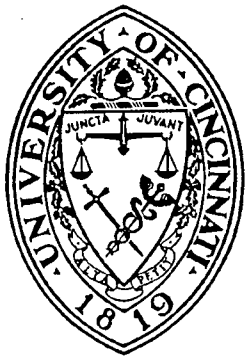

BOND CHARACTERISTICS OF OVERLAYS PLACED OVER BRIDGE DECKS SEALED WITH HMWM OR EPOXY

by

Arnol J. Gillum
Jeremiah Cole
Ahmet Turer
Bahram M. Shahrooz

Report No. UC-CII 98/02

July 1998

CINCINNATI INFRASTRUCTURE INSTITUTE

University of Cincinnati
College of Engineering

Cincinnati, Ohio 45221-0071

1. Report No.	2.	3. Recipient's Catalog No.
FHWA/OH-98/022	PB99-140865	

4. Title and Subtitle	5. Report Date
BOND CHARACTERISTICS OF OVERLAYS PLACED OVER BRIDGE DECKS SEALED WITH HMWM OR EPOXY	July, 1998
	6. Performing Organization Code
	8. Performing Organization Report No.
7. Author(s)	10. Work Unit No. (TRAIS)
Bahram M. Shahrooz	
9. Performing Organization Name and Address	11. Contract or Grant No.
The University of Cincinnati Department of Civil and Environmental Engineering Cincinnati, OH 45221-0071	State Job No. 14604(0)
	13. Type of Report and Period Covered
	Final Report
12. Sponsoring Agency Name and Address	14. Sponsoring Agency Code
Ohio Department of Transportation 1600 West Broad Street Columbus, OH 43223	

15. Supplementary Notes

Prepared in cooperation with the U.S. Department of Transportation, Federal Highway Administration

16. Abstract

The reported research examines the bond strength between overlays placed over bridge decks which are sealed with epoxy resin or high molecular weight methacrylate (HMWM) sealers. The study involved field and laboratory experimental testing of cores under direct shear, SHRP interfacial specimens, beams, and a 1/3-scale bridge subassembly of a typical steel stringer bridge. Micro-silica modified concrete, latex modified concrete, and superplasticized dense concrete overlays were used in this study. The experimental data were complemented with finite element studies. Despite often stark variations in the values of bond strength obtained from different testing methods, the data universally suggest that the use of a sealer at the interface can reduce the available bond strength. The level of the strength reduction depends on the type of sealer, but the bond strength can drop by as much as 50%. Extra surface preparation techniques, such as light sandblasting of the surface after applying the sealer or broadcasting sand over the sealed interface while the sealer is curing, are effective in restoring the bond strength. Sandblasting the HMWM sealed surface, or broadcasting sand (at approximately 100 kg/m^2 (20 lb/ft^2)) increases the strengths to 80% and 85%, respectively of the unsealed surfaces. Fatigue testing and loading well beyond service level loads do not adversely impact the bond strength so long as the sealed surface is treated before the application of the overlay. Test results indicate that bond strength at the overlay-deck interface is not critical when the deck is subjected to negative moments (i.e., those producing tension in the overlay); hence, the deck over piers can be sealed with or without a secondary treatment of the sealed surface. Although the application of sealers lower the available bond strength, finite element analyses of representative bridges show that the maximum computed shear stress is smaller than the lowest strength. Therefore, bridge decks may be sealed if either of the recommended secondary surface preparation techniques is followed to prepare the sealed deck before the application of overlays.

17. Key Words					18. Distribution Statement
Bond	Bridge decks	Field testing	Epoxy		No Restrictions. This document is available to the public through the National Technical Information Service, Springfield, Virginia 22161
HMWM	In-situ testing	Overlay	Repair		
Sealer	Shear Stress	Slab			

19. Security Classif. (of this report)	20. Security Classif. (of this page)	21. No. of Pages	22. Price
Unclassified	Unclassified		

Form DOT F 1700.7 (8-72) Reproduction of completed page authorized

BOND CHARACTERISTICS OF OVERLAYS PLACED OVER BRIDGE DECKS SEALED WITH HMWM OR EPOXY

by

Arnol J. Gillum
Jeremiah Cole
Ahmet Turer
Bahram M. Shahrooz

Report No. UC-CII 98/02

July 1998

A Report to Sponsor:
Federal Highway Administration
And
Ohio Department of Transportation

Contract # 14604(0)

Cincinnati Infrastructure Institute

University of Cincinnati
College of Engineering
Cincinnati, Ohio 45221-0071

ABSTRACT

The reported research examines the bond strength between overlays placed over bridge decks which are sealed with epoxy resin or high molecular weight methacrylate (HMWM) sealers. The study involved field and laboratory experimental testing of cores under direct shear, SHRP interfacial specimens, beams, and a 1/3-scale bridge subassembly of a typical steel stringer bridge. Micro-silica modified concrete, latex modified concrete, and superplasticized dense concrete overlays were used in this study. The experimental data were complemented with finite element studies. Despite often stark variations in the values of bond strength obtained from different testing methods, the data universally suggest that the use of a sealer at the interface can reduce the available bond strength. The level of the strength reduction depends on the type of sealer, but the bond strength can drop by as much as 50%. Extra surface preparation techniques, such as light sandblasting of the surface after applying the sealer or broadcasting sand over the sealed interface while the sealer is curing, are effective in restoring the bond strength. Sandblasting the HMWM sealed surface, or broadcasting sand (at approximately 100 kg/m^2 (20 lb/ft^2)) increases the strengths to 80% and 85%, respectively of the unsealed surfaces. Fatigue testing and loading well beyond service level loads do not adversely impact the bond strength so long as the sealed surface is treated before the application of the overlay. Test results indicate that bond strength at the overlay-deck interface is not critical when the deck is subjected to negative moments (i.e., those producing tension in the overlay); hence, the deck over piers can be sealed with or without a secondary treatment of the sealed surface. Although the application of sealers lower the available bond strength, finite element analyses of representative bridges show that the maximum computed shear stress is smaller than the lowest strength. Therefore, bridge decks may be sealed if either of the recommended secondary surface preparation techniques is followed to prepare the sealed deck before the application of overlays.

ACKNOWLEDGMENTS

The reported study was sponsored by the Ohio Department of Transportation and the Federal Highway Administration under contract number 14604(0). The contents of this report reflect the opinion the views of the authors who are solely responsible for the facts and accuracy of the data presented herein. It does not necessarily reflect the views or policies of ODOT or FHWA, and does not constitute a standard, specification, regulation, or recommendation.

The authors acknowledge Messrs. V. Dalal, R. Eltzroth, B. Weber, and L. Welker for their crucial support and advice throughout the research. The help of may ODOT personnel in districts 8 and 12 during field testing is gratefully acknowledged. The technical support personnel at the Cincinnati Infrastructure Institute were instrumental in successful completion of the reported project.

II. TABLE OF CONTENTS

III. LIST OF FIGURES

IV. LIST OF TABLES

CHAPTER 1

INTRODUCTION

A major problem for federal and state transportation departments across the country is the deteriorating condition of the highways and bridges. Reinforced concrete is used in construction of most bridges or at least a component of them. Because of the inability of concrete to resist tension, cracking occurs in bridge decks. This cracking may not be directly responsible for deterioration, but it assists other processes in creating deterioration. Cracks are formed by loads, and temperature and shrinkage effects. Cracks can also form from abrasion and everyday abuse of the wearing surface.

One way to slow down the deterioration process is to provide a protective system by the use of concrete overlays. This preventive procedure is known as an overlay because it is a layer of concrete (aggregate and binder) placed over the existing hardened portland cement concrete. The overlay creates a barrier against abrasion, water, and chemicals.

In practice, three different types of overlays are used, refer to Figure 1.1. ACI committee 345 (concrete highway bridge deck construction) recognizes the overlays as:

- Type I — Thin overlay (Polymer modified epoxy overlays)
- Type II — Concrete based overlap (Portland cement overlay)
- Type III — Combined system overlap (Asphaltic concrete over membrane)

Each of these systems attempt to create a "waterproof barrier" over the existing bridge deck, but they also must create an acceptable wearing surface and provide adequate skid resistance over the design life. Overlays only provide durability and are not considered to add strength to the structure. Therefore, if the overlay is removed, the clear cover and section modulus of the original deck would not be reduced. Through proper design and placement of bridge deck overlay systems, the service life of bridge decks can be extended which indirectly keeps the bridge open for traffic, helps prevent damage to other structural elements, and saves money.

The objective of the reported research project is to explore the possibilities of combining type I and type II overlay systems together. In the past, epoxies have been used to enhance the bond of Portland cement (PC) overlays to existing concrete (or act as a glue). However, previous studies have not examined the issues related to combining sealers and PC based concrete as a protective system and repair alternative.

1.1 Causes of Concrete Deterioration

When Portland cement is combined with water, two main products are formed, calcium - silicate - hydrate (cement paste) and calcium - hydroxide. Water dissolves the calcium - hydroxide and leaches it out of the concrete leaving voids, which lowers strength, and more importantly increases the permeability. When water is collected and trapped in these voids, it can freeze and expand in excess of 9% of its original volume (Metha and Montiero, 1993). The resulting hydraulic pressure creates cracks in the calcium - silicate - hydrate matrix. After countless freeze-thaw cycles, spalling and cracking will eventually be visible on the deck surface. A similar phenomenon can also occur in the aggregates. The resulting cracks can reflect to the surface creating a situation called D-cracking.

Chemical degradation is another major cause for deck deterioration. The expansion of steel due to corrosion will delaminate the concrete cover. Note that in order for corrosion to occur, air and water must be present at the surface of the reinforcement (a crack must be present allowing contact with air and water).

The relatively high level of pH in concrete creates a protective coating around steel reinforcing bars. When chlorides (Cl^-) from deicing salt penetrate into the concrete, the pH is lowered below 11.5 which leaves rebar susceptible to corrosion.

1.2 Concrete Overlays

As mentioned previously, three different types of overlays are recognized by ACI committee 345 (Concrete Highway Bridge Construction):

- Type I — Thin overlay

- Type II — Concrete based overlay
- Type III — Combined system Overlay

Type I and II overlay systems will be the subject of the reported research. Type III overlays are rubberized membranes bonded to the deck with tar which is covered with an asphaltic concrete riding surface. This overlay system is a very economical approach for stopping chemical and water infiltration on new decks, but it must be used in rural areas with low traffic volumes. Type I and II overlays have been successfully used to stop deterioration of existing bridge decks. The strengths and weaknesses of these methods are identified below.

Type I overlays are usually referred to as Polymer Modified Concrete overlays (PMC). These overlays are composed of multi-component polymer resins (epoxies) that are flooded onto a concrete bridge deck . The thickness is usually between 10 to 20 mm. in thickness ($^1/_2$ to $^3/_4$ inch). After application of the resin, the surface is sprayed with aggregate for traction, and control of volume changes due to temperature and shrinkage effects. When curing is completed (usually after a 24 hour period), the system provides a complete vapor barrier against infiltration of water and chlorides. Because of the low viscosity of the system, the shrinkage and flexural cracks in the existing bridge deck are also filled during the application. Several problems are associated with the use of PMC overlays. Strict guidelines (ACI 503) for mixing and application are a necessity for proper performance. The existing deck must be cleaned of all dirt, and the contaminated and unsound concrete must be removed prior to application (surface preparation for overlays is an important issue and will be discussed later). Because PMC systems are very sensitive to water during application and curing, the deck must be totally dry at the surface before placement. Additional problems may occur after application of PMC. Because the PMC overlay creates a vapor barrier, any water in the existing concrete will be trapped. Freeze - thaw cycles can debond the overlay. Furthermore, differences in thermal coefficient of PMC and concrete (thermal coefficients of PMC systems range from 17 E^{-6} to 50 E^{-6} in/in/deg °F compared to approximately 7 in/in/°F (ACI 503)) create large stresses at the interface. Abrasion

due to high volumes of traffic is also a concern for PMC overlays.

California was one of the first states to successfully use PMC as a bridge deck overlay in 1957 on the San Francisco-Oakland Bay Bridge (ACI 503). This type of overlay is an excellent option in climates with minimum freeze-thaw cycles, and no extreme temperature changes. PMC overlays do not increase the dead load of the structure, nor require changes in thickness, joints, and surface drainage requirements.

Research conducted in the mid 1980's has shown how polymer resins (2-part epoxy and methyl methacrylate) are very successful at stopping the intrusion of chlorides (tests were conducted by soaking cubes in a 15% NaCl Solution). Tests show that PC concrete with 0.4 w/c ratio sealed with epoxy and methyl methacrylate can reduce chloride penetration 92 percent better than PC concrete without treatment (Pfiefer, Perenchio, and Marusin, 1985). If this could be achieved over actual bridge decks, deterioration due to water and chloride intrusion would significantly decrease or even stop.

Type II overlays are a layer of high-performance portland cement concrete 32 to 76 mm. thick (1¼ to 3 inches) placed over the existing concrete deck. These are the most common overlays used today. Three different types of high-performance PC based concretes are used for overlays: latex modified concrete, super dense plasticized concrete, and micro-silica modified Concrete. All of these types of concrete are designed for very low permeability, resistance to abrasion, ease of placement, and bond to an existing surface. The modulus of elasticity, and thermal coefficients of Portland cement (PC) overlays are very similar to normal concrete. The moisture level in the existing deck is not an issue. The cost of installation is small compared to that of Polymer modified concrete (PMC) overlays. In 1985 Weiss Janey and Ellstner conducted a survey to compare costs between different types of specialty polymer concretes and PC concretes (Pfeifer and Perenchio, 1985). The results are summarized in Table 1.1. Although the prices are outdated, the differences in cost are apparent.

Latex Modified Concrete (LMC) has been used since the 1940's as repair material for

concrete bridge decks. The latex mixture that is added to the mix clogs voids in the cement paste and transition zones created from evaporating water (low permeability), and also makes the concrete more workable. Unfortunately LMC, overlays can have many problems due to the latex admixture. The amount of latex that is added to the concrete is very important to the permeability and strength, excess latex will increase permeability and even prohibit the concrete from setting. LMC also can exhibit plastic shrinkage greater than unmodified concrete if the surface is improperly cured. The surface must be covered to keep water from evaporating. Due to the extremely low w/c ratio, if surface water evaporates, the cement paste cannot properly hydrate and exhibit enough tensile strength resulting in cracking (ACI 548). Placement of LMC is very labor intensive. An on-site mixer must be used because of the rapid set time, and a bonding grout must be brushed on the deck prior to placement. When the cost of latex admixture is included, LMC overlays become an expensive process.

Due to the progress of water reducing admixtures for PC concrete, Superplasticized Dense Concrete became a popular alternative for overlays. SDC overlays provide a very low permeability, high strength (a very high PC content) and great workability for a price much cheaper than LMC. The concrete could be hauled in mobile mixer truck to the bridge making it a more desirable repair option.

In 1984 the Ohio Department Of Transportation began using Micro-Silica modified Concrete for bridge deck overlays (Luther, 1993). Silica fume is a fine material (1/100 the diameter of a cement particle) that is combined with portland cement to create a better gradation in the concrete mix. Silica fume also is a pozzolan which reacts with CaOH, a product of the reaction between PC and water, forming more calcium-silicate-hydrate (C-S-H). The additional C-S-H does not significantly increase strength, but it does decrease the possibility for voids in the concrete (due to leaching of CaOH dissolved by water) and lower permeability. MSC overlays are now the most common type in Ohio, low permeability and excellent bond strength are the two major reasons for this choice.

The bond strengths for each type of concrete overlay are close to being identical. MSC tends to have a slightly higher strength than LMC and SDC. The major differences found in bond strength are usually attributed to surface preparation. Of the three types of overlays recognized by ACI 345, success of PC overlays depend the most on the preparation of the existing deck. If the surface concrete on a bridge deck is deteriorated or contains dirt, no PC overlay will be effective because of debonding between the layers. Further discussion of surface preparation will be addressed in the next section. Another problem with PC overlays is shrinkage. Even with proper curing, shrinkage cracks will form which in turn decrease the effectiveness of the overlay.

Weaknesses of PC overlays do not compare with the advantages of using high performance PC concretes for bridge deck repair, abrasion resistance, low permeability, and adhesion to existing concrete. As a result, PC overlays are the main repair choice across the country.

Companies producing concrete products such as epoxy resins and sealers are creating new and better repair systems every year. New penetrating sealers which are "cousins" of PMC overlay systems have been introduced for crack sealing. Because of their low viscosity (10 cps, much less than water), they are able to penetrate into the small shrinkage and flexural cracks sealing off pathways for water and chloride intrusion. Methyl methacrylate sealers have been found to penetrate small cracks as deep as 38 mm. (1½ in.) (Florida DOT, 1996). Because PC overlays develop shrinkage and flexural cracks, water and chlorides can still find paths to the existing bridge deck and continue the deterioration process. Any procedure or procedures which successfully stop the intrusion of water and chlorides into concrete are favorable options for repair and control of concrete deterioration. It may be advantageous to seal existing voids, flexural and shrinkage cracks in the bridge deck, then place a PC overlay such as MSC on top of the sealer. If water and chlorides traveled through cracks in the overlay, the sealer would not allow penetration into the deck and reinforcing steel; thus eliminating corrosion. The MSC also

would provide a desirable surface for skid and abrasion resistance. Unfortunately, the effect of sealers on interface bond is not known. A limited number of research involving laboratory and field testing have been conducted to understand the best surface preparation procedures for ultimate bond strength between plastic and hardened concrete, but no studies relate to the amount of bond strength necessary for an overlay to work, or show what tests represent the actual field conditions best. Because the use of sealers at the concrete interface may reduce the bond strength, it may not be feasible to use sealers with concrete overlays. Advantages offered by placing concrete over a sealed surface may still compensate for the smaller bond strength, particularly if sealers result in only a slight reduction of bond strength. Therefore, it is important to create an experimental program which studies the influence of testing methods for establishing bond strength, to evaluate the influence of sealers on bond strength, and to examine the required bond strength in actual bridges.

1.3 Interface Bond Tests for Concrete to Concrete

In the past, various tests have been created to represent the bond at the interface of old concrete to new concrete. Most of these tests were created to determine methods of creating the highest bond strength. Unfortunately, the tests were not chosen to best represent behavior of the actual structure in the field.

In order for an overlay to work, the overlay and deck must act as a composite system. Mechanical bond and electrical forces are two main mechanisms which create bond between surfaces. Mechanical bond is created by friction and interlock between uneven surfaces and aggregates, electrical attraction is created by Van Der Waals forces as shown in Figure 1.2. These bond mechanisms must be constant in lab tests to get an accurate representation with acceptable variances in results.

(a) Hindo (1990)

One of the only studies that compared the practicality of test methods to actual site conditions was conducted by Hindo. Three different bond tests were considered for measuring

the quality of bond obtained from different surface preparation procedures. These tests were the split shear, direct shear, and direct tension tests. Because of the ability to use the direct tension test in the field, specimens do not need to be removed from the bridge. The direct tension test also gives a better idea of the location and nature of failure. Failure will occur over the weakest plane. If the bond strength is greater than the concrete strength, failure will be a tensile concrete failure rather than separation at the interface.

The actual purpose of the research was comparison of the surface preparation procedures. Preparation of the existing surface by mechanical means was completed by conventional mechanical chipping (scarify or jackhammer) or hydrodemolition. Hydrodemolition is a new procedure for removing damaged surface concrete by blasting it with water jets from 82 to 240 MPa (12,000 to 35,000 psi). Immediately prior to overlay placement, epoxy or cement slurry was painted on the surface as bonding agents.

Results showed that the use of bonding agents made very little impact on bond strength but the use of hydrodemolition for concrete removal provided much greater bond strength than mechanical chipping. Mechanical chipping was found to leave micro-cracks or "bruises" in the existing concrete at the interface. The use of hydrodemolition reduced the amount of micro-cracks and increased bond strength from a mean of 940 kPa to 1.4 MPa (136 psi to 203 psi), a 33% increase. In all cases the average bond strengths were above the ACI minimum of 100 psi (ACI committee 503).

(b) Saucier, Bastien, Pigeon and Fafard (1991)

The study separated bond tests into four different categories, i.e. direct tension, direct shear, indirect tension, and shear-compression. Each test was judged by space efficiency of the bond line, specimen construction, and mechanics of failure.

Finite element studies indicated that tests using a direct shear approach would be most practical. The direct shear or guillotine test caused some problems. The point of contact of the guillotine created stress concentrations which led to premature failures. In order to eliminate

these problems, compression was applied simultaneously as the shear force was being increased. Results indicated that the higher the compressive stress, the results varied less (variation as low as 3%).

The authors proposed this test method as a new ASTM method for finding bond strength between new and old concrete. Nevertheless, several problems can be identified for this test. A special test apparatus would be required to complete the test. Also, the size of the specimens would have to be very small and aggregate sizes would be limited. Performance of different surface preparation techniques cannot be compared with this testing method.

(c) O'Connor and Saiidi (1993)

This research led to the development of the California Test 551, i.e. a specimen tested in flexure made from a beam with a vertical interface in the middle. The test was developed for evaluating the performance of PMC overlays in cyclic behavior and under effects of high temperatures (up to 200 degrees °F). The specimens were constructed by creating 75x75x400mm. (3x3x16") beams and cutting them in half after curing. New concrete is placed against the old concrete and allowed to cure. The specimens were loaded as beams. The failure stress was simply the modulus of rupture.

(d) Keeran (1994)

An in house testing program conducted by ODOT used the direct shear or guillotine test to compare the performance of different types of PC overlays with different types of surface preparation. The testing was performed because of questions about ODOT's specification for PC overlays. The specification requires that the surface must be dry and a PC based grout be brushed onto the surface before placement of an overlay. Six 2.1x4.3m, (7x14') test slabs were made from normal ODOT class "S" concrete and allowed to properly cure before applying an overlay. Three slabs received overlays of MSC and SDC concrete each. Each of the three slabs received different surface conditions; wet, surface dry, and dry. Each slab was divided into three sections to receive different surface preparation through the use of bonding grouts;

equal parts cement and sand, no grout, and brushing the mix onto the surface as a bonding grout. After curing, 100 mm. (4") cores were taken from each of the slabs and tested in direct shear. Bond strength values were found by dividing the load by the bonded area of the core. The test procedure worked very well with some variance in results. The research indicates that the existing deck does not have to be surface dry before placing an overlay, and the same mix as the overlay may be brushed onto the surface as a bonding grout to increase bond strength.

(e) Strategic Highway Research Program Product No. 2025

This report (SHRP-C-361, 1993) proposes a new test method for bonding new concrete to old concrete. The test provides interfacial bond strength and the corresponding deformation. The specimen is shaped as 2 L segments on top of each other (Figure 1.3). Due to the large size of the specimen, uniform shear stress should be achieved over the interface without stress concentrations. One specimen must be cast and allowed to cure. The surface is then prepared, and the same L specimen is cast on top. After proper curing, two displacement transducers are mounted vertically across the interface and the specimen is ready to test. Bond stress is found by dividing the maximum load by the bonded area of concrete (232 cm^2 or 36 in^2 for the proposed test).

This test requires special equipment in the form of displacement transducers, a data acquisition system, and a testing machine capable of loading at a constant rate (proposed 6.7 MN/min or 1500 lb/min). Because of the large area of bonded region, surface flaws may have less effect on the final strength of the test leading to results with low variance.

1.4 Objectives

As noted in the preceding paragraphs, no previous study has examined the influence of sealers on bond strength of an overlay to an existing bridge deck. Considering the need for experimental results and the limitation of available information, an experimental test program reported herein was undertaken. The specific objectives of this research are (1) to establish expected bond strength of overlays to sealed bridge decks using epoxy resin and high

molecular weight methacrylate sealers, and (2) to evaluate the influence of different testing methods for establishing bond strength.

1.5 Scope

In an effort to achieve the above-mentioned objectives, an experimental program was conducted. The tests were separated into two main categories, (1) field tests, and (2) laboratory tests.

Field testing consisted of evaluation of 12 total overlaid bridge decks in Ohio Department of Transportation (ODOT) districts 8 and 12 (Southwestern Ohio, and Cleveland respectively). Of the 12 total bridges, four had overlays with latex modified concrete, four with super dense plasticized concrete, and four with micro-silica modified concrete. None of the bridges tested had been sealed prior to having an overlay placed on them. The bridges were all tested using the direct shear and direct tension (pull-out) test methods. By conducting the field tests, an idea of the magnitude of the actual bond stress of different overlays can be found along with the influence of each test method on bond strength.

Laboratory testing consisted of fabricating test specimens for three different test methods, (1) direct shear, (2) SHRP, (3) a beam with an overlay in flexure, and (4) flexural testing of a bridge subassembly subjected to fatigue and static loading. Specimens constructed for each test method varied with the type of sealer applied along with surface preparation at the interface prior to overlay placement. By combining the test results, a database can be formed showing the effect of a sealed surface, the effect of different brands and types of sealers, the influence of surface preparation, and the influence of test methods on bond strength.

In Chapter 2 the four test methods are described in detail.

In Chapter 3, the experimental data are presented. The performance of the 12 bridges tested is reported. Laboratory results of the influence of sealers and surface preparation is also evaluated. Chapter 3 also attempts to compare the bond strength results for each test and identify a test procedure which best represents bond strength.

In Chapter 4, flexural beam tests are presented. The measured data from each of the tests are utilized to explain the expected mode of failure for overlaid decks with sealers and no sealers.

To further examine the results obtained from the laboratory and field tests, a 1/3-scale model of a typical bridge with three girders and concrete deck was constructed and tested. The deck was prepared, and overlaid based on optimum methods developed in Chapters 3 and 4. The test specimens, testing methods, measured data, and relevant observations are summarized in Chapter 5.

The research is summarized in Chapter 6. Based on the experimental information presented in this report, appropriate conclusions and recommendations are made.

Table 1.1 Concrete Overlay Material Costs

Concrete Type	Cost /ft^2
Latex Modified PC concrete	\$1.55[*1] (extra cost not included for full depth repairs)
Super Dense Plasticized PC Concrete	\$0.25[*1] (extra cost not included for full depth repairs)
Methyl Methacrylate PMC	\$1.50[*2]

*Note:

1. Assuming 1½" overlay thickness
2. Assuming ½" overlay thickness

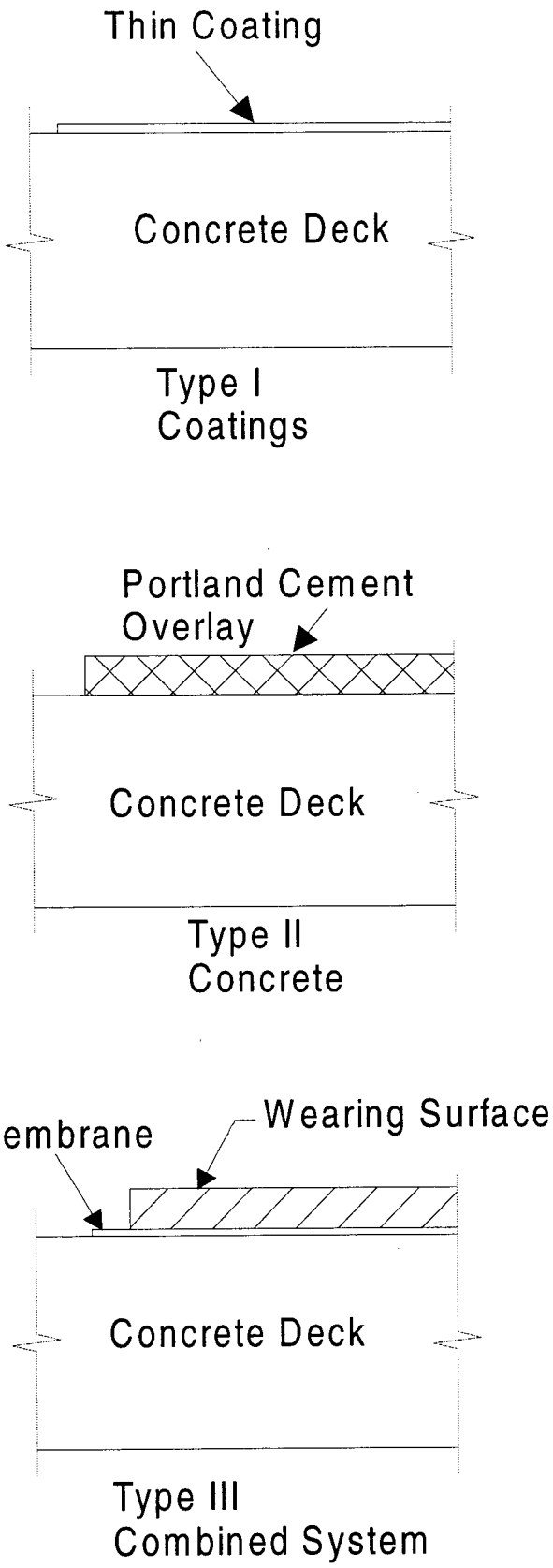

Figure 1.1 Types of Bridge Deck Overlays

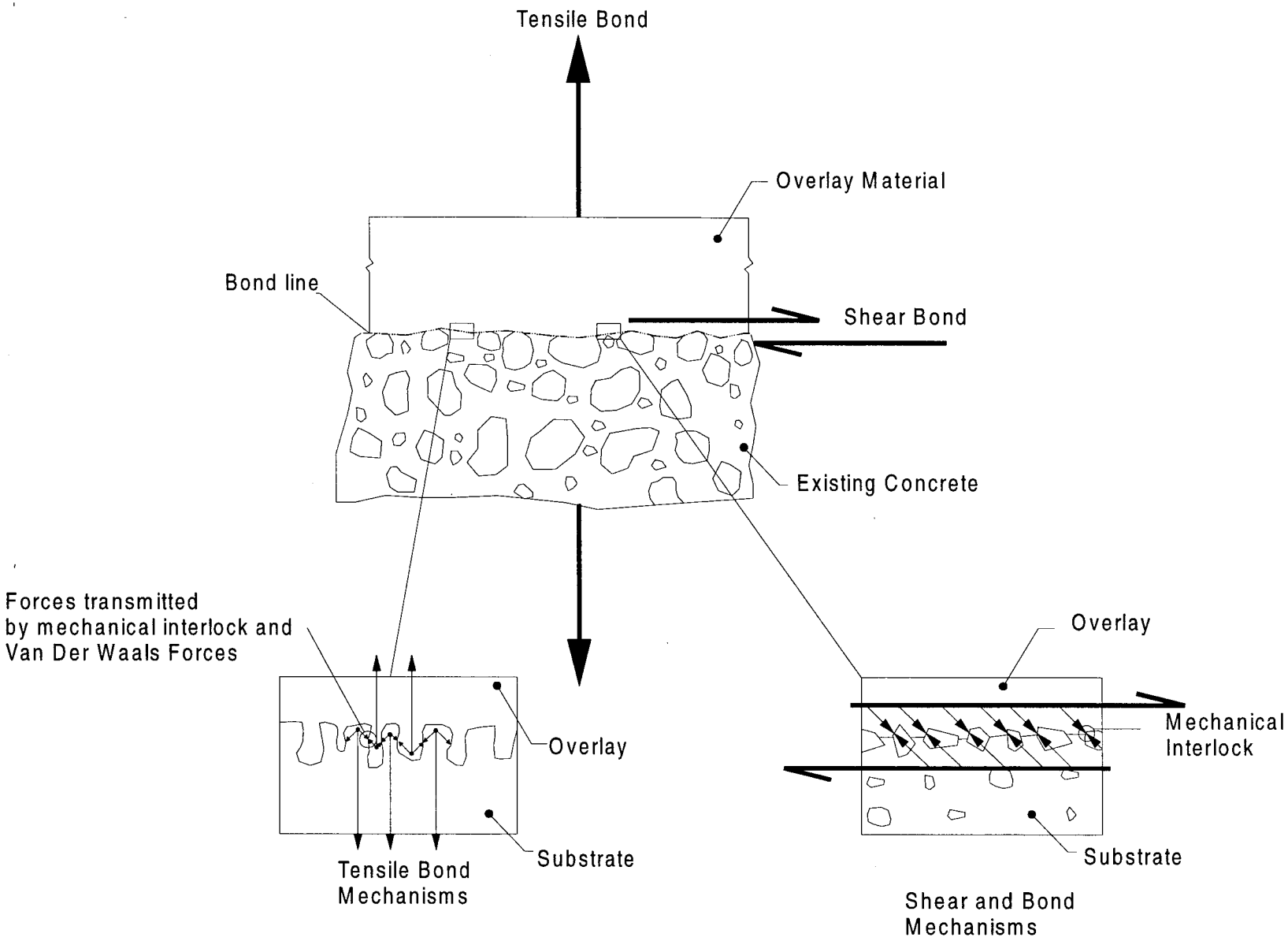

Figure 1.2 Bond Mechanisms

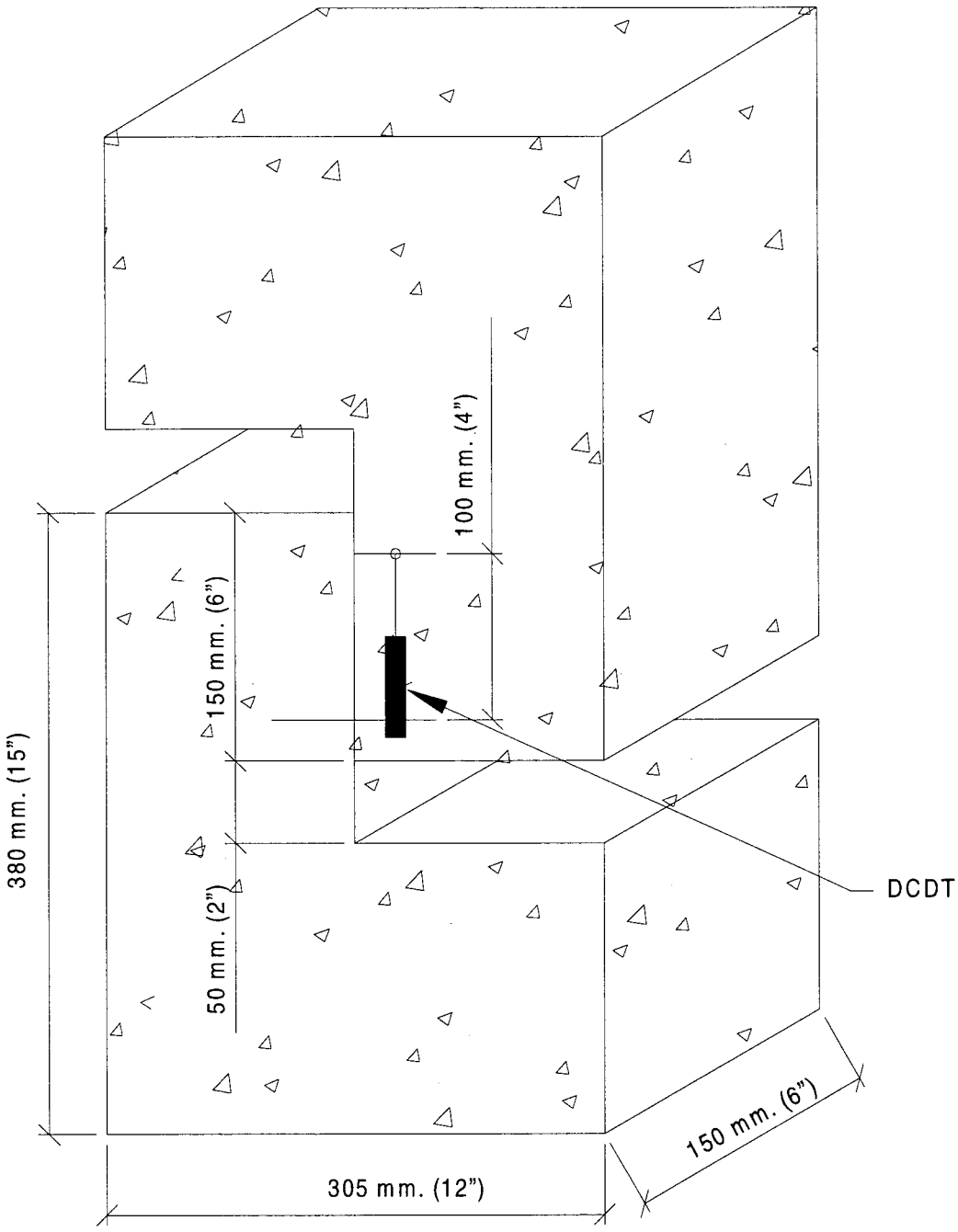

Figure 1.3 SHRP Test Specimen

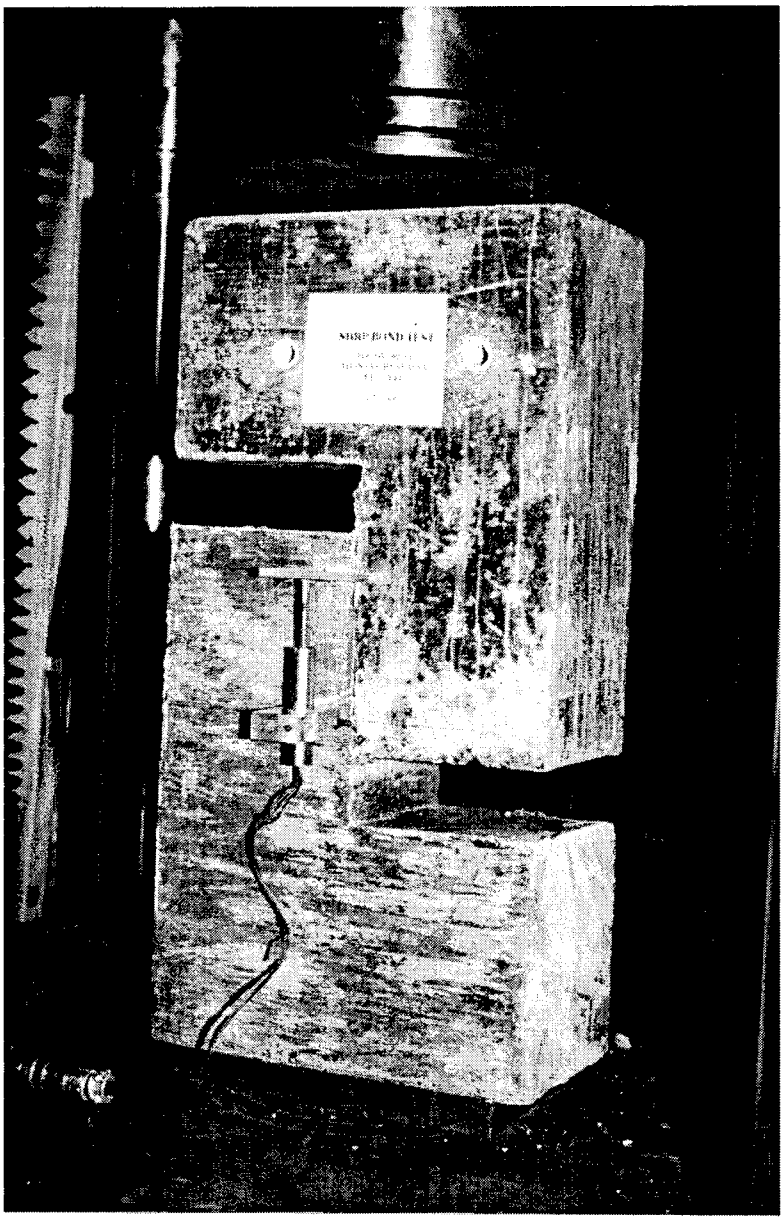

Figure 1.4 Photograph of SHRP Specimen During Testing

CHAPTER 2

DESCRIPTION OF TEST METHOD

In order to represent the bond between the interface of existing concrete to new concrete, different methods of testing were selected based on comprehensive review of literature along with the practicality of fabricating and testing the specimens. Four different types of tests were selected for this investigation:

- Direct Shear (Guillotine)
- Direct Tension (Pull-Out)
- SHRP Bond Test
- Flexural Beam Test

The first two tests were designed for use in the field and laboratory. The last two, SHRP and flexural beam tests are strictly laboratory tests and require more extensive instrumentation.

2.1 Direct Shear Test

The direct shear or guillotine test is a very practical test and can be performed on cylinders made in the laboratory, or cores removed from bridges. The test apparatus consists of a base which holds a core or cylinder, and a sliding head (Figure 2.1). The test specimens must be inserted so the load is applied at the overlay-base concrete interface. The bond stress is the maximum applied load divided by the bonded area which is the area of the core. This test relies upon both bond mechanisms, aggregate interlock, and the Van Der Waals forces for the bond strength. The test requires that the specimen be positioned properly; otherwise the bond strength will be artificially increased as part of the load is resisted by the monolithic concrete. Precise positioning can be very difficult with cores from actual bridge decks where there is no unique interface as evident from Figure 2.2.

2.2 Direct Tension Test

Another test which is applicable to both the field and laboratory is the direct tension or

pull-out test. The test is completed by coring below the interface line into the existing concrete, attaching a plate to the surface, and pulling the core out (Figure 2.3). The bond stress is the maximum load divided by the bonded area, i.e. area of the core. Unlike the direct shear test, pull-out tests can be conducted on site and give immediate results on the quality of bond. The failure in pull-out tests can occur at the interface, base, or overlay depending on the relative tensile strength of the base or overlay concrete versus the bond strength. Direct tension test is also useful to examine the influence of variables such as surface preparation, bonding agents, overlay type, etc. The attachment of the plate to the surface is typically achieved by epoxy adhesives. Hence, the bond strength of the adhesive must be larger than the expected bond strength.

2.3 SHRP Bond Test

Recently, a new test method for interfacial bond strength has been developed by the Strategic Highway Research Program (SHRP-C-361,1993). The test specimens involve two L shaped pieces of concrete bonded together as represented in Figure 2.4. The first segment receives a proper cure along with surface preparation prior to placing the overlay which is also a L shaped segment. The two segments must be cast such that the interface is within the plane of applied load. Similar to the direct shear/guillotine test, the bond interface is once again subjected to pure shear. In contrast to direct shear test, the interface is expected to be subjected to a more uniform shear force. Furthermore, the larger bonded surface would reduce the effects of local flaws. The variation of the measured bond strength is anticipated to be less as pronounced. Aggregates do not protrude at the interface and do not affect results.

The testing involves measurement of the applied load and slip at the interface. The primary use of the measured load-slip relationship is to ensure that the specimen is loaded without eccentricity. The maximum bond strength is obtained by dividing the ultimate load by the bonded area.

2.4 FLEXURAL BEAM TEST

The bond stress between bridge decks and concrete overlays may be best simulated by a flexural beam test. The specimen consists of a reinforced concrete beam with an overlay which is intended to represent a slab strip on a bridge. The beam is loaded until failure. Note that the beam has to be proportioned adequately to prevent beam failure, i.e. flexural or shear failure, and to ensure bond failure.

The calculated in-plane shear stress at the interface represents the bond strength. Due to material non-linearity of concrete, the fundamental equation $\tau=VQ/It$ cannot be used. In lieu of detailed analysis, fundamental principles can be used to calculate the shear stress. The basic procedure is identical to the derivation of $\tau=VQ/It$. However, appropriate modifications are necessary to account for cracking and the nonlinear behavior of concrete. The method implemented herein is described in the following.

1. Fiber analysis techniques are used to establish the cross-sectional response of the overlaid beam. Proper steel and concrete constitutive relationships are used to ensure reliable results. For a range of concrete compressive strain at the extreme fiber, the values of the neutral axis and bending moment are generated.
2. The test beam is divided into a number of nodes of the length dx.
3. For a given distribution of bending moment along the beam, the depth of the neutral axis and concrete strain at each node are obtained.
4. Knowing the material properties of the overlay concrete as well as the strain, the stress distribution over the overlay thickness is obtained.
5. By integrating the material stress distribution curve at each node, the in-plane compressive force can be calculated. The difference between the forces in two adjacent nodes is the in-plane shear. Dividing the calculated shear force by the bonded area between nodes results in the in-plane shear stress.

6. The load at which the overlay is debonded is used to calculate the maximum shear stress, i.e. bond strength.

Figure 2.5 provides a graphical representation of the process for calculating in-plane shear stress.

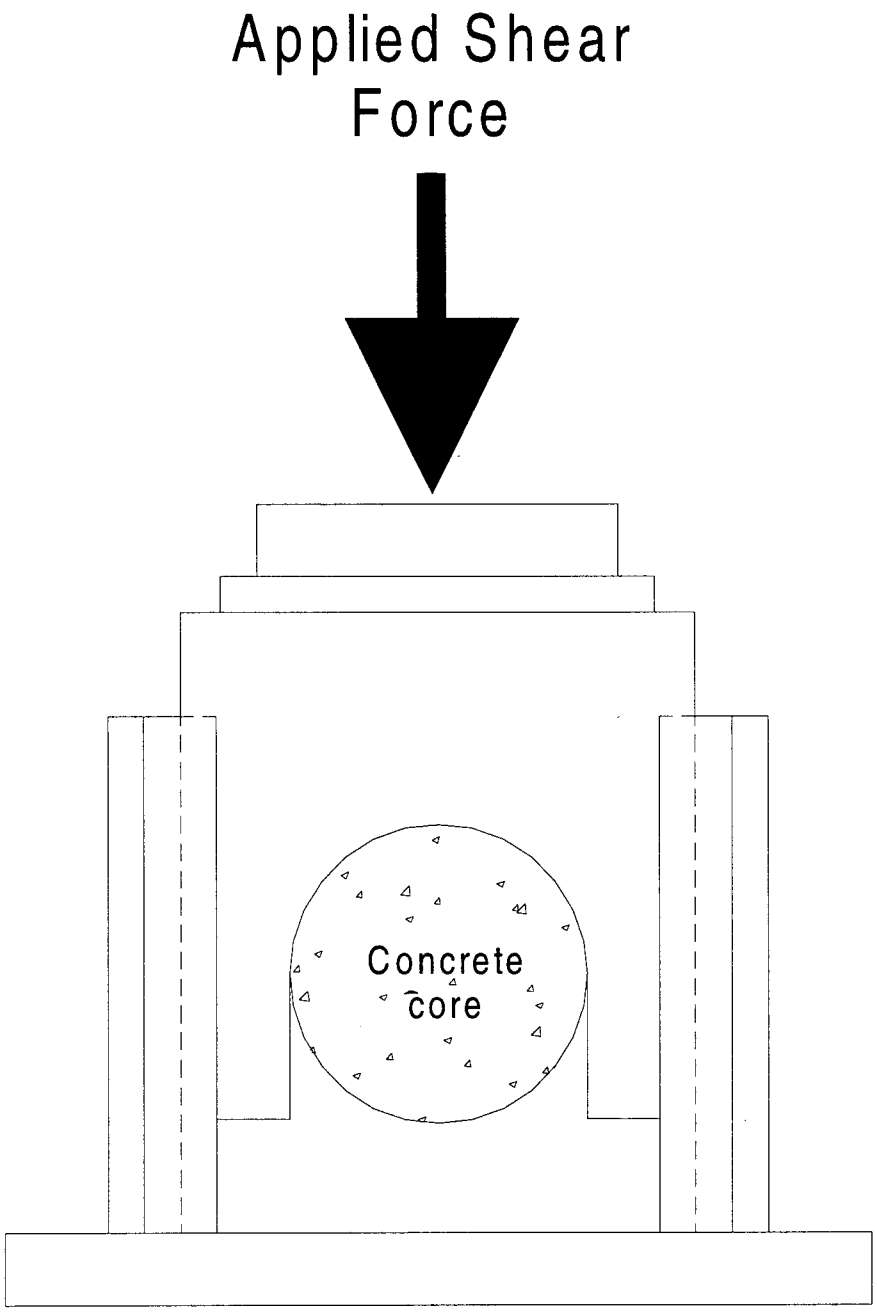

Figure 2.1 Direct Shear Test Device

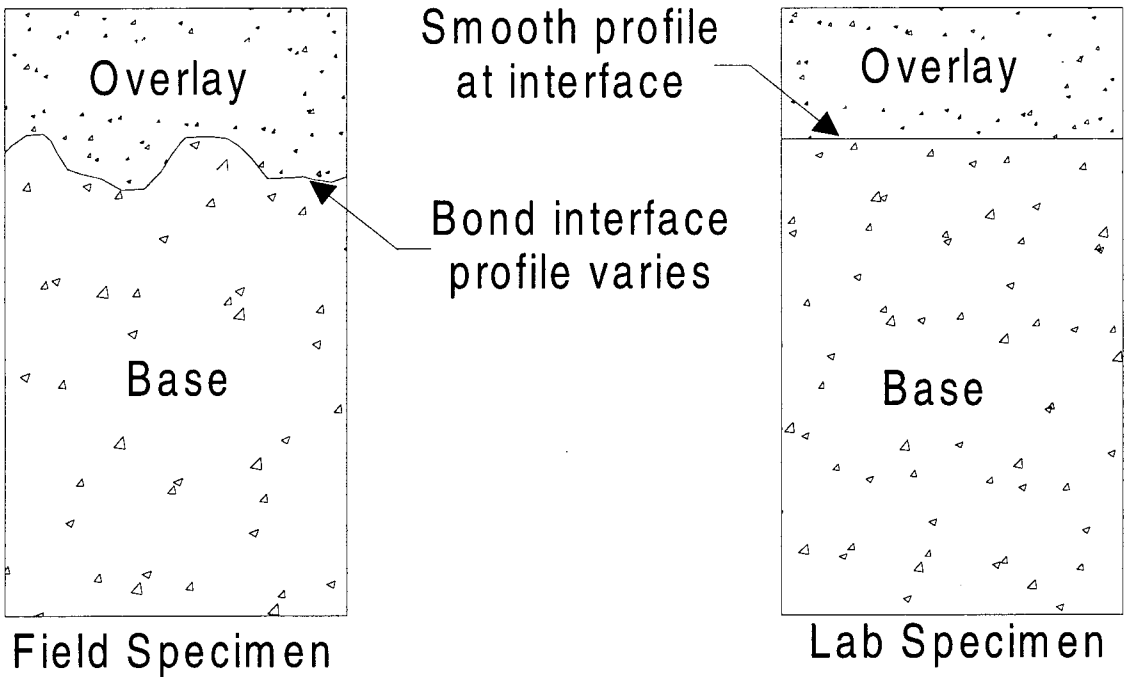

Figure 2.2 Direct Shear Core

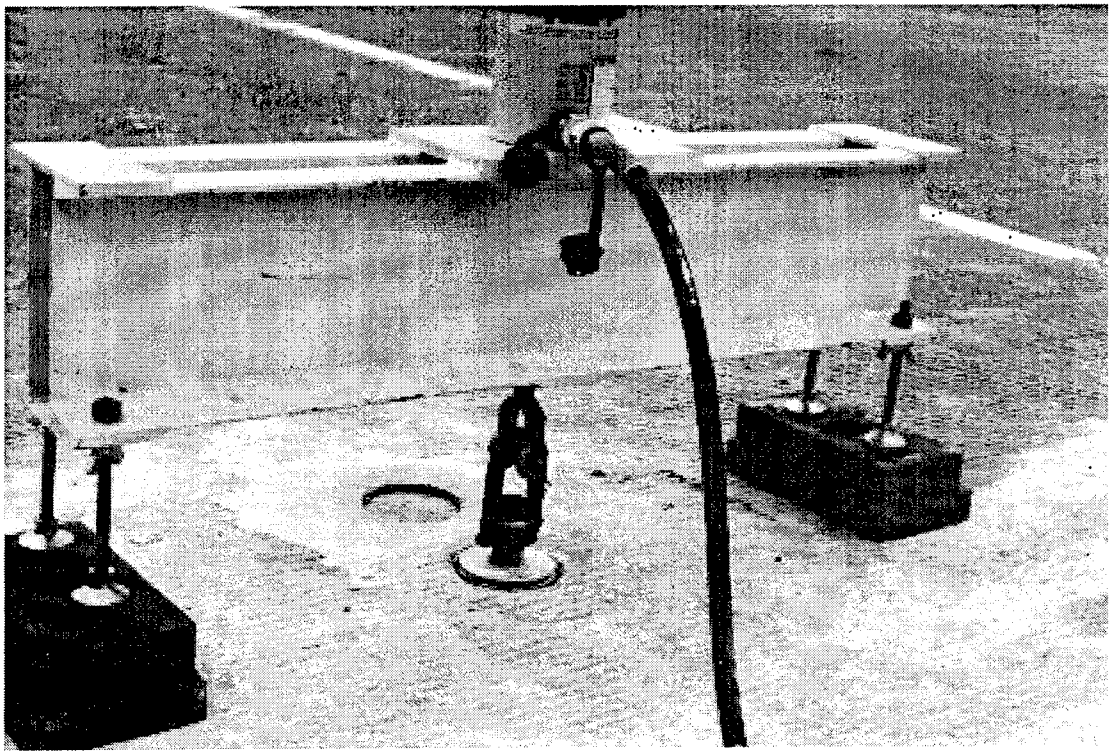

Figure 2.3 Pullout Test Frame

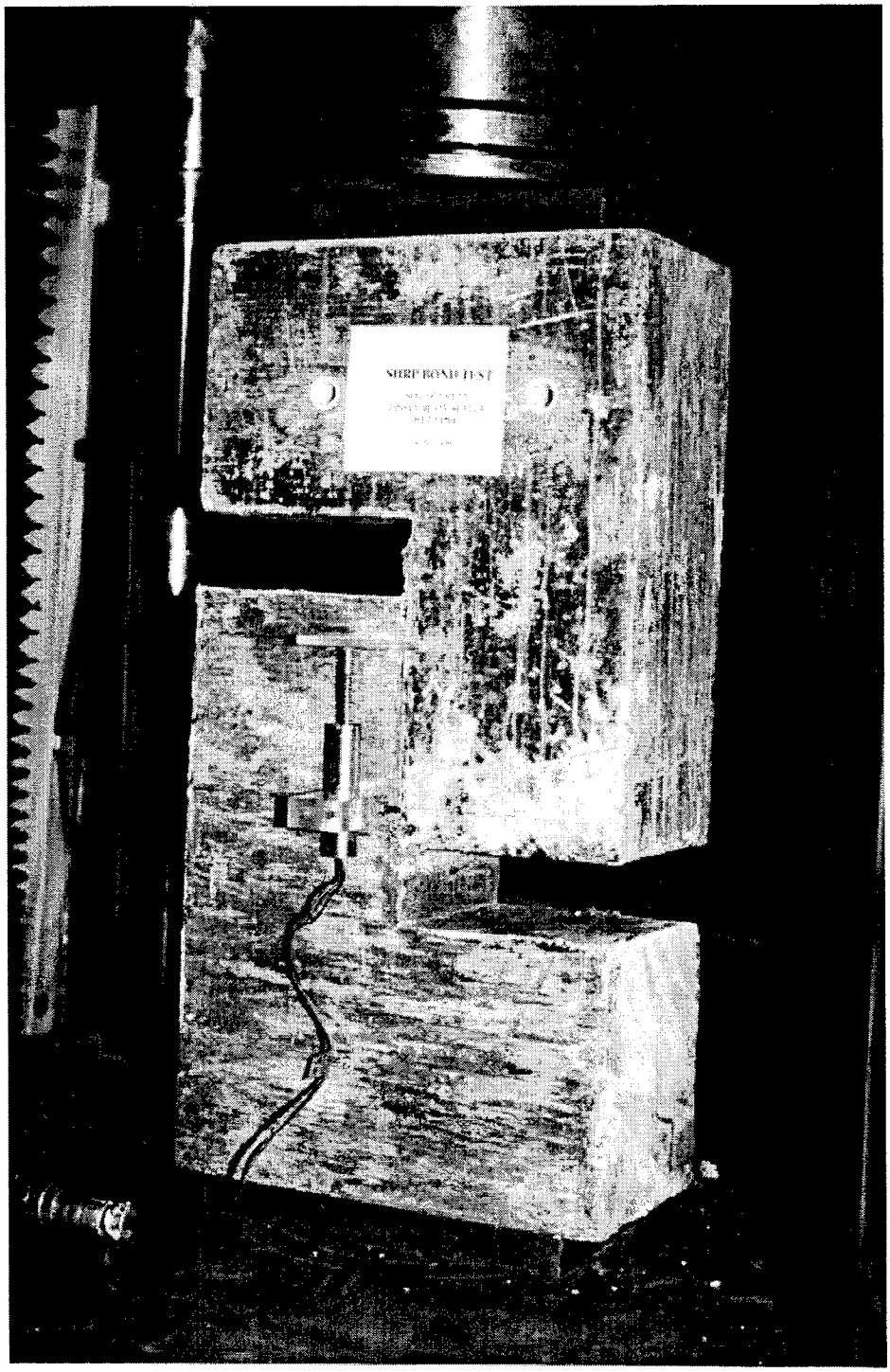

Figure 2.4 SHRP Test Specimen

A. Beam section with applied load.

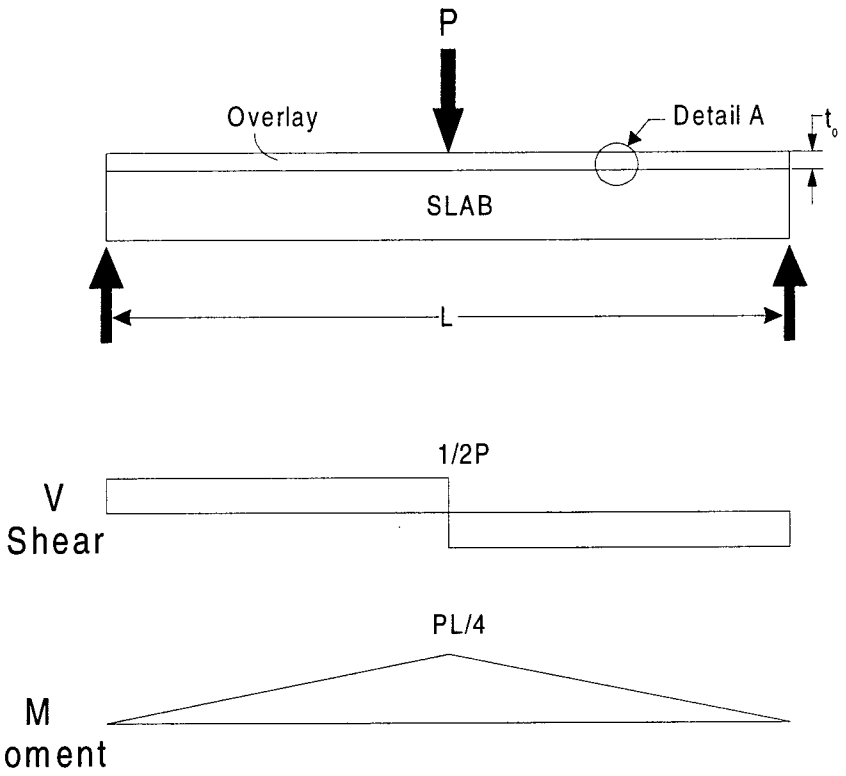

If the material is linear elastic, the stress and strain distributions are linear over the cross-section as shown below.

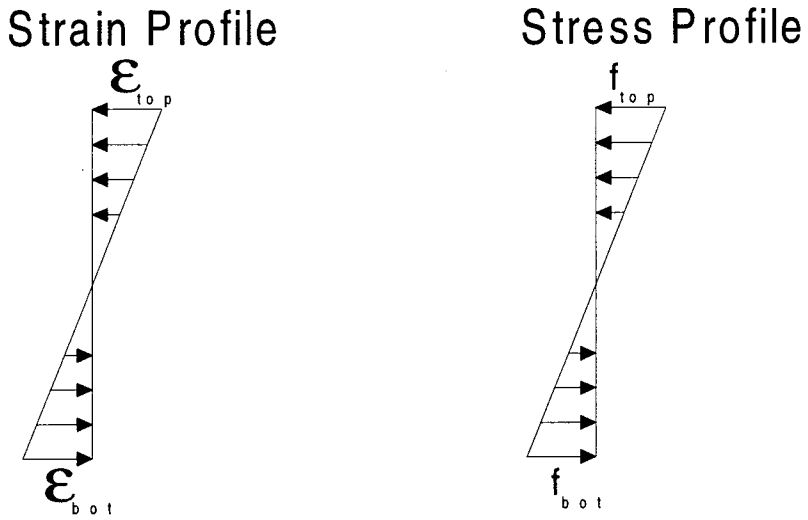

The equation $\tau = VQ/It$ can be used to calculate the shear stress.

Figure 2.5 Calculation of In-Plane Shear Stress at the Overlay Interface

B. Concrete is nonlinear. The strain profile remains the same as that for linear, elastic materials; however, the stress profile changes.

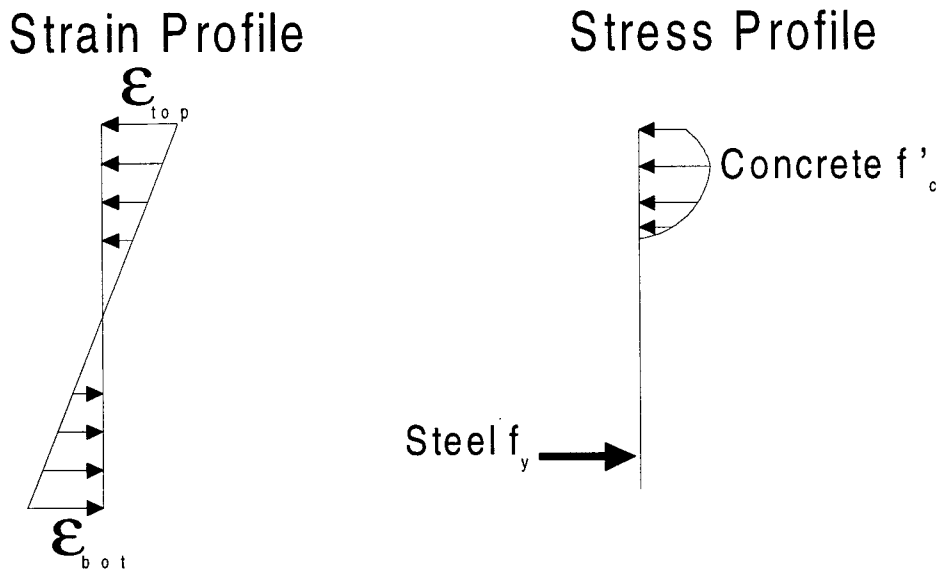

C. Using fiber analysis, behavior of the section can be investigated under a range of applied moments.

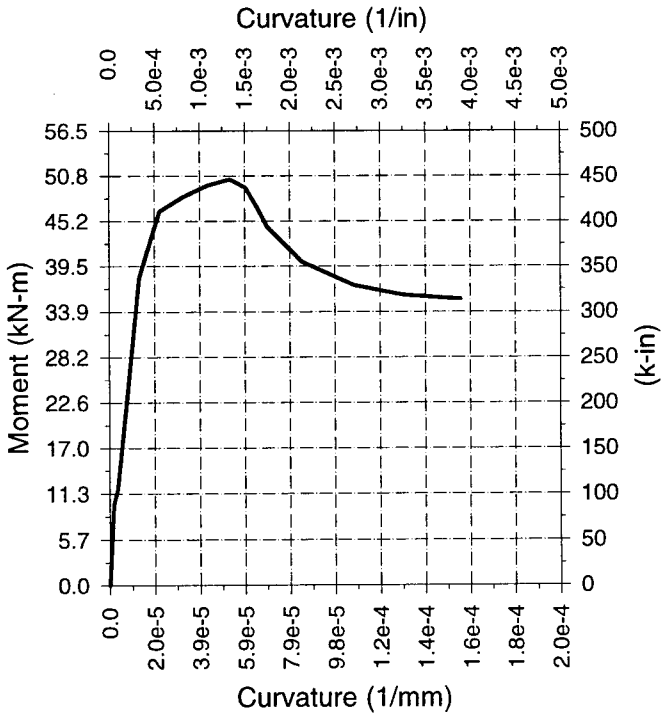

Figure 2.5 (Cont.)

D. Distribution of compressive stress in overlay between two nodes.

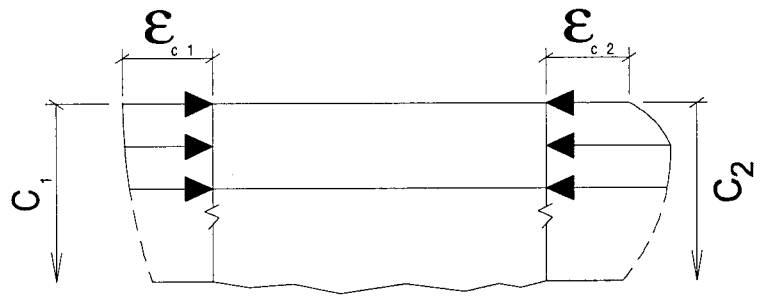

Detail A

F. Calculate in-plane shear at each node.

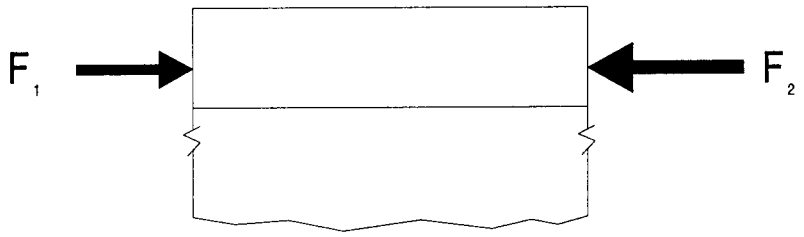

Detail A

$$F_1 = \int_{c_1 - t_o}^{c_1} f_c \, dc \qquad F_1 = \int_{c_1 - t_o}^{c_1} f_c \, dc$$

G. Calculate in-plane shear stress from

$$\tau = \frac{F_1 - F_2}{bdx}$$

Figure 2.5 (Cont.)

CHAPTER 3

Testing Program and Results

In this chapter, testing will be separated into two different sections, (1) field testing and (2) laboratory testing. Information of testing equipment and the variables of each test are discussed along with illustration and interpretation of results. The properties of materials used, calibration of instruments, and the selection and placement of instrumentation are also included.

3.1 Field Testing Program

Twelve bridges were selected for field tests. The bridges were located in Ohio Department of Transportation districts 8 and 12 (Southwestern Ohio and Cleveland area, respectively). In each district, two bridges had latex modified concrete overlays (LMC), two had superplasticized dense concrete (SDC), and two with micro-silica modified concrete (MSC). An ODOT core truck was provided in order to drill the proper 100 mm. (4 in.) cores for direct shear and direct tension testing. Cores for the direct shear test were taken from both the driving lane and the median of the bridge. The location of the coring is important because the concentration of chloride due to deicing salt is more significant in the median than in the driving lanes. The level of bond strength between overlays and existing slab is likely to be impacted by high concentrations of chlorides. Figures 3.1 and 3.2 show the examples of core locations for two bridges. Core locations for the other ten test bridges are presented in Appendx D. Table 3.1 lists the bridges tested along with the number of tests conducted.

All of the bridges in the study were multiple span concrete slab over steel stringers. In most cases the deck was around 200 mm. (8 in.) in thickness. Ages of the overlays varied from 8 years and older. All the bridge decks had been scarified before receiving an overlay.

3.1.1 Direct Shear Test

A total of 45 cores were taken from the test bridges. Because a pachometer or other means to locate reinforcing bars was not present, some of the core samples contained bars

near the interface and had to be excluded. Each core was measured to obtain thickness of the overlay, thickness of portion of slab within the core, and the diameter. The profile of the overlay was also traced around the outside edge of the core so that only the interface would be subjected to shear. In order for the cores to be held properly in the test apparatus, cores had to have a minimum overlay thickness of least 25 mm. (1 in.), and a base thickness of at least 150 mm. (6 in.) as shown in Figure 3.3.

Testing was conducted using the direct shear device described in Chapter 2. A 100- kN Tinius Olsen servo controlled universal testing machine was used to apply the loads. The compressive force was applied at 675 N (3 kips) per minute with the goal of keeping the test time around 2 minutes. Before testing the overlaid cores, a monolithic concrete core was tested to establish the expected shear capacity. The shear strength was found to be 6.6 MPa (960 psi). Using this value and data from previous research (Keeran,1995), the bond strength was anticipated to be approximately 4.4 MPa (640 psi). Therefore, if failure did not occur before 4.4 MPa (640 psi), the specimen was unloaded, repositioned, and tested to failure. This procedure was necessary to ensure that the shear load was being applied along the interface of the test core. The failure load was recorded along with significant observations such as whether the failure had occurred at the interface, in the base, or in the overlay. The results will be presented and discussed later in Section 3.1.3.

3.1.2 Direct Tension Test

The second field test used for evaluation of bond strength of bridge decks was the direct tension test. As described in Chapter 2, this test requires a small load frame, hydraulic jack and pump for loading, and an instrument to measure the applied load.

The loading frame (Figure 3.4) used consisted of two channels, laced together back to back with a 40 mm. (1½ in.) gap. The channels rested on 4 legs which could be adjusted to level the test frame. Load was applied by an Enerpac 10,000 psi hollow plunger, hydraulic cylinder with a 13.5 kN (60 kips) capacity. Pressure and hydraulic fluid were supplied by a

hand pump. A pressure transducer was connected to the hand pump to monitor the applied load. The pressure transducer in conjunction with the complete hydraulic system was calibrated prior to testing. As part of calibration, a self equilibrating frame was loaded by the hydraulic system. A load cell had been positioned in the system to record the applied load. The voltage change from the pressure transducer and the corresponding load from the load cell were monitored. The measured data were used to obtain a calibration factor relating pressure transducer voltage to load. A factor of 3.20 kN/Volt (14.26 kips/Volt) was used for testing. In order to read the voltage in the field, a Hewlett Packard hand held voltmeter accurate to ±0.005% (±1.1 N) was selected. The voltmeter also had a function capable of recording maximum and minimum voltage output from the pressure transducer.

The direct tension test required a 100mm. core be drilled to a depth of 40 mm. below the overlay into the existing slab concrete (Figure 3.5). The cores taken for direct shear tests provided an effective means to determine the exact depth of overlay for each bridge. Hence, proper drill depth for direct tension tests was established. Note that the locations for direct tension tests and cores taken for direct shear tests were within immediate vicinity of each other. This coring sequence ensured a proper comparison of the two methods. Special attention was made to ensure level bonding surface before attaching a load plate. The load plate was 10 mm. thick and 100 mm. in diameter. The plate was bonded to the top of the core with Master Builders SPL epoxy. Because it was not necessary to test immediately, the epoxy was allowed to cure overnight to ensure proper strength. To perform the test, the bonded plate was connected to the hydraulic system using a universal joint and a 20 mm. (3/4 in.) high strength threaded rod. Load was applied until the core was broken from the bridge deck. The maximum load and failure mode were observed and documented.

Due to earlier problems with the loading system and epoxy, the bridges in District 8 could not be tested successfully. Six bridges in district 12 were successfully tested using the direct tension test system (Table 3.1). The results are presented in Section 3.1.3.

3.1.3 Field Test Results

The test results are presented in graphical and abridged tabular form in Figures 3.6 and 3.7 and Tables 3.2 to 3.7, respectively.

Failure of each test occurred at the interface, in the overlay, or in the base slab concrete. Generally, failure occurred at the interface for LMC or SDC overlays by a clean break at the bond line for direct shear and direct tension. Apparently, the base concrete and overlay concrete were stronger than the bonded interface. In the case of MSC, the failure in the direct shear test was at the interface. However, the location of failure in the direct tension test occurred in the overlay concrete on two occasions. This observation indicates that experimental results and corresponding conclusions can be significantly impacted by testing method.

Values for bond strength from the direct shear test are listed in Tables 3.2 to 3.5, and Figure 3.6. The trends for bond strength of LMC, SDC, and MSC overlays were different for the bridges tested in District 8 and 12. This difference is attributed to conditions such as age of the overlay, and care of surface preparation and concrete placement. Based on direct shear tests conducted on cores taken from the bridges in District 8, the highest average bond strength was for LMC overlay followed by SDC and MSC. However, the highest average bond strength for district 12 bridges was for MSC overlay (5.1 MPa or 738 psi) followed by SDC and LMC (4.5 MPa or 625 psi). The average bond strength was practically identical for the bridges with LMC in District 8 and 12.

Values for bond strength from the direct tension test are shown in Table 3.6 and in Figure 3.7. Based on the direct tension test, micro-silica modified (MSC) overlays provided the highest bond strength followed by super dense plasticized concrete (SDC) and latex modified concrete (LMC). This trend in terms of relative bond strength between overlays is similar to that obtained for direct shear tests conducted for cores taken from District 12 bridges. Values of bond strength were much lower for the direct tension test than for the direct shear test. Stresses recorded for the direct tension test were 35% less, on average, than the values found

by direct shear. Since the state of stresses and transfer of load to the base concrete are dissimilar between the tests, different values for bond strength are expected.

Bond strength measured by direct shear and direct tension test has a high level of variance as seen from Tables 3.3, 3.5, and 3.7. The variance does not apparently depend on the type of overlay. One needs to recognize this scatter when evaluating bond strength.

Trends of the bond strength obtained by each method are identical; therefore, either method can be used to obtain the relative magnitudes for bond strength. Although each test method may show similar trends in bond strength, the values of bond strength and types of failure at the interface are different and cannot be directly compared to one another. Because of the high scatter in the results for both test methods, there is a lack of confidence with the absolute bond strength values.

3.2 Laboratory Testing Program

The available bond strength was evaluated by direct shear test, Strategic Highway Research Program (SHRP) interfacial bond test, and flexural beam test. Different test variables were examined through two different series of tests. To simulate field conditions (i.e. shrinkage of concrete in the deck has effectively stopped when the overlay is appled), the "base concrete" for the test specimens was not overlaid immediately after fabrication. The overlays were cast after the shrinkage had stabilized and was insignificant. Tables 3.8 to 3.10 show the test variables along with the type of test used in each series. Prior to describing the test results, a brief discussion of the materials used in the fabrication of specimens is provided.

3.2.1 Materials

The materials used for the laboratory tests in series 1 and 2 all conformed with the State of Ohio Department of Transportation Construction and Material Specifications, i.e. ODOT specification 499: for the deck concrete (ODOT Class "S" concrete); ODOT supplemental specification 845: Bridge Deck Repair and Overlay with Latex Modified Concrete; ODOT supplemental specification 850: Bridge Deck Repair and Overlay with Superplasticized Dense

Concrete; ODOT proposal note no. 315-88: Bridge Deck Repair and Overlay with Micro-Silica Modified Concrete; ODOT proposal note no. 824-88: Item Special - Treating Concrete Bridge Decks with HMWM Resin; ODOT proposal note no. 825-93: Treating Concrete Bridge Decks with Gravity-Fed Resin. All of the materials used during the research project are listed in Table 3.11. The concrete mix designs used for the tests in series 1 and 2 are illustrated in Tables 3.12a through 3.12d.

The concrete used in the construction of the laboratory specimens was tested in accordance with all relevant ASTM specifications. The ASTM tests performed for material properties were C490: Standard Practice for Use of Apparatus for the Determination of Length Change of Hardened Cement Paste, Mortar, and Concrete; and C39: Standard Test Method for Compressive Strength of Cylindrical Concrete Specimens. Separate compressive strength properties were recorded for series one and series two tests. Tables 3.13 and 3.14 show compressive strength results for concrete used in each series. Figure 3.8 shows the shrinkage of each type of concrete used over time.

3.2.2 Series 1 Tests

This series focused on studying the influence of the type of polymer sealers on bond strength. Epoxy resin, and high molecular weight methacrylate (HMWM) were considered. The bond strength was measured by direct shear test and SHRP interfacial bond test. Thirty six specimens were cast for each test method. As seen from Tables 3.8 and 3.9, four specimens of each type of overlay were cast with no sealer at the interface, four with epoxy resin at the interface, and four with HMWM.

Each specimen was sealed and overlaid at 56 days. This age ensured that the shrinkage in the concrete had reached insignificant levels. The interface in direct shear specimens was sandblasted for one minute. Due to the larger surface area of SHRP specimens, the interface was sandblasted for three minutes. After sandblasting, sealer was applied to the interface and allowed to cure for one day. Sikadur 55 SLV epoxy resin and Sika

Pronto 19 HMWM were used in this study. An overlay was placed over the interface and wet cured for three days in accordance with the Ohio Department of Transportation specifications. The specimens were tested 56 days after being overlaid to ensure most of the shrinkage in the overlay concrete had already occurred. The tests were conducted according to the procedures described in Chapter 2. A 100-kN Tinius Olsen servo controlled universal testing machine was used to load the specimens. The load was applied at 675 N (3 kips) per minute for direct shear tests, and 1.35 kN (6 kips) per minute for SHRP interfacial bond tests. The failure load was recorded along with significant observations such as location of failure. The load-interface slip was also recorded for the SHRP specimens using two ±13mm. (0.5 in.) direct current displacement transducers.

The test results are presented in graphical and abridged tabular form in Figures 3.9 and 3.10 and Tables 3.15 to 3.16, respectively. Generally, failure occured at the interface for both test procedures. In each test method, bond strength decreased when the interface was sealed. Direct shear tests indicated that specimens treated with epoxy resin experienced a 35% reduction in bond strength, while the presence of HMWM resulted in a 52% bond strength reduction. SHRP interfacial bond specimens showed a reduction of 60% or 43% in bond strength for specimens sealed with epoxy resin or HMWM, respectively.

Despite this large reduction in bond strength, treated surfaces may be acceptable if the actual bond strength demand is less than the available strength. Finite element analysis of three representative bridges (see Appendix B) indicate a maximum in-plane shear stress of 0.65 MPa (95 psi) under service loads. This value is significantly smaller than the available bond strength of surfaces which are treated by epoxy resin or HMWM (see Table 3.15 and 3.16). Although the remaining bond strength is adequate to resist the applied in-plane shear stress due to service loads, additional stresses due to shrinkage and temperature may overcome available bond strength.

Direct shear specimens which were not sealed exhibited the same trends in bond

strength as those established based on cores taken from District 8. Latex modified concrete possessed the highest bond strength followed by super dense plasticized concrete, and micro-silica modified concrete. Due to the small difference between the highest and lowest bond strength (about 230 kpa or 33 psi), a clear trend could not be established based on SHRP Specimens.

Bond strength from SHRP specimens was on the average 55% lower than those from direct shear tests. This observation is attributed to the differences in the state of stresses at the interface for the two test procedures. Hence, one needs to consider such variability when evaluating the quality of bond.

3.2.3 Series 2 Tests

The second test series focused on examining the influence of different types of surface preparation in an effort to enhance bond strength of sealed surfaces. High molecular weight methacrylate (HMWM) has a lower viscosity than epoxy resin; hence, it penetrates deeper and appears to be more effective in sealing cracks. Considering such advantages, ODOT engineers will likely choose HMWM over epoxy. Therefore, the focus of this series of tests was placed on HMWM. HMWM sealer from two manufactures (Sika and Transpo Industries) were tested. To incorporate a relatively large number of specimens, only direct shear specimens were fabricated and tested. The test matrix is summarized in Table 3.10.

Similar to series one, the specimens were sealed and overlaid at 56 days. Each specimen was sandblasted for one minute. Twelve specimens were left unsealed as a benchmark. The remaining 76 specimens were sealed with Transpo Sealate T-70 and SikaPronto 19 HMWM. To remedy the bond strength reduction observed in series one, two secondary surface preparation techniques were explored. The first method involved sprinkling sand (sand broadcast) over the surface immediately after applying sealer. The second procedure was to sandblast the surface before overlaying. Both of these procedures were expected to remove residue left from HMWM which was believed to be the main reason for the

observed lower bond strength in series one. The additional surface treatment would also roughen the surface to enhance concrete overlay bond. The effectiveness of the secondary surface preparation techniques was studied through 48 specimens.

All specimens received an overlay of latex modified concrete(LMC), super dense plasticized concrete (SDC), or micro-silica modified concrete (MSC). Tests were conducted 56 days after being overlaid in accordance to direct shear test procedures outlined in Chapter 2.

Test results are presented in graphical and abridged tabular form in Figures 3.11 and 3.12 and Table 3.17. Failure occured at the interface for all of the specimens. For unsealed specimens, LMC had the highest bond strength with 5.9 Mpa (856 psi) followed by MSC (5.1 Mpa, 735 psi) and SDC (4.3 Mpa, 618 psi). The measured values of bond strength were smaller in this series than those found in series one. Variation in the compressive strength of the base concrete (Tables 3.13 and 3.14) are believed to have caused the differences. The use of Sika HMWM sealer in seies two resulted in a 49% reduction. The corresponding value for series one was 52%. The percent reduction of overlaid specimens is not apparently affected by the compressive strength of the base concrete. Bond strength was improved when the sealed surface was sand broadcast or sandblasted before applying the overlay. In case of Sika HMWM, bond strength dropped to 85% or 80% of otherwise unsealed surface by sand broadcast or sandblasting, respectively.

Tests conducted using Transpo T-70 Sealer showed much lower bond strengths than those using Sika HMWM. Without secondary surface treatment, specimens sealed with transpo T-70 had effectively no bond strength. Bond strength was only 3% of the available bond in the unsealed specimens. When the sealed surface was sand braodcast or sandblasted, the bond strength increased to 31% and 43% of the specimens without HMWM.

These results indicate that simple procedures such as sandblasting or sand broadcasting are effective means to improve bond strength of sealed surfaces. Even though bond strength can be improved by additional surface preparation procedures, the study has

shown that all types of HMWM may not be appropriate for sealing decks before placing concrete overlay.

3.3 Summary

The testing for bond strength in this chapter involved using tests conducted in the field and laboratory. Field tests were performed to compare bond strength from different test procedures. Laboratory tests were performed to compare test methods and investigate the effects of using sealers (at the interface) on bond strength.

The direct shear and direct tension tests both show identical trends for bond strength. Either test method may be used to obtain relative magnitudes for bond strength on bridge decks with concrete overlays.

Trends in bond strength from various test methods appear to be the same, but the values of bond strength are different and cannot be directly compared. This difference is expected because of the different state of stresses and load transfer between the overlay concrete and base concrete. Chapter Four will provide further discussion regarding the influence of testing procedure on measured bond strength.

The use of a high molecular weight methacrylate (HMWM) or epoxy resin sealer at the interface surface of the test specimens will affect bond strength. The direct shear and SHRP interfacial bond test procedures indicate that the use of epoxy resin or HMWM sealers will lower bond strength in comparison to identical unsealed specimens. The level of the strength reduction was found to be influenced by the type (manufacturer) of HMWM sealer.

Extra surface preparation techniques applied to the SikaPronto 19 HMWM sealed specimens increased the bond strength close to the values of the unsealed specimens. These surface preparation techniques included sandblasting the interface surface after applying HMWM sealer, or broadcasting sand over the interface surface while the sealer was curing.

Table 3.1 Field Test Log

Bridge No. (_) Indicates District	Overlay Type	No. of Direct Shear Tests	No. of Direct Tension Tests
(8) BUT 27-1402	LMC	3	--
(8) BUT 129-0908	LMC	2	--
(12) CUY I90-1372	LMC	5	2
(12) CUY I90-1391	LMC	4	2
(8) BUT 4-0040	SDC	3	--
(8) BUT 4-0191	SDC	3	--
(12) CUY I480-1842R	SDC	3	2
(12) CUY I271-0232L	SDC	5	2
(8) WAR 73-1838	MSC	4	---
(8) WAR 741-0209	MSC	2	---
(12) CUY I480-2075R	MSC	5	2
(12) CUY I480-2139R	MSC	5	2

Table 3.2 District 8 Direct Shear Test Results

Core #	Overlay Type	Stress MPa	* Comments
1	SDC	4.7	2,4
2	SDC	4	2
3	SDC	3.3	2,4
4	SDC	3.3	2
5	SDC	5.6	2,4
6	SDC	3.6	2
1	MSC	3.9	2,4,5
2	MSC	3	2,6
3	MSC	2.9	2,5
4	MSC	3	2,6
5	MSC	3	2,5
6	MSC	6	2,4
1	LMC	5	2,4,5
2	LMC	4.4	2,4,5
3	LMC	4.6	2,4,5
4	LMC	4.1	2,5

1.Failure in Overlay
2.Failure at interface
3.Failure in Base Slab
4.Loaded to 35 kN, repositioned and failed
5.Cracked aggregates present at interface
6.Voids present at interface

Table 3.3 Direct Shear Strength (District 8)

Overlay Type	Average Bond Strength (MPa)	Standard Deviation (MPa)
SDC	4.1	±0.9
MSC	3.6	±1.2
LMC	4.5	±0.4

Table 3.4 District 12 Direct Shear Test Results

Core #	Overlay Type	Stress (MPa)	* Comments
1	SDC	3.6	2
2	SDC	3.9	2
3	SDC	4	2
4	SDC	5.5	2,4
5	SDC	3.9	2
6	SDC	5.5	2
7	SDC	5.9	2,4
8	SDC	5.9	2,4
1	MSC	7.6	2,4
2	MSC	5.9	2,4
3	MSC	6.5	2,4
4	MSC	4.5	2
5	MSC	5.3	2,4
6	MSC	4.9	2
7	MSC	5.1	2
8	MSC	2.9	2
9	MSC	5.8	2,4
10	MSC	3.8	2
1	LMC	3.2	2
2	LMC	3.8	2
3	LMC	3.9	2
4	LMC	4.7	2
5	LMC	3.7	2
6	LMC	5.8	2,4
7	LMC	6.3	2,4
8	LMC	2.4	2,6
9	LMC	2.2	2,6

1.Failure in Overlay
2.Failure at interface
3.Failure in Base Slab
4.Loaded to 35 kN, repositioned and failed
5.Cracked aggregates present at interface
6.Voids present at interface

Table 3.5 Direct Shear Strength (District 12)

Overlay Type	Average Bond Strength (MPa)	Standard Deviation (MPa)
SDC	4.6	±1.3
MSC	5.46	±1.3
LMC	4.5	±1.1

Table 3.6 District 12 Direct Tension Test Results

Core #	Overlay Type	Stress (MPa)	* Comments
1	SDC	1.32	2
2	SDC	1.12	2
3	SDC	2.29	2
4	SDC	1.56	2
1	MSC	2.16	2
2	MSC	2.52	1
3	MSC	2.55	1
4	MSC	1.95	2
1	LMC	2.33	2
2	LMC	0.69	2
3	LMC	1.04	2

1.Failure in Overlay
2.Failure at interface

Table 3.7 Direct Tension Strength (District 12)

Overlay Type	Average Bond Strength (MPa)	Standard Deviation (MPa)
SDC	1.57	±0.51
MSC	2.29	±0.29
LMC	1.36	±0.87

Table 3.8 Series 1 Direct Shear Test Matrix

Overlay Type	Type of Sealer	Number of Specimens
MSC	No Sealer	4
SDC	No Sealer	4
LMC	No Sealer	4
MSC	HMWM	4
SDC	HMWM	4
LMC	HMWM	4
MSC	Epoxy Resin	4
SDC	Epoxy Resin	4
LMC	Epoxy Resin	4

Table 3.9 Series 1 SHRP Test Matrix

Overlay Type	Type of Sealer	Number of Specimens
MSC	No Sealer	4
SDC	No Sealer	4
LMC	No Sealer	4
MSC	HMWM	4
SDC	HMWM	4
LMC	HMWM	4
MSC	Epoxy Resin	4
SDC	Epoxy Resin	4
LMC	Epoxy Resin	4

Table 3.10 Series 2 Test Matrix

Overlay Type	Type of Sealer	Type of Surface Preparation	Number of Specimens
MSC	No Sealer	N/A	4
SDC	No Sealer	N/A	4
LMC	No Sealer	N/A	4
MSC	Sika (HMWM)[*1]	None[*3]	4
SDC	Sika (HMWM)	None	4
LMC	Sika (HMWM)	None	4
MSC	Transpo (HMWM)[*2]	None	4
SDC	Transpo (HMWM)	None	4
LMC	Transpo (HMWM)	None	4
MSC	Sika (HMWM)	Sandblasting[*4]	4
SDC	Sika (HMWM)	Sandblasting	4
LMC	Sika (HMWM)	Sandblasting	4
MSC	Transpo (HMWM)	Sandblasting	4
SDC	Transpo (HMWM)	Sandblasting	4
LMC	Transpo (HMWM)	Sandblasting	4
MSC	Sika (HMWM)	Sand Broadcast[*5]	4
SDC	Sika (HMWM)	Sand Broadcast	4
LMC	Sika (HMWM)	Sand Broadcast	4
MSC	Transpo (HMWM)	Sand Broadcast	4
SDC	Transpo (HMWM)	Sand Broadcast	4
LMC	Transpo (HMWM)	Sand Broadcast	4

1. Sika Pronto 19 High Molecular Weight Methacrylate
2. Transpo Sealate T-70 High Molecular Weight Methacrylate
3. No secondary surface preparation performed
4. Interface surface was sandblasted after application of HMWM sealer
5. Sand was broadcast over the interface surface after application of HMWM Sealer

Table 3.11 Materials Used for Fabrication of Specimens

Material	Supplier
Cement	Type I Portland Cement
Fine Aggregate	Sand aggregate per ODOT Specification 703.02 from Hilltop Basic Resources, Inc.
Coarse Aggregate #1	#57 aggregate from Hilltop Basic Resources, Inc.
Coarse Aggregate #2	#8 aggregate from Hilltop Basic Resources, Inc.
Air Entrainment	Sika AEA-15 by the Sika Corp.
Superplasticizer	Sikament 10ESL by the Sika Corp.
Latex Emulsion	SikaLatex by the Sika Corp.
Micro-Silica	Sikacrete 950 Micro-Silica Fume by the Sika Corp.
Epoxy Resin	Sikadur 55 SLV Healer/Sealer by the Sika Corp.
High Molecular Weight	SikaPronto 19 HMWM by the Sika Corp.[*1]
Methacrylate	Transpo Sealate T-70 by Transportation Industries.[*2]

1. SikaPronto 19 HMWM was used in both series 1 and 2 tests
2. Transp Sealate T-70 was used in series 2 tests only

Table 3.12a ODOT Class "S" Concrete Mix Proportions

Material	Quantity
Cement	420 kg/m^3 (715 lbs./Yd^3)
Coarse Aggregate #1	1030 kg/m^3 (1735 lbs./Yd^3)
Fine Aggregate	670 kg/m^3 (1125 lbs./Yd^3)
Maximum Water/Cement Ratio	0.44
Air Entrainment	8 ± 2%

Table 3.12b Superplasticized Dense Concrete (SDC)

Material	Quantity
Cement	490 kg/m^3 (825 lbs./Yd^3)
Coarse Aggregate #2	770 kg/m^3 (1300 lbs./Yd^3)
Fine Aggregate	770 kg/m^3 (1300 lbs./Yd^3)
Maximum Water/Cement Ratio	0.36
Air Entrainment	8 ± 2%
Superplasticizer	6 ± 2" Slump

Table 3.12c Micro-Silica Modified Concrete (MSC)

Material	Quantity
Cement	415 kg/m^3 (700 lbs./Yd^3)
Micro-silica Fume	42 kg/m^3 (70 lbs./Yd^3)
Coarse Aggregate #2	750 kg/m^3 (1265 lbs./Yd^3)
Fine Aggregate	850 kg/m^3 (1430 lbs./Yd^3)
Maximum Water/(Cement-Pozzolan) Ratio	0.36
Air Entrainment	8 ± 2%
Superplasticizer	6 ± 2" Slump

Table 3.12d Latex Modified Concrete (LMC)

Material	Quantity
Cement	390 kg/m^3 (658 lbs./Yd^3)
Coarse Aggregate #2	770 kg/m^3 (1300 lbs./Yd^3)
Fine Aggregate	975 kg/m^3 (1645 lbs./Yd^3)
Maximum Water	86.5 L/m^3 (17.5 Gal/Yd^3)
Latex Emulsion	121.5 L/m^3 (24.5 Gal/Yd^3)

Table 3.13 Series 1 Average Compressive Strengths

Type of Concrete	28 Days	At Time of Testing
ODOT Class "S"	53.5 MPa (7760 psi)	64.4 MPa (9350 psi)
SDC	53.4 MPa (7740 psi)	59.3 MPa (8610 psi)
MSC	51.5 MPa (7480 psi)	58.6 MPa (8500 psi)
LMC	28.8 MPa (4180 psi)	30.6 MPa (4440 psi)

Table 3.14 Series 2 Average Compressive Strengths

Type of Concrete	28 Days	At Time of Testing
ODOT Class "S"	31.4 MPa (4560 psi)	33.9 MPa (4930 psi)
SDC	53.0 MPa (7700 psi)	N/A
MSC	44.2 MPa (6420 psi)	N/A
LMC	30.1 MPa (4368 psi)	N/A

Table 3.15 Direct Shear Strength (Series 1 Tests)

Overlay Type	Average Bond Strength (MPa)	Standard Deviation (MPa)
SDC/No Seal	7.3	±0.16
MSC/No Seal	5.3	±1.13
LMC/No Seal	7.6	±0.18
SDC/Epoxy Resin	5.4	±0.61
MSC/Epoxy Resin	3.4	±1.29
LMC/Epoxy Resin	4.3	±0.28
SDC/HMWM	4	±0.54
MSC/HMWM	2.5	±0.39
LMC/HMWM	3.2	±0.08

Table 3.16 SHRP Interfacial Bond Strength (Series 1 Tests)

Overlay Type	Average Bond Strength (MPa)	Standard Deviation (MPa)
SDC/No Seal	3.79	1.9 ±
MSC/No Seal	3.46	1.4 ±
LMC/No Seal	3.68	1.0 ±
SDC/Epoxy Resin	1.81	0.2 ±
MSC/Epoxy Resin	1.44	0.3 ±
LMC/Epoxy Resin	2.07	0.8 ±
SDC/HMWM	1.57	0.9 ±
MSC/HMWM	1.67	0.9 ±
LMC/HMWM	2.88	0.2 ±

Table 3.17 Direct Shear Strength (Series 2)
SikaPronto 19 HMWM

Overlay Type	Average Bond Strength (MPa)	Standard Deviation (MPa)
SDC/No Seal	4.3	±0.97
MSC/No Seal	5.1	±0.26
LMC/No Seal	5.9	±0.52
SDC/HMWM	2	±0.28
MSC/HMWM	3.3	±0.18
LMC/HMWM	2.5	±0.28
SDC/HMWM	3.8	±1.2
with Sand Broadcast MSC/HMWM	4.4	±1.1
with Sand Broadcast		
LMC/HMWM with Sand Broadcast	4.4	±1.3
SDC/HMWM Sandblasted	3.6	±1.0
MSC/HMWM Sandblasted	4.2	±1.1
LMC/HMWM Sandblasted	4.4	± 0.70

Table 3.18 Direct Shear Strength (Series 2)
Transpo Sealate T-70 HMWM

Overlay Type	Avg. Bond Strength (MPa)	Standard Deviation (MPa)
SDC/No Seal	4.3	±0.97
MSC/No Seal	5.1	±0.26
LMC/No Seal	5.9	±0.52
SDC/HMWM	No Bond	N/A
MSC/HMWM	No Bond	N/A
LMC/HMWM	No Bond	N/A
SDC/HMWM with Sand Broadcast	2.7	±0.5
MSC/HMWM with Sand Broadcast	1.5	±0.9
LMC/HMWM with Sand Broadcast	3	±0.3
SDC/HMWM Sandblasted	1.1	±0.5
MSC/HMWM Sandblasted	1.5	±0.2
LMC/HMWM Sandblasted	1.3	±0.70

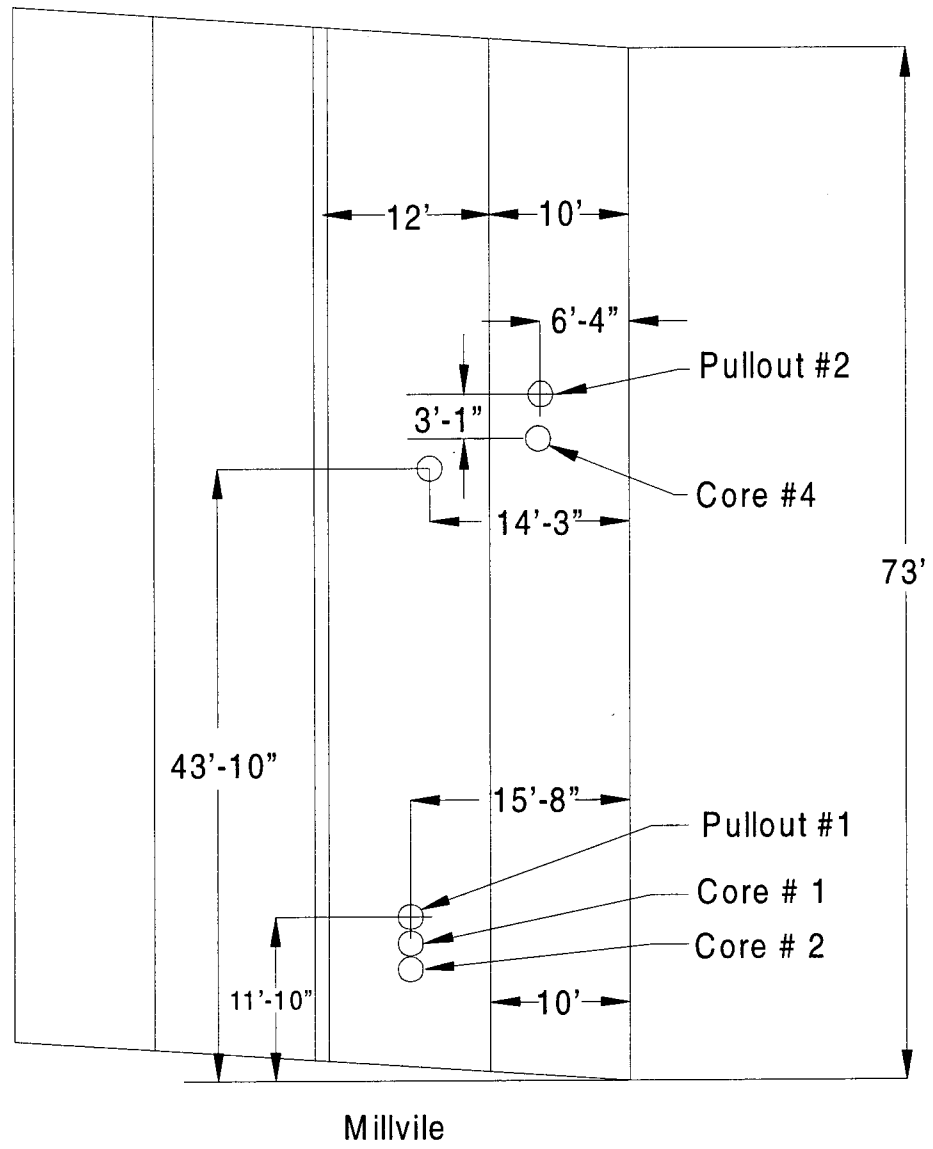

Figure 3.1 Coring Locations for Direct Shear and Pullout Tests Conducted in ODOT District 8

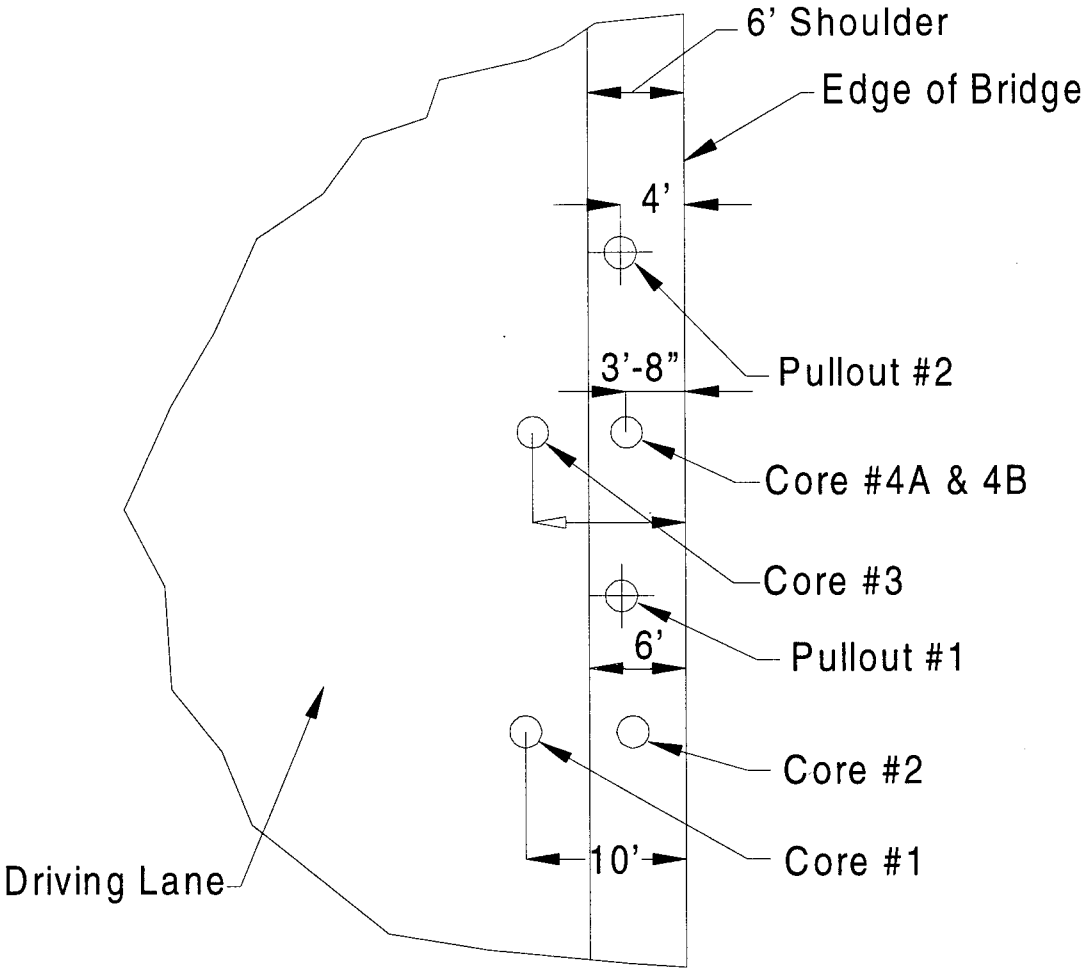

Guyahoga 271-0232 L

Super Dense Plasticized Concrete Overlay

Figure 3.2 Coring Locations for Direct Shear and Pullout Tests Conducted in ODOT District 12

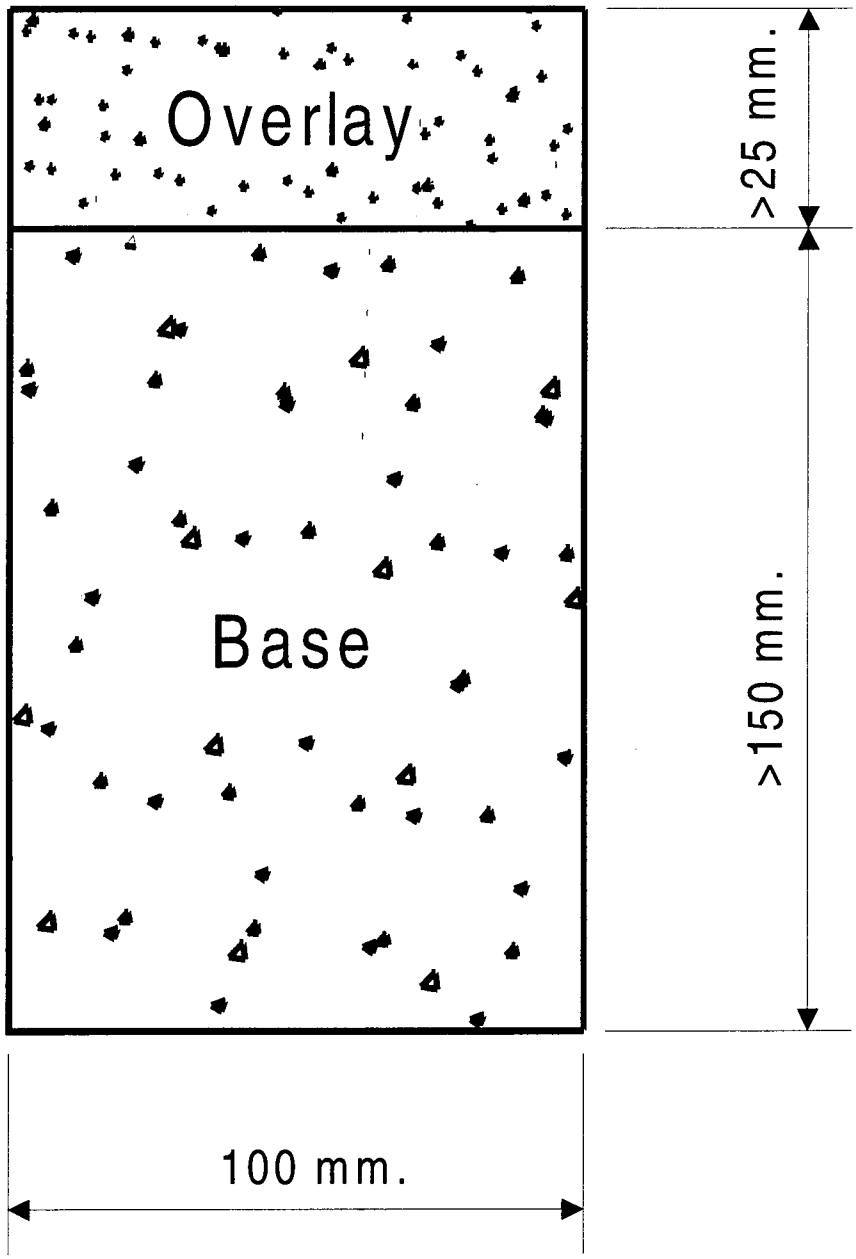

Figure 3.3 Direct Shear Test Specimens

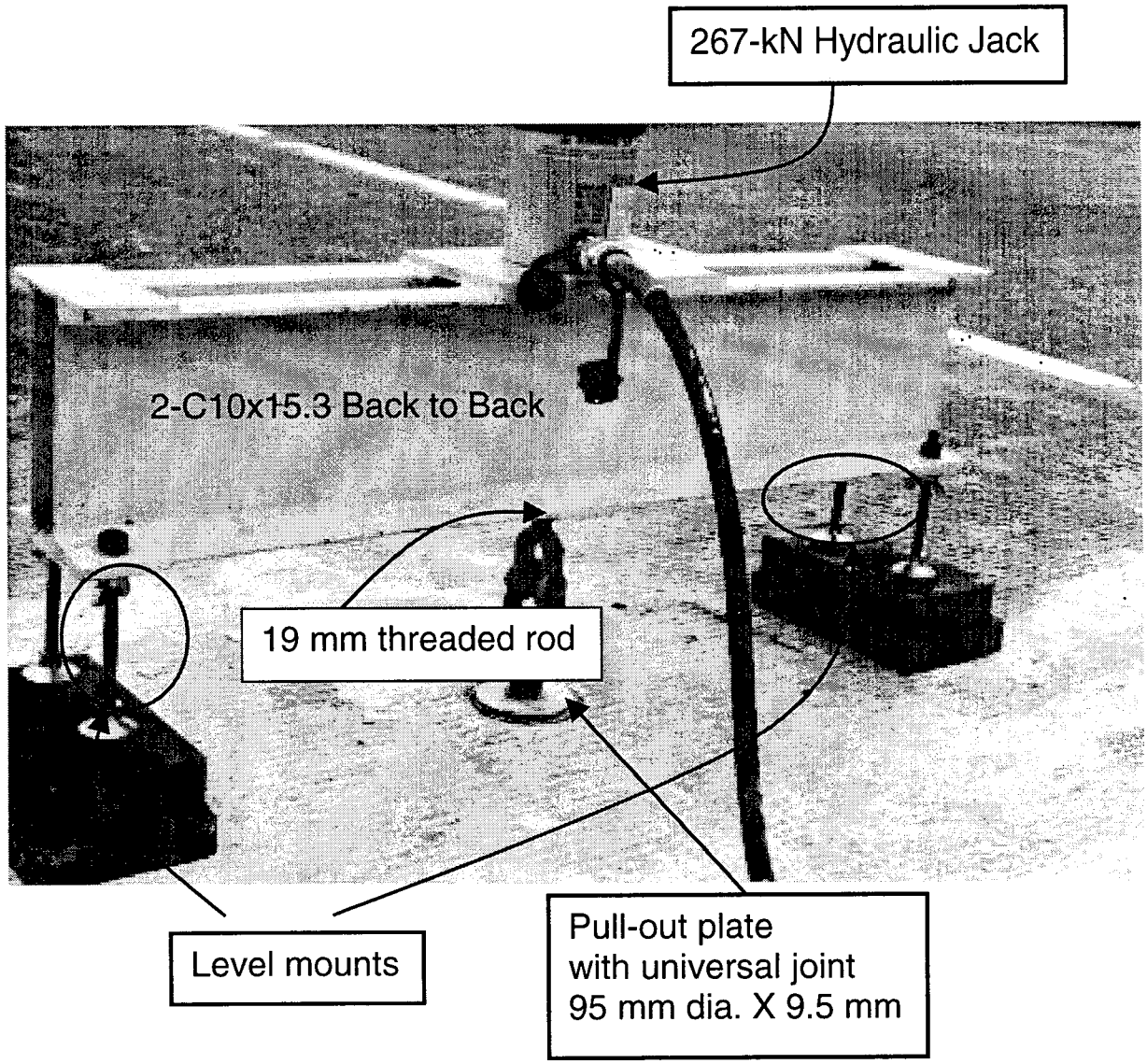

Figure 3.4 Direct Tension Test Apparatus

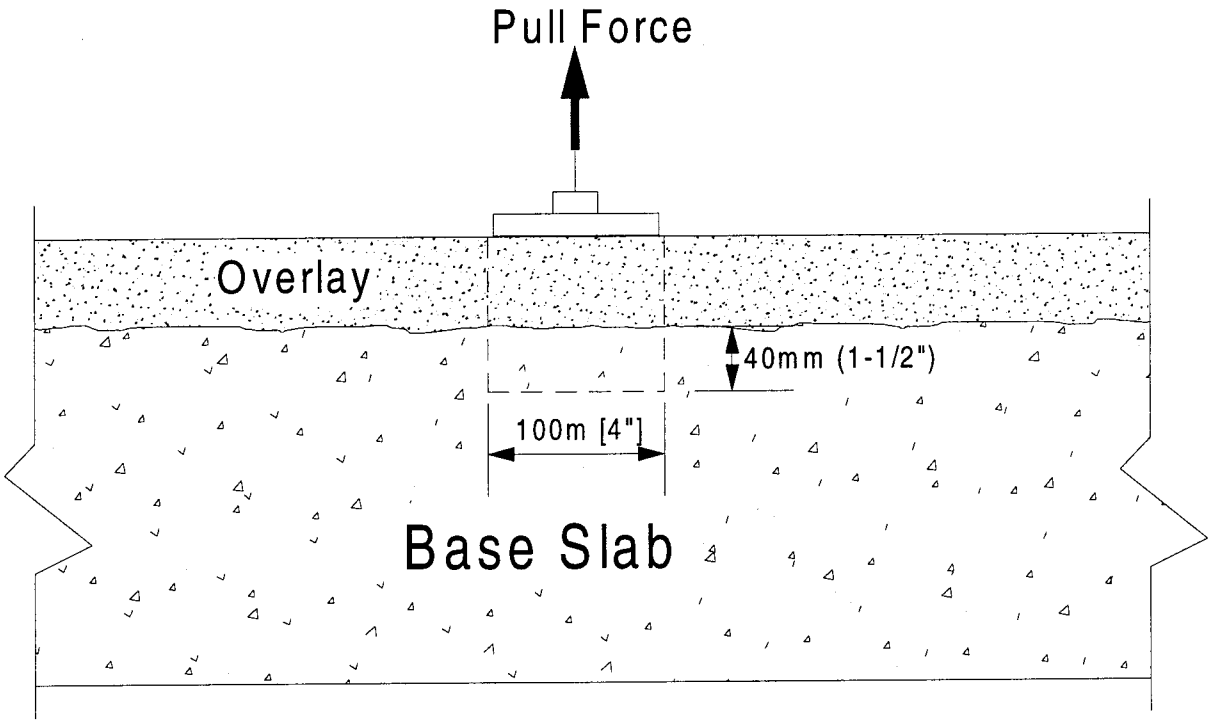

Figure 3.5 Direct Tension Core

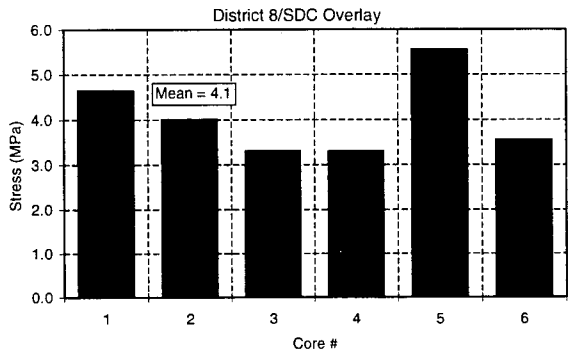

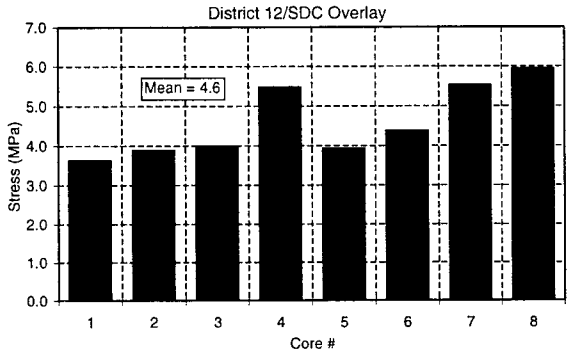

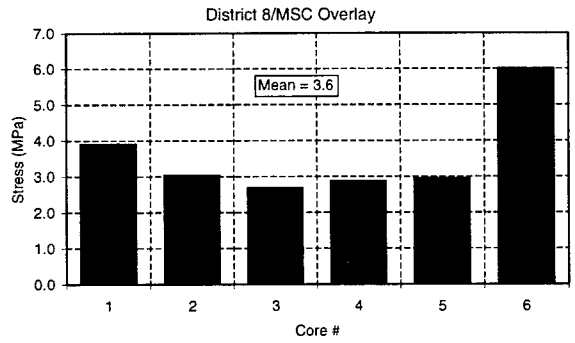

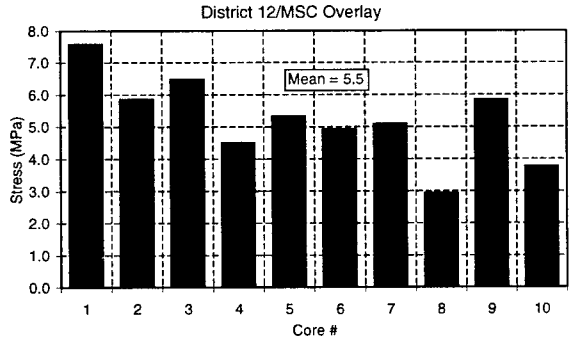

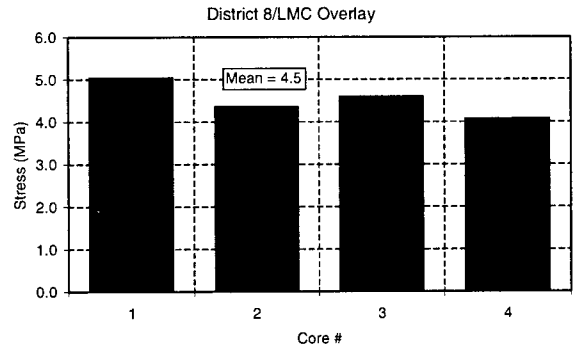

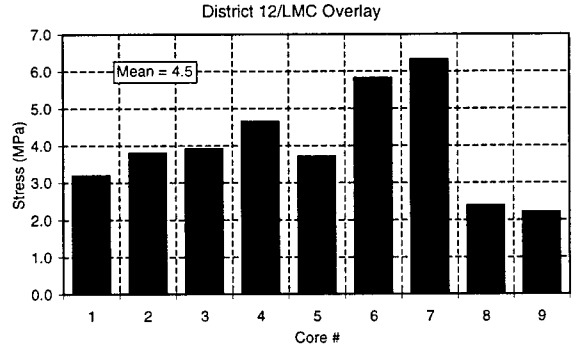

Figure 3.6 Direct Shear Test Results (Field Test)

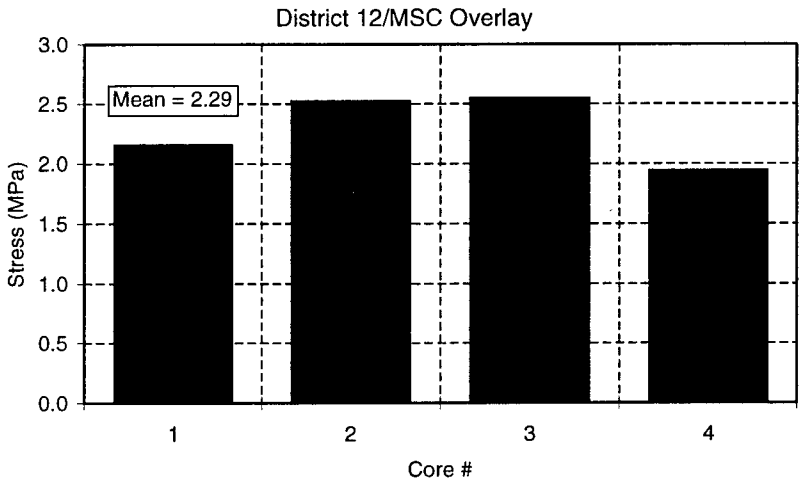

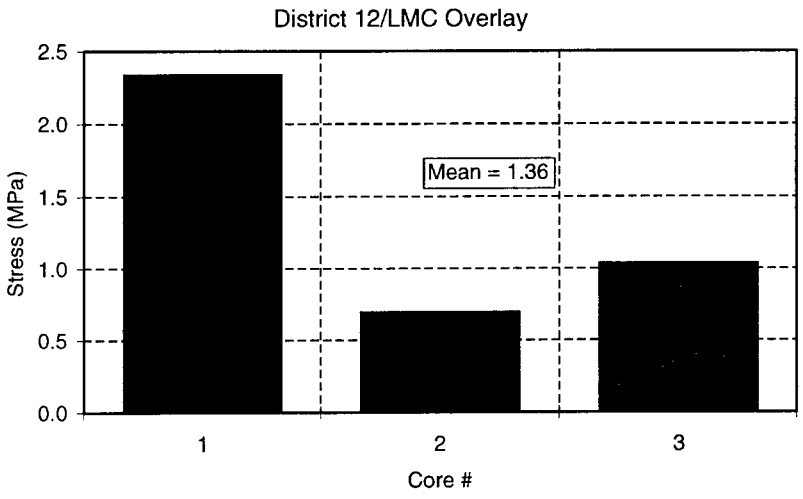

Figure 3.7 Direct Tension Test Results

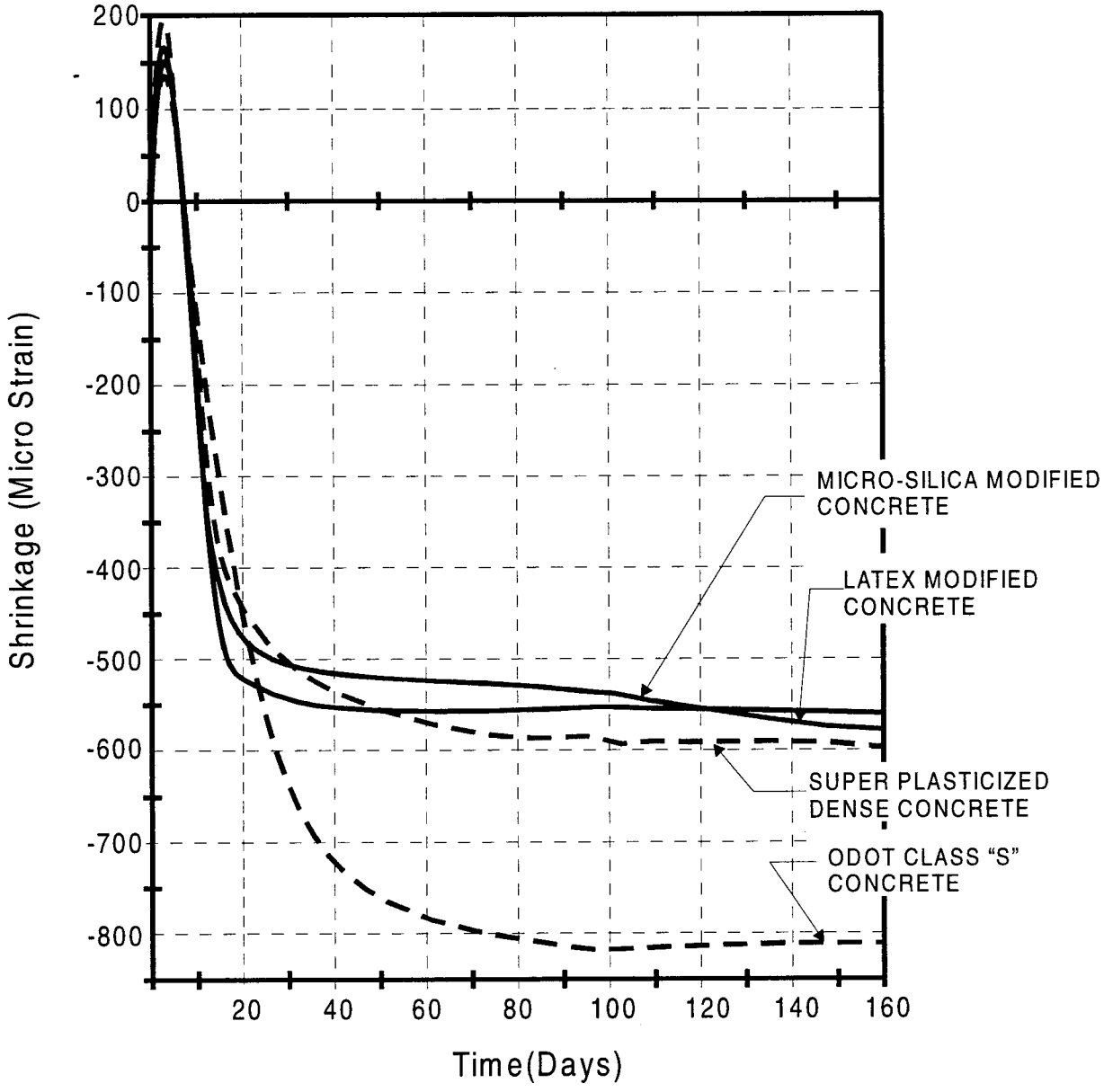

Figure 3.8 Drying Shrinkage of Concrete Used for Test Specimens

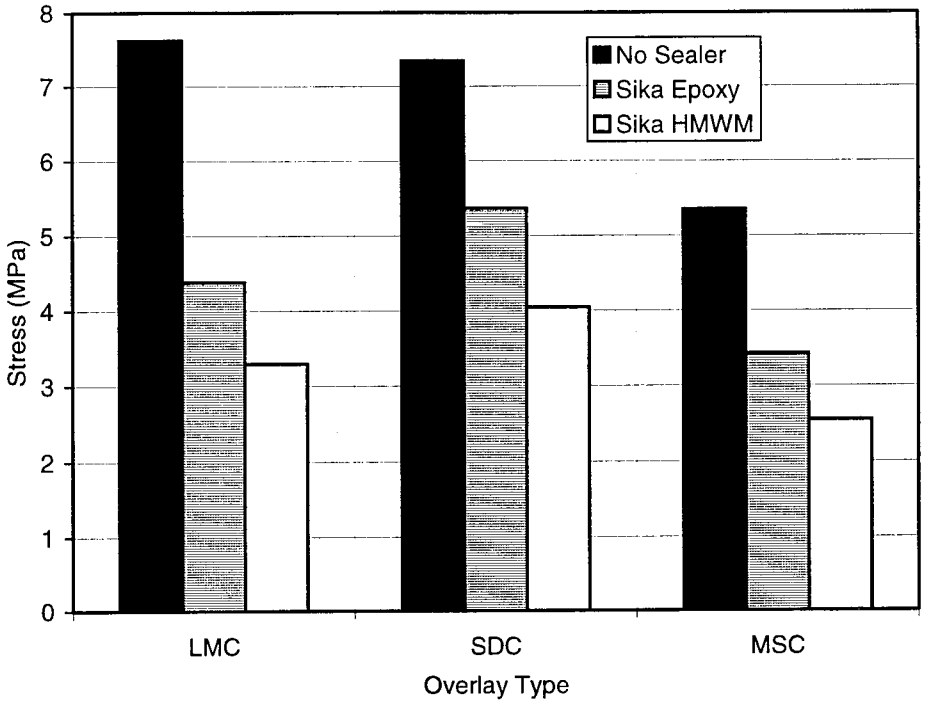

Figure 3.9 Direct Shear Test Results (Series 1)

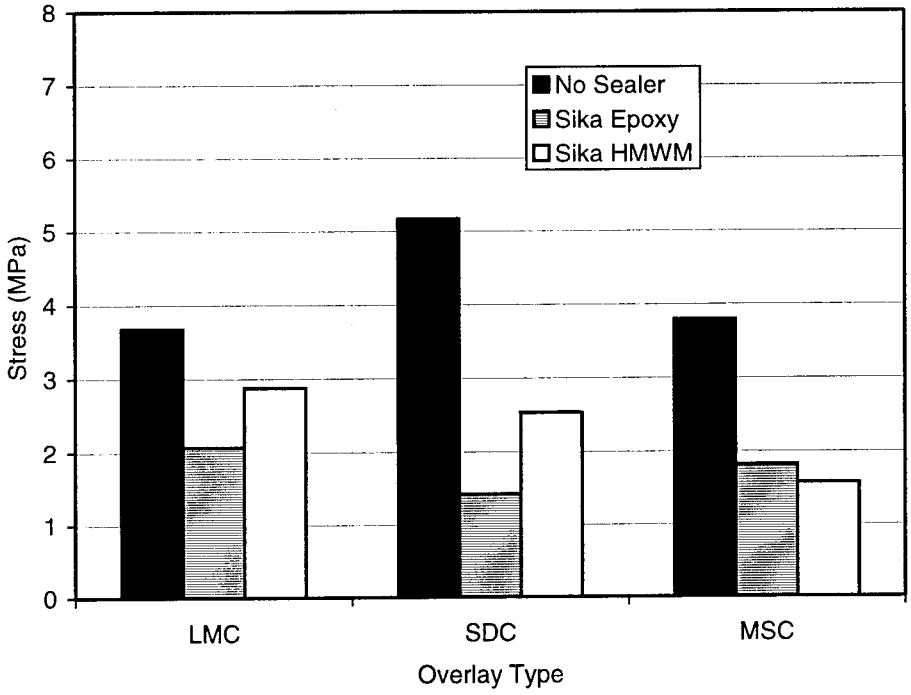

Figure 3.10 SHRP Test Results (Series 1)

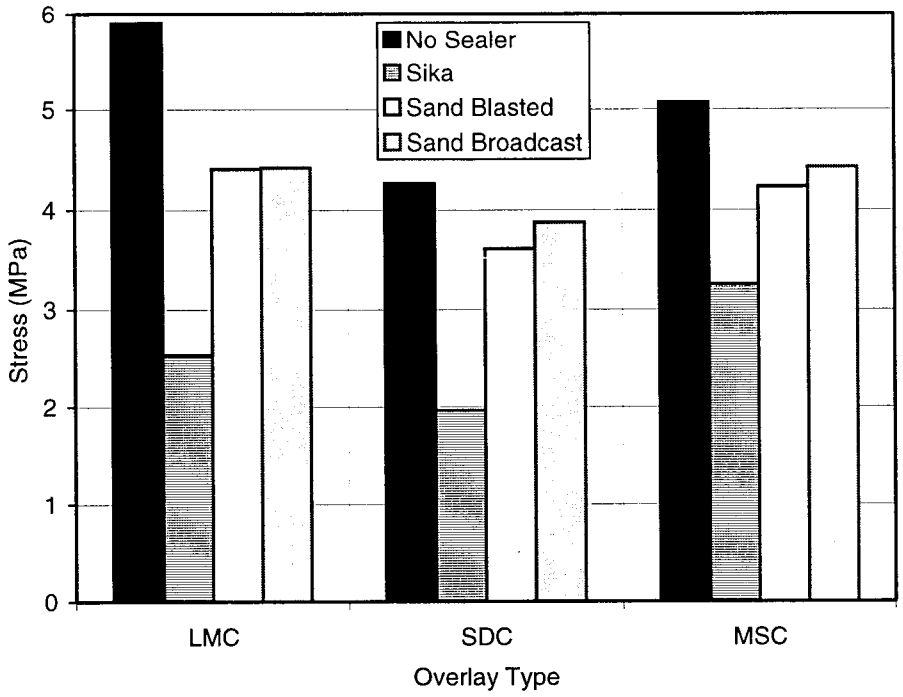

Figure 3.11 Direct Shear Test Using Sika HMWM at the Interface With Alternate Surface Preparation Procedures (Series 2)

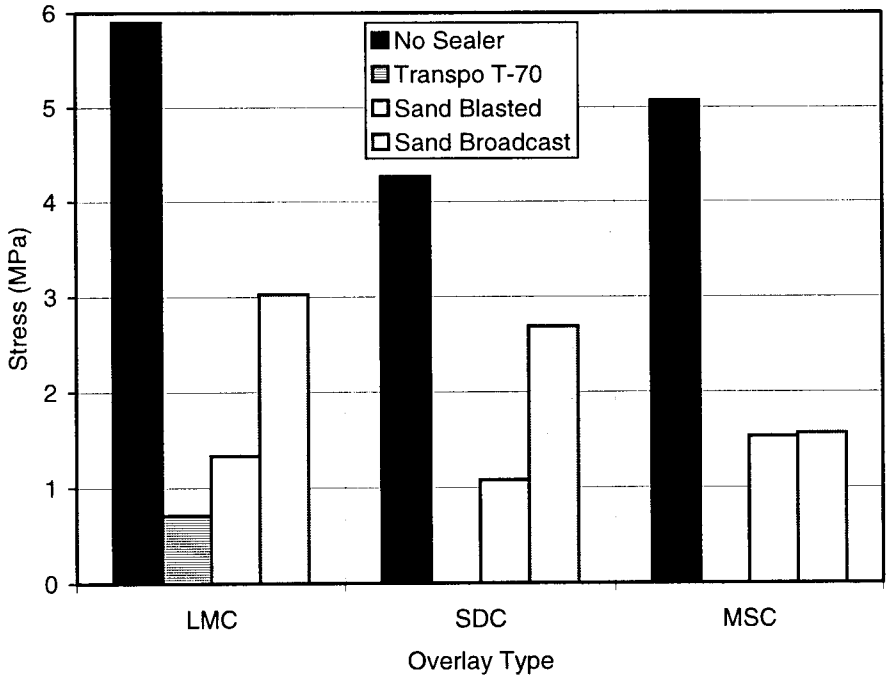

Figure 3.12 Direct Shear Test Using Transpo HMWM at the Interface With Alternate Surface Preparation Procedures (Series 2)

CHAPTER 4
BEAM TESTS

As discussed previously, the bond stress between bridge decks and concrete overlays is best simulated by inducing shear stress at the bond interface by testing a beam. The beam will represent a strip along the deck, and will simulate the deck behavior more realistically than other test methods. In this chapter, the test specimens and experimental program will be discussed. The measured data will be utilized to explain the expected mode of failure for overlaid decks with sealers and no sealers. The experimental data will also be used to infer bond strength.

4.1 Test Program

Ten reinforced concrete beams were cast and tested to examine: (a) the influence of sealer on bond strength, (b) whether direction of bending (i.e., the sealed surface will be subjected to compressive stresses (positive bending) or tensile stresses (negative bending)) impacts the bond strength and mode of failure, (c) study mode of failure of sealed and unsealed surfaces, (d) infer bond strength for sealed and unsealed surfaces, and (e) compare the bond strength from a flexural test against that obtained from direct shear and SHRP tests. The main test variables, as seen from Table 4.1, were presence or lack of sealer at the overlay-concrete interface, and direction of bending. For each variable, two identical specimens were tested to average out the impact of experimental variabilties. The test results (most importantly, the initial stiffness and maximum load) were compared against those obtained from the two benchmark specimens with no overlay.

4.2 Test Specimens

The test specimens represented a half-scale model of a 300 mm. (12 in.) strip along a typical reinforced concrete deck, which was assumed to be 400 mm. (16 in.) thick. Hence, the benchmark specimens were 200 mm. (8 in.) deep and 150 mm. (6 in.) wide. Following ACI design provisions (ACI 318-95), the beam was designed by using 41.2 MPa (6,000 psi) concrete, and 1.5% longitudinal reinforcement ratio. The required transverse reinforcement was

calculated based on developing the expected flexural overstrength which was taken as $1.5M_n$ where M_n = nominal moment capacity. The nominal moment capacity was computed by assuming Gr. 420 (60) reinforcement and 41.2 MPa (6,000 psi) concrete. The beam details are illustrated in Figure 4.1.

A number of overlay thicknesses were considered before selecting the final value. Although the nominal specified overlay thickness is typically 38 mm. (1.5 in.), the actual thickness may vary significantly. The overlay thickness of the cores taken from the test bridges in District 8 and 12 were observed to vary between 25 mm. (1 in.) to about 89 mm. (3.5 in.). The overlay thickness was selected based on analytically generated moment-curvature responses of the benchmark beam, and the benchmark beam with 25 mm. (1 in.), 38 mm. (1.5 in.), and 50 mm. (2 in.) thick overlays. These thicknesses are equivalent to full-scale overlays of 50 mm. (2in.), 76 mm. (3 in.), and 100 mm. (4 in.). The computed moment-curvature responses under positive bending (overlay is in compression) are shown in Figure 4.2. As expected, the beams with a thicker overlay exhibit a higher stiffness and load-carrying capacity. In comparison to the benchmark beam (i.e., the beam with no overlay), the additional stiffness and strength due to 25 mm. (1 in.) of overlay was deemed too small to be detected reliably in the test specimens, and was not selected. The additional stiffness and strength due to a 38 mm. (1.5 in.) thick overlay or larger would easily be measurable. For the half-scale test specimens, overlay thicknesses larger than 38 mm (1.5 in.) were deemed to be excessive. Therefore, the overlay thickness was selected to be 38 mm. (1.5 in.).

The length of the specimens was selected to ensure that a reasonable level of shear stress at the overlay-beam interface can be introduced. The selected span of 2286 mm. (90 in.) does not correspond to the half-scale equivalent of a typical span.

4.3 Fabrication

The beams for all the specimens were cast simultaneously. The beam longitudinal bars were placed at the top and bottom of the forms depending on whether the specimen was to be subjected to negative or positive bending. Ohio Department of Transportation Class S concrete

and micro-silica concrete (per ODOT proposal note no. 107-91) were used for the beams and overlay, respectively. The overlay was placed on the finished surface of the concrete beam for all of the specimens. Specimens No. 3, 5, 8, 9, which were subjected to negative bending, were turned before testing; while the remaining specimens were placed directly in the test frame and tested. Before applying the overlay, the finished surface of the concrete beam was sand blasted for 15 minutes. For specimens No. 2, 3, 9, 10 (i.e., those with no sealer), the overlay was placed directly on the sandblasted surface. In case of sealed specimens (No. 4, 5, 6, 8), HMWM sealer was applied to the sandblasted surface. The sealed surfaces were not treated prior to the placement of the overlay concrete.

4.4 Experimental Program

The test specimens were tested under a three-point bending as shown in Figure 4.3. The load at the midspan was applied by a servo-valve controlled 670-kN (150-kip) actuator. The closed-loop control of the specimens was accomplished by a two-channel, 5900-series Pegasus digital servo controller. The specimens were tested through a combination of load-control and displacement-control steps. Initially, the actuator was operated in load control by increasing the magnitude of the applied load. After formation of cracks and inducing adequate displacements, position control was utilized to finish the tests. That is, the midspan displacement of the specimens was increased until the load required to displace the beam did not increase significantly or began to drop, i.e., failure limit state.

Each specimen was instrumented to monitor (a) beam deflections at the midspan and quarter points, (b) rotations at each support, (c) strains through the depth at the midspan and quarter points, (d) strain at the midspan on one of the longitudinal bars, and (e) the applied load. The instrumentation layouts are shown in Figures 4.4 and 4.5. Photographs illustrating the instruments are shown in Figures 4.6 and 4.7. In addition to the measured data, crack and damage patterns were recorded at approximately identical load and displacement levels.

4.5 Material Properties

Critical material properties of the reinforcing bars, concrete in the beam, and overlay

concrete were obtained according to ASTM A370 and ASTM C683, respectively. The measured properties are summarized in Table 4.2.

4.6 Damage and Crack Patterns

The behavior of the benchmark specimens (Specimen No. 1 and 7) was as expected, i.e., identical to that for under-reinforced beams. The crack patterns, illustrated in Figure 4.8, consisted of flexural and flexural-shear cracks. At a mid-span displacement of 56 mm. (2.2 in.), the crack widths were as much as 3 mm. (0.12 in.), and the compression concrete started to crush. The tests were stopped after the beams sustained large deformations.

The performance of the remaining specimens varied for each particular test variable. The crack patterns for Specimens No. 2 and 10 (which had not been sealed before the application of the overlay, and were subjected to positive bending, i.e., the overlay was subjected to compressive stresses) were generally similar to those found for the benchmark specimens. A number of localized, minor cracks were observed at the overlay-beam interface. As explained later, these cracks are attributed to local bond defects, and do not suggest bond failure. At midspan deflection of 17 mm. (0.667 in.), the overlay concrete failed in a brittle fashion. A significant portion of the beam was peeled off when the overlay failed, refer to Figures 4.9 and 4.10. The overlay appears to have been adequately bonded to the beam. The observed mode of failure does not suggest a true interface shear failure, i.e., the overlay did not slide off the base concrete. The failure is believed to be due to outward buckling of the overlay which appears to have acted as a column, with "fixed" and "free" boundary conditions at the midspan (which was restrained by the actuator) and at the support, respectively. As the overlay concrete buckles outward, tensile stresses perpendicular to the overlay are developed and lead to separation of the overlay. Note that the failure of the overlay was not symmetrical about the north and south ends of the beam specimens because of local variations in bonded surface.

On the other hand, Specimens No. 4 and 6 (those sealed with HMWM and tested under positive bending) experienced a classical bond failure. From Figures 4.11 and 4.12, it is evident that the overlay slid off the beam once the bond strength was exhausted. The bond failure of

the overlay concrete was again sudden, and occurred at small deformations. For example, in Specimen No. 4, the beam midspan deflection was 15 mm. (0.59 in.) when the overlay slid off the beam. Once again, the failure was not symmetrical. Local flaws such as the variation of bonded surface and level of sealer are deemed to result in uneven failure of the overlay.

When the overlay concrete was subjected to negative bending moment (i.e., the overlay was subjected to tensile flexural stresses), the observed damage and crack patterns were similar for the specimens with and without sealer. In contrast to the specimens subjected to positive bending, the overlay failure in Specimens No. 3,9, 5, and 8 was not apparently due to bond failure. Delamination and separation of the overlay from the beam was gradual, and occurred after formation of excessive flexural cracks. Towards the end of testing, the overlay delaminated completely at a number of locations along the beam length, refer to Figures 4.13 through 4.16 and Figures 4.17a and 4.17b. The observed damage pattern is similar to that for monolithic reinforced concrete beams in which "concrete teeth" form between cracks. At advanced deformations, the concrete teeth usually separate and fall. Formation of similar concrete teeth was evident in the test specimens. The overlay-beam interface clearly accelerated separation of the concrete teeth.

4.7 Measured Responses

Measured values were successfully recorded for load, deflection (at quarter points), bottom reinforcement bar strain, and rotations at each end of the beam. Representative load - deflection curves for each beam are shown in Figures 4.18 to 4.23. The maximum load resisted by each specimen is summarized in Table 4.3. The complete measured data are available electronically upon request.

Specimens No. 2, 4, 6, and 10 had overlays and were subjected to positive bending. Comparing the load - deflection curves of the benchmark Specimen No. 7 to those from Specimens No. 2, 4, 6, and 10, the overlay concrete is seen to act compositely with the base concrete as evident from the higher values of stiffness. When the deflection reached 10mm.; the corresponding load for the benchmark beam and average load for the overlaid beams

subjected to positive bending were 38kN (8.5 kips) and 67 kN (15 kips), respectively. After the overlay debonded from Specimens No. 2, 4, 6, and 10, the load - deflection response nearly resembled that of the benchmark beam. Specimens No. 2 and 10, which did not have sealer at the interface, debonded at loads of 106 kN (23.8 kips) and 119 kN (26.7 kips) with the corresponding mid - span deflections of 11.5 mm. (0.45in.), and 17mm. (0.667in.), respectively. Specimens 4 and 6 were sealed prior to receiving an overlay. Up to failure of the overlay, these specimens were also much stiffer than the benchmark specimen. Failure occurred at 117 kN (26.2 kips) and 107 kN (24 kips) when the corresponding mid-span deflection reached 15 mm. (0.59in.) and 9 mm. (0.35in.) For Specimens No. 4 and 6, respectively.

As seen from Figures 4.21 and 4.22 beams subjected to negative bending (Specimen No. 3, 5, 8, and 9) show a similar load-deflection response for sealed and unsealed beams. The loss of stiffness in these specimens was gradual and similar to that for the benchmark specimen (Specimen No. 7). As discussed previously, the overlay in Specimens No. 3, 5, 8, and 9 did not debond. Hence, the loss of stiffness is attributed to cracking and yielding of the longitudinal bars. The cracking in the overlay eliminated the influence of sealer on the behavior.

4.8 Synthesis of Experimental Results

The main goal of the beam tests was to examine the expected mode of failure for overlays placed over sealed and unsealed bridge decks. The experiments provided an opportunity to infer the maximum in - plane shear stress at the overlay - deck interface before failure (i.e., bond strength). In - plane shear stress in cracked reinforced concrete members cannot be computed by elementary equations for linear, elastic materials. After describing the method and its necessary steps, the experimental results are evaluated.

4.8.1 General Description of Analytical Method

In Chapter 2.4, a procedure to calculate in - plane shear stress beyond cracking was described briefly. A key component of the procedure is to generate the moment - curvature relationship for the beam section.

Using the computer program RESPONSE (Felber, 1989), the moment – curvature

response for each beam was obtained. This program is based on fiber analysis in which a reinforced concrete beam is discretized into finite sections. Using basic equations of equilibrium in conjunction with strain compatability (which is based on assuming a linear strain distribution) and constitutive relationships, the moment - curvature response is generated. Uniaxial stress - strain relationships of steel and concrete are utilized. Figure 4.24 illustrates how a beam is discretized. The computer program RESPONSE uses a basic parabolic model for modeling concrete in compression as indicated in Equation 4.1.

$$f_c = f'_c\left(2\frac{\varepsilon_{cf}}{\varepsilon'_c} - \left(\frac{\varepsilon_{cf}}{\varepsilon'_c}\right)^2\right) \qquad 4.1$$

In which
f_c = Concrete Stress
f'_c = Ultimate Concrete Stress

Tensile behavior (tension stiffening) of concrete is also included in the analysis. Tension stiffening will have a significant impact of the stiffness of the section immediately after cracking. The program RESPONSE uses a model proposed by Vecchio and Collins (Vecchio and Collins, 1986) shown in Equation 4.2

if $\epsilon_{cf} > \epsilon_{cr}$

$$f_c = \frac{\alpha_1\alpha_2 f_{cr}}{1+\sqrt{500\varepsilon_{cf}}} \qquad 4.2$$

In which
α_1 = factor for bond characteristics of reinforcement
α_2 = factor for sustained or repeated loading

In this study, the tensile capacity was ignored beyond strains exceeding 15 ϵ_{cr}. The stress-strain relationship for steel is simulated by a linear range, yield plateau, and a linear strain hardening range. The material models are presented in Figures 4.25 to 4.26.

At the completion of the fiber analysis, a moment - curvature response of a cross section is obtained. Note that for the test specimens the cross section was identical throughout the beam length; hence, a single moment - curvature was needed. This response is assumed to be

correct, but must be calibrated with the data obtained from each flexural beam specimen. The beam deflection is obtained by integrating the curvature twice along the length. Therefore, a theoretical load - deflection response can be calculated at each point. In this study, the theoretical load - deflection curve at the midspan was guaged against the measured data. Matching the calculated load - deflection response ensures a reliable calculated moment - curvature response. A representative comparison is shown in Figure 4.27.

For calculation of in - plane shear stress, each beam was divided into thirty-six segments (63.5 mm. or 2.5 in. each) and thirty-seven nodes over the entire length. This number of segments was necessary to ensure that the effects of cracking, sudden changes in neutral axis depths, etc. on the computed shear stresses are detected. Integrating the concrete stress over the depth of the overlay at each node provides the in-plane shear along the length. The difference in the shear between each node in a segment, divided by the horizontal contact area results in the in-plane shear stress (refer to Figure 2.5, Chapter 2).

For negative bending specimens (overlay concrete in tension), the concrete stress - strain relationship was assumed to be linear until cracking, then changing according to the tension stiffening model described by Equation 4.2. For the specimens subjected to positive bending (overlay concrete in compression), compressive stresses on the overlay were represented by the parabolic concrete model in Equation 4.1. Integration of concrete stresses over the depth of the overlay was completed using the program MathCad.

The maximum in-plane shear stress occurring along the length of the beam was taken as the bond strength, or the maximum bond-stress prior to failure. The following section will describe the variables involved for analysis of each test beam, and the corresponding bond-stress.

4.8.2 Synthesis of Experimental Data

Based on the procedure described above, bond stress was calculated for each specimen. Specimens No. 2, 4, 6, and 10 were tested in positive bending, i.e., the overlay was in compression. As expected, the presence of overlay resulted in a significantly higher stiffness

than the benchmark beam until delamination of the overlay. Figures 4.28 through 4.31 represent the computed shear stress corresponding to the applied loads of 2.2 kN (0.5 kips), 14.8 kN (3.3 kips), 29.7 kN (6.7 kips), 59.3 kN (13.3 kips), and the maximum load occurring prior to delaminating of the overlay. In these figures, the mode of failure is also sketched. Due to symmetry, the results for one half of the span are shown. Note that although crack patterns were generally symmetrical in the test specimens, only one side of the overlay delaminated. Local variations in surface condition are deemed to be the primary reason for the observed unsymmetrical mode of failure. The maximum calculated shear stress for each specimen is listed in Table 4.5.

Specimens No. 2 and 10 (which were unsealed) achieved the highest shear stress 1.5 MPa (225psi) and 1.8 MPa (266 psi), respectively. This trend was expected because of the absence of sealer at the bond interface. As discussed previously and shown schematically in Figures 4.28 and 4.31, the overlay failure was not a "classical" shear bond failure, i.e., the overlay did not slide off the beam at failure. Therefore, the maximum computed shear stress is not the bond strength. This stress can only be viewed as the maximum bond-stress occurring at the interface when the overlay failed. On the other hand, Specimens No. 4 and 6 (which were sealed with HMWM before the application of overlay) failed in a manner corresponding to shear failure. In these specimens, the overlay debonded and slid off the edge of the beam (refer to Figures 4.11, 4.12, 4.29, and 4.30). Hence, the maximum measured shear stress of 1.4 MPa (206 psi) (for Specimen No. 4) and 1.5 MPa (217 psi) (for Specimen No. 6) correspond to the bond strength. Comparing the flexural beam test values to bond strengths obtained from the direct shear and SHRP tests (with MSC overlay and HMWM sealer) the results are similar. The direct shear test gave the highest bond strength of 2.5 MPa, but the SHRP test indicated an average value of 1.7 MPa. The average bond strength values obtained from the SHRP test is very close to that from the flexural beam test. However, the bond strength values can not be directly related because the specimens were not cast at the same time.

As seen from Figures 4.28 through 4.31, shear stress at the overlay-base concrete

interface is distributed rather similarly for the sealed or unsealed specimens. Prior to cracking, shear stress is essentially identical to that obtained from the fundamental equation ($\tau = VQ/It$). Slight variations in the calculated bond stress, particularly for Specimen No. 4 and Specimen No. 8 are attributed to the fact that the computer program used to generate the moment-curvature relationships relationships (Felber, 1989) outputs only 2 significant figures. The resulting round off errors will impact the accuracy of the computed bond stresses for small loads, but will diminish for higher loads.

Upon cracking, a noticeable jump in the calculated bond stress is observed for all the specimens subjected to positive bending. When the section cracks, the concrete compressive force has to become larger to balance the steel tensile force. The higher compressive force results in a larger bond stress at the overlay-concrete interface. After the section cracks, the forces do not change as rapidly; hence, the changes in the bond stress are more gradual.

For Specimen No. 10, a significant drop in shear stress is observed when the applied load reaches 119.1 kN (26.8 kips). This trend can be explained with reference to the location of the neutral axis and distribution of stresses on either side of the block at which the stress drops sharply. At near ultimate limit state, the neutral axis and concrete stresses on the sides tend to become very similar as the load-deformation response of the member near the ultimate capacity flattens, refer to Figure 4.32. Therefore, as seen from Figure 4.33, the difference between the longitudinal forces on the sides of the block diminishes, and the shear force (the difference between the longitudinal forces) and shear stress drop accordingly.

For the specimens subjected to negative bending (Specimens No. 3, 5, 8, and 9), cracking once again resulted in a noticeable rise in shear stress. Beyond cracking, the longitudinal forces leading to shear stress (at the overlay-concrete interface) are developed due to concrete tension stiffening behavior which tends to drop as the concrete strain is increased. Therefore, as seen from Figure 4.34 the computed shear stress is reduced and becomes negative with an increase in the distance from the support. This trend can easily be explained from Figures 4.35 and 4.36 in which the computed longitudinal forces for Specimen No. 8 at a

load equal to 39.5 kN (8.9 kips) are summarized. From Figure 4.34, it is evident that the largest shear stress occurs in the uncracked sections. After cracking, the shear stress drops significantly. The maximum computed shear stress for Specimen No. 8 is 0.90 MPa (130 psi) when the applied load is 89 kN. Note that beyond this level, the section has cracked along the entire length, and the computed in - plane shear stress would be considerably less than that found for the applied load equal to 89 kN. It is clear that the maximum shear stress of 0.9 MPa (130 psi) was not sufficient to result in overlay debonding. This assessment is in accordance with the experimental observations and measured data.

The test results and associate analytical studies clearly indicate that bond between overlays and concrete under negative moments is not critical. Therefore, the possibility of bond failure of sealed or unsealed surfaces needs to be investigated for regions subjected to positive bending moment.

4.9 Summary

Ten flexural beams representing one-half scale models of a 300 mm. (12") strip of a typical slab bridge were fabricated and tested to (a) examine the effects of High Molecular Weight Methacrylate (HMWM) sealer on bond strength, (b) evaluate the influence of bending direction, and (c) investigate the influence of testing procedure on the measured bond strength.

When the overlay is in compression (positive bending moment), it fails as a result of bond failure (i.e., the overlay slides off after bond failure) or due to apparent buckling depending on whether the surface is sealed or not, respectively. For specimens subjected to negative bending (the overlay is in tension), the overlay did not delaminate. The behavior of these specimens was similar to typical under-reinforced concrete beams in which "concrete teeth" form between wide flexural cracks.

Table 4.1 Test Variables

Specimen No.	Overlay	Surface Condition	Direction of Bending
1	None	No Sealer	Benchmark
2	40 mm. Microsilica	No Sealer	Positive Bending
3	40 mm. Microsilica	No Sealer	Negative Bending
4	40 mm. Microsilica	HMWM Sealer	Positive Bending
5	40 mm. Microsilica	HMWM Sealer	Negative Bending
6	40 mm. Microsilica	HMWM Sealer	Positive Bending
7	None	No Sealer	Benchmark
8	40 mm. Microsilica	HMWM Sealer	Negative Bending
9	40 mm. Microsilica	No Sealer	Negative Bending
10	40 mm. Microsilica	No Sealer	Positive Bending

Negative Bending = Overlay in Tension
Positive Bending = Overlay in Compression

Table 4.2 Measured Material Properties

Material	f'_c (28 day)	f_y	E	f_u
Base Concrete	47.9 MPa (6960 psi)	N/A		N/A
Micro-silica Modified Overlay Concrete	60.8 MPa (8830 psi)	N/A		N/A
#5 Reinforcing Bars	N/A	450 MPa (65 ksi)	179x103 MPa (25.9x103 ksi)	723 MPa (105 ksi)

f'_c = Concrete Ultimate Stress

f_y = Steel Yield Stress

E = Steel Modulus of Elasticity

f_u = Steel Ultimate Stress

Table 4.3 Measured Maximum Load

Specimen No.	Maximum Load	* Overlay Failure Type
1	N.A.	N.A.
2	106.2 kN (23.5 kips)	C
3	105.3 kN (23.7 kips)	A
4	117.0 kN (26.3 kips)	B
5	97.7 kN (22.0 kips)	A
6	107.2 kN (24.1 kips)	B
7	104.8 kN (23.6 kips)	A
8	98.6 kN (22.2 kips)	A
9	98.8 kN (22.2 kips)	A
10	119.0 kN (26.8 kips)	C

A. Flexural failure in beam.
B. Shear failure at overlay bond interface.
C. Buckling of overlay at bond interface.

Table 4.4a Deck Concrete Properties Used for Modeling

Specimen	f'_c	ε_c	f_{cr}
2	46.5 MPa (6.75 ksi)	2.75×10^{-6}	2.87 MPa (417 psi)
3, 5, 8, 9	46.5 MPa (6.75 ksi)	2.75×10^{-6}	2.87 MPa (417 psi)
4	46.5 MPa (6.75 ksi)	2.75×10^{-6}	2.87 MPa (417 psi)
6	46.5 MPa (6.75 ksi)	2.75×10^{-6}	2.87 MPa (417 psi)
10	46.5 MPa (6.75 ksi)	2.75×10^{-6}	2.87 MPa (417 psi)

Table 4.4b MSC Overlay Concrete Properties Used for Modeling

Specimen	f'_c	ε_c	f_{cr}
2	67.2 MPa (9.75 ksi)	2.65×10^{-6}	3.37 MPa (490 psi)
3, 5, 8, 9	67.2 MPa (9.75 ksi)	2.65×10^{-6}	3.37 MPa (490 psi)
4	55.1 MPa (8.00 ksi)	2.65×10^{-6}	3.37 MPa (490 psi)
6	51.7 MPa (7.50 ksi)	2.65×10^{-6}	3.37 MPa (490 psi)
10	67.9 MPa (9.85 ksi)	2.65×10^{-6}	3.37 MPa (490 psi)

f'_c : Concrete compressive strength

ε'_c: Strain at concrete compressive strength

f_{cr}: Concrete cracking stress

Table 4.4c Steel Reinforcement Properties Used for Modeling

Specimen	f_y	E_s	f_u
2	503 MPa (73.0 ksi)	162x103 MPa (23.5x10^3 ksi)	751 MPa (109 ksi)
3, 5, 8, 9	503 MPa (73.0 ksi)	200x103 MPa (29.0x10^3 ksi)	751 MPa (109 ksi)
4	506 MPa (73.5 ksi)	158x103 MPa (23.0x10^3 ksi)	751 MPa (109 ksi)
6	489 MPa (71.0 ksi)	152x103 MPa (22.0x10^3 ksi)	751 MPa (109 ksi)
10	537 MPa (73.0 ksi)	162x103 MPa (23.8x10^3 ksi)	751 MPa (109 ksi)

f_y: Steel yield stress

E_s: Steel modulus of elasticity

f_u: Ultimate steel stress

Table 4.5 Maximum Shear Stress
(Under Positive Bending)

Specimen	Shear Stress
2	1.5 MPa (225 psi)
4	1.4 MPa (206 psi)
6	1.5 MPa (217 psi)
10	1.8 MPa (266 psi)

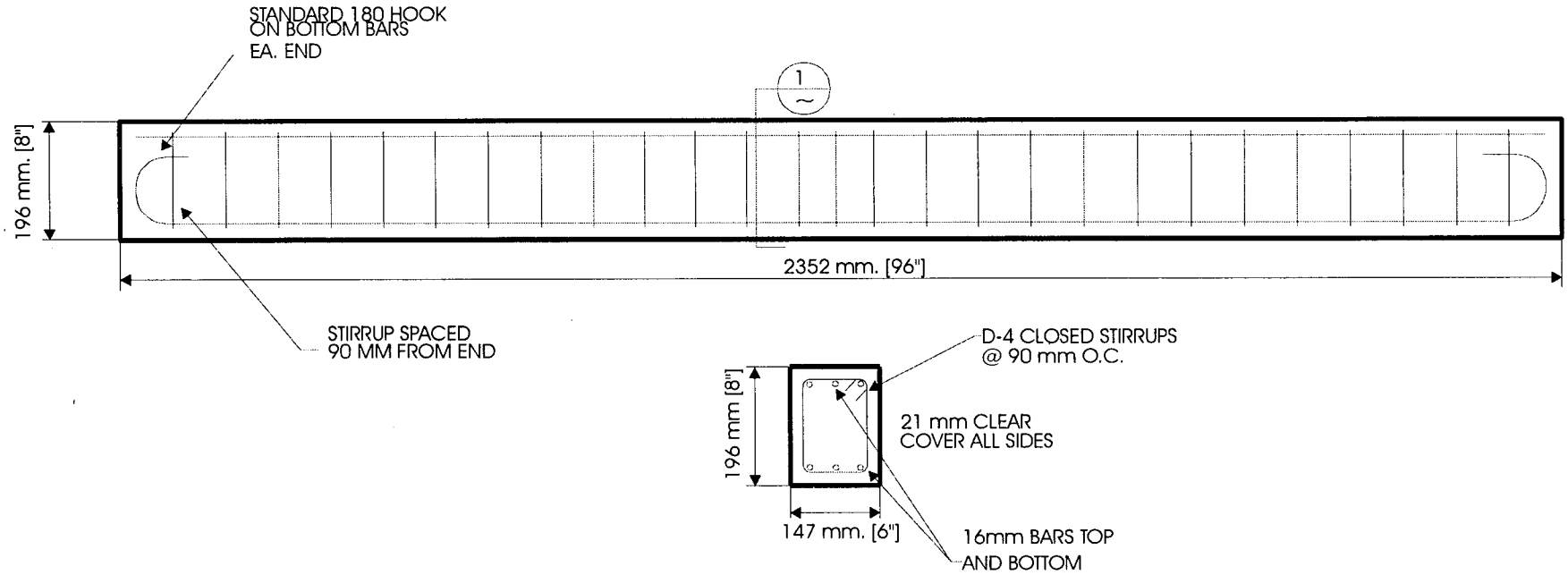

Figure 4.1 Flexural Beam Reinforcement Layout

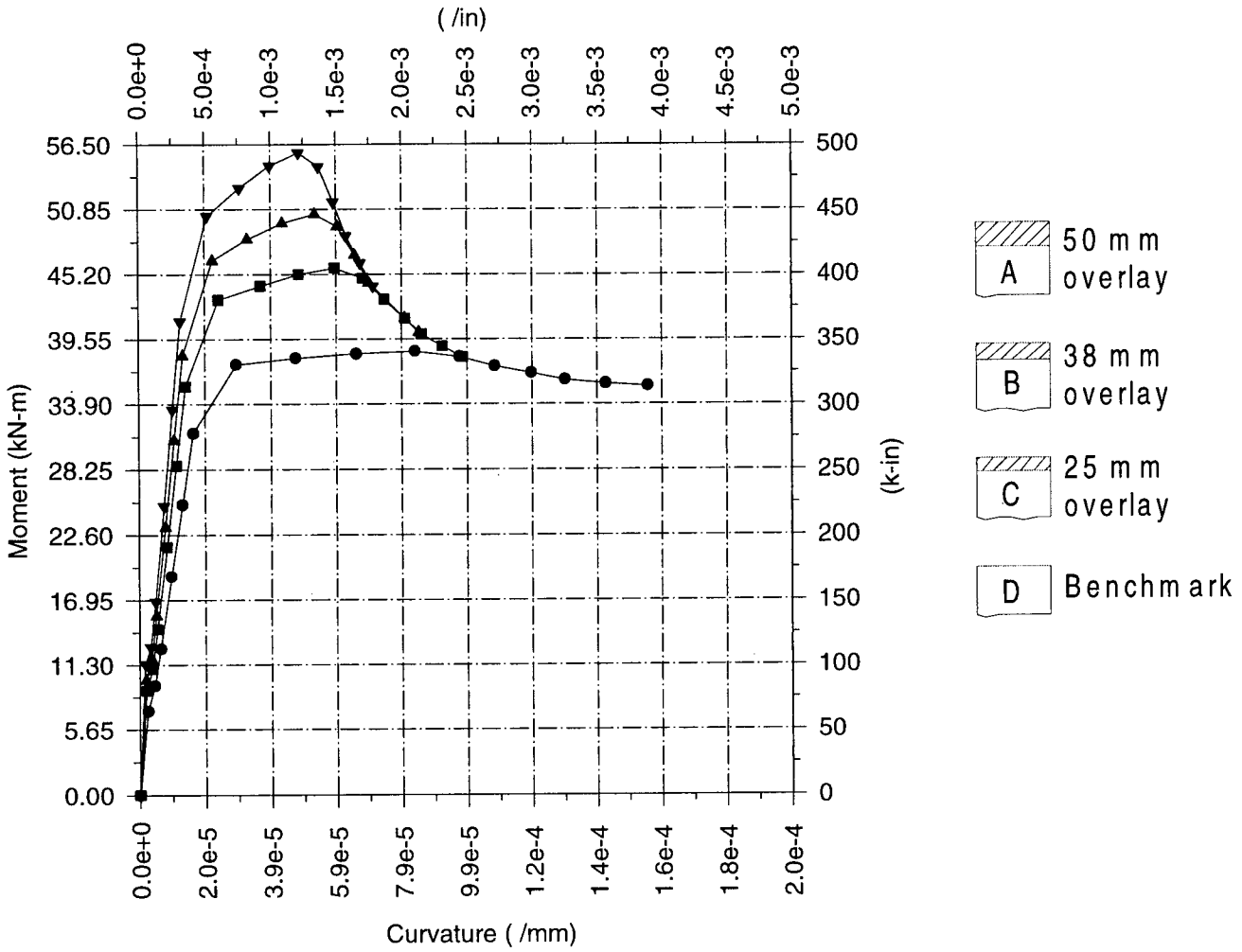

Figure 4.2 Moment-Curvature Comparison for Overlay Thickness Selection

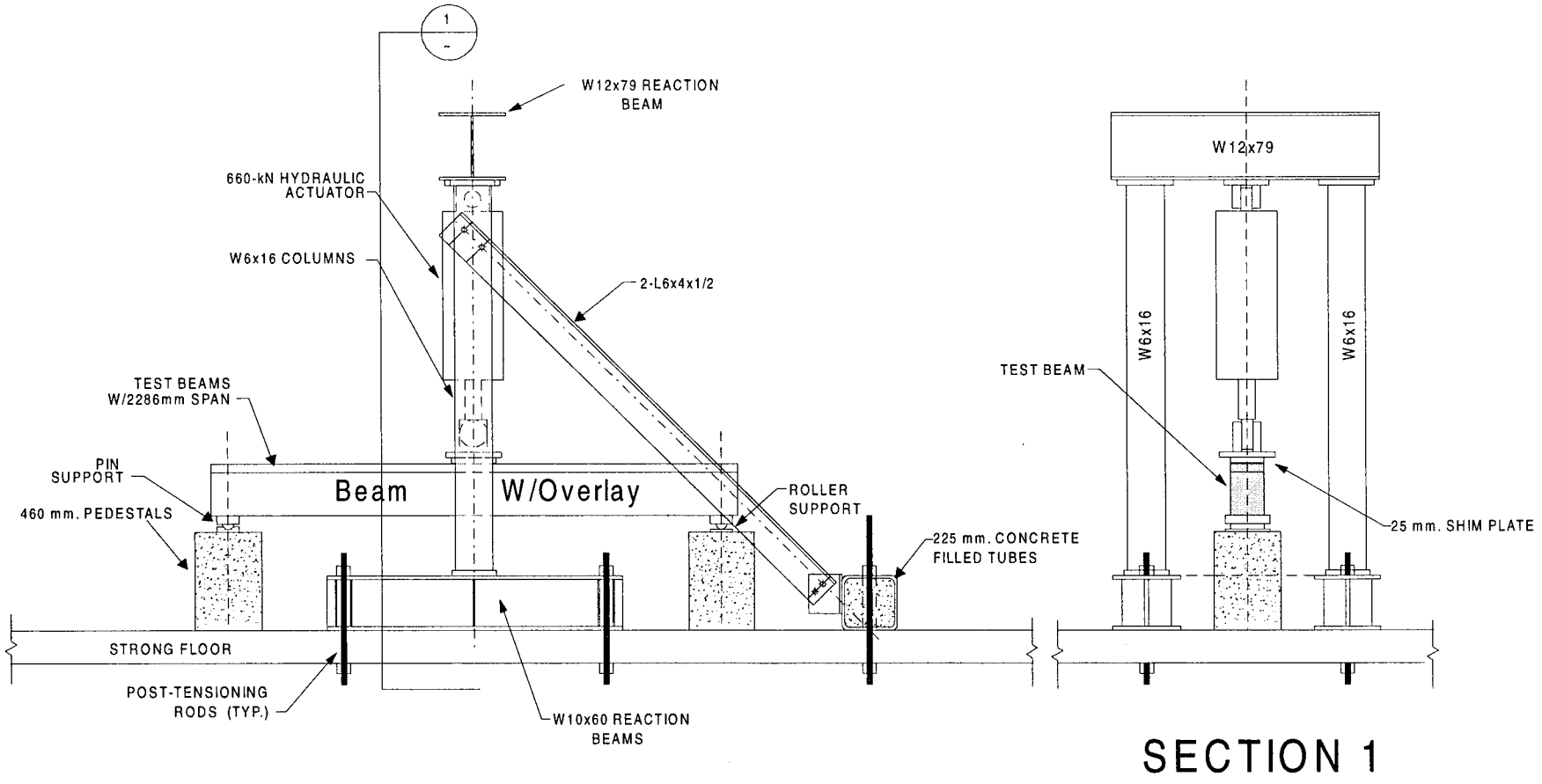

Figure 4.3 Test Setup for Flexural Beam Test

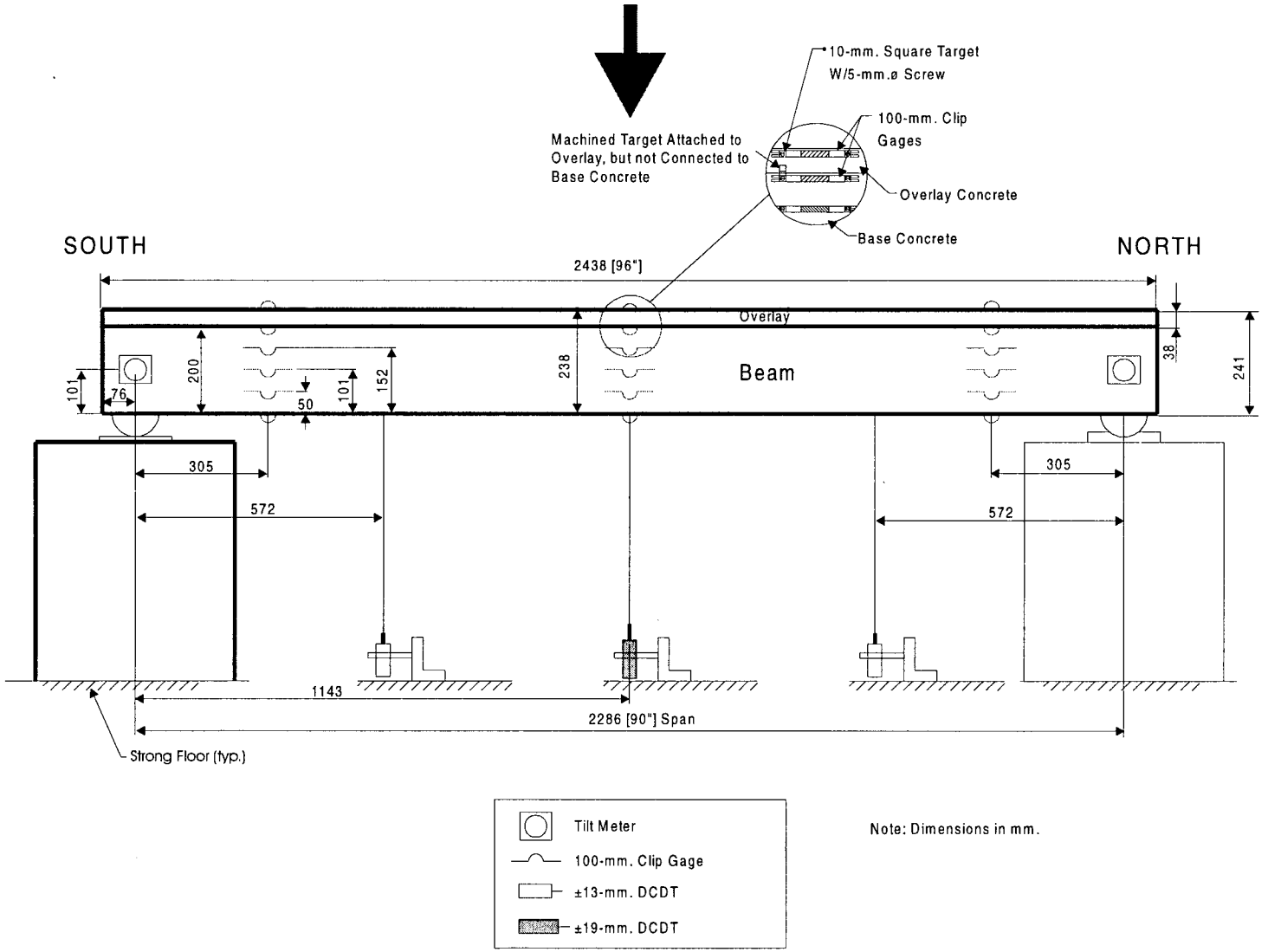

Figure 4.4 Positive Bending Instrumentation Layout

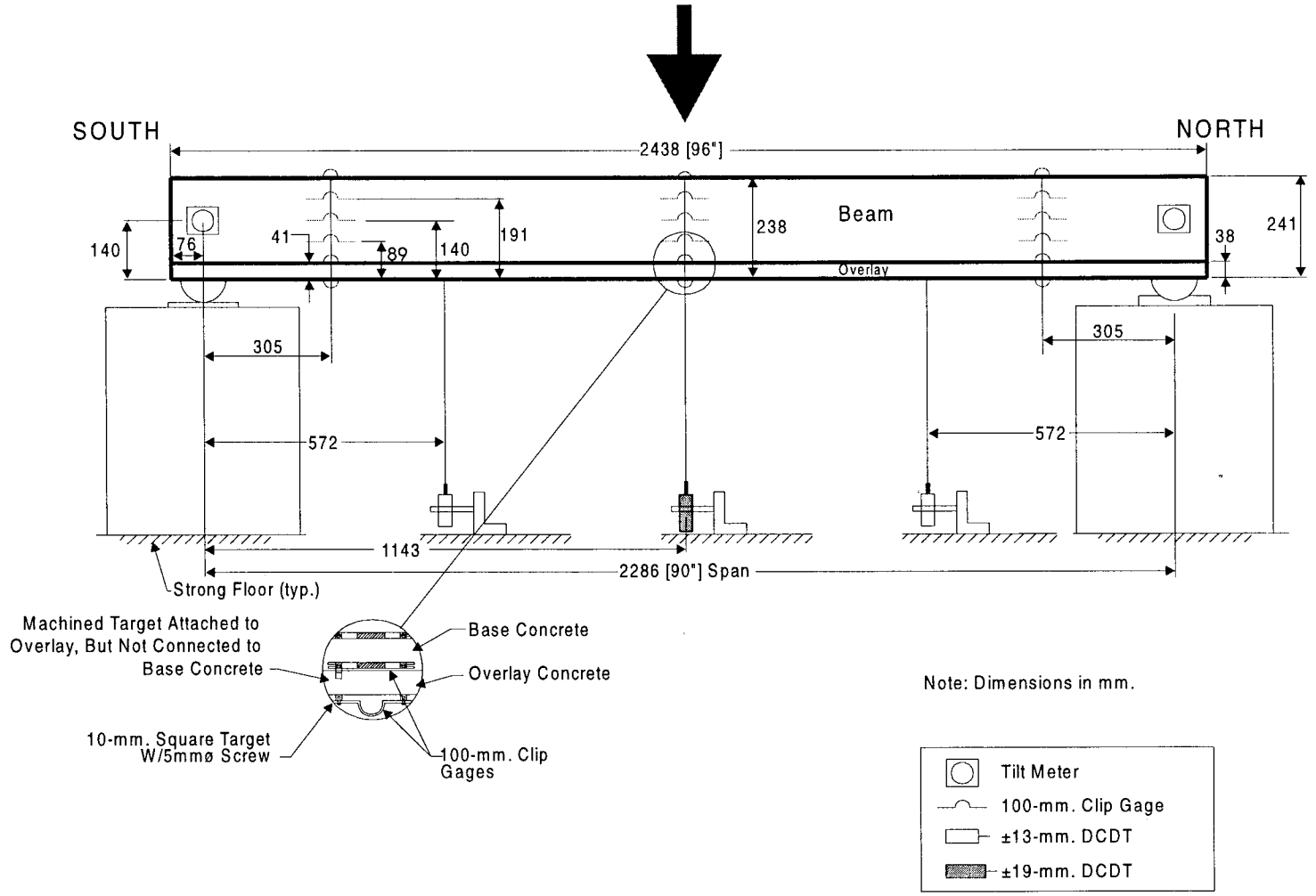

Figure 4.5 Negative Bending Instrumentation Layout

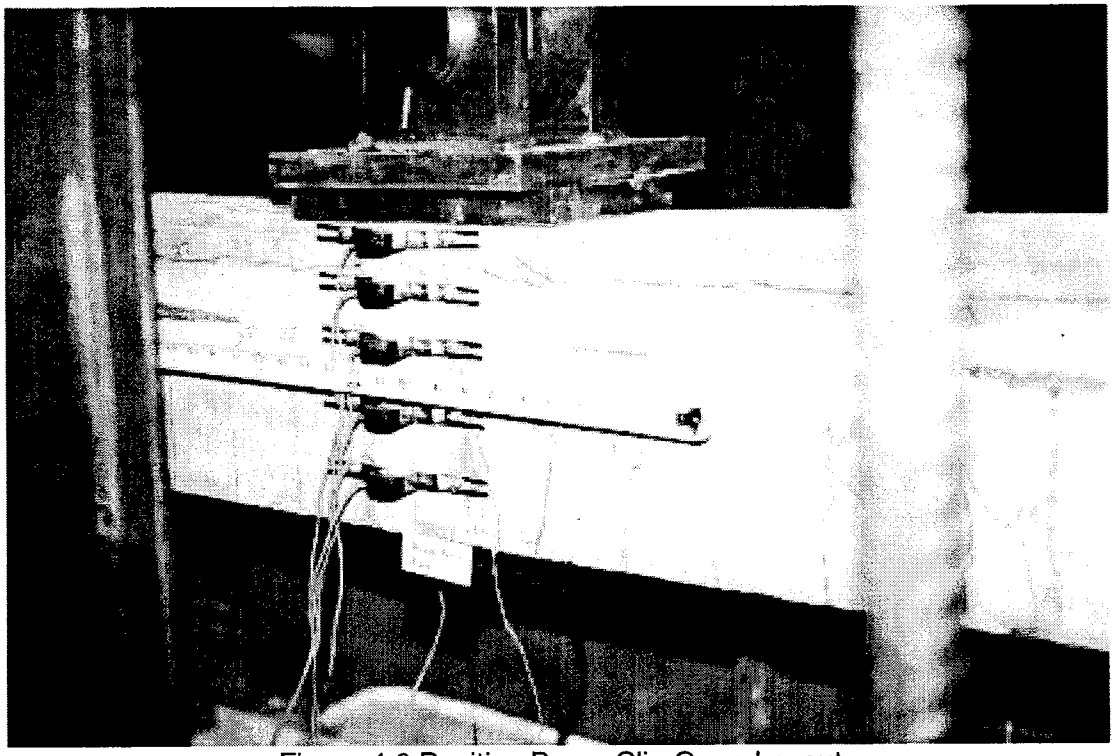

Figure 4.6 Positive Beam Clip Gage Layout

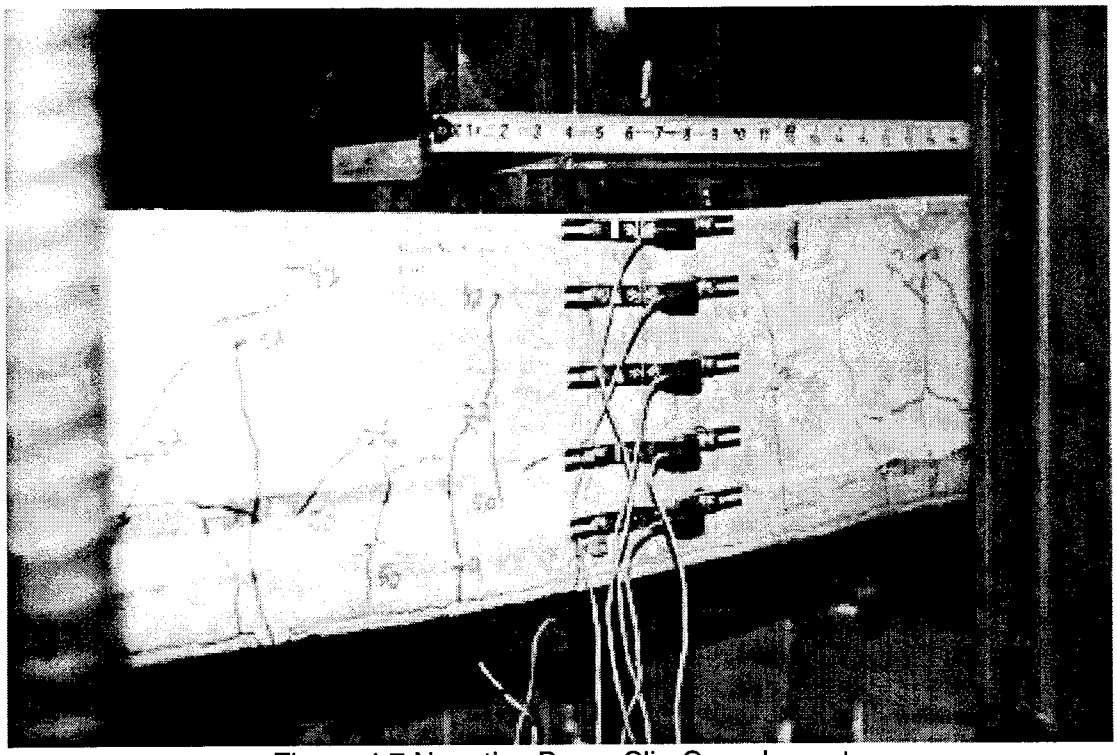

Figure 4.7 Negative Beam Clip Gage Layout

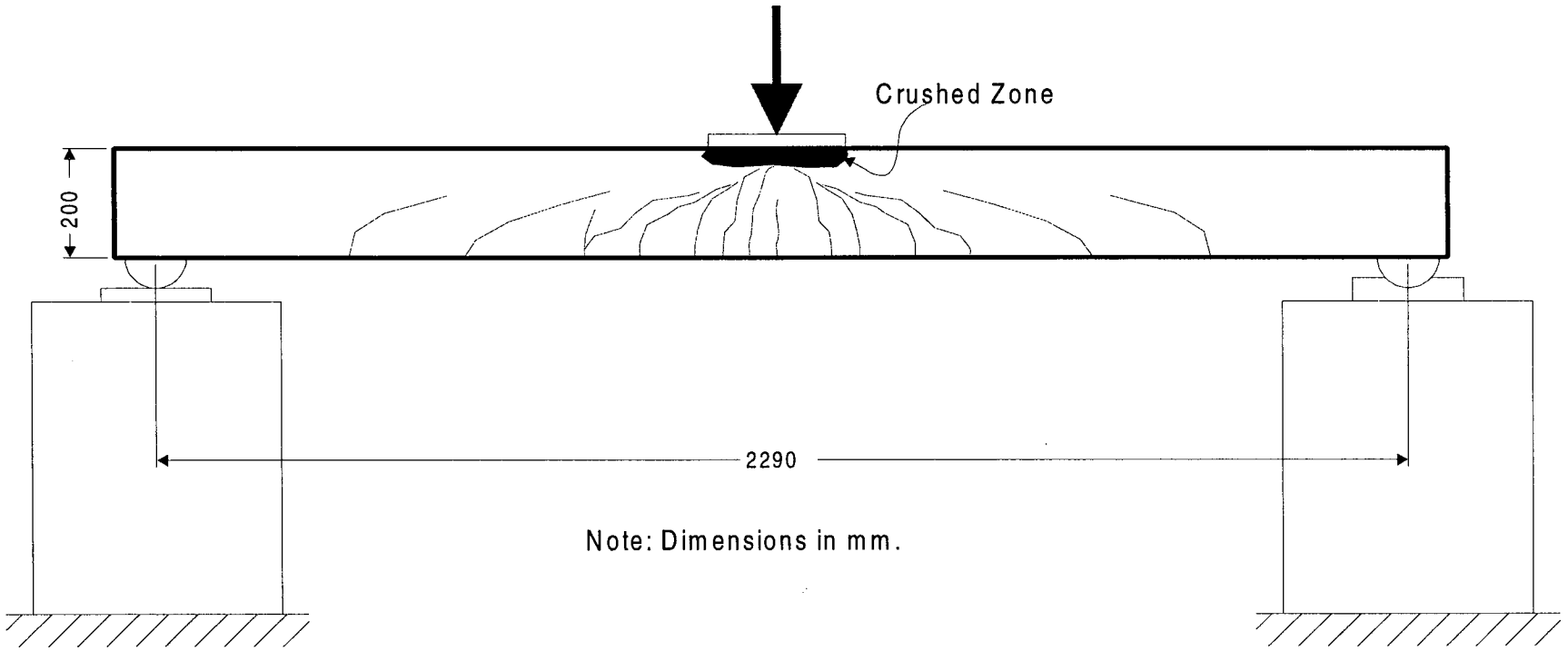

Figure 4.8 Crack Pattern in Benchmark Specimen No. 7 at Conclusion of Testing

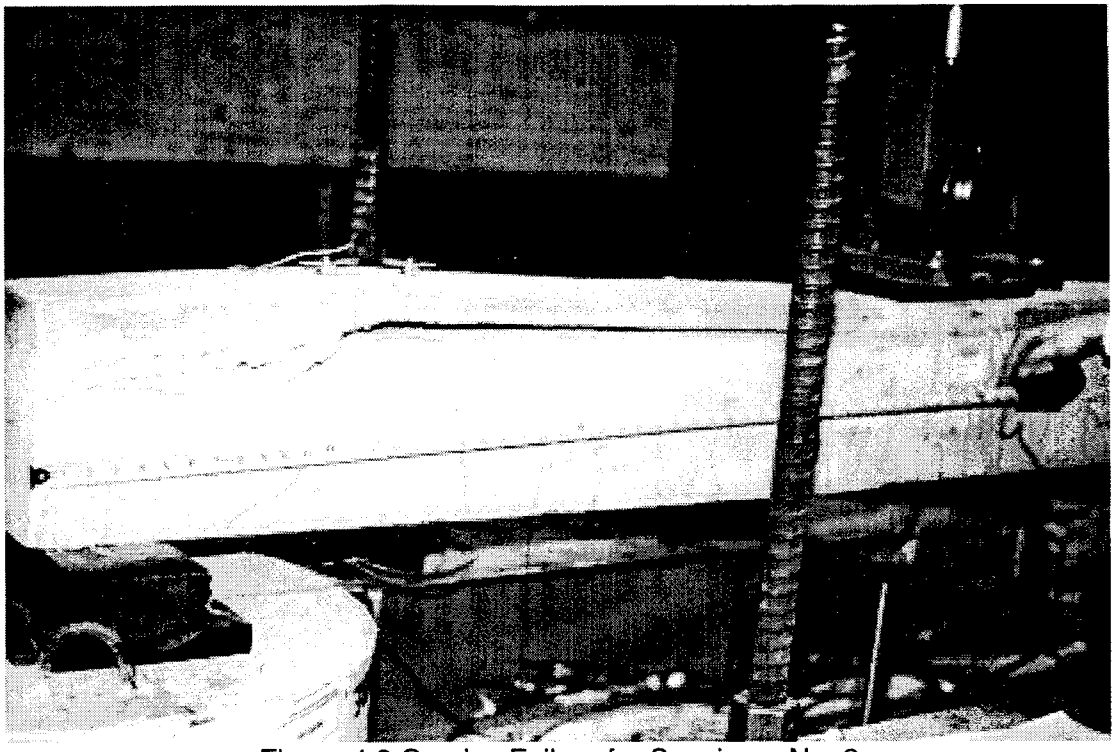

Figure 4.9 Overlay Failure for Specimen No. 2

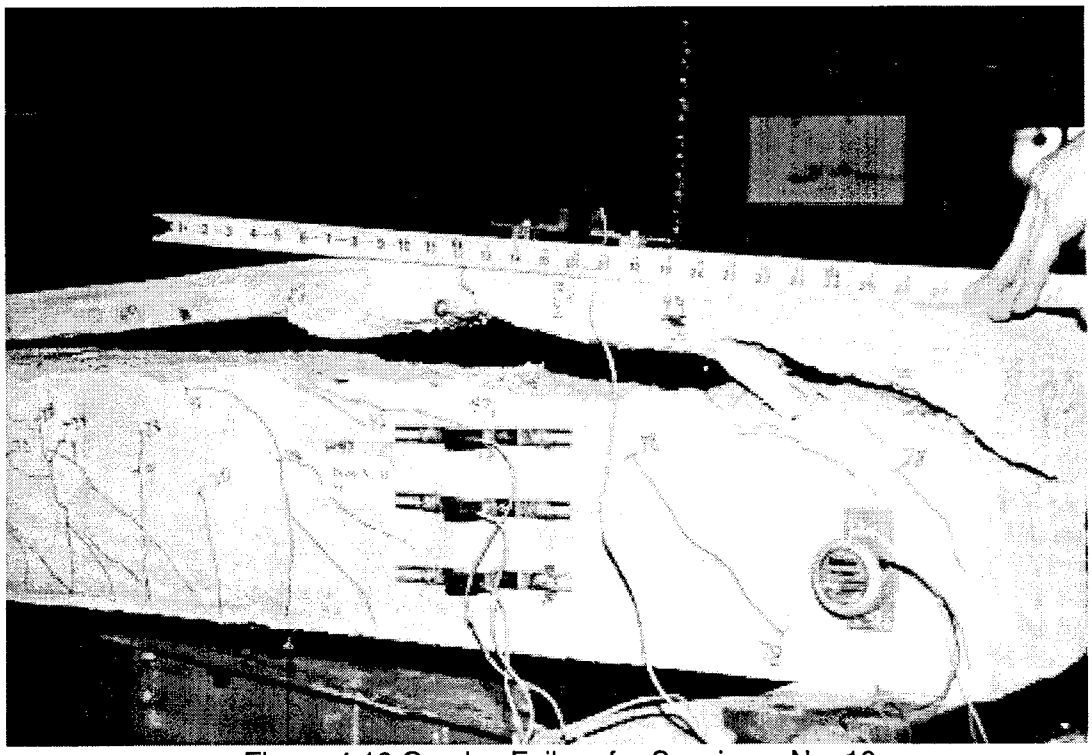

Figure 4.10 Overlay Failure for Specimen No. 10

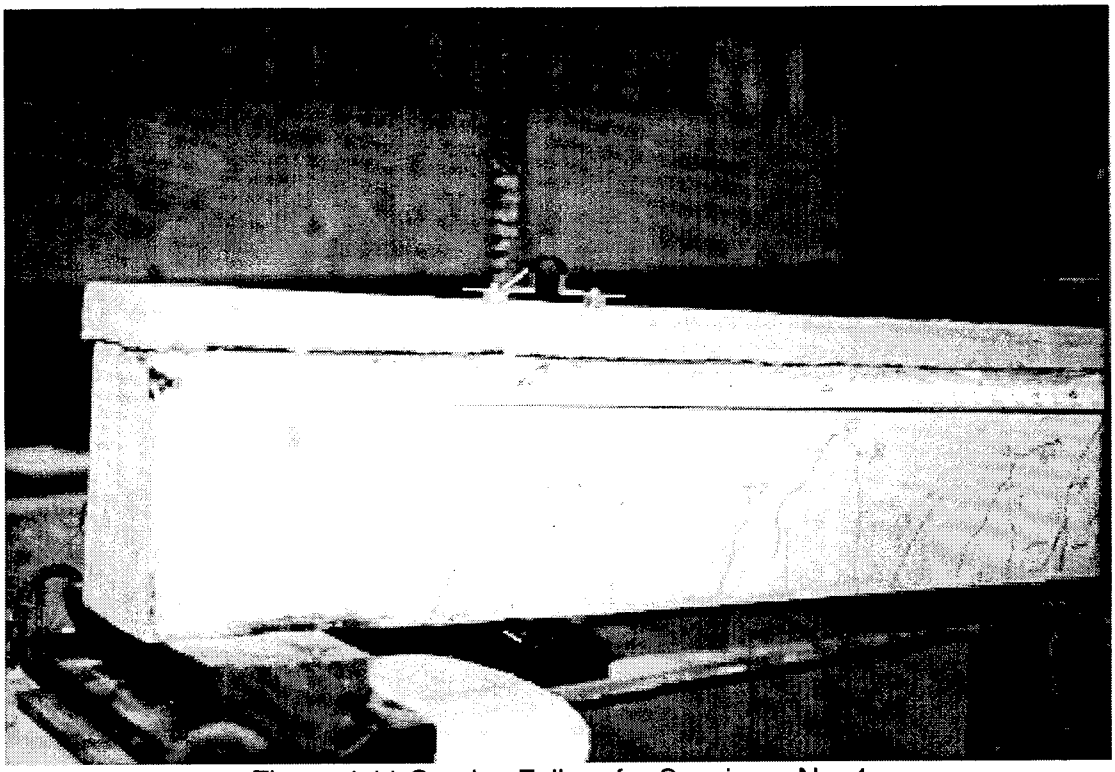

Figure 4.11 Overlay Failure for Specimen No. 4

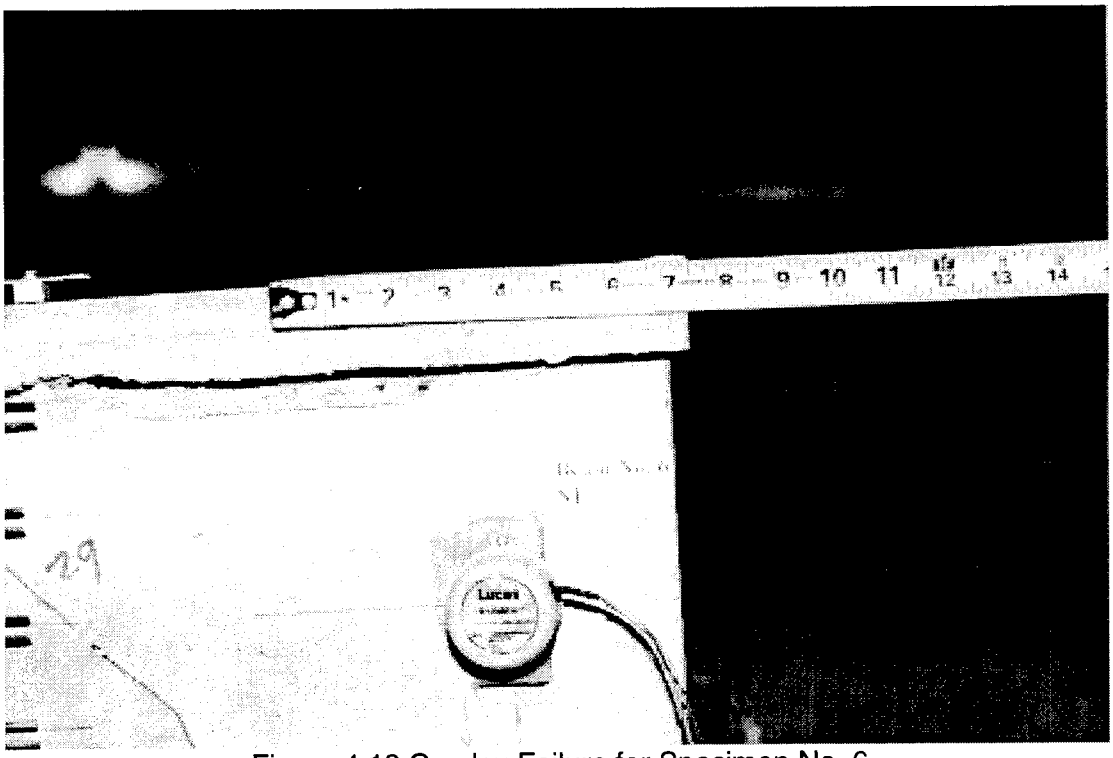

Figure 4.12 Overlay Failure for Specimen No. 6

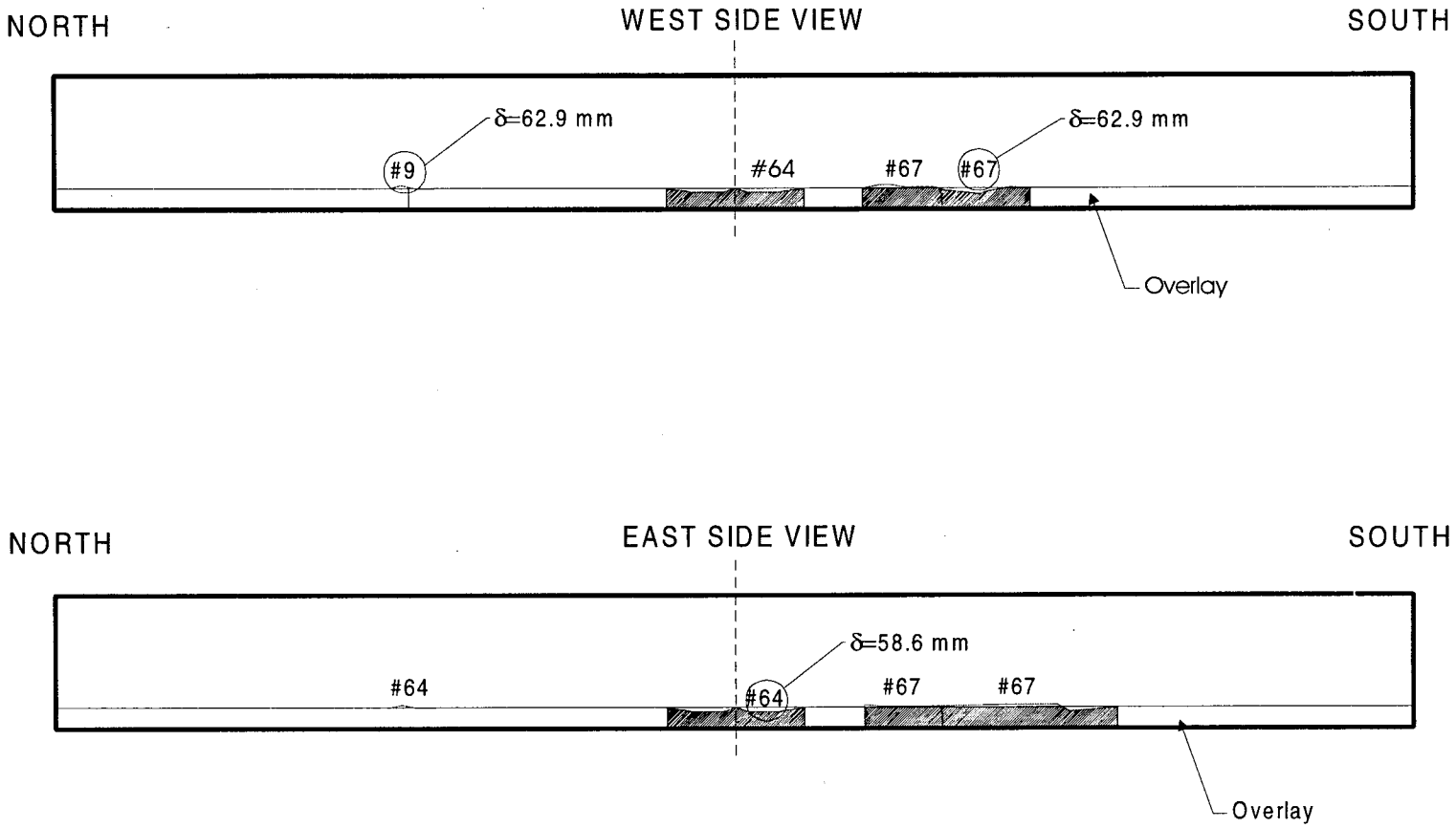

Figure 4.13 Specimen No. 3 Overlay Delamination Pattern (Unsealed/Negative Bending)

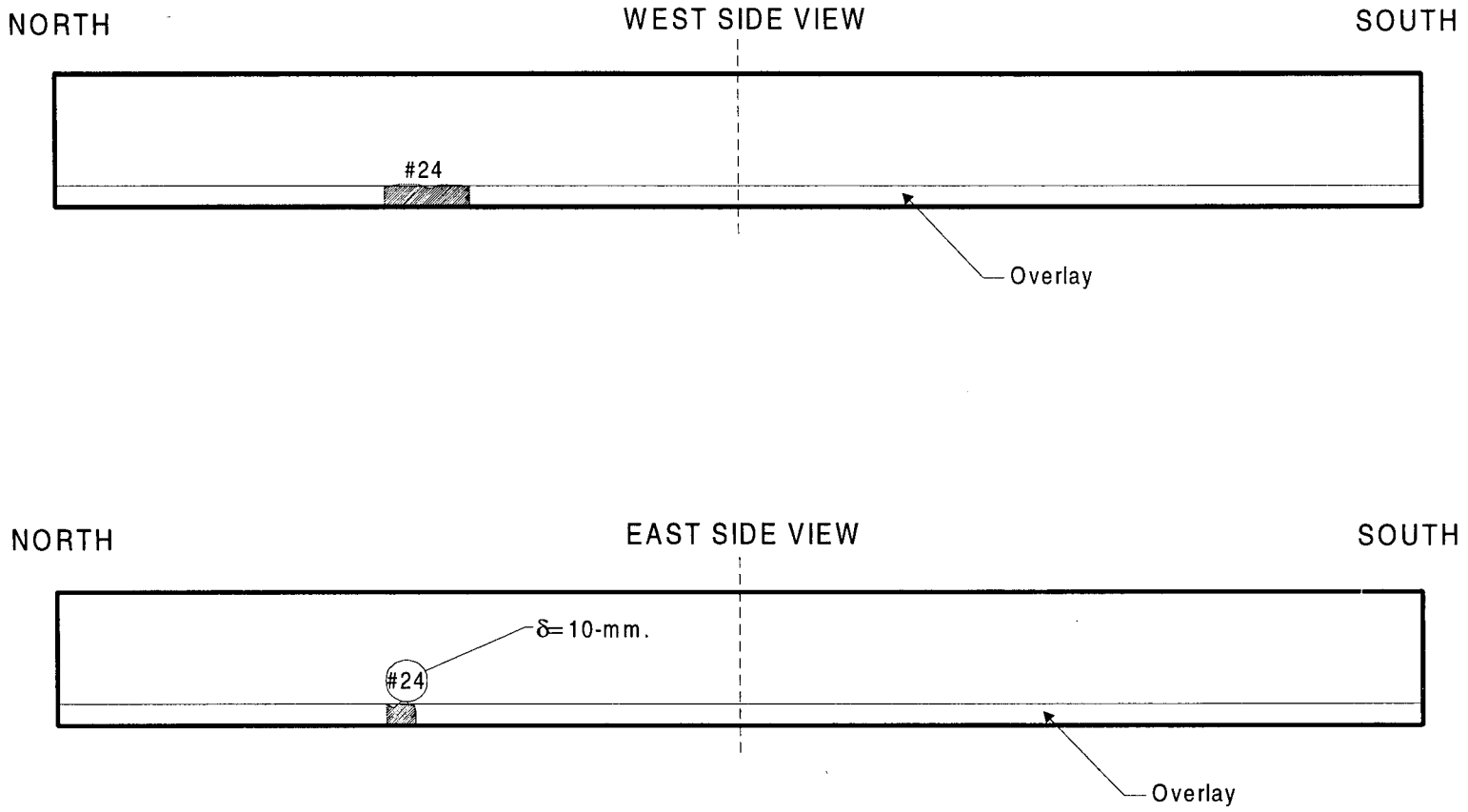

Figure 4.14 Beam 5 Overlay/Delamination Pattern (Sealed/Negative Bending)

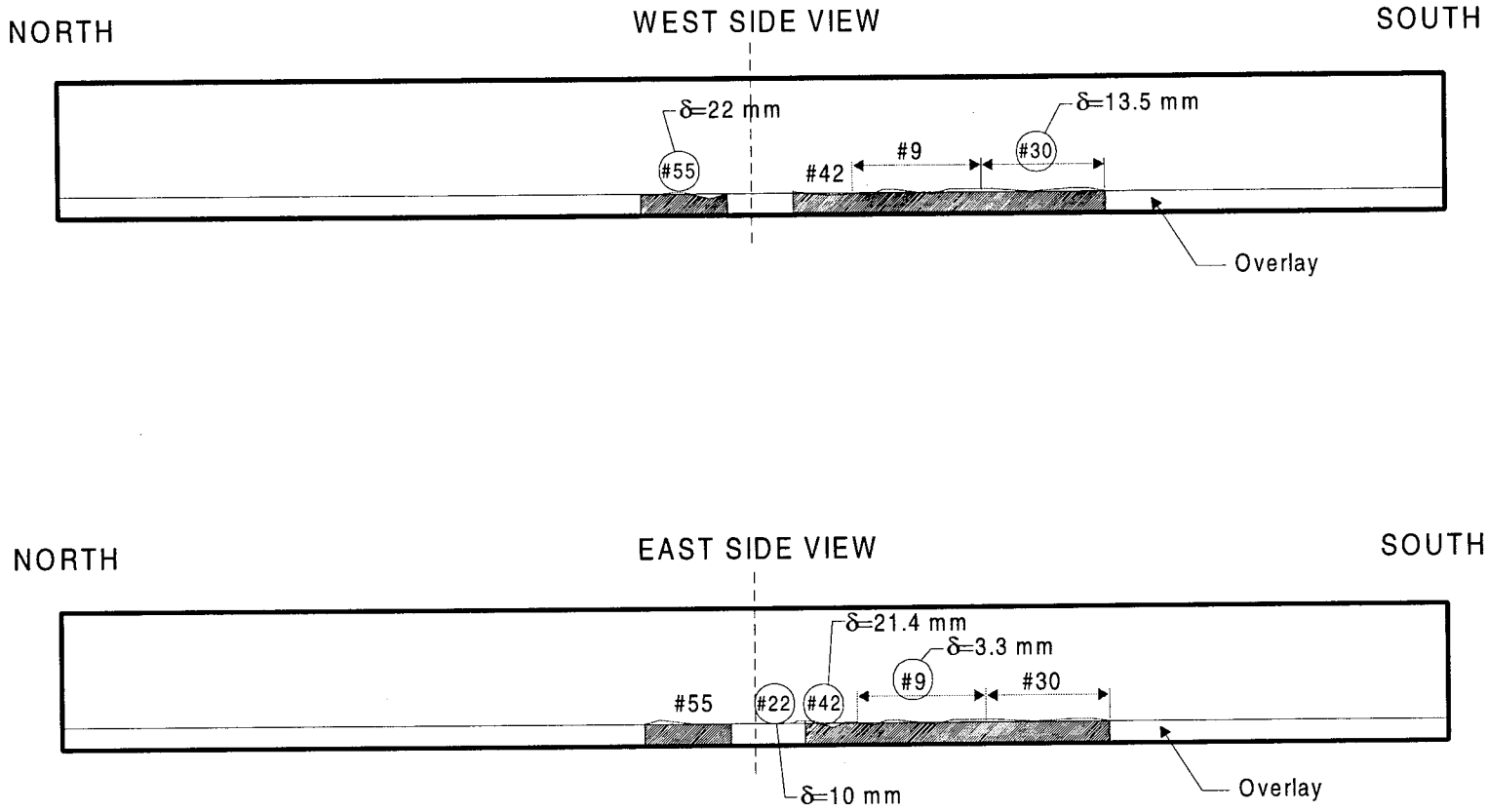

Figure 4.15 Specimen No. 8 Overlay/Delamination Pattern (Sealed/Negative Bending)

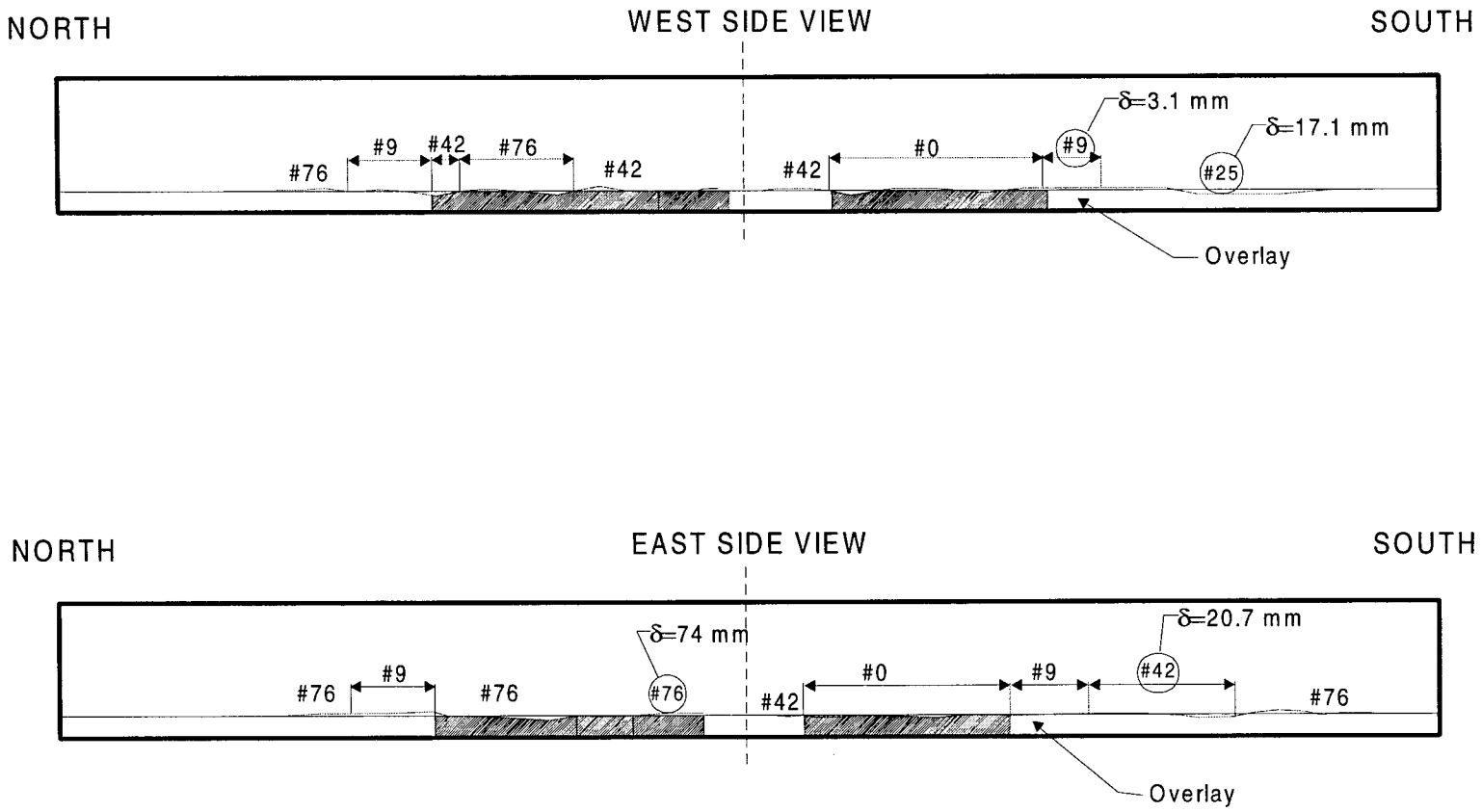

Refers to load application number in loading sequence.

δ = Midspan Deflection

Delamination

Crack

Figure 4.16 Specimen No. 9 Overlay Delamination Pattern (Unsealed/Negative Bending)

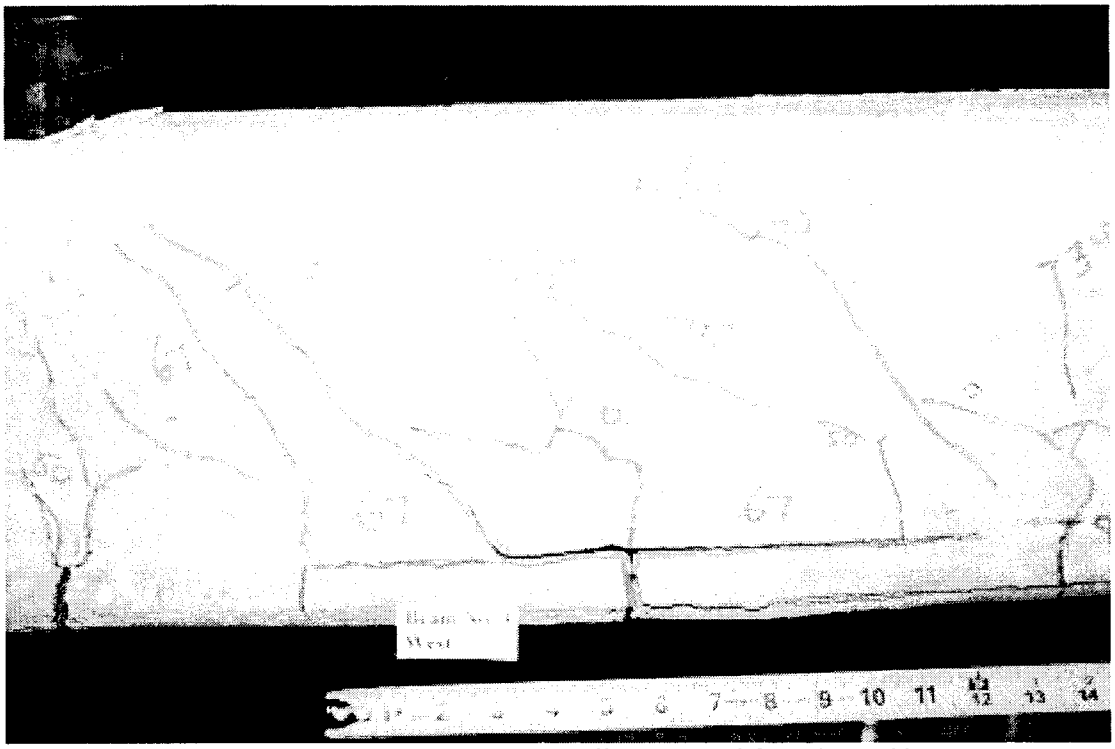

Figure 4.17a Overlay is Peeling off Bottom of Specimen No. 3

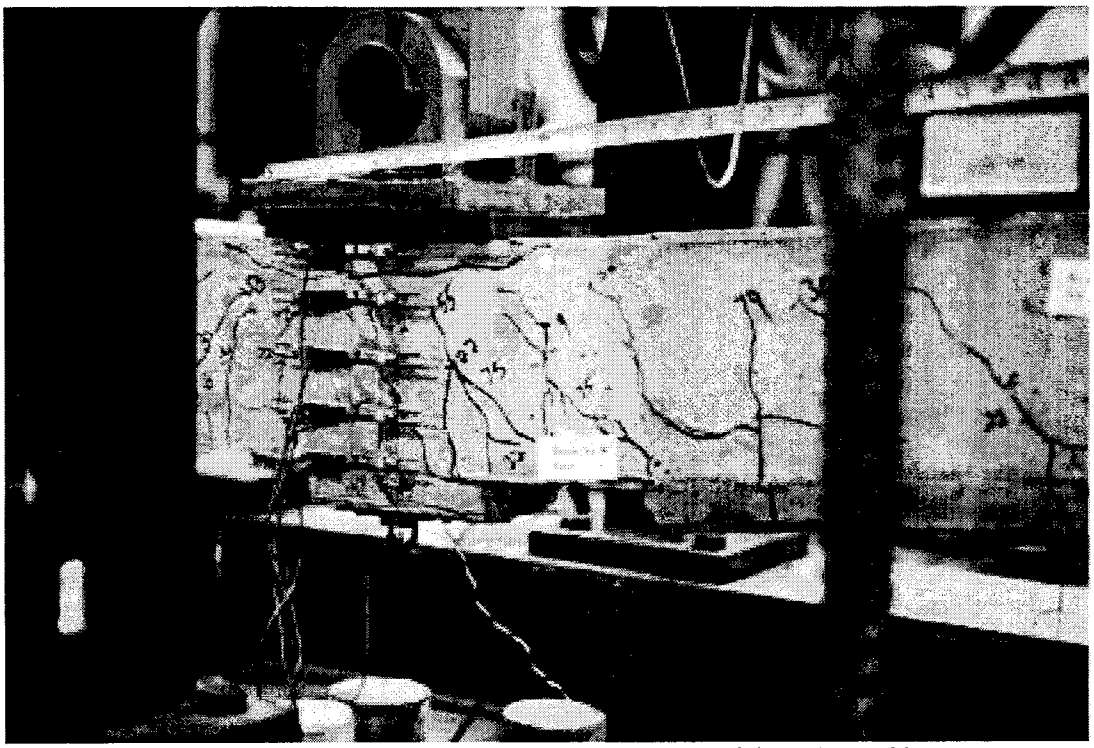

Figure 4.17b Overlay is Peeling off Bottom of Specimen No. 3

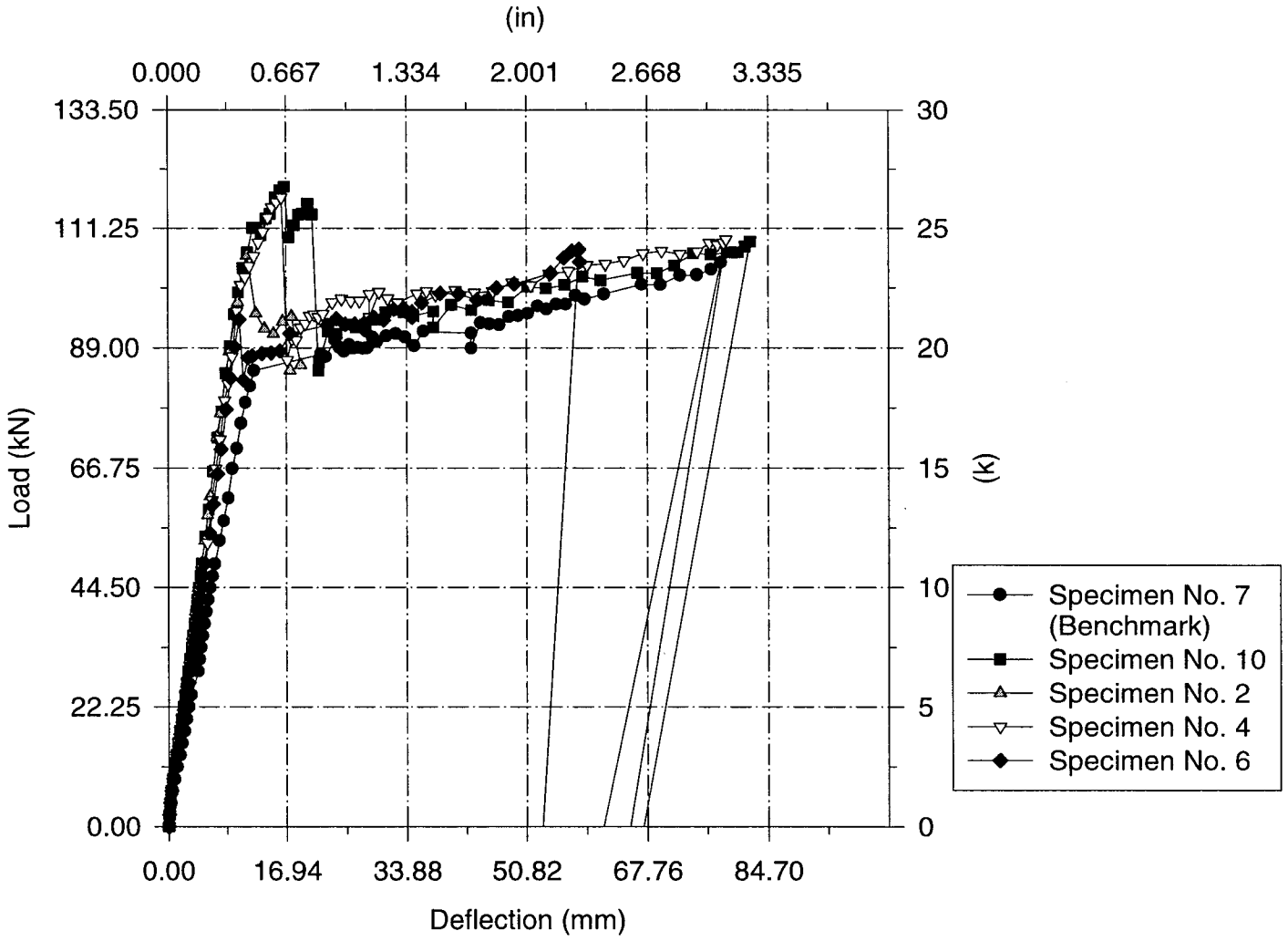

Figure 4.18 Load vs. Midspan Deflection for Beams Tested in Positive Bending

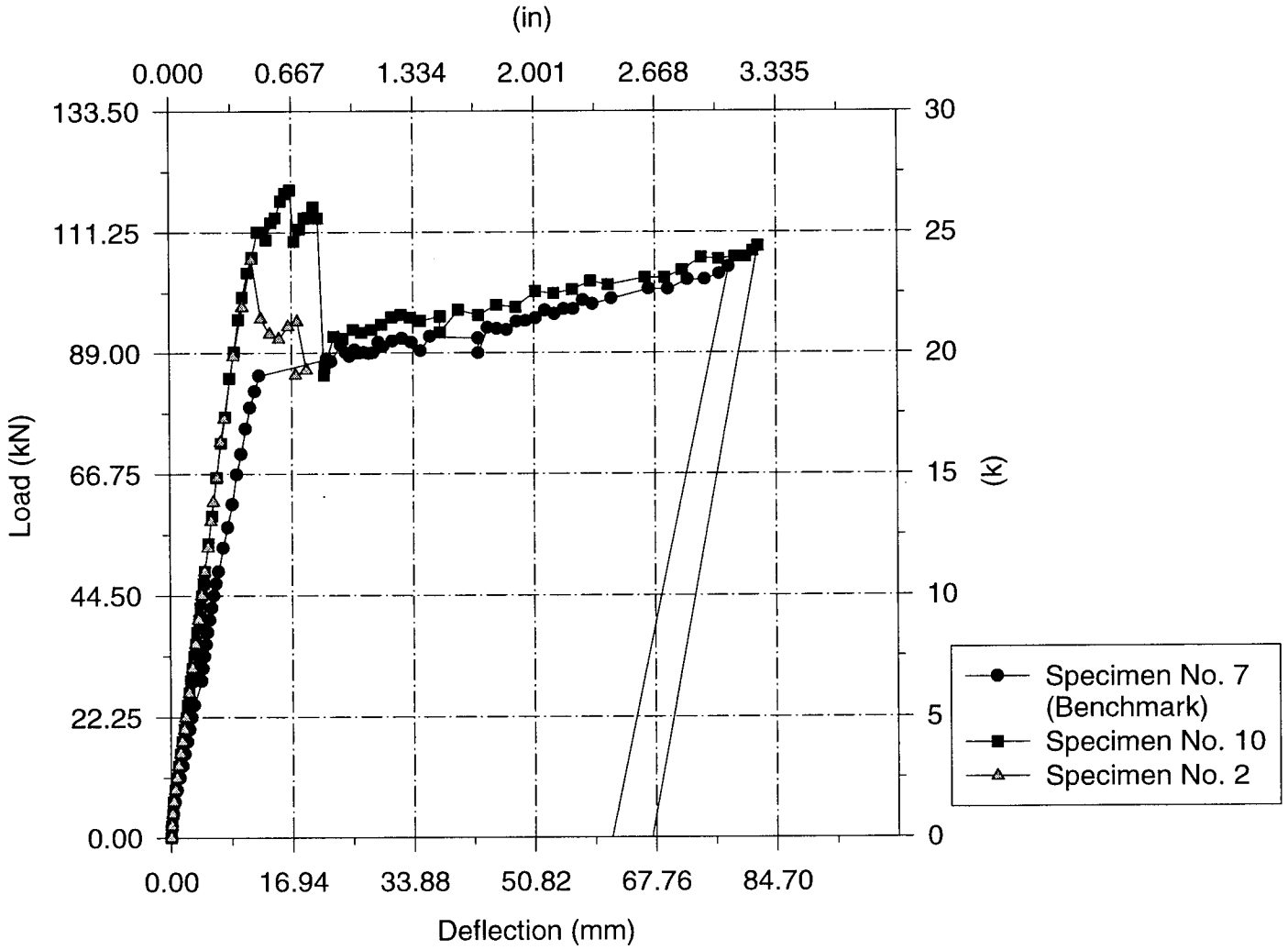

Figure 4.19 Load vs. Midspan Deflection for Beams Tested in Positive Bending Without Sealer

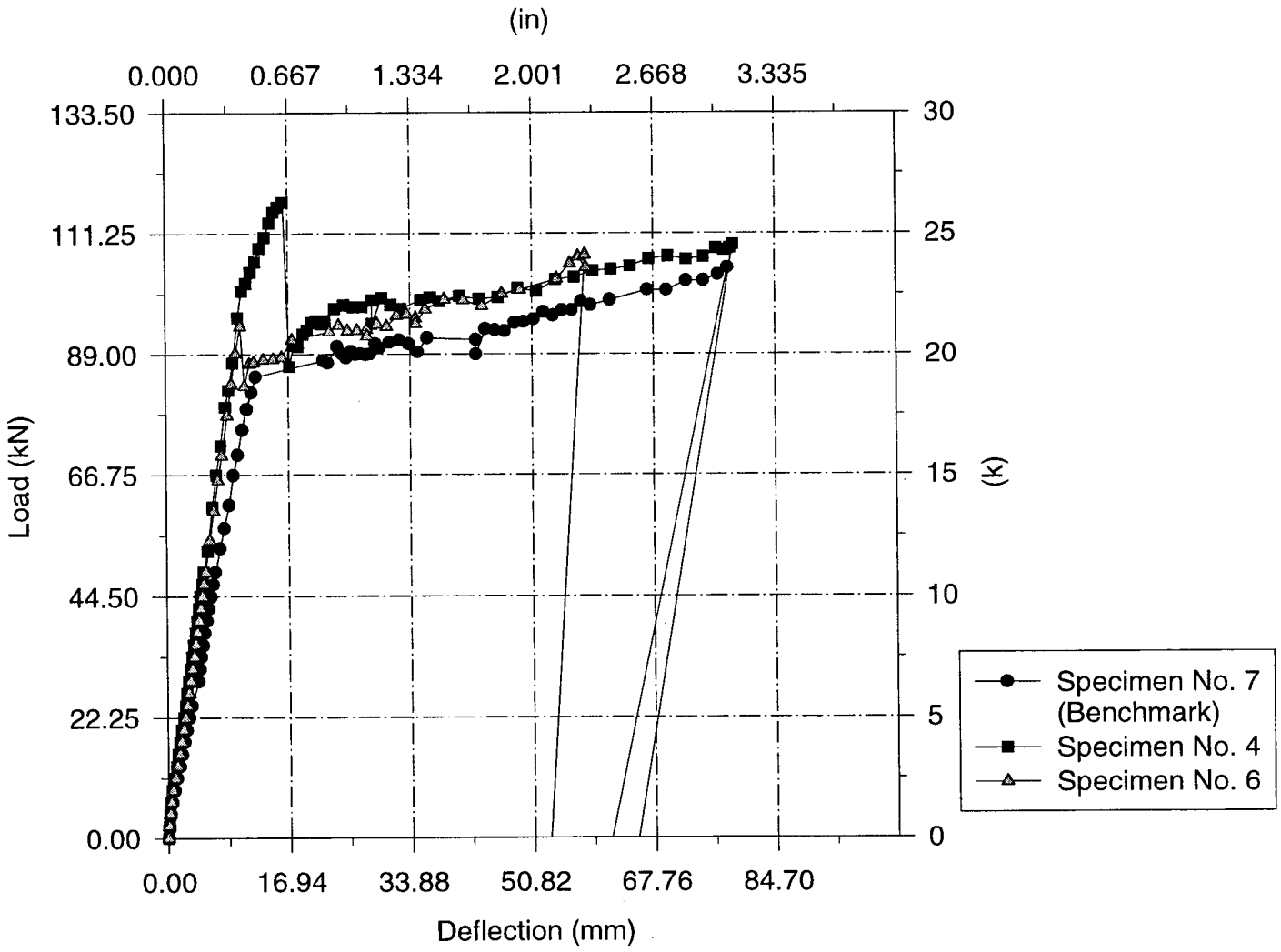

Figure 4.20 Load vs. Midspan Deflection for Beams Tested in Positive Bending With HMWM Shear

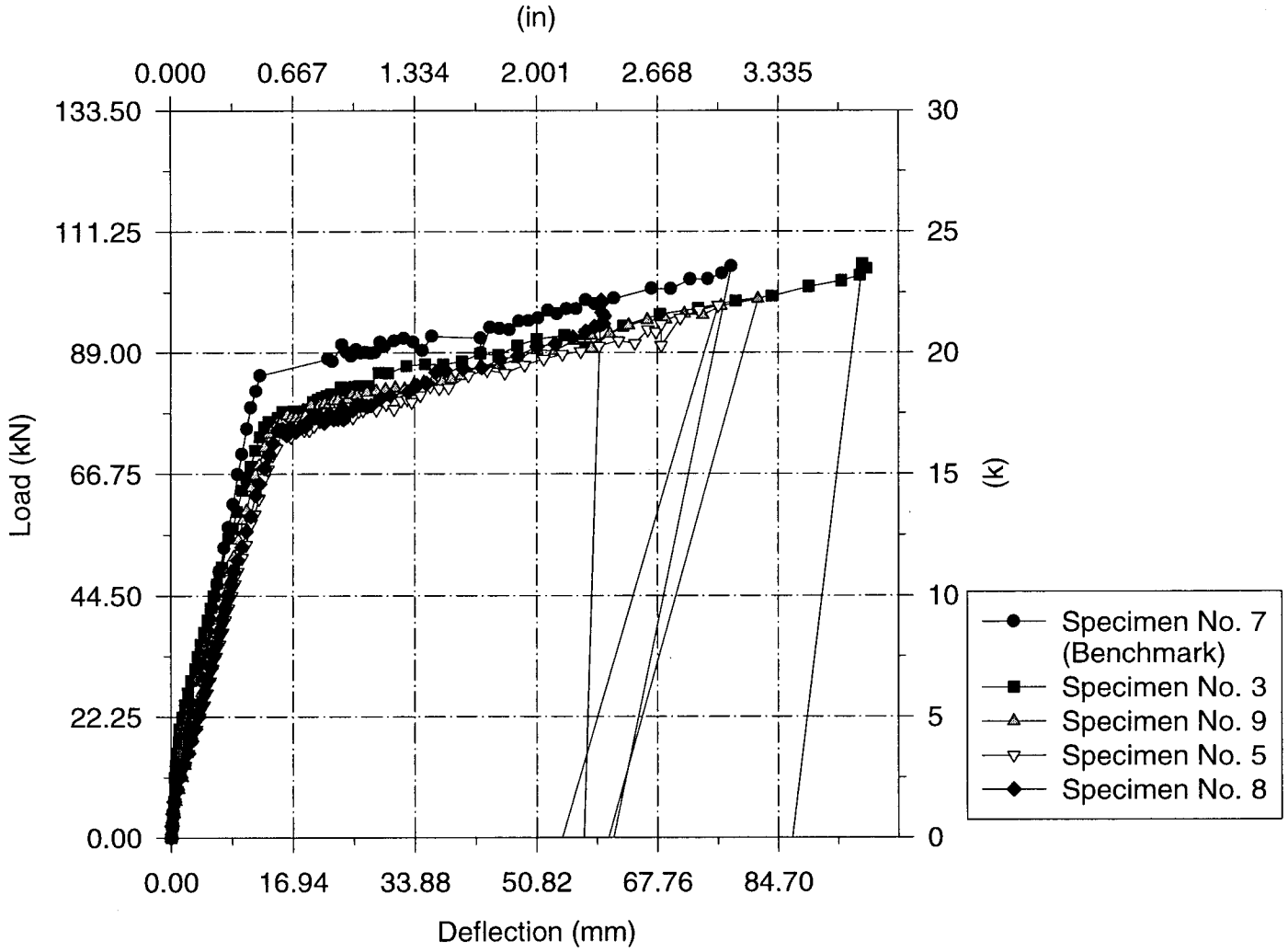

Figure 4.21 Load vs. Midspan Deflection for Beams Tested in Negative Bending

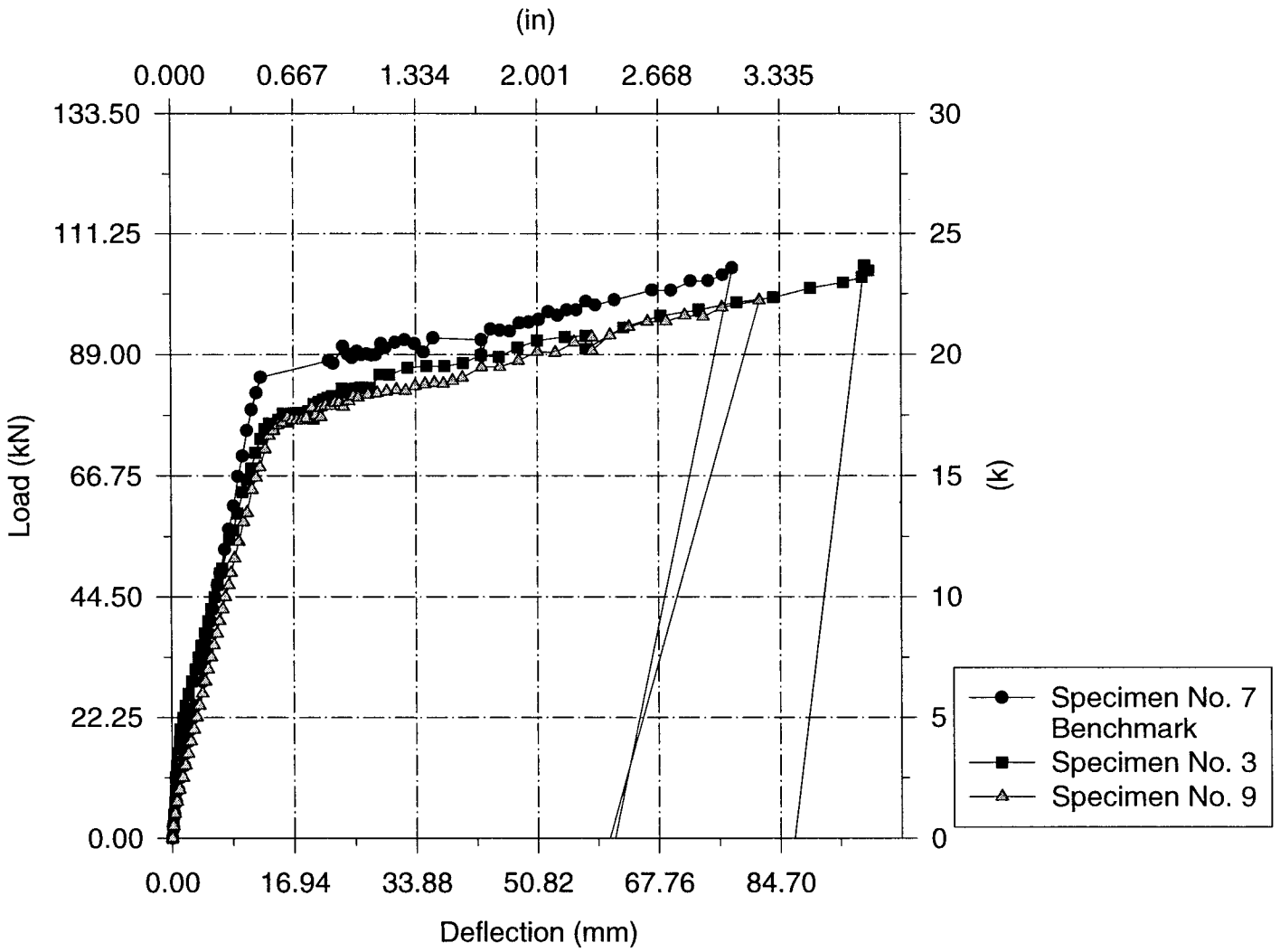

Figure 4.22 Load vs. Midspan Deflection for Beams Tested in Negative Bending Without Sealer

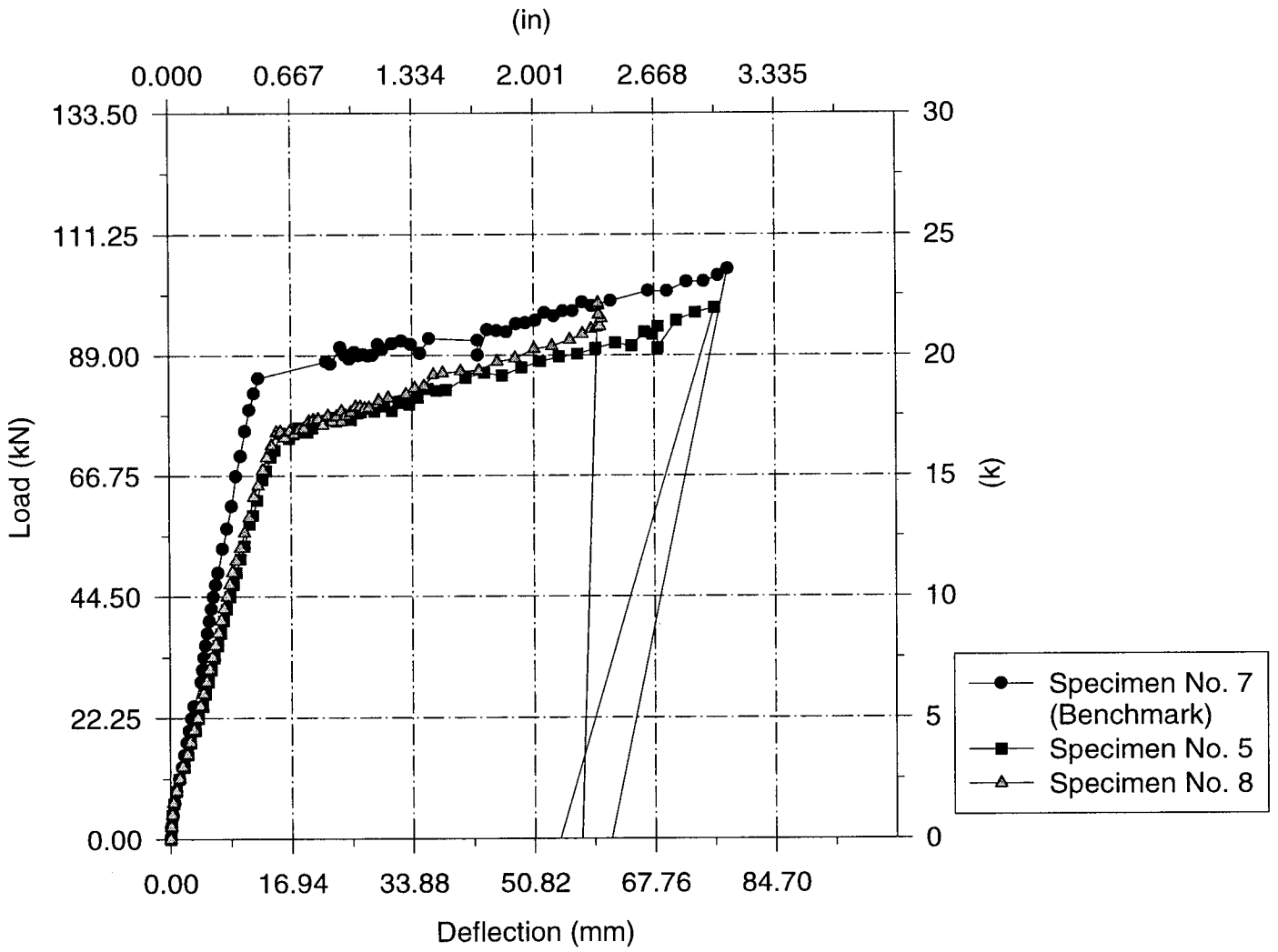

Figure 4.23 Load vs. Midspan Deflection for Beams Tested in Negative Bending With HMWM Sealer

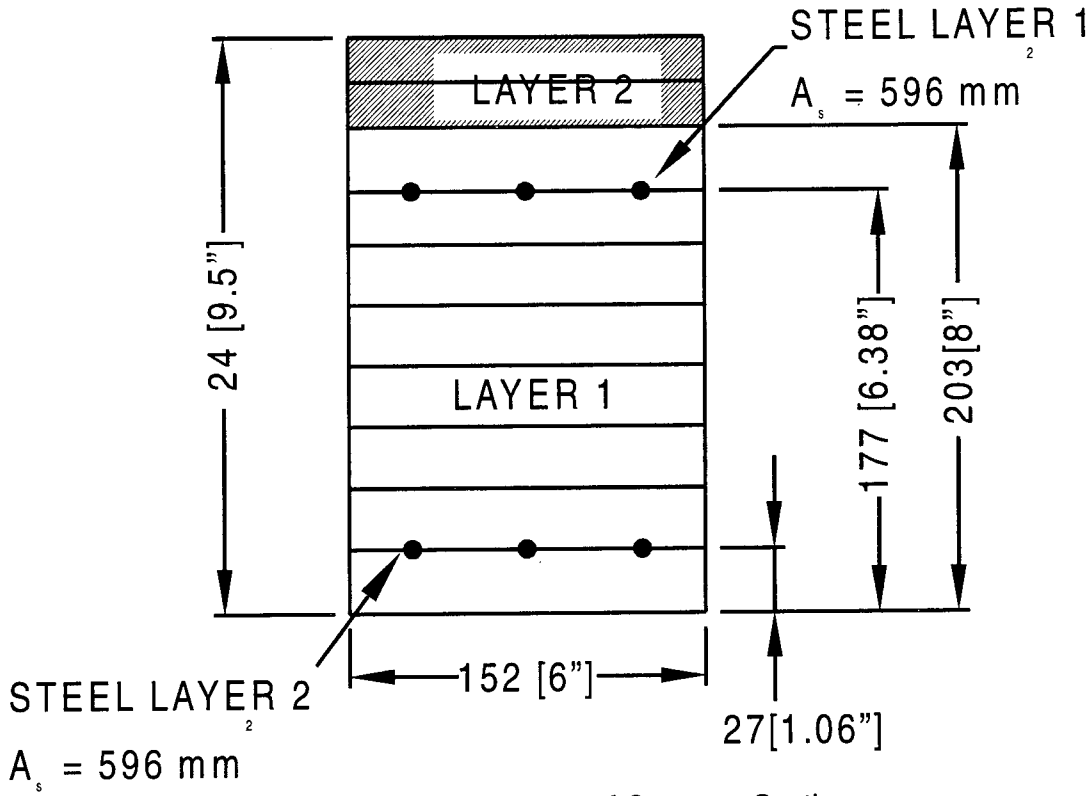

Figure 4.24 Discretization of Concrete Section

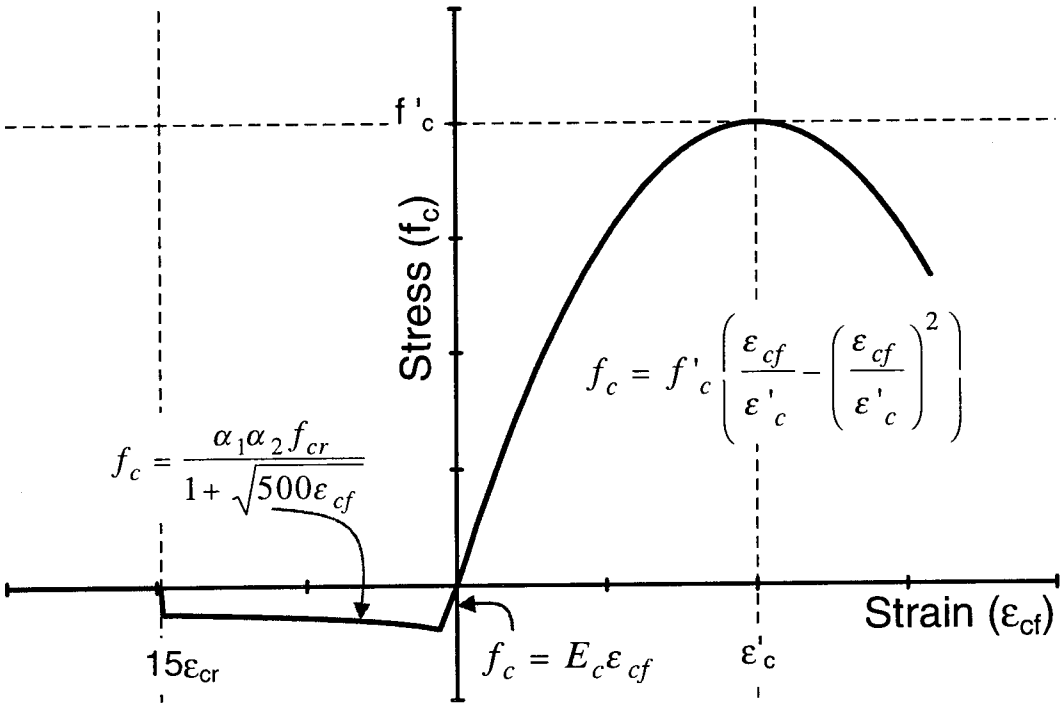

Figure 4.25 Concrete Stress-Strain Model

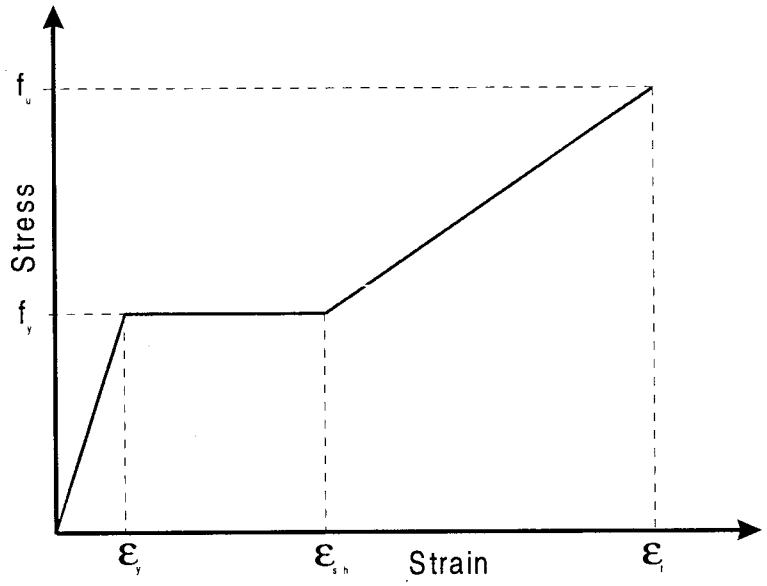

Figure 4.26 Steel Model

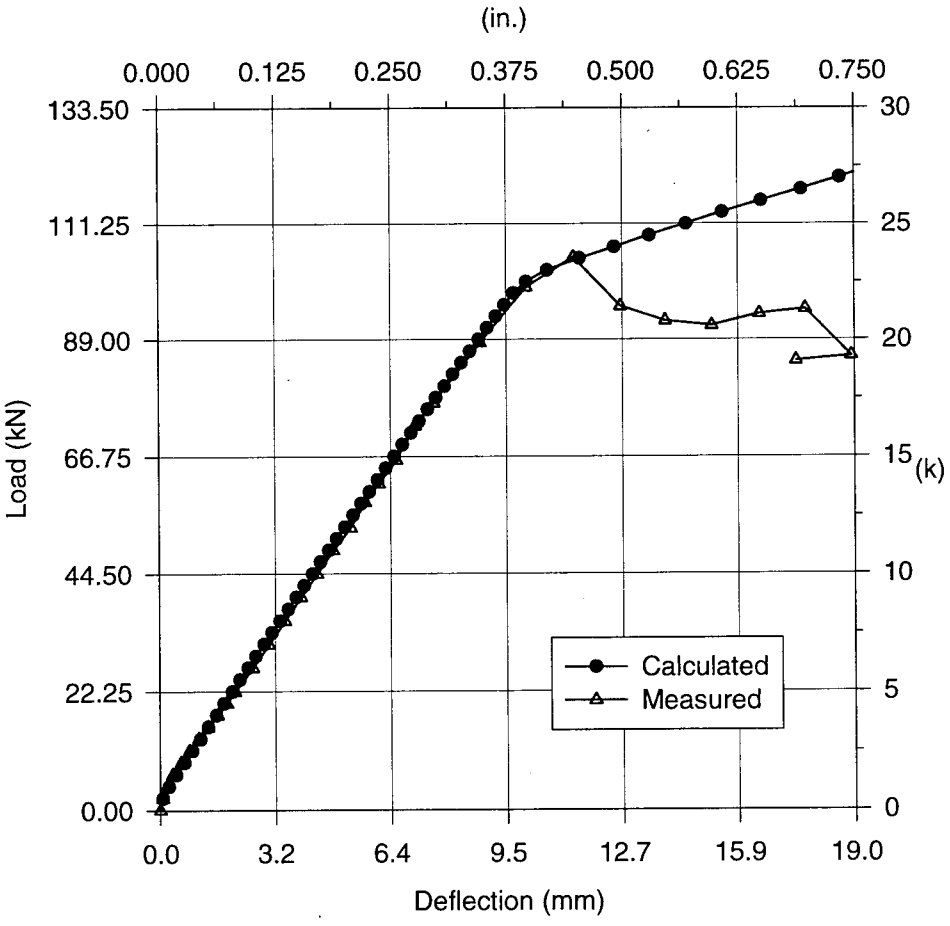

Figure 4.27 Load-Deflection Calibration for Specimen No. 2

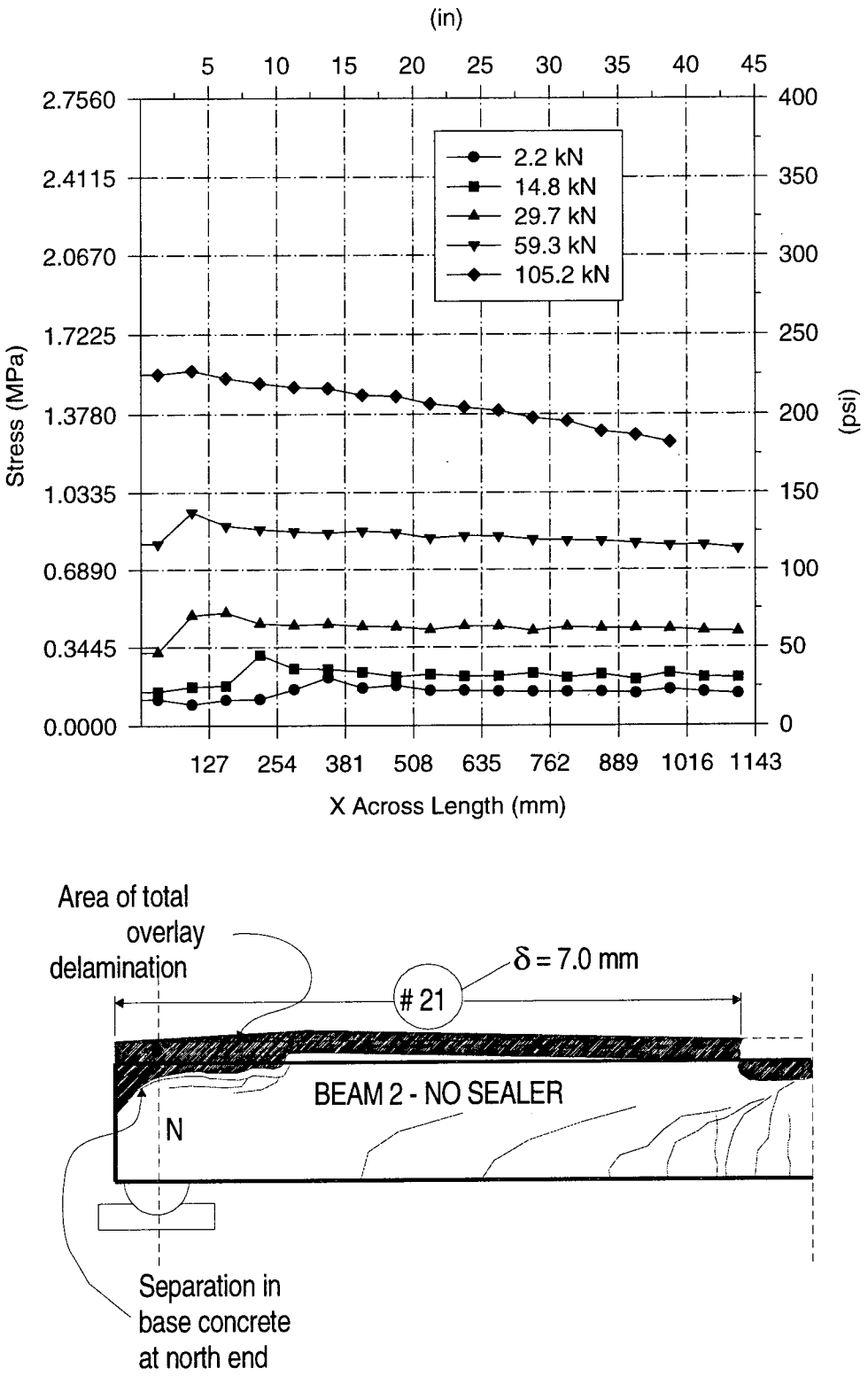

Figure 4.28 Shear Stress at Bond Interface for Specimen No. 2
Positive Bending/No Sealer at the Interface

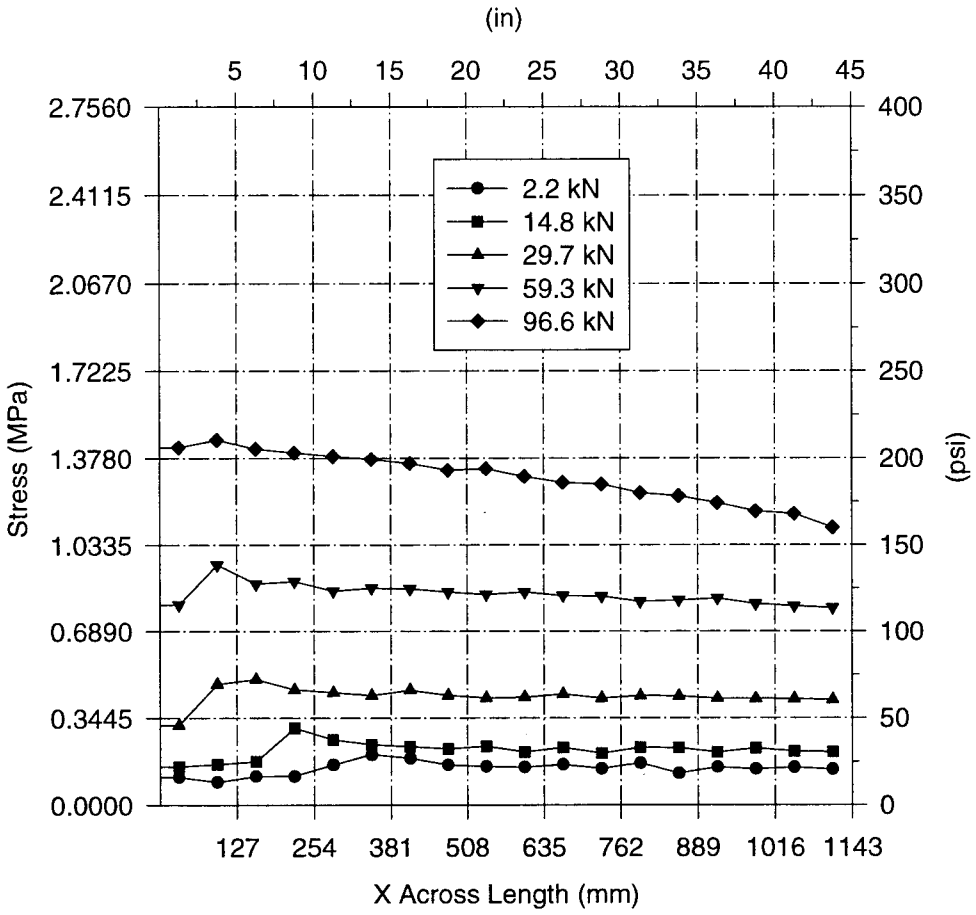

Figure 4.29 Shear Stress at Bond Interface Specimen No. 4
Positive Bending/Sealed with HMWM Sealer at the Interface

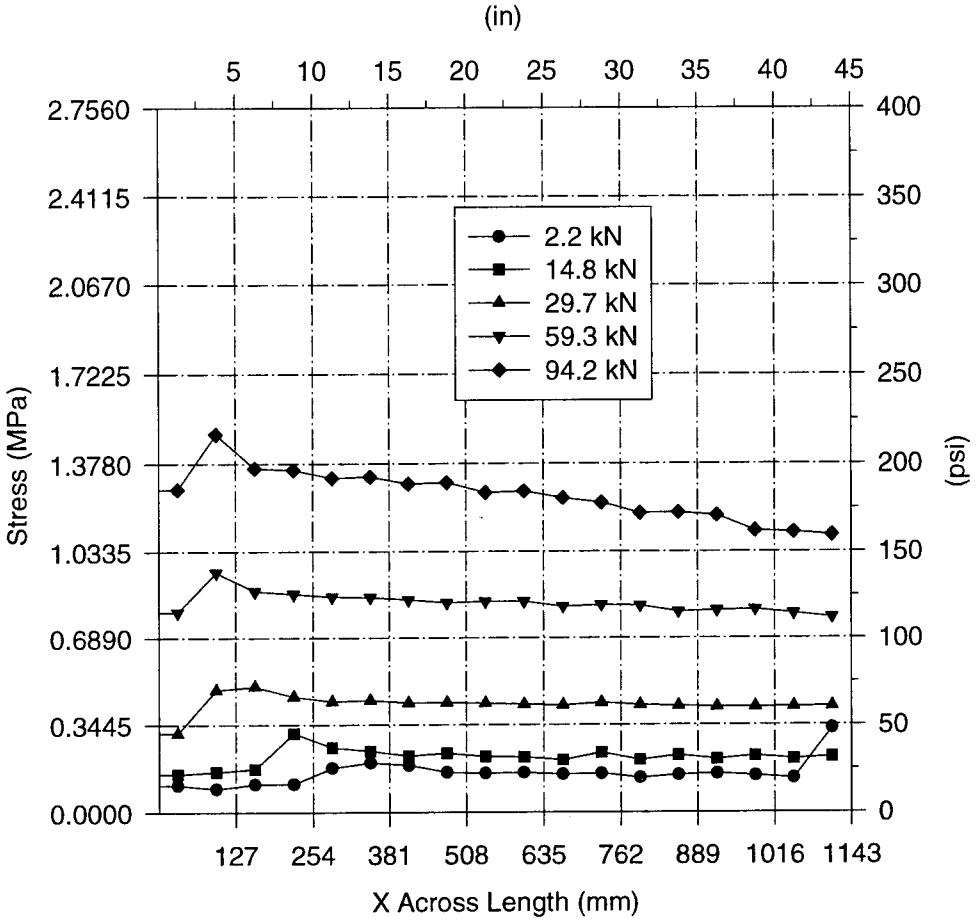

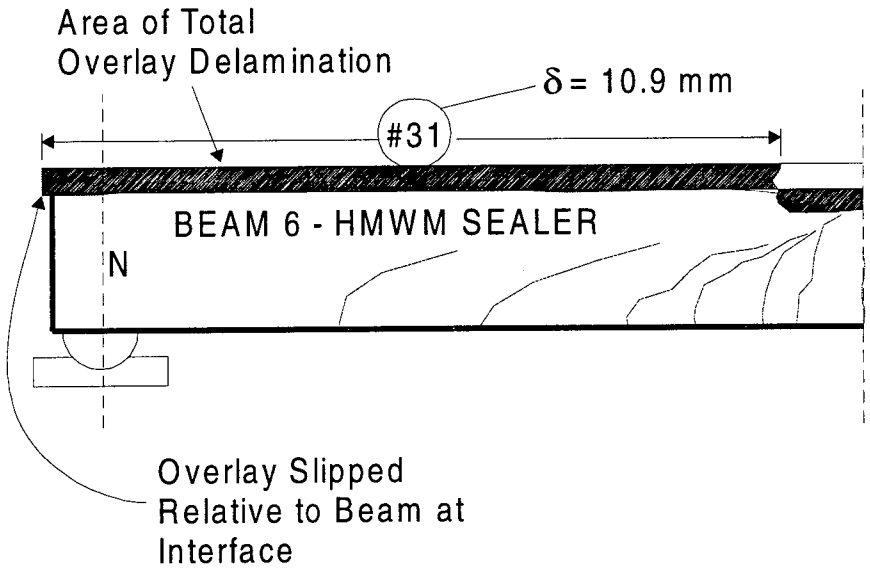

Figure 4.30 Shear Stress at Bond Interface Specimen No. 6
Positive Bending/Sealed with HMWM at the Interface

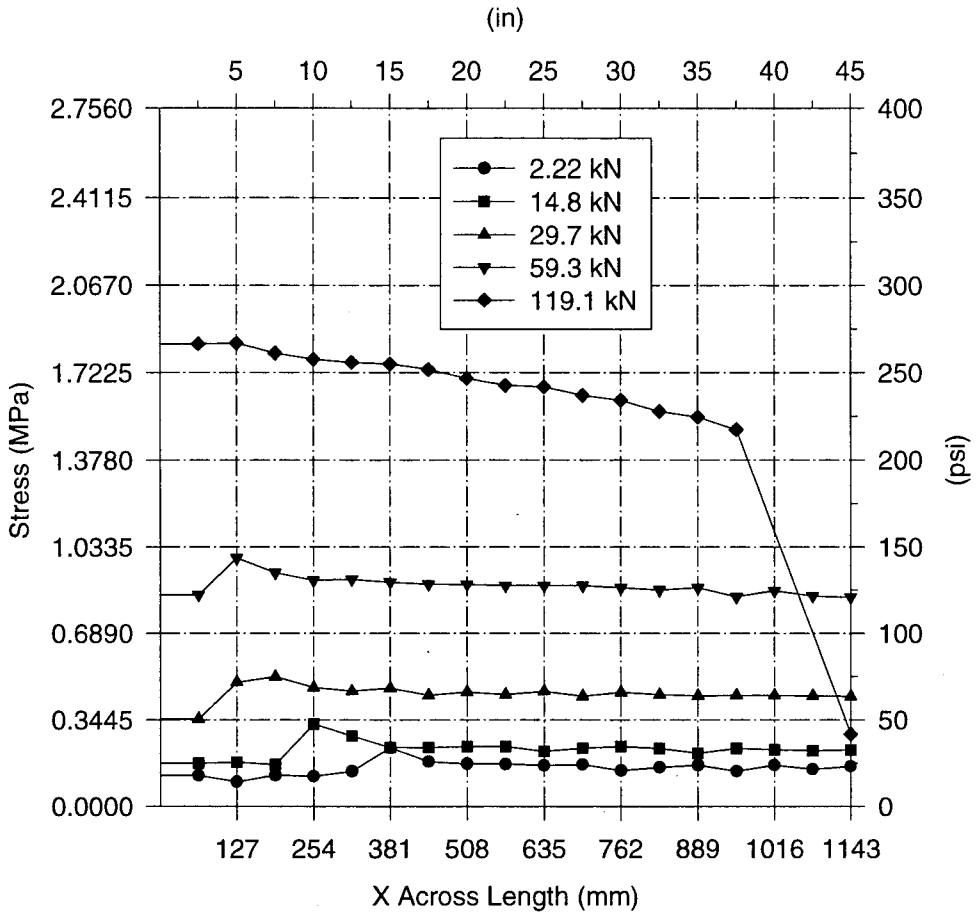

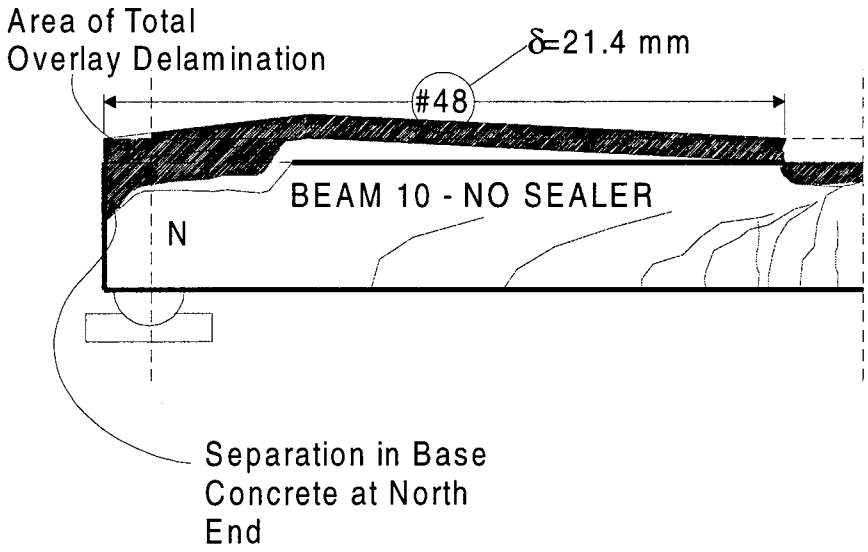

Figure 4.31 Shear Stress at Bond Interface Specimen No. 10
Positive Bending/No Sealer at the Interface

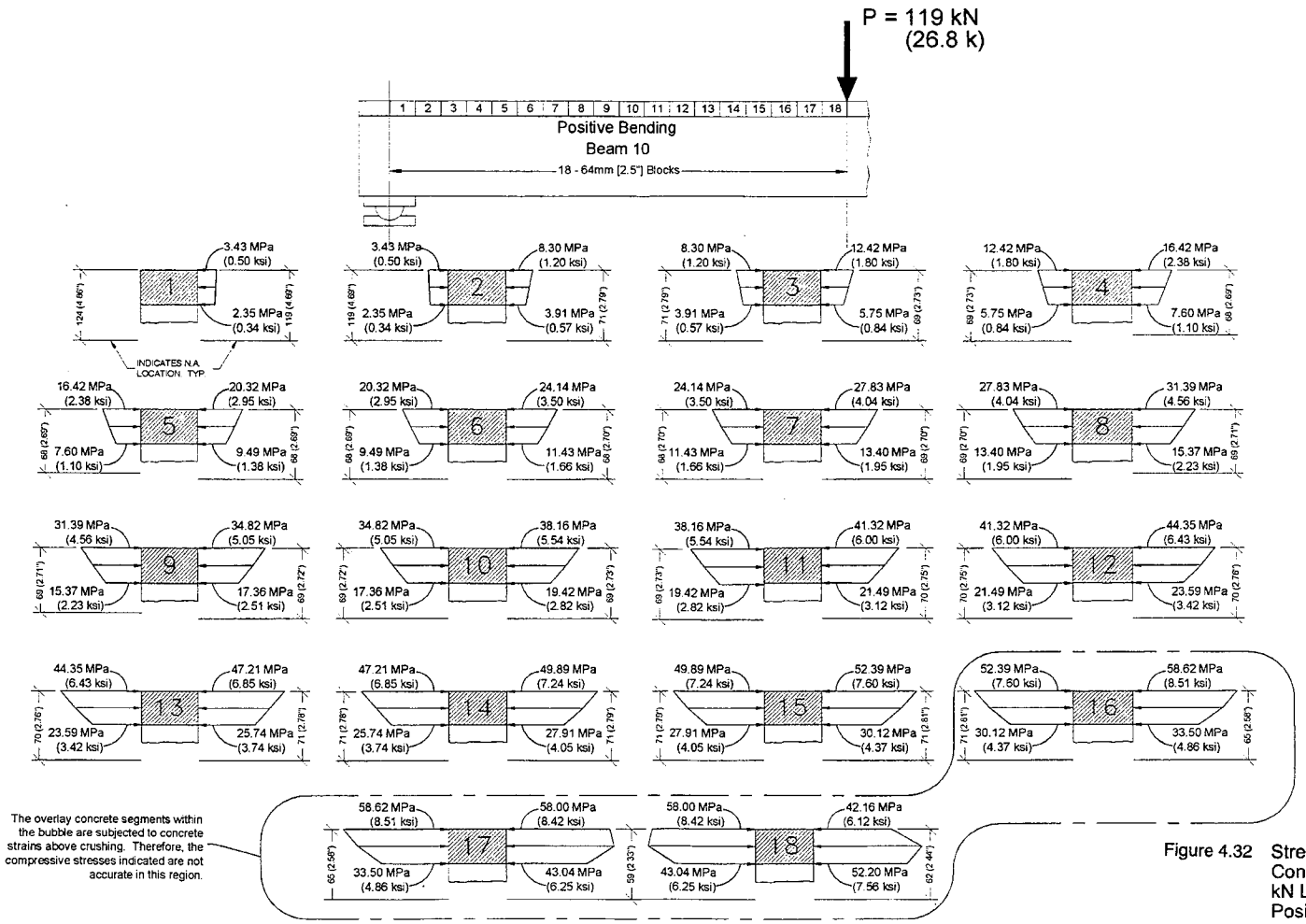

Figure 4.32 Stress Profiles on Overlay Concrete Blocks with 119 kN Load Applied Creating Positive Bending.

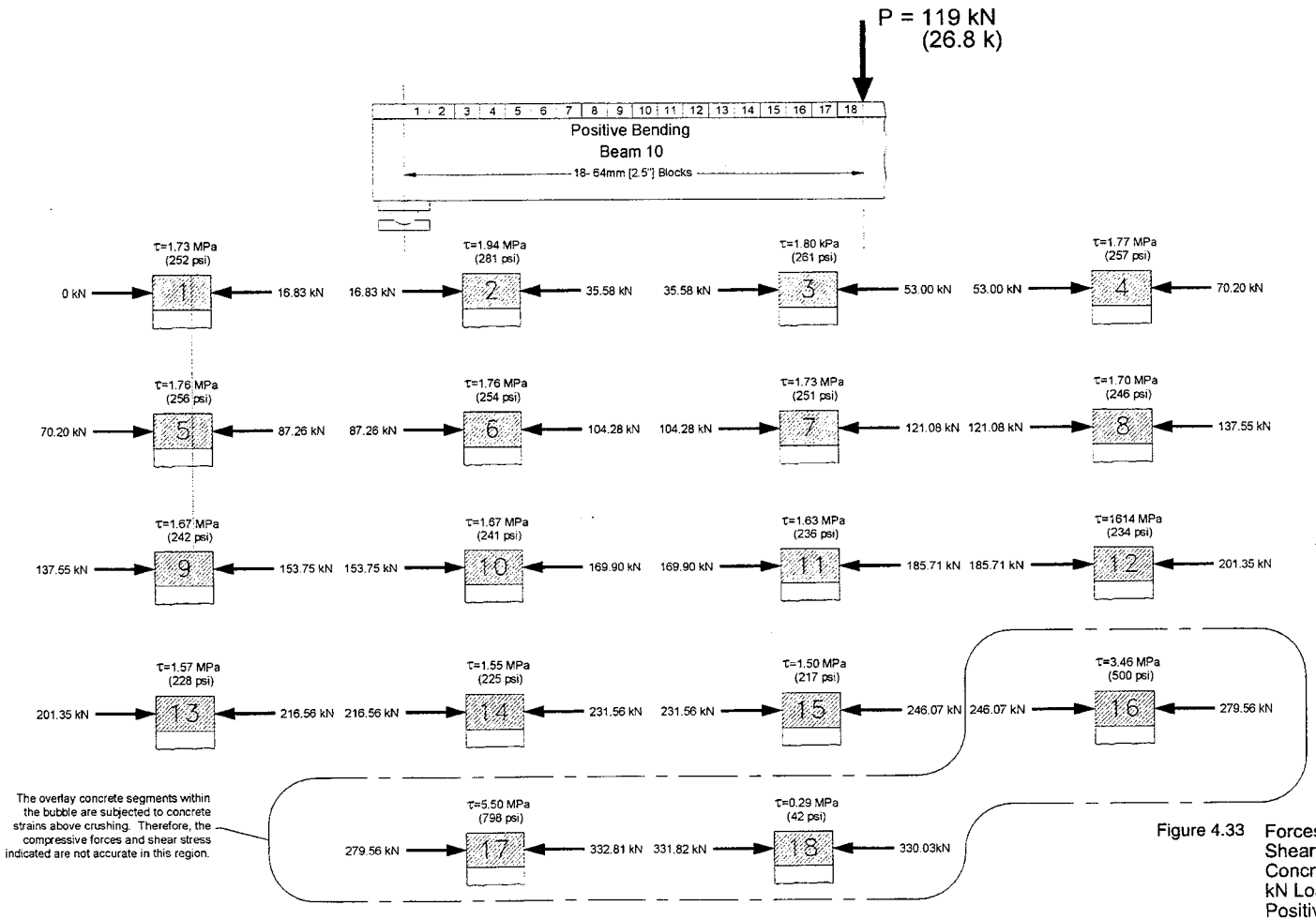

Figure 4.33 Forces and Corresponding Shear Stress on Overlay Concrete Blocks with 119 kN Load Applied Creating Positive Bending.

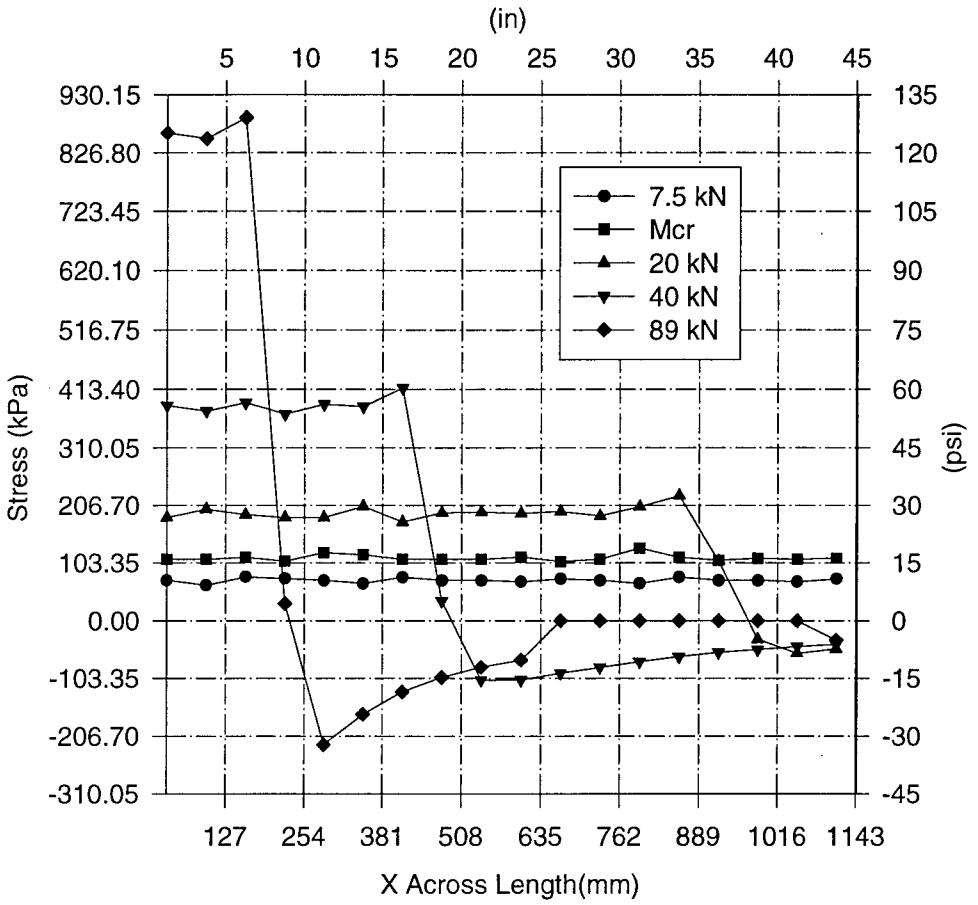

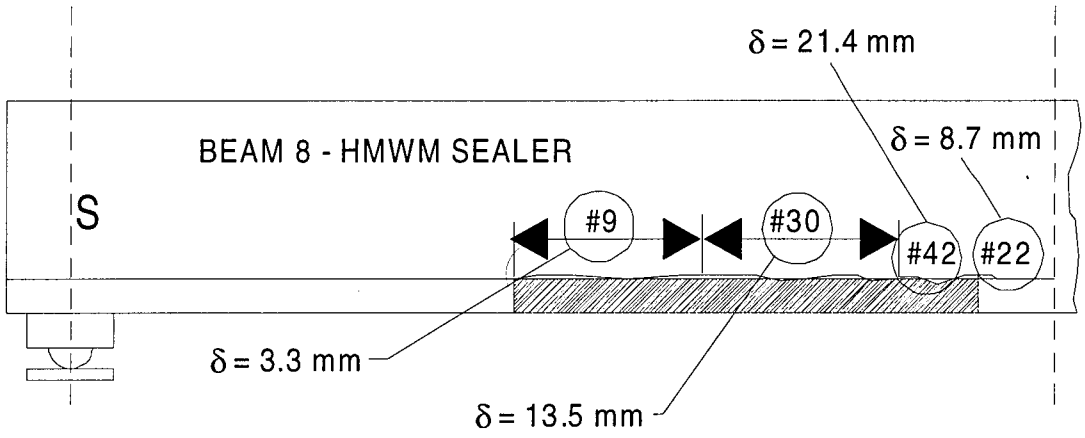

Figure 4.34 Shear Stress at Bond Interface for Negative Bending

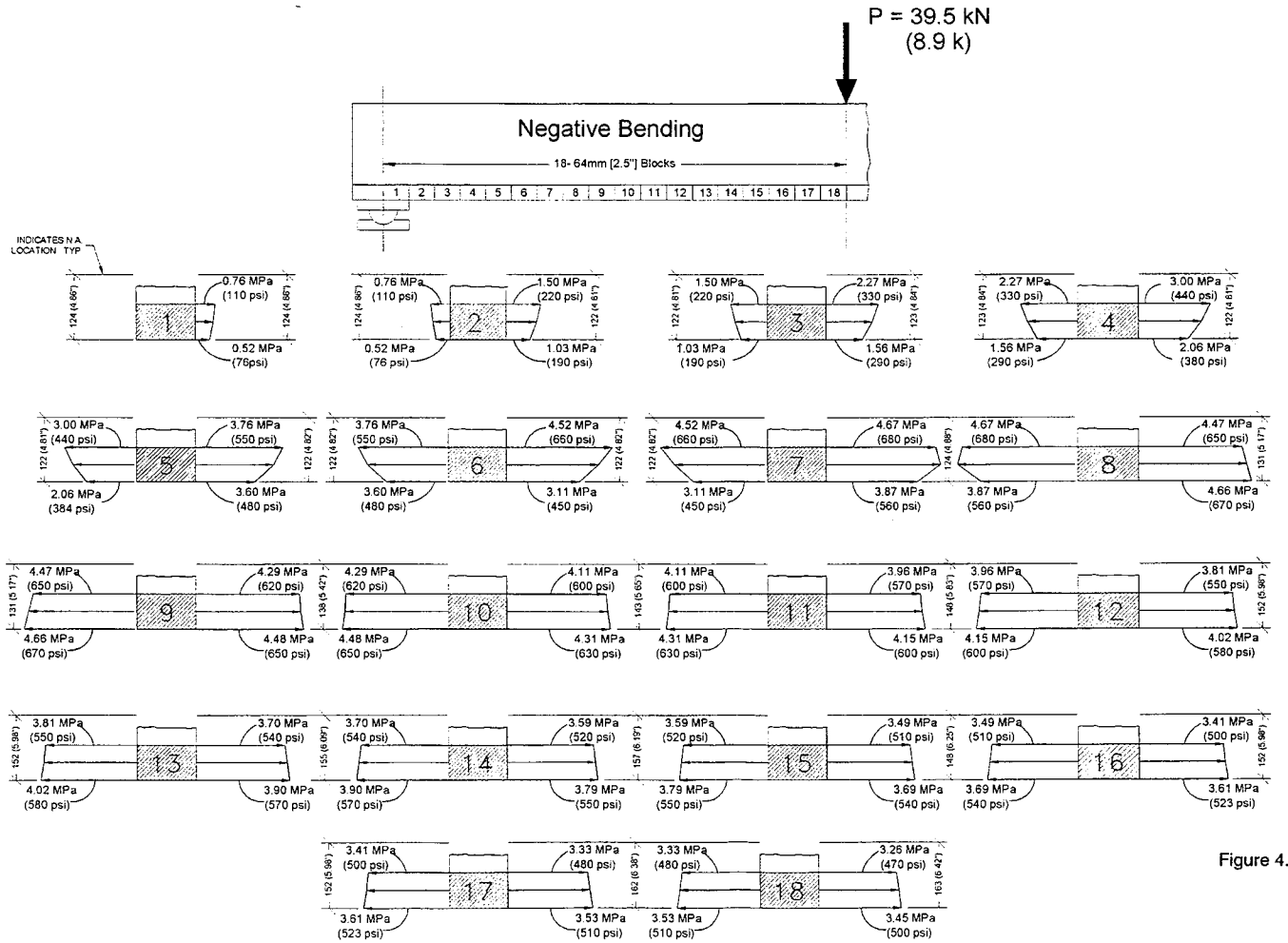

Figure 4.35 Stress Profiles on Overlay Concrete Blocks with 8.9 kN Load Applied Creating Negative Bending.

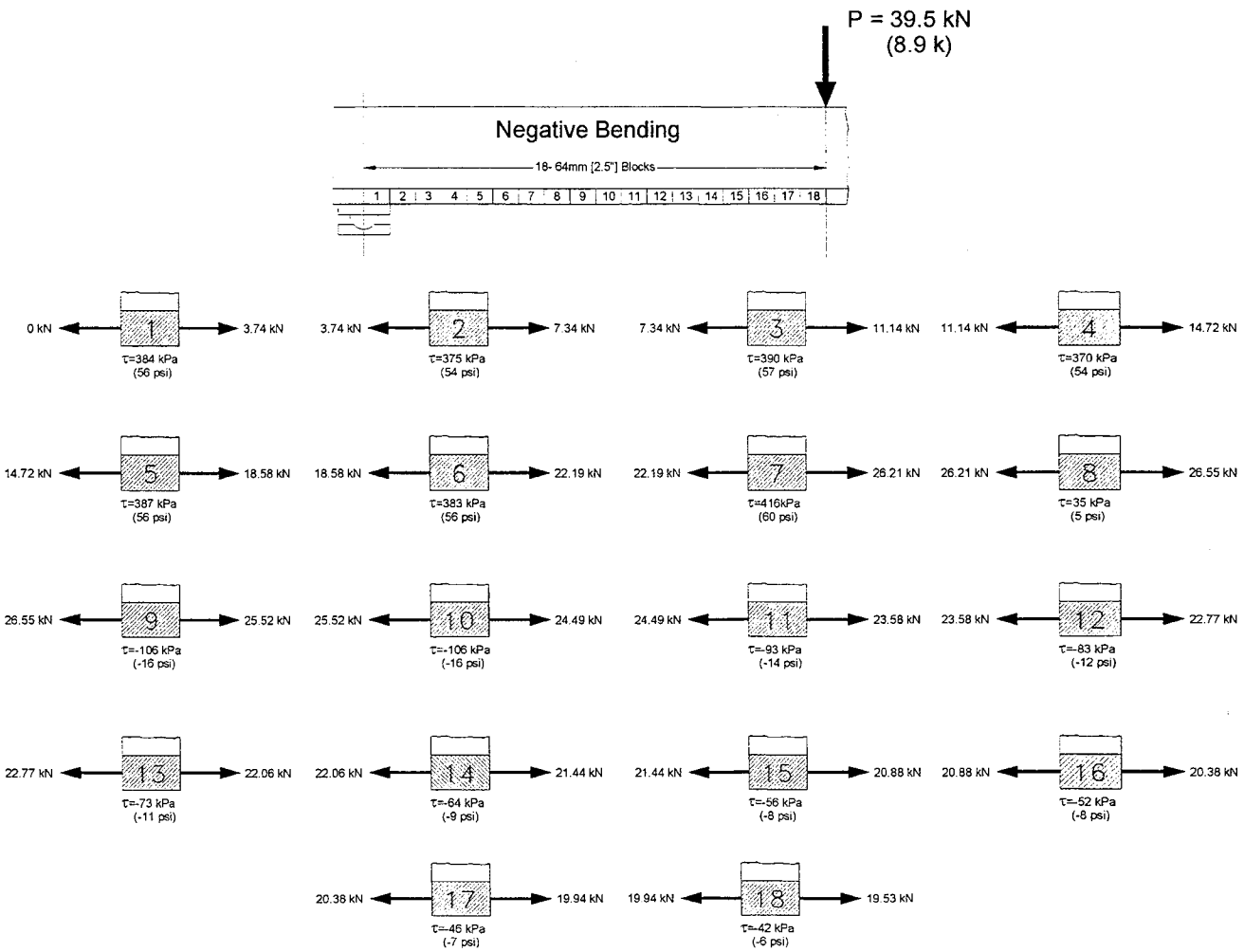

Figure 4.36 Forces and Corresponding Shear Stress on Overlay Concrete Blocks with 8.9 kN Load Applied Creating Negative Bending.

CHAPTER 5

TESTING OF A BRIDGE SUBASSEMBLY

The observations made in Chapters 3 and 4 are based on specimens that do not necessarily represent the state of stress and deformations in an actual bridge. Therefore, a 1/3-scale bridge specimen was constructed and tested in order to more realistically evaluate the behavior of overlays placed over sealed decks. Prior to loading the specimen to its ultimate limit state, multi-reference modal tests and service-level fatigue loading were conducted. The test specimen, its behavior under service loads, and responses beyond service loads are described in this chapter.

5.1 Description of Test Specimen

The test specimen was modeled after HAM-126-0881 which was deemed to be a representative steel stringer bridge in Ohio. Moreover, a detailed analytical model of the bridge was available from a previous study (K.A. Grimmelsmann, 1997), and could readily be used for the analytical studies required to establish the test specimen. Pertinent details of this bridge are shown in Figures 5.1 to 5.3. As discussed in Chapter 4, bond strength between overlays and decks is more critical when the overlay is subjected to positive moments. Therefore, a simply-supported specimen was selected, and was subjected to loads producing positive moment in the deck. The test specimen represented a 1/3-scale model of the free-body diagram of the prototype bridge (HAM-126-0881) between the inflection points of the midspan. A simple two-dimensional computer model of the prototype bridge was constructed and loaded by a moving truck. For the load position producing the most critical midspan positive moment, the inflection points for the midspan were established by examining the deflected shape and moment diagram. The distance between the inflection points was found to be 16.8 m. (55.1 ft.) which would correspond to a simple span length of 5.6 m. (18.4 ft.) for the 1/3-scale test specimen. The actual span in the test specimen was rounded to 5.49 m. (18 ft.). The test specimen was

further simplified by using only three girders instead of five girders in the prototype structure. The transverse distance between adjacent girders corresponded to 1/3 of that in the prototype structure (see Figure 5.2). The slab on either side of the edge girders was extended by 305 mm. (12 in.) similar to common practice in steel stringer bridges. Therefore, the specimen was 2.4 m. (8 ft.) wide as seen from Figure 5.4.

Standard similitude principles were followed closely to establish the member sizes in the test specimen. For example, the girders in the prototype bridge are W36x182; therefore, the corresponding members in the test specimen should be 1/3 as deep; the flange width, and flange thickness and web thickness be 1/3 of those in W36x182; moment of inertia be $(1/3)^4$ of that for W36x182; and the cross-sectional area be $(1/3)^2$ of that for W36x182. Keeping these constraints in mind, W12x19 was selected for the girders in the test specimen. This member is a very reasonable 1/3-scale model of W36x182. The same concepts were followed to size the bracing members and their spacing in the test specimen. In the prototype bridge, 22 mm.x127 mm. (7/8 in. x5 in.) studs are spaced at 305 mm. (12 in.) on center. The smallest available studs are 6.4 mm.x35 mm. (1/4 in.x1.375 in.) or 9.5 mm.x41.3 mm. (3/8 in.x1.625 in.). The former size studs were used in the test specimen as the stud diameter could be scaled down more closely. The studs were spaced at 102 mm. (4 in.) on center in the test specimen. The deck thickness of 76 mm. (3 in.) was simply 1/3 of that in the prototype bridge. Assuming a 76 mm. (3 in.) thick overlay for the prototype bridge, the overlay thickness in the test specimen was set to 25 mm. (1 in.). The specimen details are summarized in Figure 5.4.

Selection of the slab reinforcement proved to be more challenging due to the availability of deformed bars. As seen from Figure 5.2, the longitudinal and transverse reinforcing bars in the prototype bridge vary in size and spacing. To simplify fabrication of the test specimen, it was decided to minimize the spacing and size of the reinforcing bars. Maintaining the appropriate scaled area of steel per unit length, the spacing and bar sizes shown in Figure 5.5 were obtained.

5.2 Fabrication

A steel subassembly consisting of the steel girders and cross braces was fabricated first by a bridge fabricator. The cross braces were welded to the girders. At the location of the supports, 13 mm. (0.5 in.) stiffener plates were welded on both sides of the web to prevent the possibility of local buckling. At five locations, the girders were supported on load cells which had been anchored to concrete pedestals which were 610 mm. (24 in.) in diameter and 508 mm. (20 in.) high. As seen in Figure 5.6, each load cell was capped by a roller. The sixth support was exactly identical to the other supports except that it had not been strain gauged. The pedestals were aligned and leveled, and were hydrostoned to the laboratory's strong floor. Special care was taken to ensure that the web stiffeners would line up with the rollers on top of the supports.

The formwork was constructed, and the top and bottom reinforcing bars were tied in place. The bridge deck was poured. The deck concrete was standard ODOT class S concrete, except that the coarse aggregate was 9.5 mm. (3/8 in.). The deck was wet cured for one week. Similar to the previous specimens described in Chapters 3 and 4, the overlay was not applied until after the shrinkage of the deck concrete had effectively stopped. The data from two shrinkage bars were monitored. From Figure 5.7, it is apparent that the specimen could have been overlaid at the end of the second week in April; however, the application of the overlay was conservatively delayed by one week to allow further reduction of shrinkage. At the end of the third week of April, surface preparation for overlaying the deck commenced.

Surface preparation began with sandblasting the existing deck. Shortly after completion of sandblasting, Sika Pronto High Molecular Weight Methylmethacrylate (HMWM) was applied with a paint roller according to the product literature.

Based on the observations made earlier in Chapters 3 and 4 and product literature, 6.8 to 9.1 kg (15 to 20 lbs.) of sand was broadcast over HMWM while the sealer was curing. The sealer was allowed to cure beyond the recommended 12 to 16 hours to allow adequate

penetration of HMWM into the deck and sufficient curing. After completion of the surface preparations, ODOT standard mircosilica overlay concrete was applied. Once again, the microsilica overlay mix was identical to ODOT's specifications except that 9.5 mm. (3/8 in.) coarse aggregates were used. The deck was 48 days old when the overlay was applied. The overlay was wet cured for three days. Service-level fatigue loads were applied to the specimen when the overlay was 9 days old.

5.3 Material Properties

The material properties of steel girder web and flanges, and the reinforcing bars were established by ASTM E8 standards. The concrete properties were measured according to ASTM C469 standard tests. The concrete compressive strengths for the deck and overlay concrete, and modulus of elasticity are summarized in Table 5.1. The measured stress-strain curves for the reinforcing bars, flange and web of the steel girders, and bracing angles are illustrated in Figures 5.8, and presented in Table 5.2.

5.4 Experimental Program

The test specimen was subjected to fatigue service-level loading as well as statically-applied loads beyond service loads. In either case, the loading was intended to simulate one HS-20 truck which was represented by four wheel loads for simplicity. That is, the front two axles of a HS-20 truck were combined into one axle located at the centroid of the front two axles, as shown in Figure 5.9. Therefore, the distance between the axles for the one-third scale, two-axle equivalent truck is 5.12/3 = 1.71 m. (16.8/3 = 5.6 ft.). This distance was rounded to 1.68 m. (66 in.). The transverse distance between the wheels is 610 mm. (24 in.) which corresponds to 1/3-scale equivalent of the distance for HS-20 trucks. As loads are scaled down by $(1/3)^2$, the front and back axles for the one-third scale, simplified HS-20 truck have to induce 178/9 = 19.8 kN (40/9 = 4.44 kips) and 142/9 = 15.8 kN (32/9 = 3.56 kips), respectively. The one-third scale, equivalent two-axle truck is illustrated in Figure 5.9.

The test setup for the fatigue and static tests was different due to the differences

between the required level of loads. Each test apparatus is described in the following.

5.4.1 Test Setup

For the fatigue tests, the force from a single 668-kN (150-kip) servo-controlled actuator was transferred to the bridge through a transfer frame (made of three W10x30 members) representing the two-axle equivalent truck. The transfer frame rested on 152mm.x152mm.x12.7mm. (6 in.x6 in.x1/2 in.) steel plates to simulate the contact between truck wheels and bridge deck. The general layout of the test setup is shown in Figure 5.10 with additional details provided in Figure 5.11. A number of wood blocks surrounding the transfer frame were glued to the deck in order to prevent potential sliding of the frame during fatigue testing. The actuator was positioned at the centroid of the equivalent two-axle equivalent truck, refer to Figure 5.11c.

The reaction frame used for the fatigue tests was inadequate to resist 890 kN (200 kips) which was the level of load anticipated (based on preliminary nonlinear analyses) to produce a significant level of inelastic deformations and yielding in the test specimen. In lieu of fabricating a very large and expensive reaction frame similar to that used for fatigue tests, static loading of the test specimen beyond service load was accomplished by four 267-kN (60-kip) center-hole hydraulic jacks. These jacks reacted against 28.5 mm. (1.125 in.) high-strength threaded rods connected to two W14x68 reaction beams which had been post-tensioned to the laboratory's strong floor. The threaded rods passed through 38 mm. (1.5 in.) holes in the deck. The jacks were positioned on the specimen at the same locations where the transfer frame was in contact with the deck during the fatigue tests. Under each jack, 292 mm.x197 mm.x25 mm. (11.5 in.x7.75 in.x1in.) plates were used as bearing plates. (The plates were positioned such that their long dimension was along the specimen's transverse direction.) The hydraulic jacks were connected to a single pump; hence, the load at each point would be fairly close to each other. Note that for the equivalent two-axle truck, the loads at the front and rear axles are different by 25% (see Figure 5.9). Therefore, the static loads applied to the specimen do not exactly

correspond to those expected for a truck. The small difference between the front and rear axle loads was deemed insignificant. The test setup for static tests is shown in Figure 5.12.

5.4.2 Instrumentation

The instrumentation layout was essentially the same for the fatigue and static tests. The test specimen was instrumented to measure (a) deflections of the steel girders, (b) strains in the webs and flanges at selected locations along the steel girders, (c) strains in selected bracing elements, (d) concrete strain in the top and bottom faces of the slab near the midspan of the middle girder (e) strains in the slab top and bottom reinforcing bars close to the midspan over the middle girder, (f) rotation of the west and middle girders over the supports, (g) applied loads, and (h) reactions at five supports. The instrumentation details are summarized in Figures 5.13 to 5.16. In order to measure the support reactions, special load cells were fabricated and calibrated, as summarized in Appendix F.

5.4.3 Testing Procedure

Multi-reference impact testing was originally conducted to establish the frequencies and mode shapes of the virgin specimen. A detailed description of the modal testing is provided in Appendix G. As seen from Figure 5.9, the total load from a 1/3-scale HS-20 truck is 35.6 kN (9 kips). Assuming an impact factor of 1.3, the expected service load is about 48.9 kN (11 kips). Following the modal tests, the specimen was loaded statically up to 48.9 kN (11 kips) to obtain data regarding its initial behavior, mostly stiffness and load distribution. Subsequently, the specimen was subjected to 1,000,000 cycles of fatigue loading. The fatigue load of 48.9 kN (11 kips) was applied at 5 Hz. After completion of 200,000, 400,000, 600,000, 800,000, and 1,000,000 cycles, fatigue testing was stopped to evaluate the specimen's behavior. For each test, the specimen was statically loaded up to 48.9 kN (11 kips) in order to monitor changes in stiffness, strains, and load distribution. In addition, the deck was inspected visually for cracks and any signs of overlay delamination. Upon completion of fatigue loading, multi-reference modal tests were once again conducted. Finally, the test specimen was loaded statically

beyond service loads to examine its behavior at or near ultimate limit state.

5.5 Test Results

Relevant results from each phase of testing are summarized in the following sections.

5.5.1 Modal Tests

The frequencies and mode shapes of the first 6 modes before and after the application of fatigue loads are summarized in Table 5.3, and compared in Figure 5.17, respectively.

The measured frequencies after fatigue loading are generally smaller. Such a trend may suggest a reduction in the stiffness due to opening of the existing micro shrinkage cracks in the deck and/or overlay, delamination of the overlay, and reduction of concrete stiffness as a result of low-cycle fatigue. Note that, however, the frequency reductions are within acceptable resolution of modal testing which is generally taken as about ± 5%. Moreover, the mode shapes before and after fatigue loading are essentially identical, and do not show any shift in the original dynamic characteristics of the specimen.

The aforementioned discussion indicates that the stiffness of the test specimen remained apparently unchanged after it was subjected to 1,000,000 cycles of service-level loads similar to those for actual bridges. Therefore, the bond strength of overlays placed over sealed bridge deck is adequate, and is not influenced by service-level loads. This conclusion was also verified by examining the changes in a number of critical responses obtained by subjecting the specimen to service loads higher than those imparted during modal testing.

5.5.2 Intermediate Static Tests During Fatigue Loading

As mentioned previously, fatigue loading was stopped intermittently to examine the influence of repeated loading on the performance of bond between the overlay and deck. After completion of 200,000, 400,000, 600,000, 800,000, and 1,000,000 cycles, the specimen was statically loaded up to 48.9 kN (11 kips). The measured strains for each phase are summarized in Table 5.4, and the corresponding deflected shapes of the girders are plotted in Figure 5.18.

The measured strains and deflections point to the same observations made from examining the specimen's dynamic characteristics. The strains at various locations did not essentially change. The small variations in the measured deflections are within the accuracy of the displacement transducers (± 0.076 mm. (± 0.003 in.)). The values reported in Table 5.4 and Figure 5.18 are for the total static load equal to 48.9 kN (11 kips). Similar trends were observed for smaller loads. Therefore, service-level fatigue loading did not deteriorate the available bond between the overlay and sealed deck

5.5.3 Ultimate Static Loading

To examine the available bond strength between overlays and decks under overload conditions, the test specimen was statically loaded as described in Section 5.4.1. The loading was continued until a significant level of yielding and/or deformations was produced.

The measured load-deflection curves at various locations (refer to Figure 5.13 for the locations of the displacement transducers) are shown in Figure 5.19. The experimental data show the extensive level of inelastic deformations experienced by the specimen. The maximum load applied to the specimen was 805 kN (181 kips). This load is equivalent to approximately 20 times the load from one HS-20 truck. The specimen experienced a maximum deflection of 58 mm. (2.28 in.). The maximum deflection corresponds to L/94 where L = span of the test specimen. Hence, the specimen had effectively reached its ultimate limit state when testing was stopped.

The extent of inelastic deformations may also be seen from the measured strains. The girders at a number of locations were found to have significantly yielded, and the concrete strain close to the midspan of the middle beam reached a maximum value 2300 micro strain. Note that the capacity of slab is established based on a usable strain of 3000 micro strain.

At the conclusion of testing, a careful examination of the test specimen did not reveal any evidence of bond failure. Therefore, the specimen could develop its capacity without any

problems associated with bond strength of the overlay placed over the sealed deck.

A comprehensive synthesis of the measured data is currently underway to examine the load distribution at various stages of testing and evaluate composite interaction between the deck and girders. Moreover, detailed analytical studies are also being conducted in order to improve modeling of steel stringer bridges under service loads and beyond the elastic limit state. These studies are reported in another report (Cole, 1999).

5.6 Summary

In an effort to validate the reliability of the lessons learned in Chapters 3 and 4, a large-scale test specimen closely representing steel stringer bridges was fabricated and tested. The deck was sealed with HMWM and overlaid with micro-silica concrete. Prior to the application of the overlay, sand was broadcast over the sealed deck. The specimen was subjected to 1,000,000 cycles of service-level fatigue loads, as well as static loads producing significant inelastic deformations and yielding. A detailed evaluation of the measured data does not suggest any adverse influence of HMWM sealers on the available bond strength so long as the sealed deck is prepared by a secondary process (such as broadcasting sand) prior to the application overlay.

Table 5.1 Deck and Overlay Concrete Compressive Strength

Deck Concrete	60.7 MPa (8.8 ksi)
Overlay Concrete	51.8 MPa (7.5 ksi)

Table 5.2 Summary of Measured Structural Steel Properties

Region	Es (ksi)	Fy (ksi)	Fu (ksi)	εsh	εf
Flange	28750	53.5	68.1	0.0186	0.251
	33159	51.2	68.4	0.0145	0.232
Avg.	30954	52.3	68.2	0.0165	0.242
Web	29998	56.6	76.5	0.0207	0.329
	29730	57.7	75.6	0.0148	0.495
Avg.	29864	57.1	76.1	0.0177	0.412
Brace	31804	52.3	74.2	0.0346	0.330
	30635	52.5	73.6	0.0274	0.329
Avg.	31219	52.4	73.9	0.0310	0.330

Table 5.3 Measured Frequencies (Hz) Before and After Fatigue Loading

Mode	Pre-Fatigue Test	Post-Fatigue Test	% Change
1	19.45	19.07	-1.97
2	26.48	25.43	-3.97
3	58.84	60.64	3.07
4	67.66	63.88	-5.59
5	80.43	76.97	-4.30
6	105.07	102.87	-2.09

Table 5.4 Measured Strains Under 48.9- kN (11-kip) Static Load
After Reaching Target Fatigue Cycles

Gage (μ strain)	Initial	After 200,000 Cycles	After 400,000 Cycles	After 600,000 Cycles	After 800,000 Cycles	After 1,000,000 Cycles
SG1	7	5	8	14	8	15
SG2	-5	-7	-5	-4	-7	-4
SG3	3	1	3	7	3	7
SG4	76	74	77	79	77	79
SG5	9	4	7	12	4	9
SG6	104	99	102	106	101	104
SG7	4	-2	2	8	-3	5
SG8	83	77	81	88	76	85
SG9	48	45	45	47	46	48
SG10	22	15	16	19	15	18
SG11	-15	-21	-22	-17	-21	-20
SG12	-11	-17	-17	-13	-17	-15
SG13	22	19	19	21	19	21
SG14	41	41	42	42	44	45
SG15	2	2	1	1	2	2
SG16	104	101	103	104	104	106
SG17	10	5	6	10	6	10
SG18	43	38	39	43	40	44
SG19	83	77	80	83	78	82
SG20	122	116	121	126	121	128
SG21	3	2	2	2	3	3
SG22	103	101	102	103	102	104
SG23	10	10	10	14	11	16
SG24	-16	-16	-17	-16	-17	-16
SG25	1	1	1	1	1	1
SG26	61	61	62	64	62	63
SG27	-1	-1	-2	-1	-1	-1
SG28	62	61	62	63	62	63
SG29	-2	-3	-8	-2	-3	-2

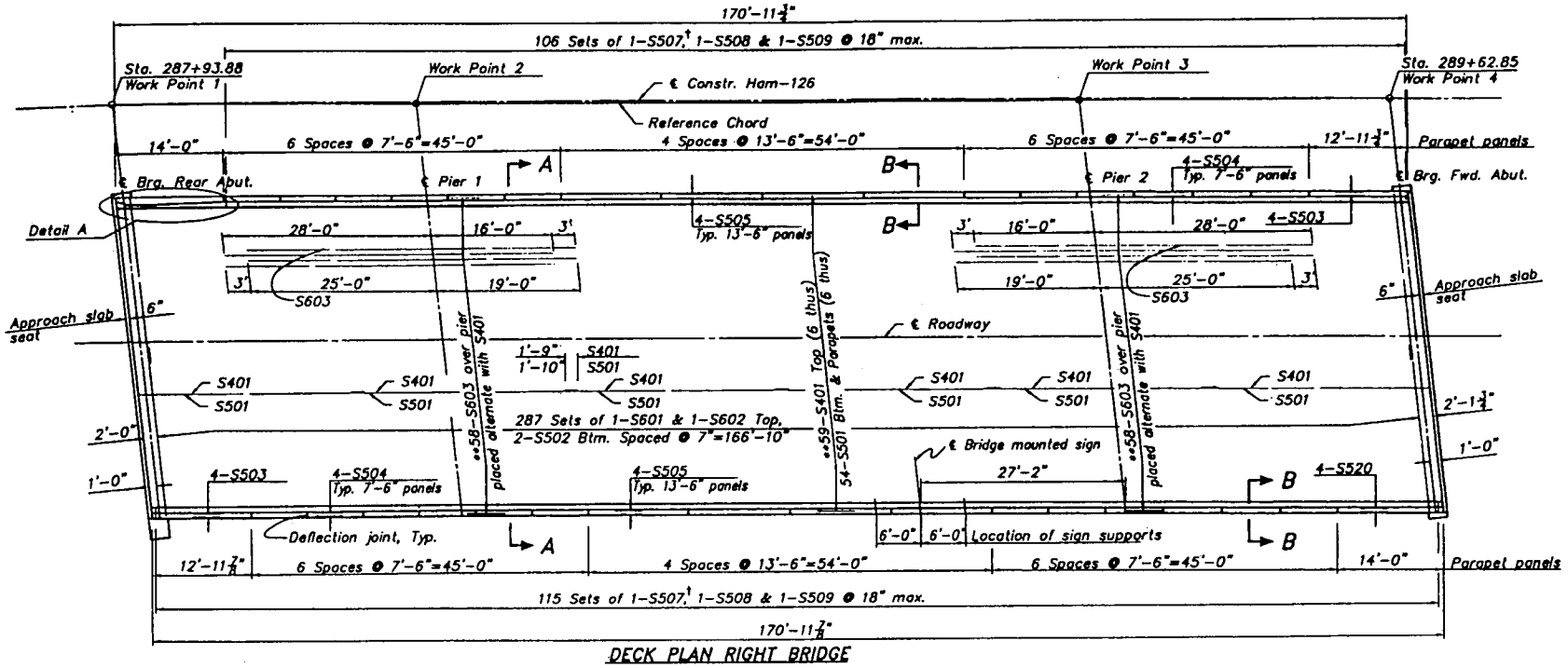

(Note: 1 in. = 25.4 mm.)

Figure 5.1 Floor Plan of Prototype Bridge (HAM-126-0881)

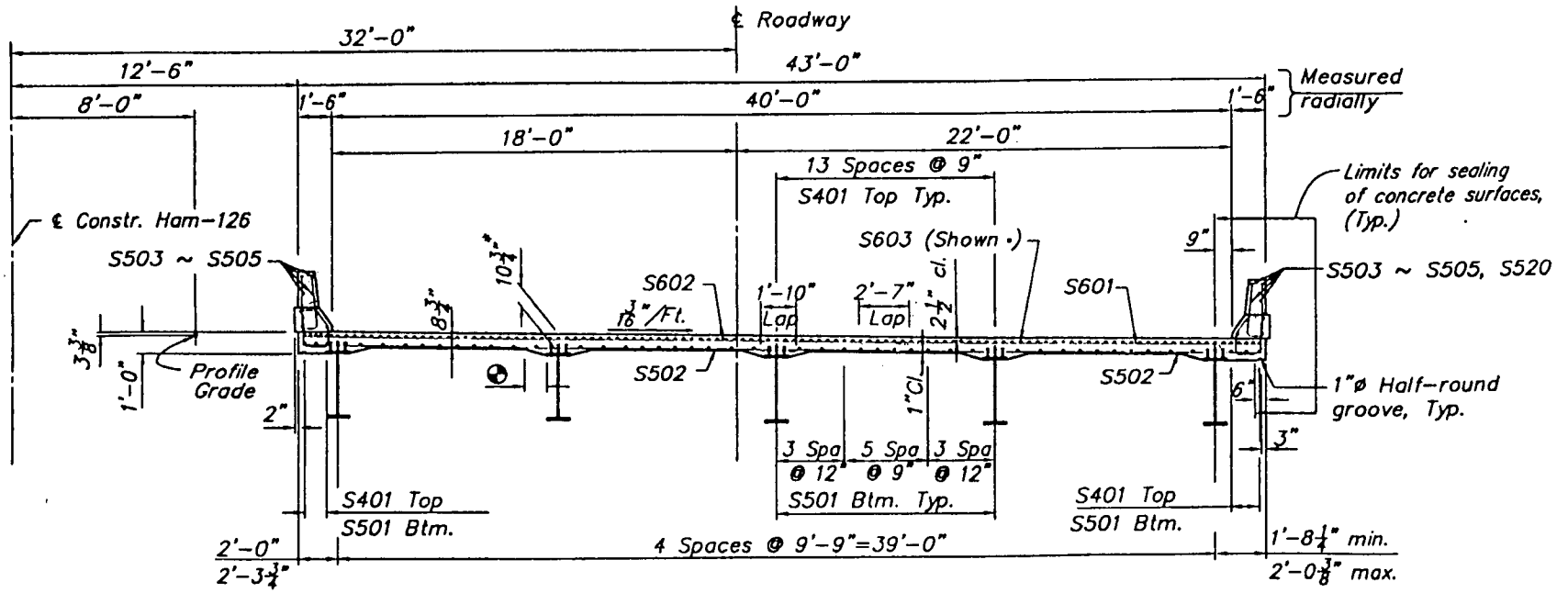

(Note: 1 in. = 25.4 mm.)

Figure 5.2 Cross Section View of Prototype Bridge (HAM-126-0881)

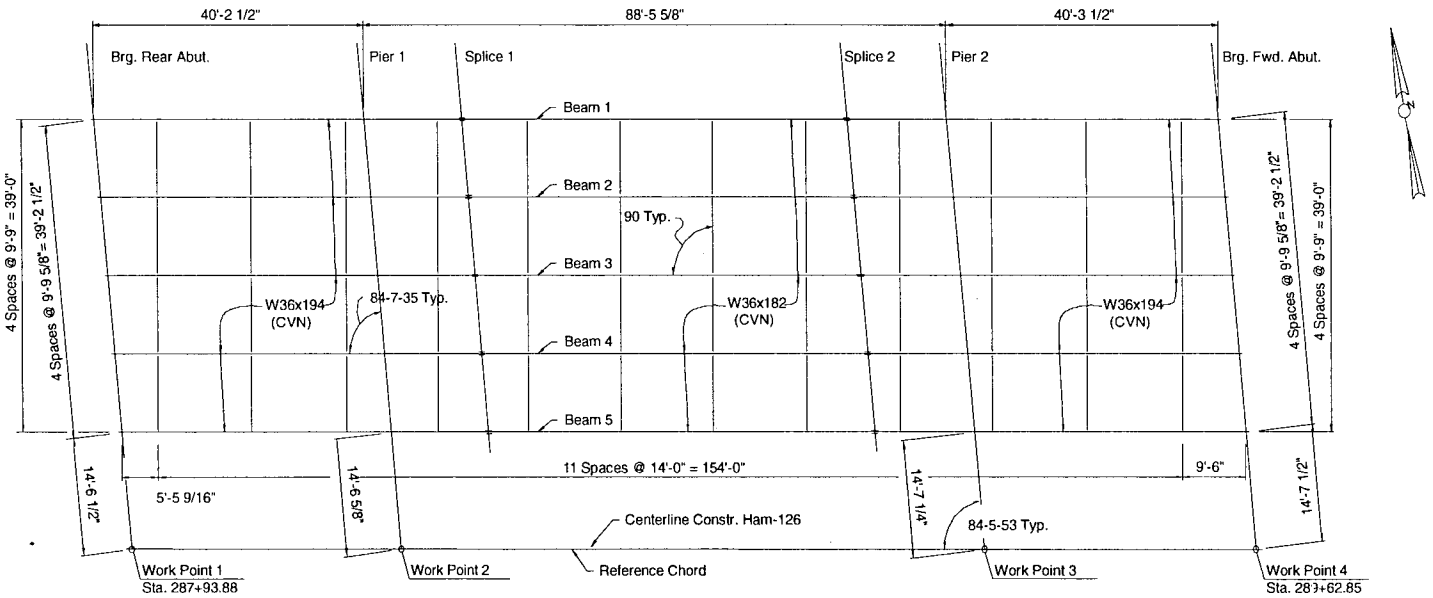

Framing Plan

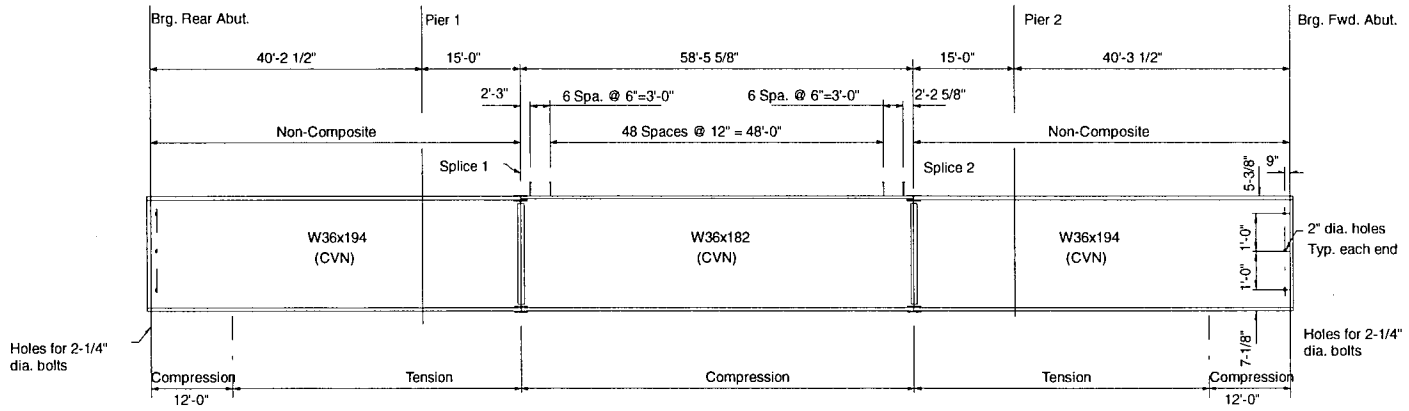

Beam Elevation

Figure 5.3 Details of Steel Girders in Prototype Bridge (HAM-126-0881)

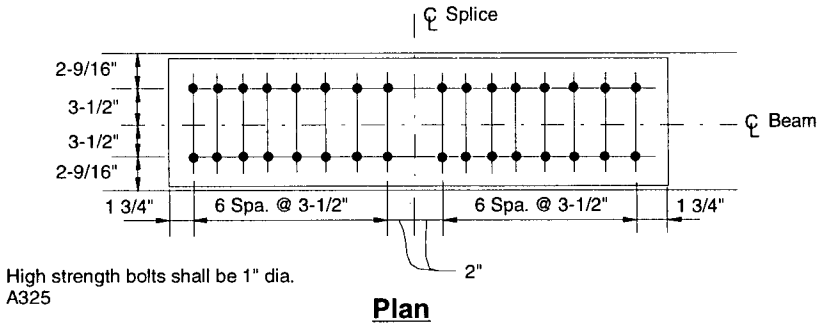

Plan

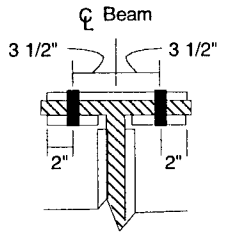

Section A-A

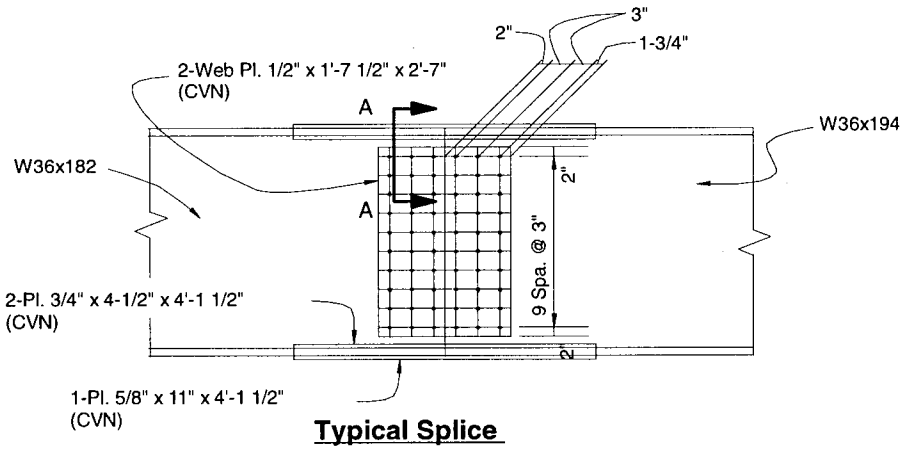

Typical Splice Detail Elevation

Shear Connector Detail

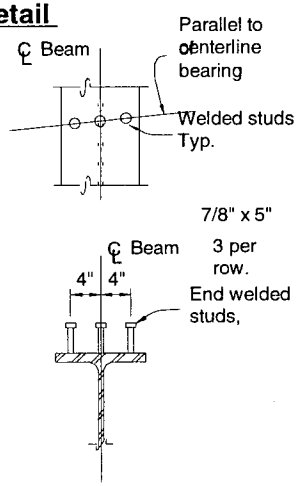

(Note: 1 in. = 25.4 mm.)

Figure 5.3 (Cont.) Details of Steel Girders in Prototype Bridge (HAM-126-0881)

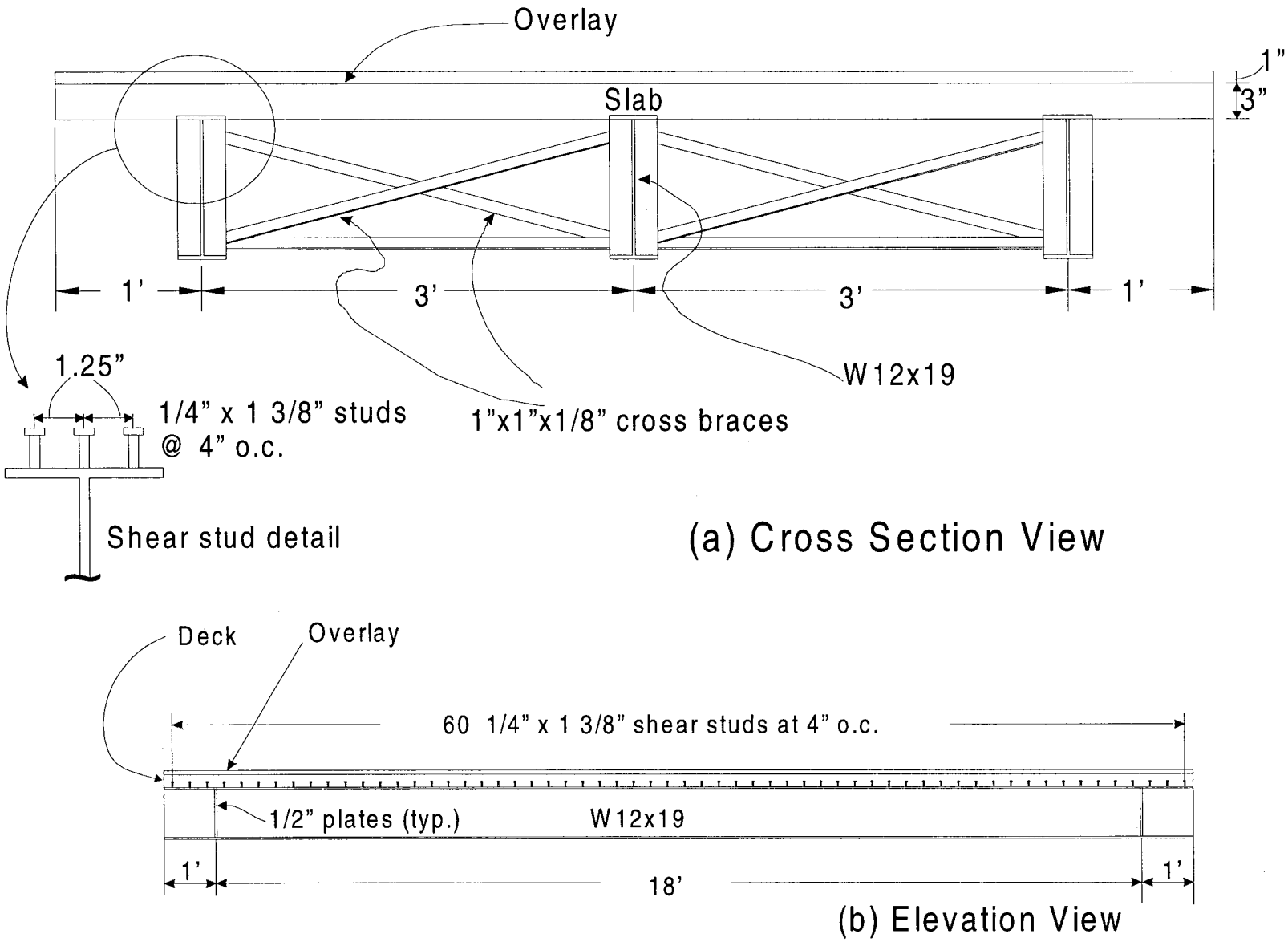

(Note: 1 in. = 25.4 mm.)

Figure 5.4 Specimen Details

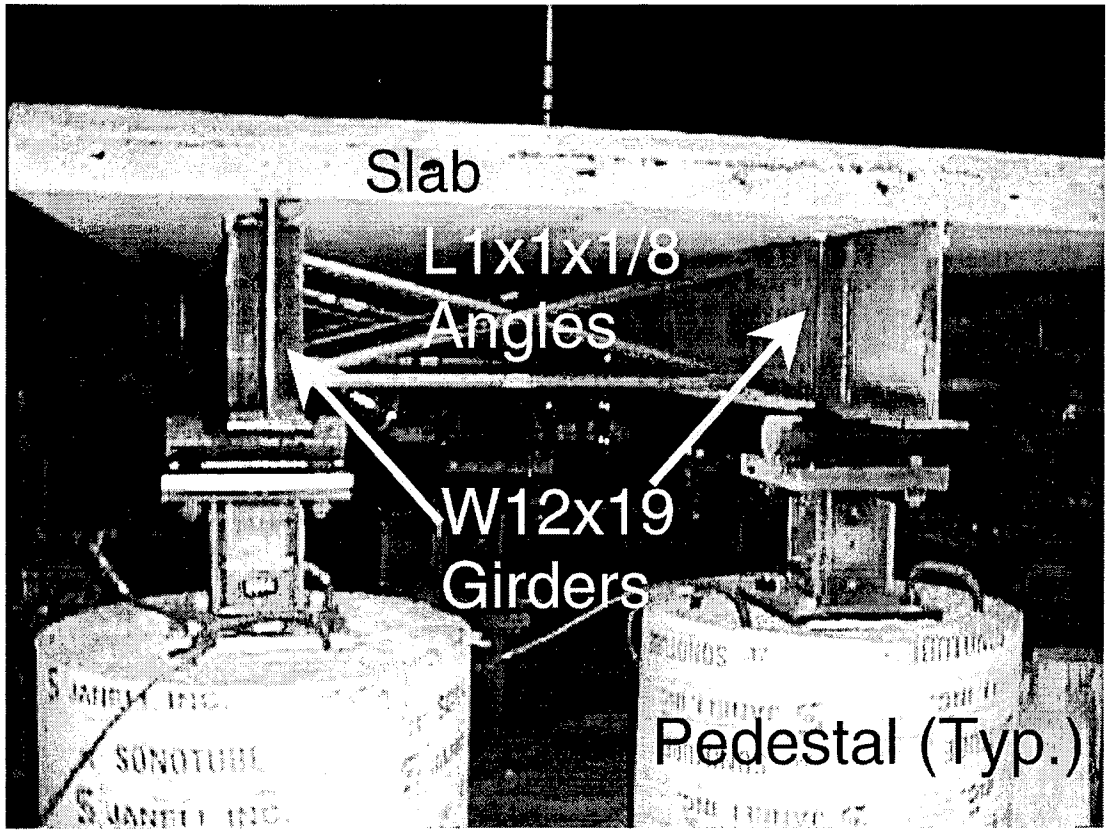

(C)General Layout

Figure 5.4 (Cont.) Specimen Details

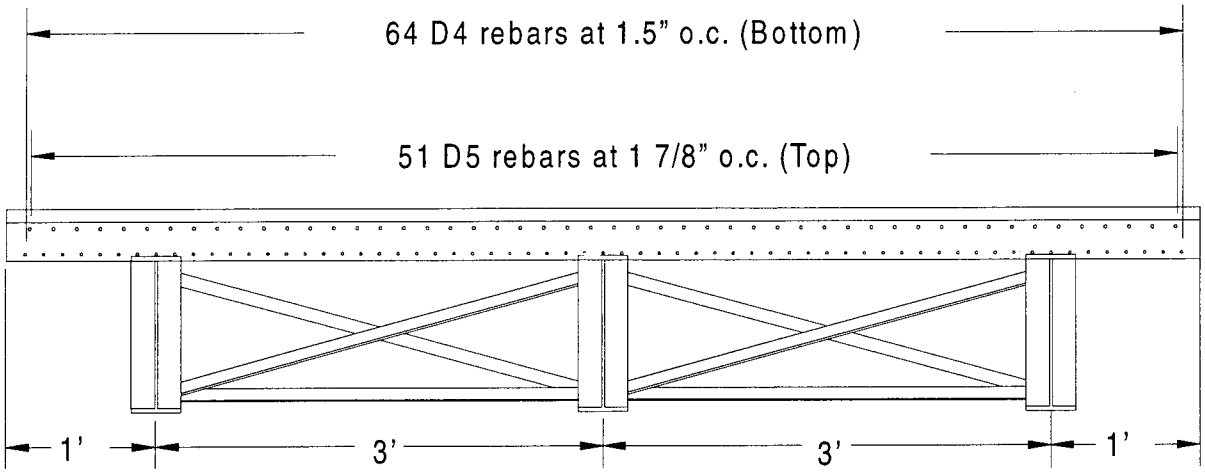

D4 : Deformed wire (d_b = 0.225 in; A_s = 0.04 in^2)

D5 : Deformed wire (d_b = 0.252 in; A_s = 0.05 in^2)

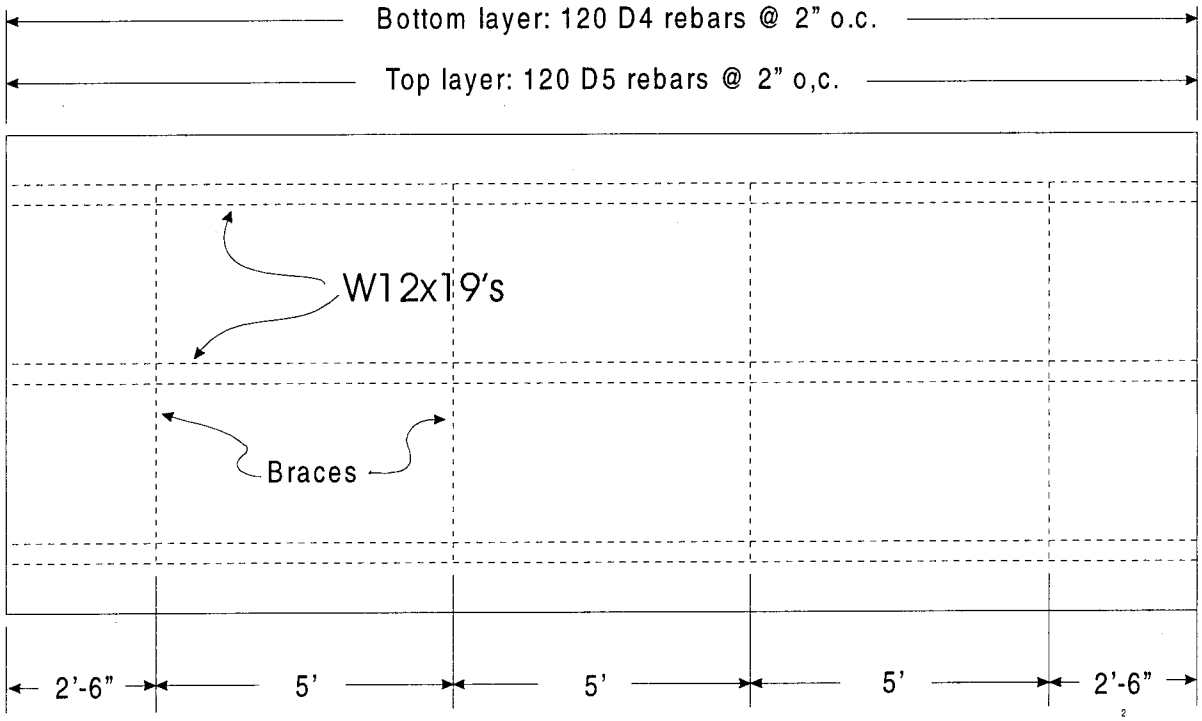

D4 : Deformed wire (d_b = 0.225 in; A_s = 0.04 in^2)

D5 : Deformed wire (d_b = 0.252 in; A_s = 0.05 in^2)

(Note: 1 in. = 25.4 mm.)

Figure 5.5 Slab Reinforcement

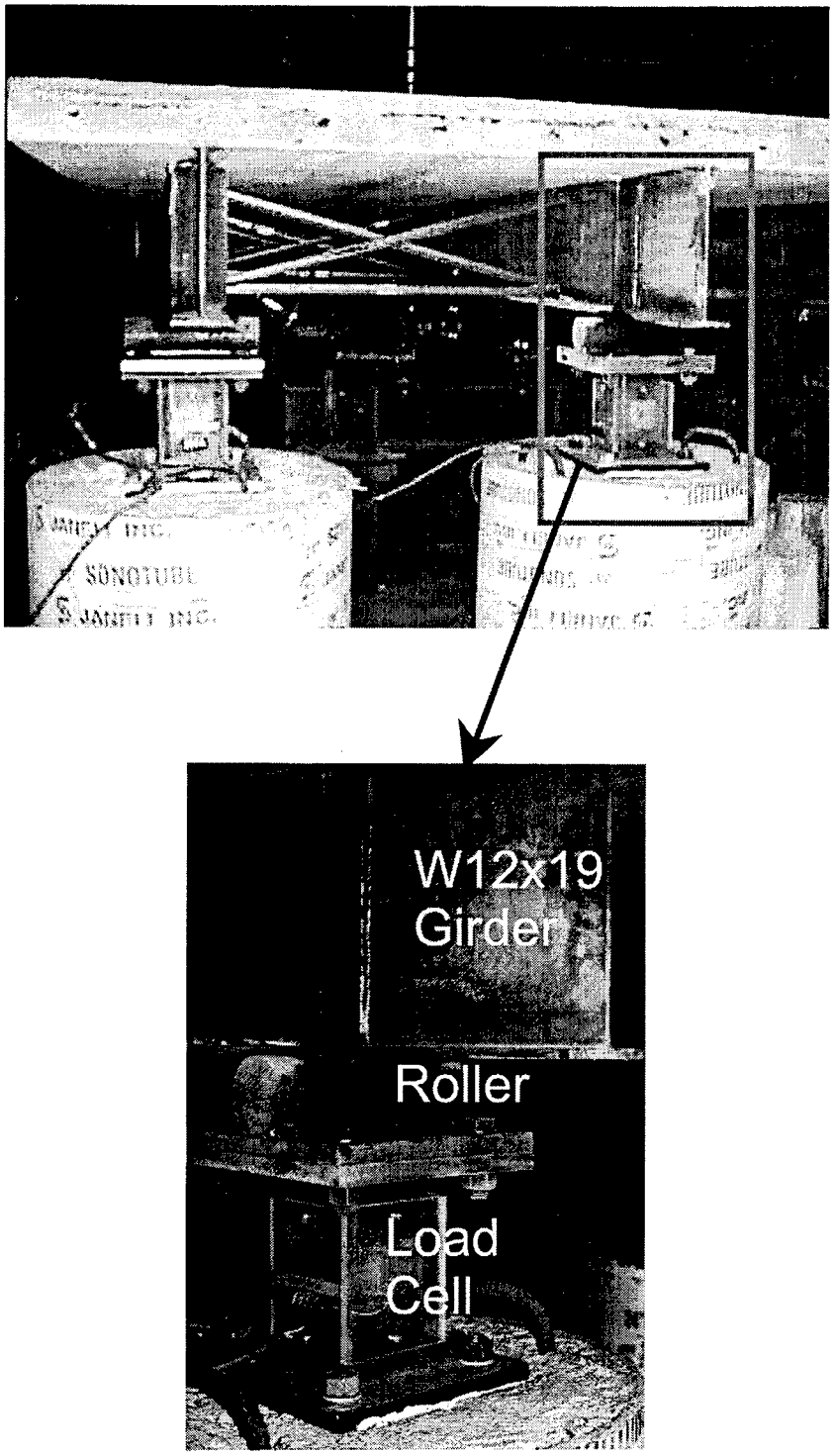

Figure 5.6 Details of Supports With Load Cells

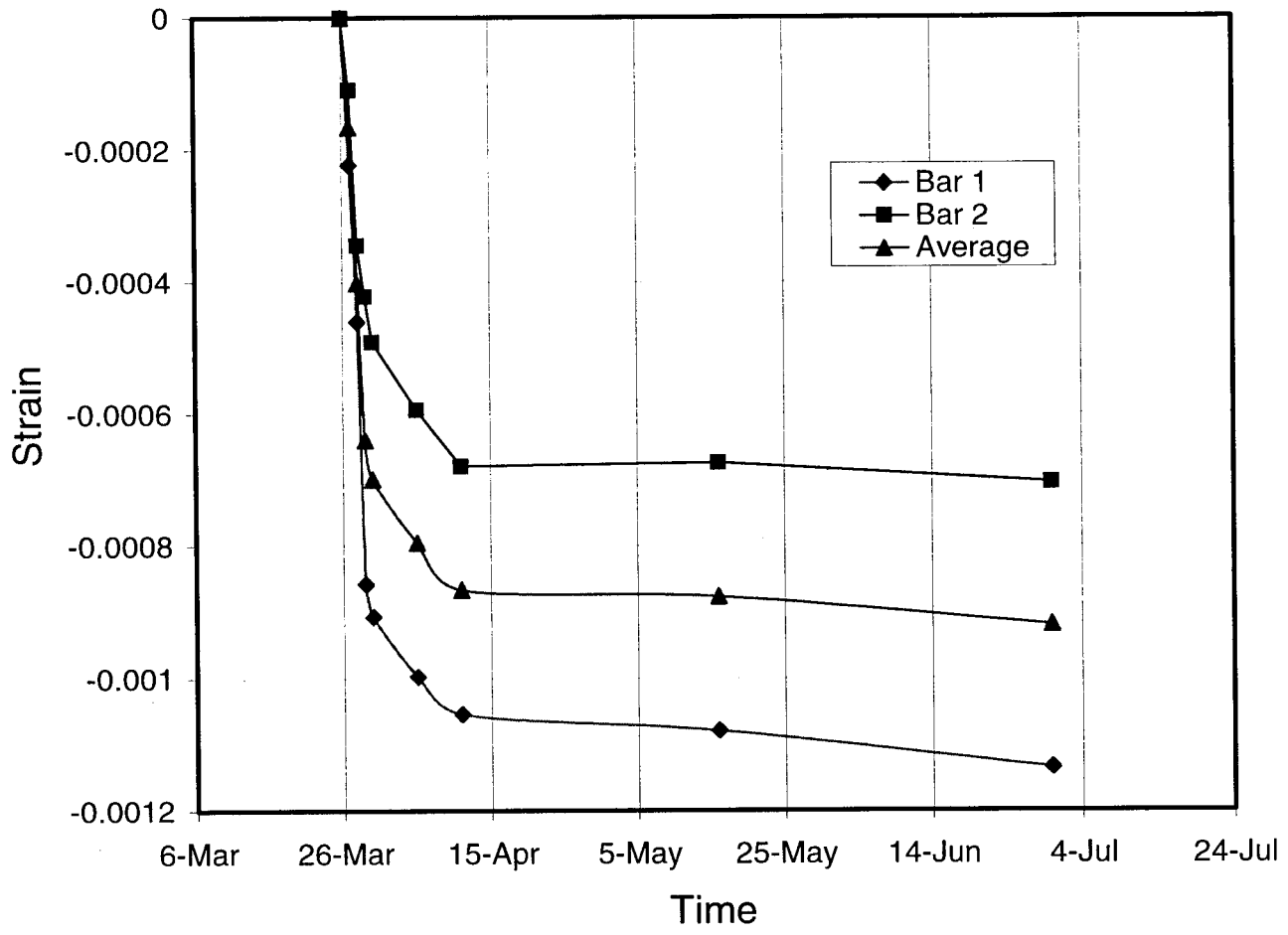

Figure 5.7 Shrinkage Behavior of Bridge Deck Concrete

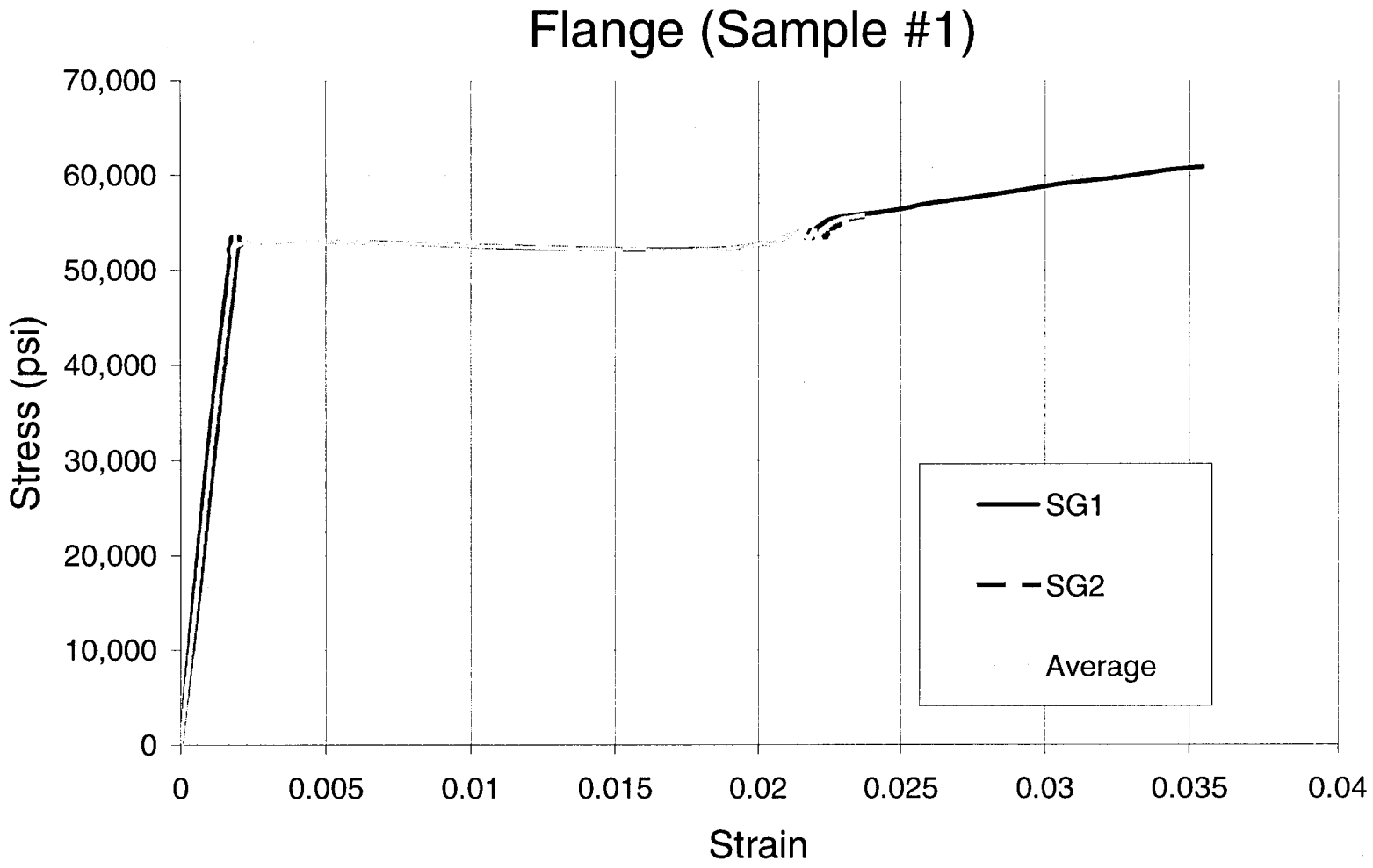

Figure 5.7 Representative Stress-Strain Curve for Structural Steel

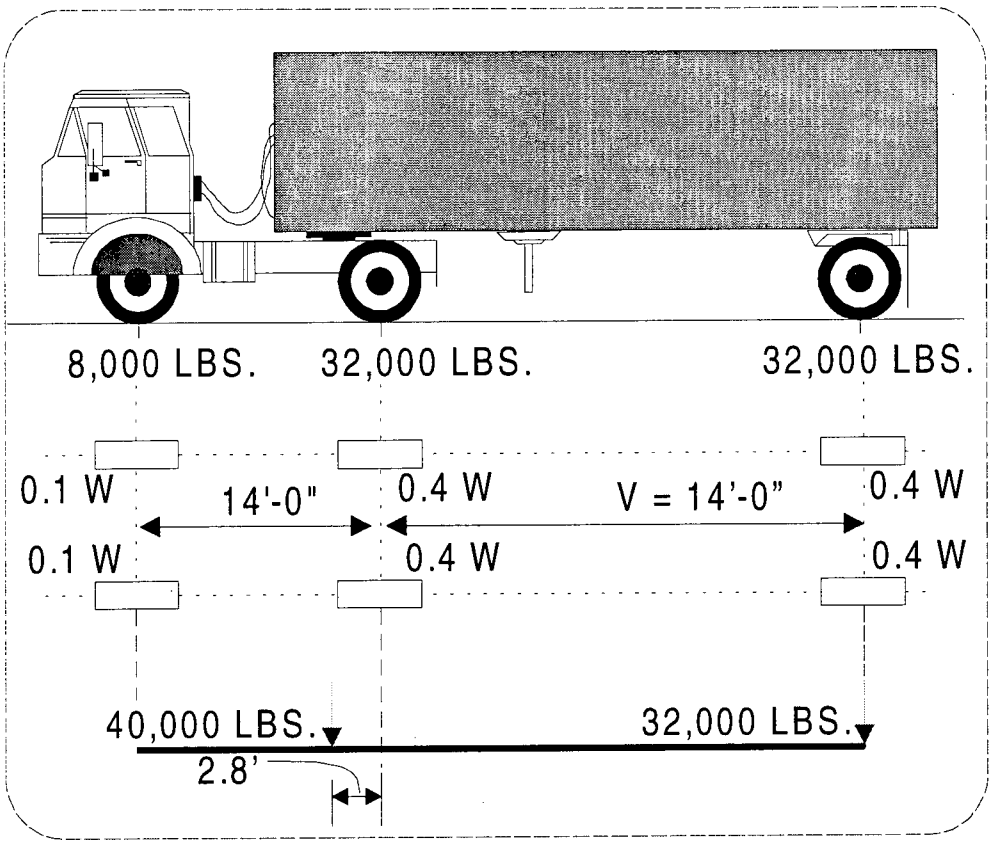

HS20-44

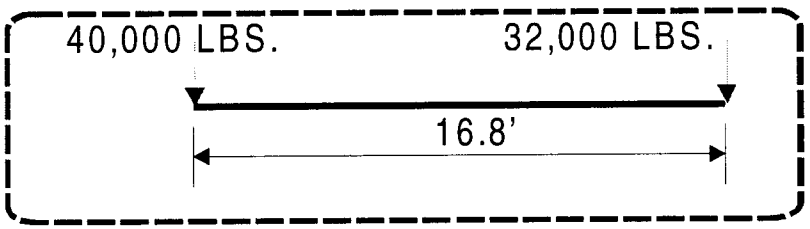

Equivalent two-axle truck
(Full scale)

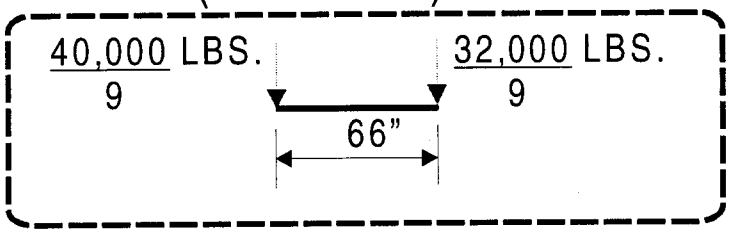

Equivalent two-axle truck
(One-third scale)

Note: 1 in. = 25.4 mm.

Figure 5.9 Idealization of HS-20 Truck for Testing

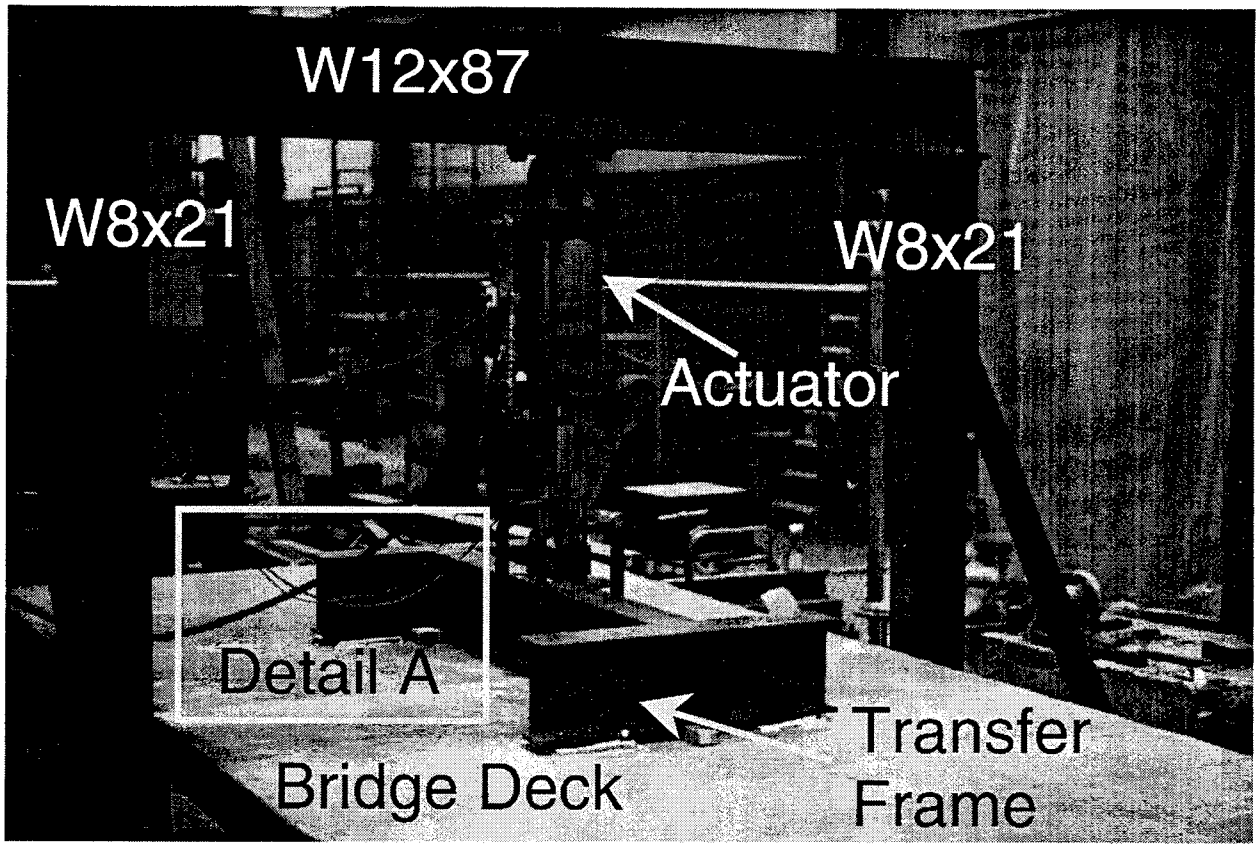

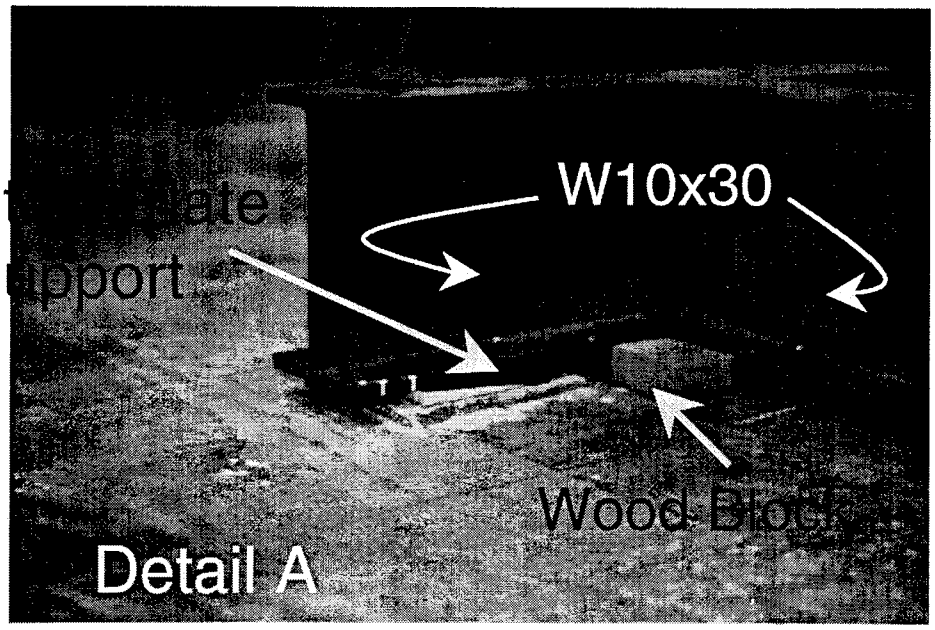

Figure 5.10 General Layout of Fatigue Test Setup

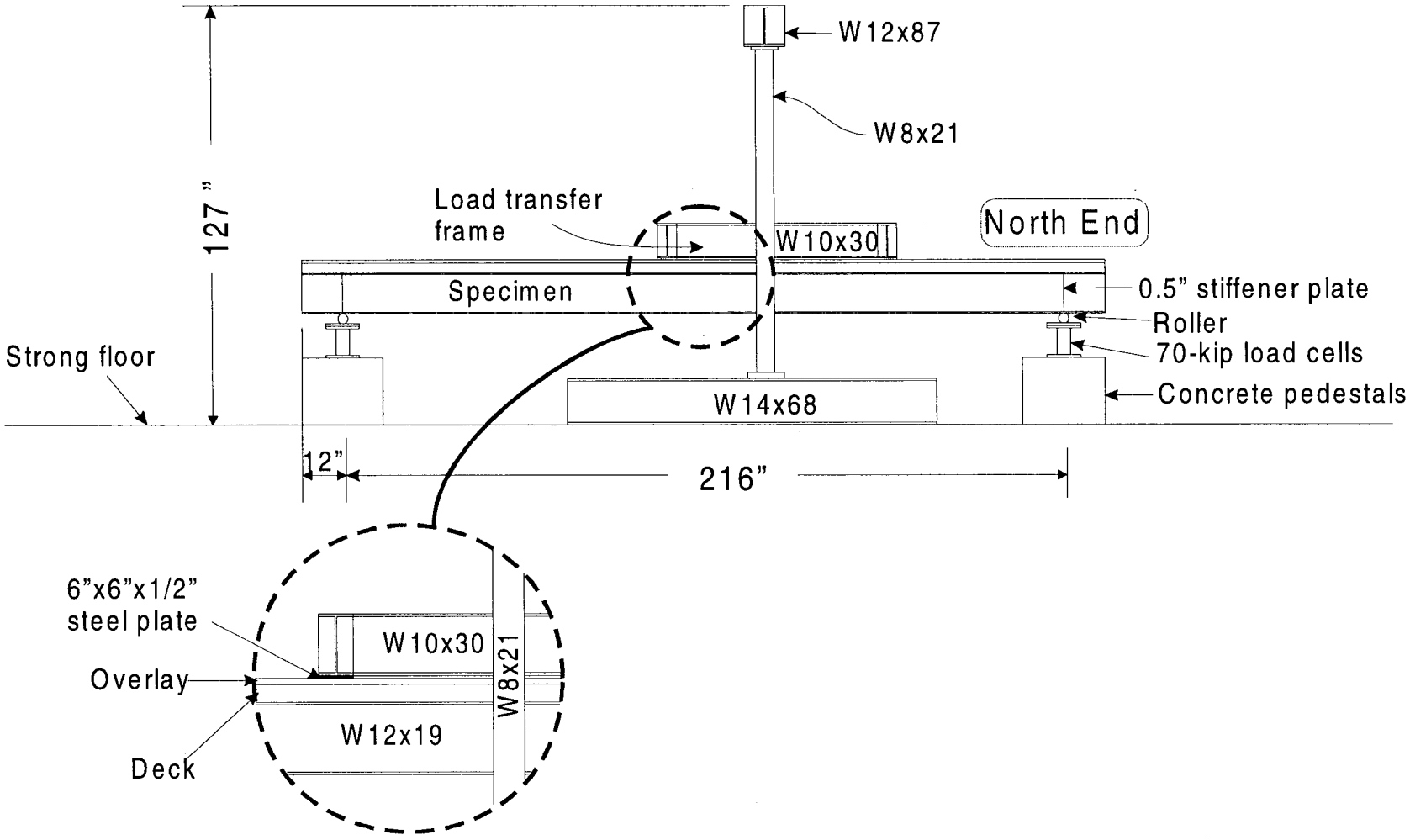

(a) Side View

Note: 1 in. = 25.4 mm.

Figure 5.11 Details of Test Setup for Fatigue Tests

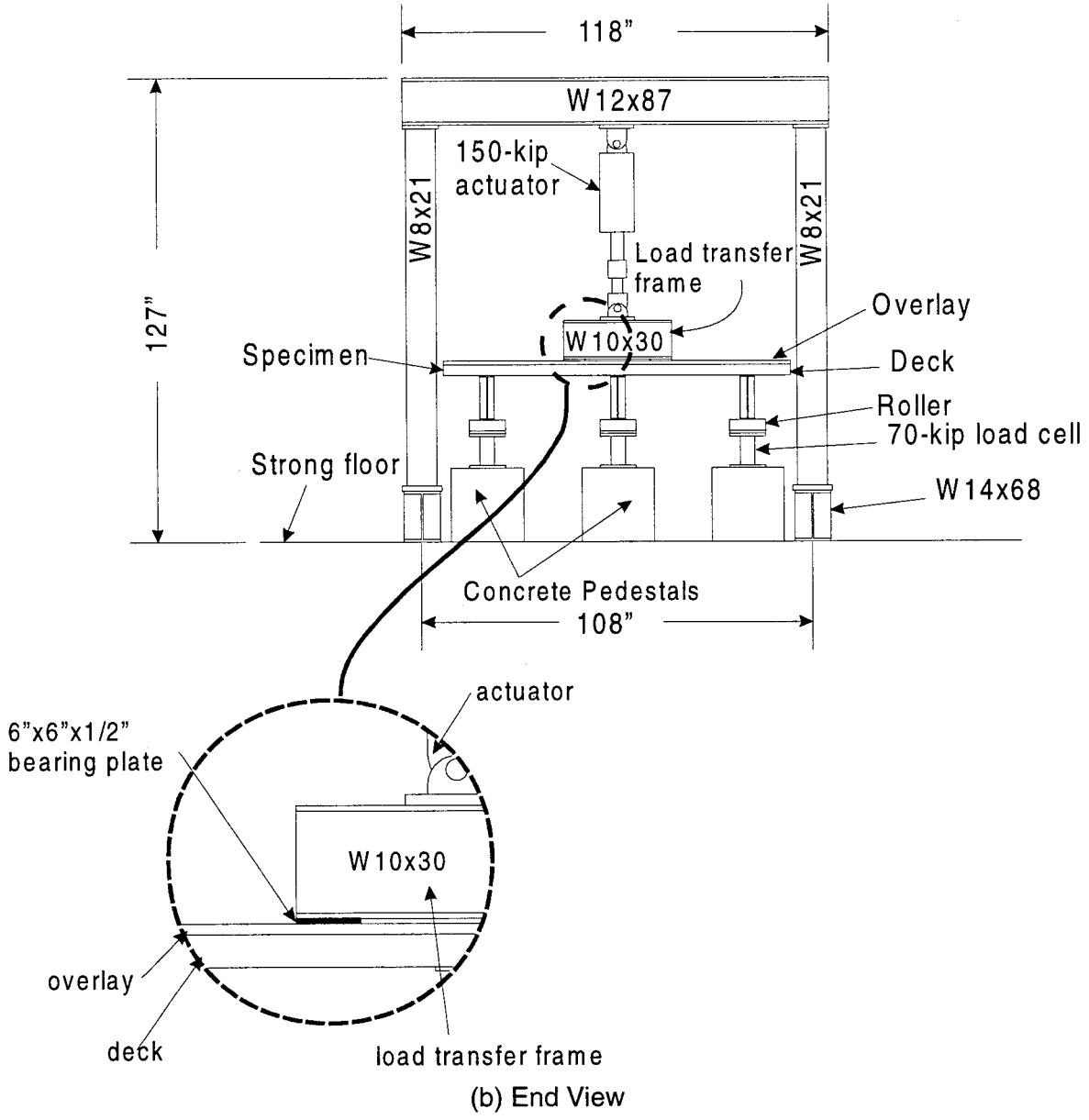

Note: 1 in. = 25.4 mm.

Figure 5.11 Details of Test Setup for Fatigue Tests (Cont.)

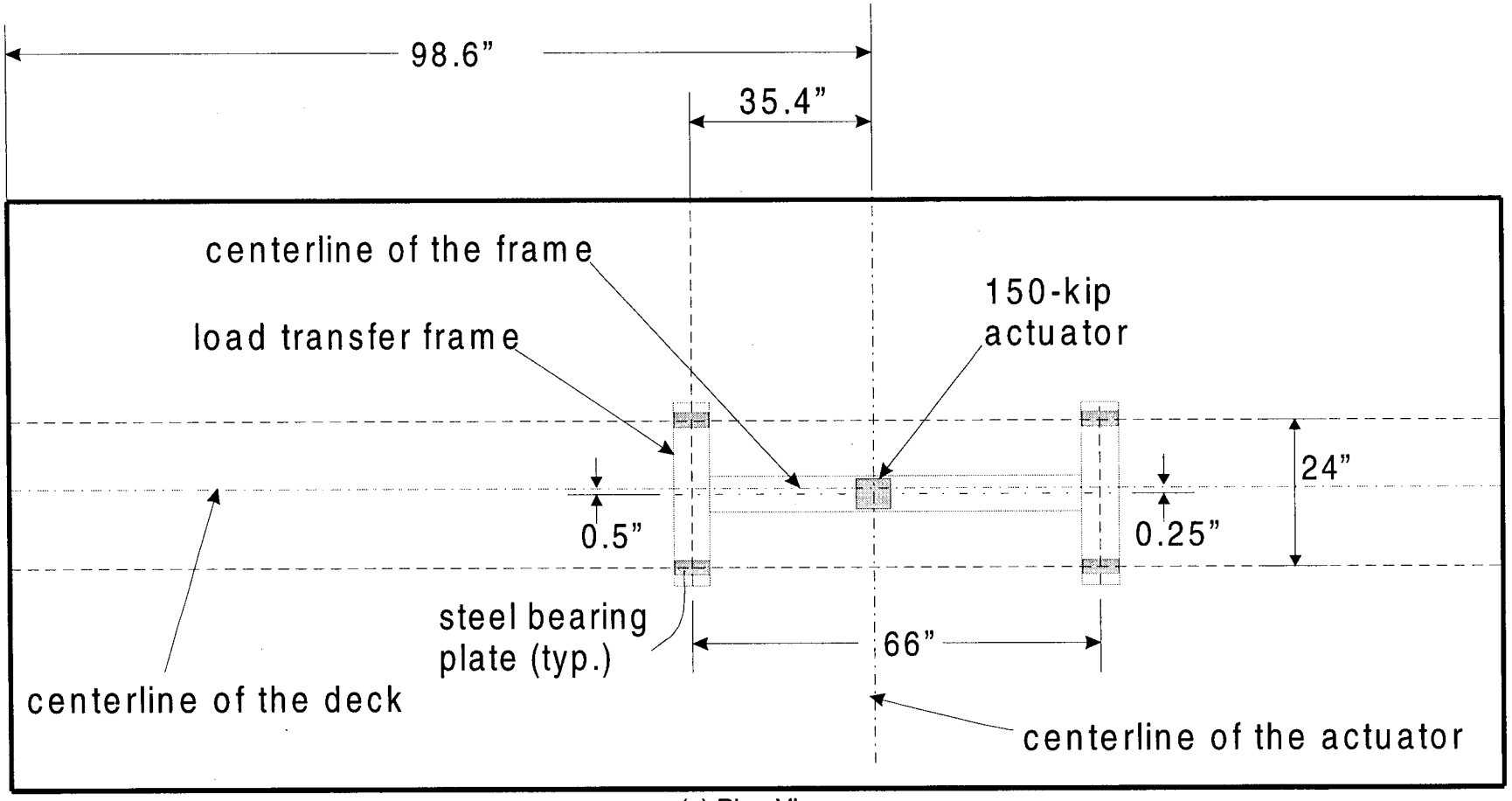

(c) Plan View

Note: 1 in. = 25.4 mm.

Figure 5.11 Details of Test Setup for Fatigue Tests (Cont.)

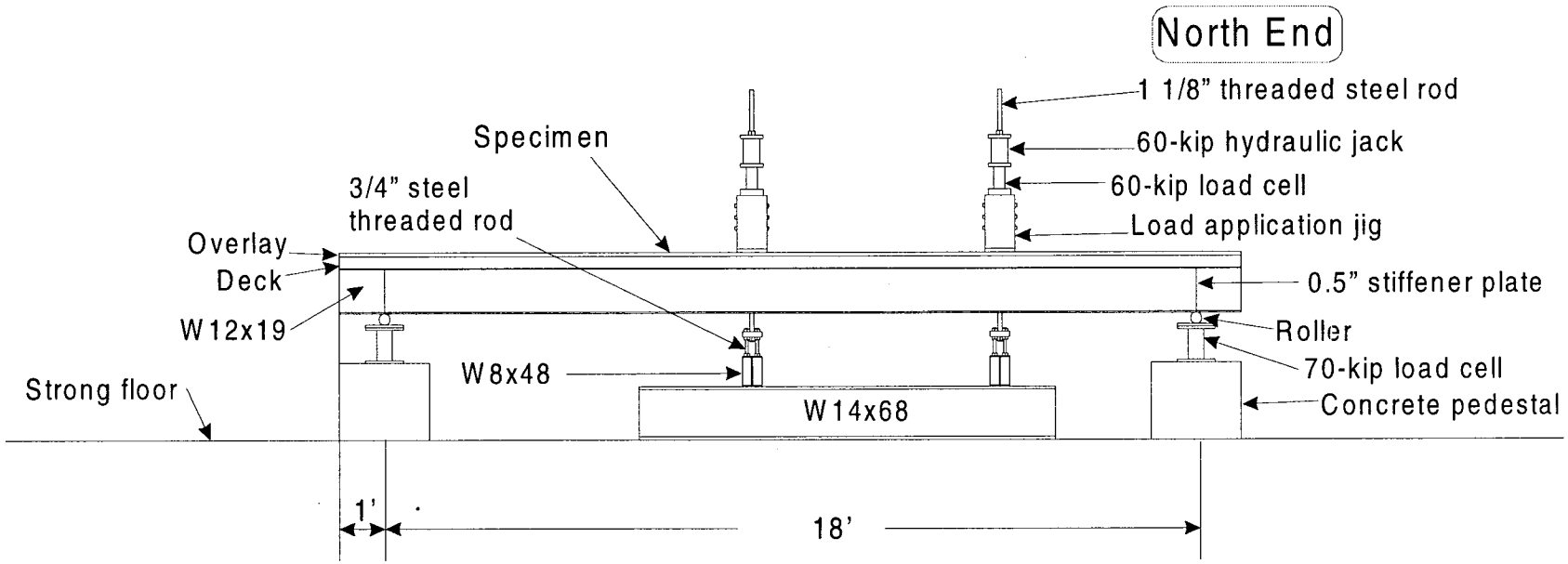

(a) Side View

Note: 1 in. = 25.4 mm.

Figure 5.12 Test Setup for Static Tests

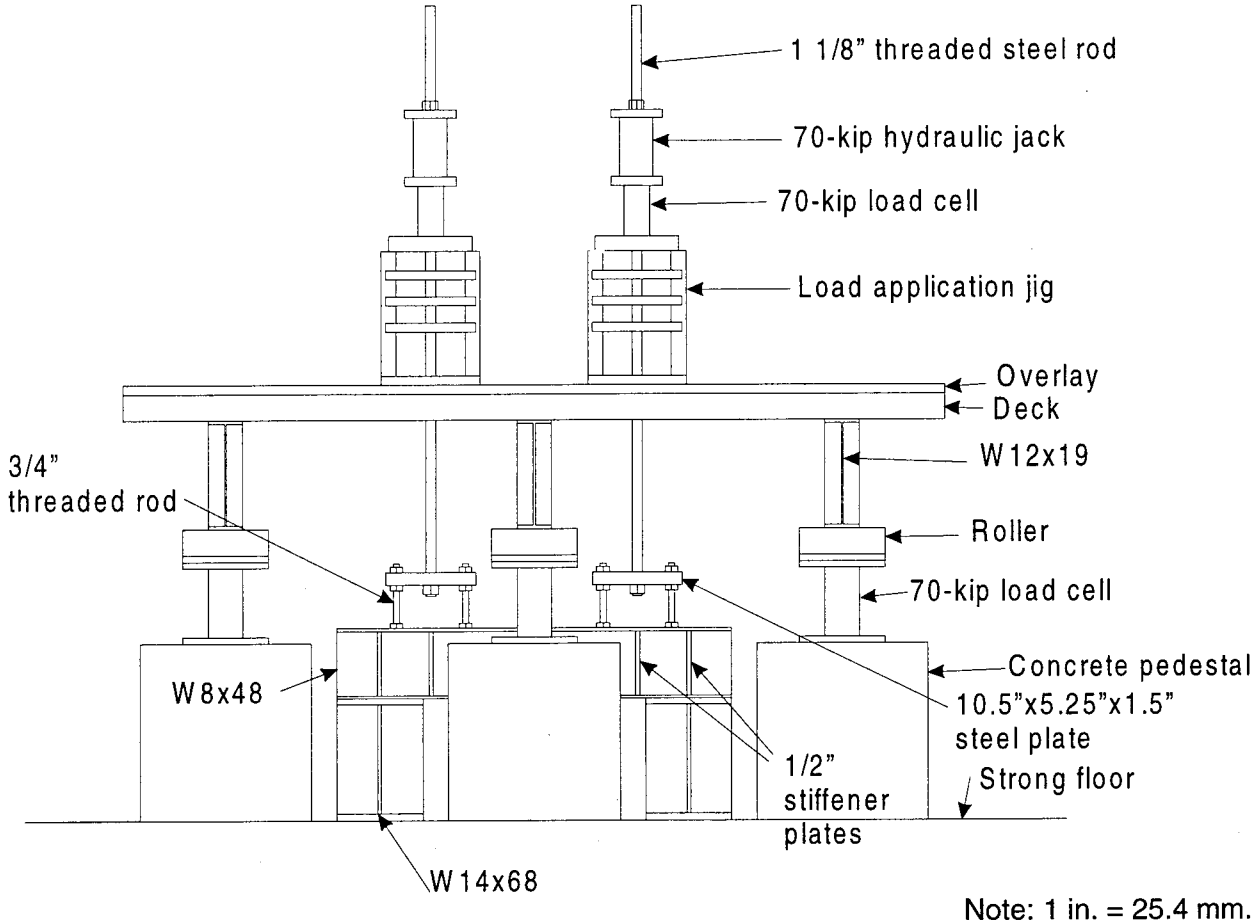

(b) End View

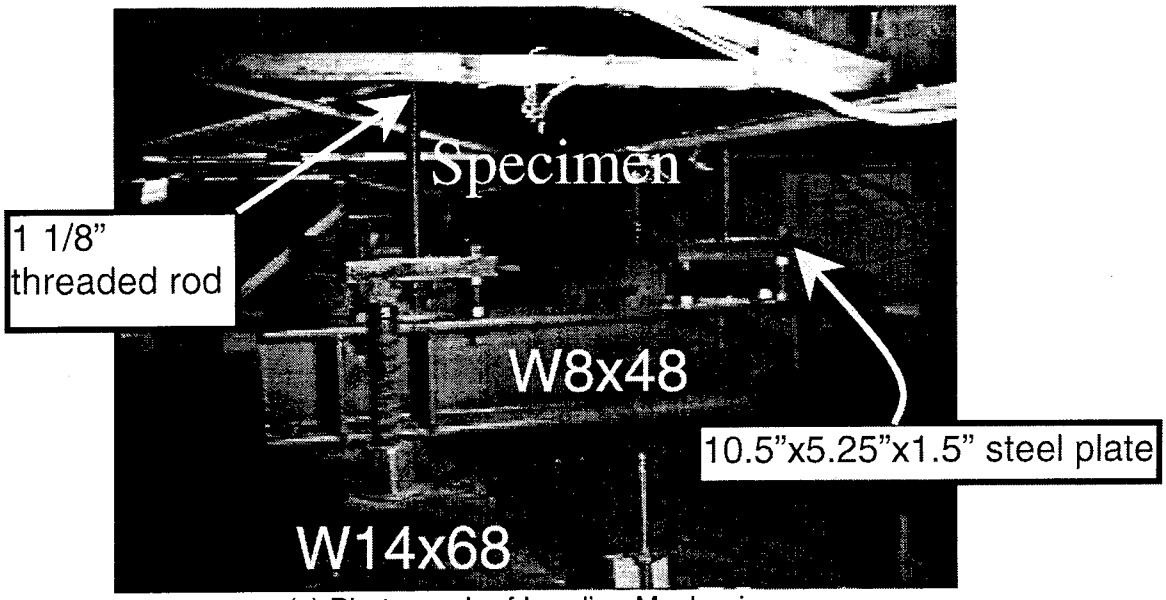

(c) Photograph of Loading Mechanism

Figure 5.12 Test Setup for Static Tests (Cont.)

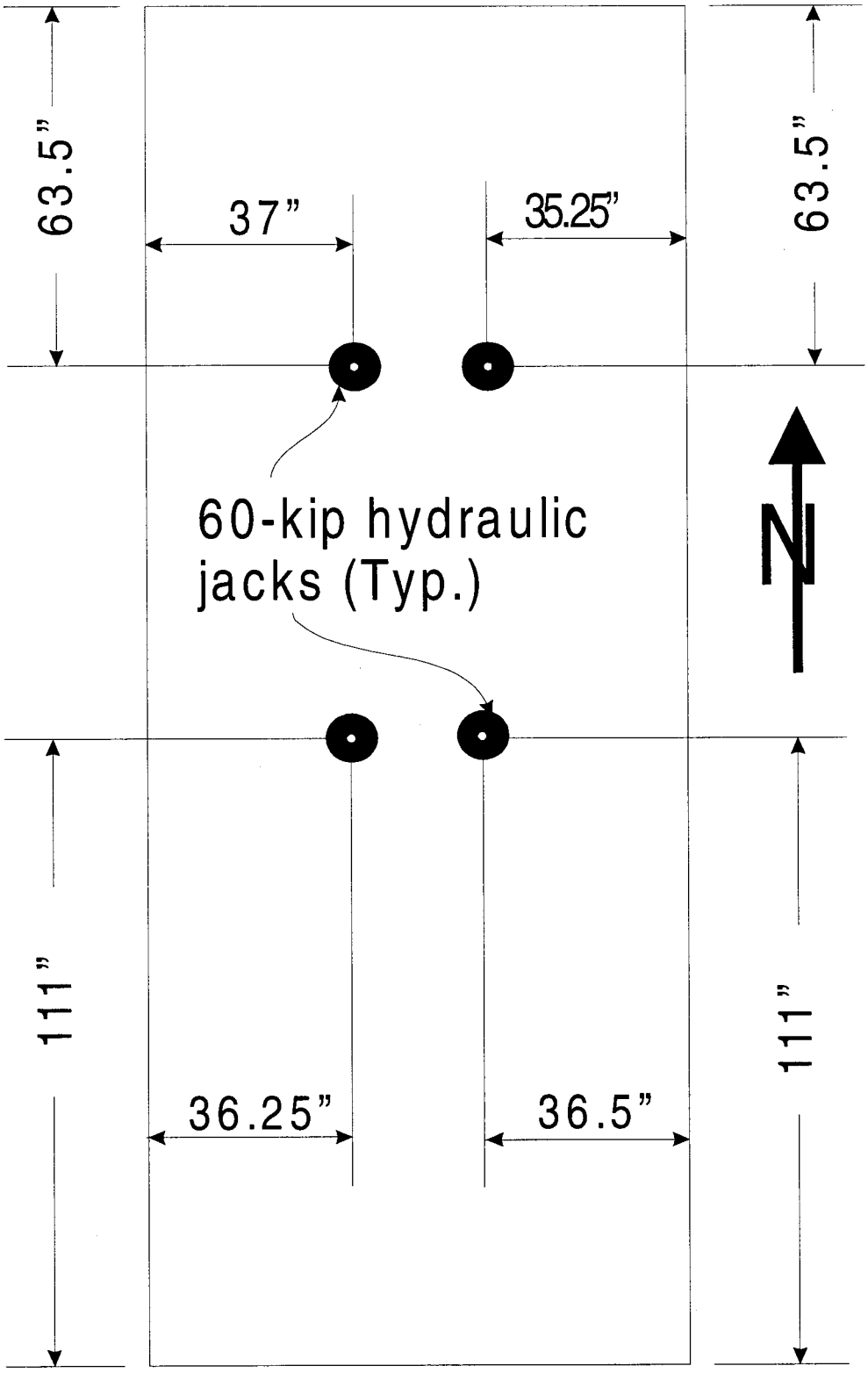

(d) Plan View

Note: 1 in. = 25.4 mm.

Figure 5.12 Test Setup for Static Tests (Cont.)

	0 CYCLES	200,000 Cycles	1,000,000 Cycles	Failure loading
A	3'	3'	3'	3'-3/8"
B	2 11/16"	2 11/16"	2 11/16"	2 3/8"
C	2'-6 1/16"	2'-6 1/16"	2'-5 13/16"	2'-5 13/16"
D	1 18"	1 18"	2 7/8"	2 7/8"
E	2'-1/8"	2'-1/8"	2'-1/8"	1'-11 11/16"
F	2"	2"	2"	2"
G	1'-11 3/8"	2'-11/16"	2'-11/16"	2'-11/16"
H	2 13/16"	2 11/16"	2 11/16"	2 11/16"
I	2'-6 3/16"	2'-6 3/16"	2'-6 3/16"	2'-6 1/4"
J	1 3/8"	1 3/8"	1 3/8"	2 1/16"
K	1'-11 1/16"	1'-11 1/16"	1'-11 1/16"	1'-9 3/8"
L	2 5/8"	2 5/8"	2 5/8"	1 1/2"

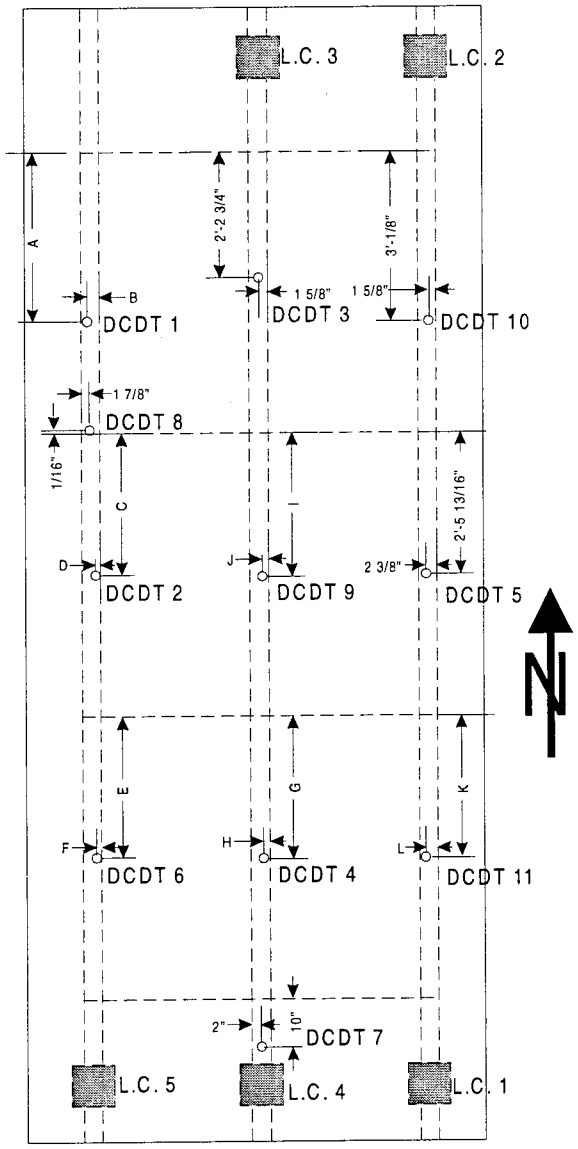

Note: 1 in. = 25.4 mm.

Figure 5.13 Locations of Displacement Transducers and Support Load Cells

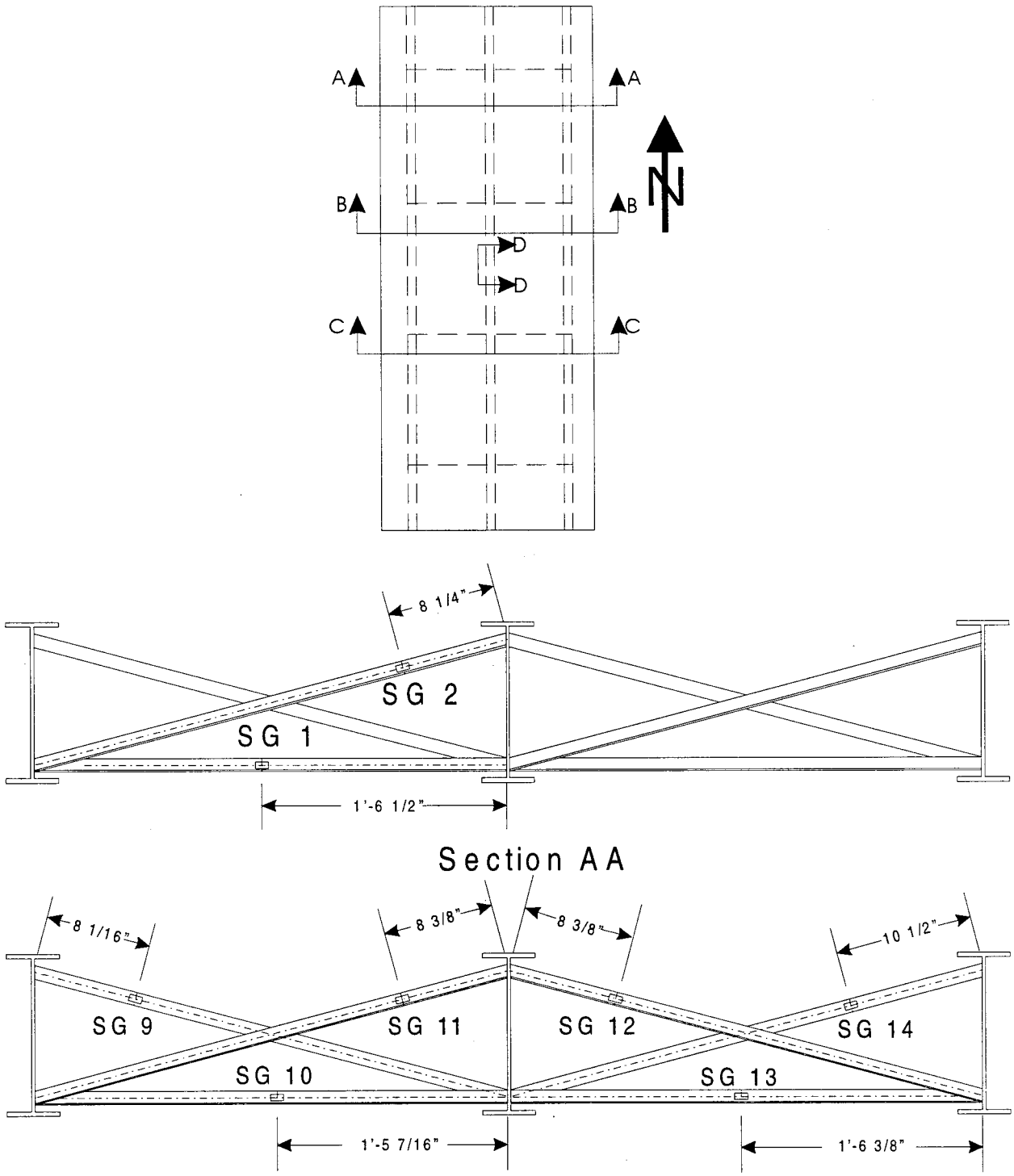

Note: 1 in. = 25.4 mm.

Figure 5.14 Locations of Strain Gages and Clip Gages

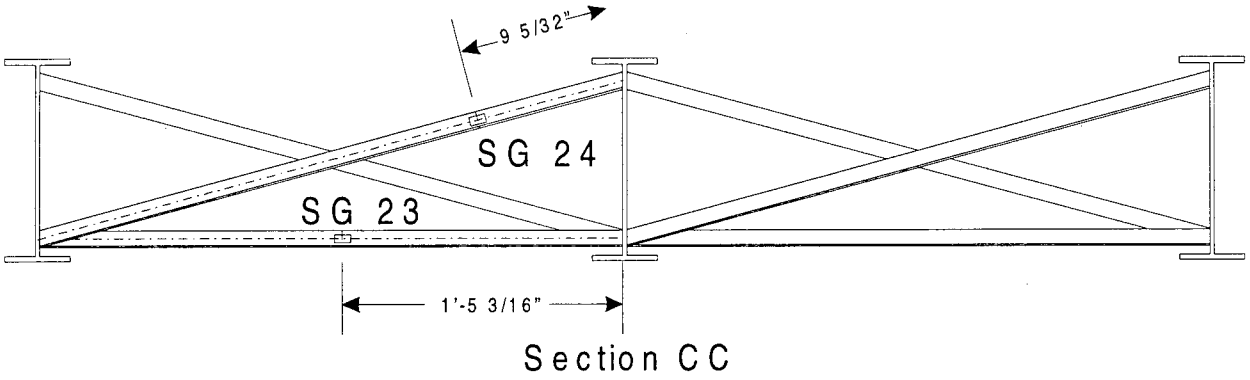

Section CC

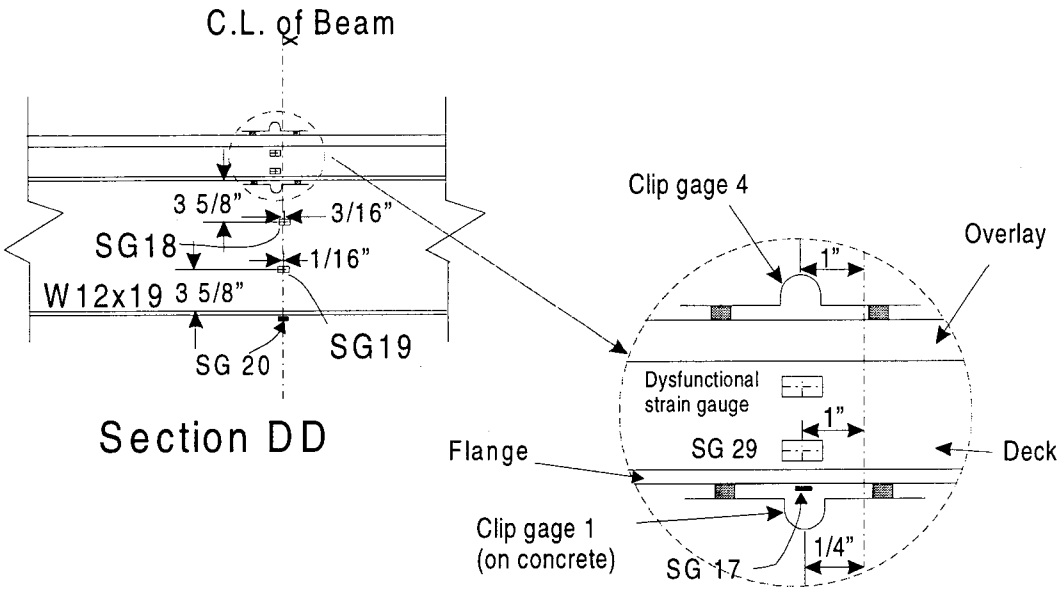

Section DD

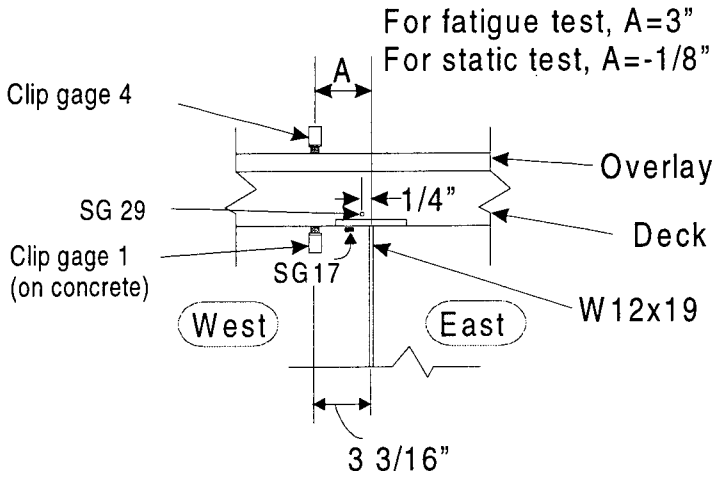

Note: 1 in. = 25.4 mm.

Figure 5.14 Locations of Strain Gages and Clip Gages (Cont.)

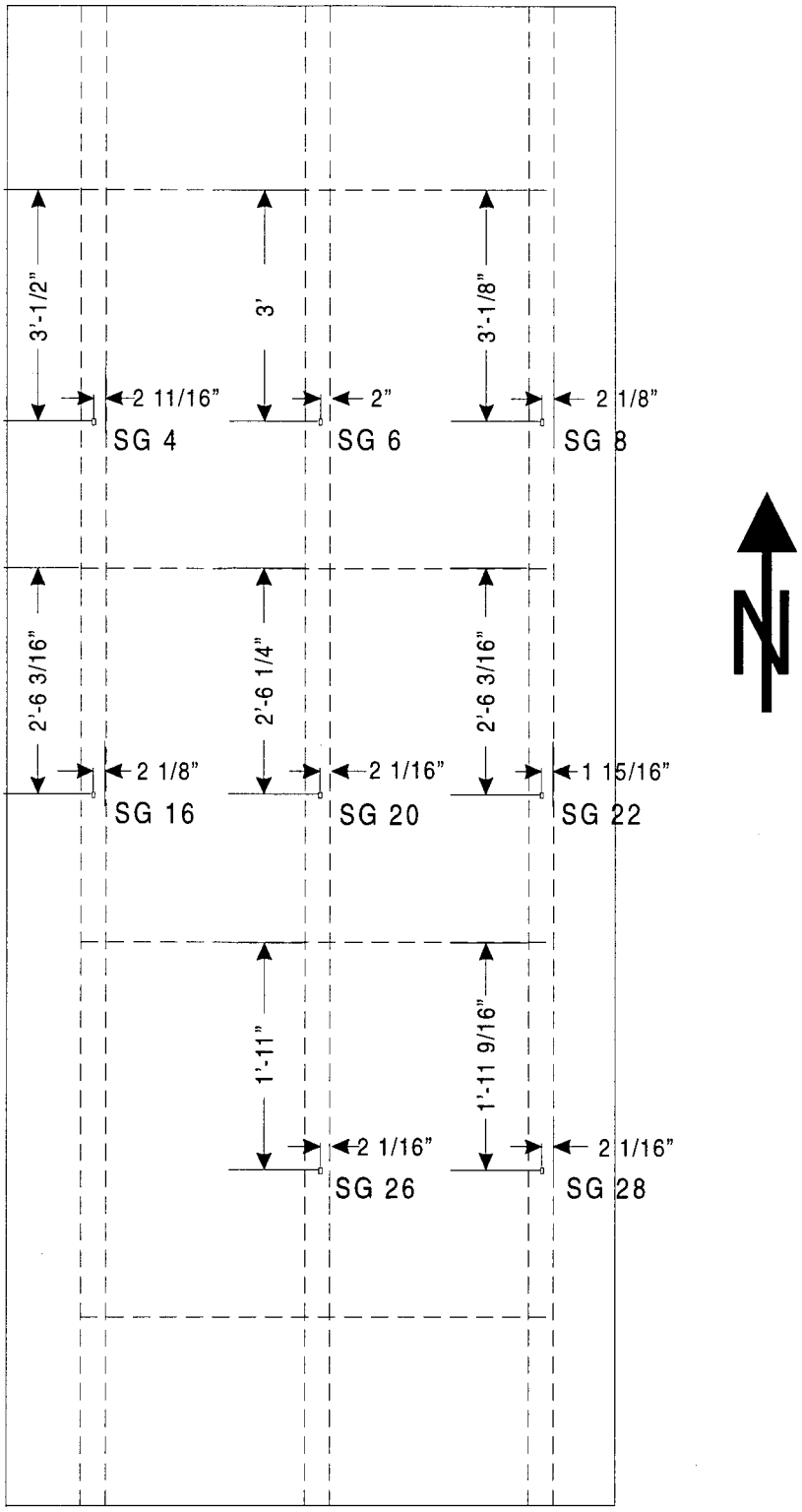

Bottom Flange Gages

Note: 1 in. = 25.4 mm.

Figure 5.14 Locations of Strain Gages and Clip Gages (Cont.)

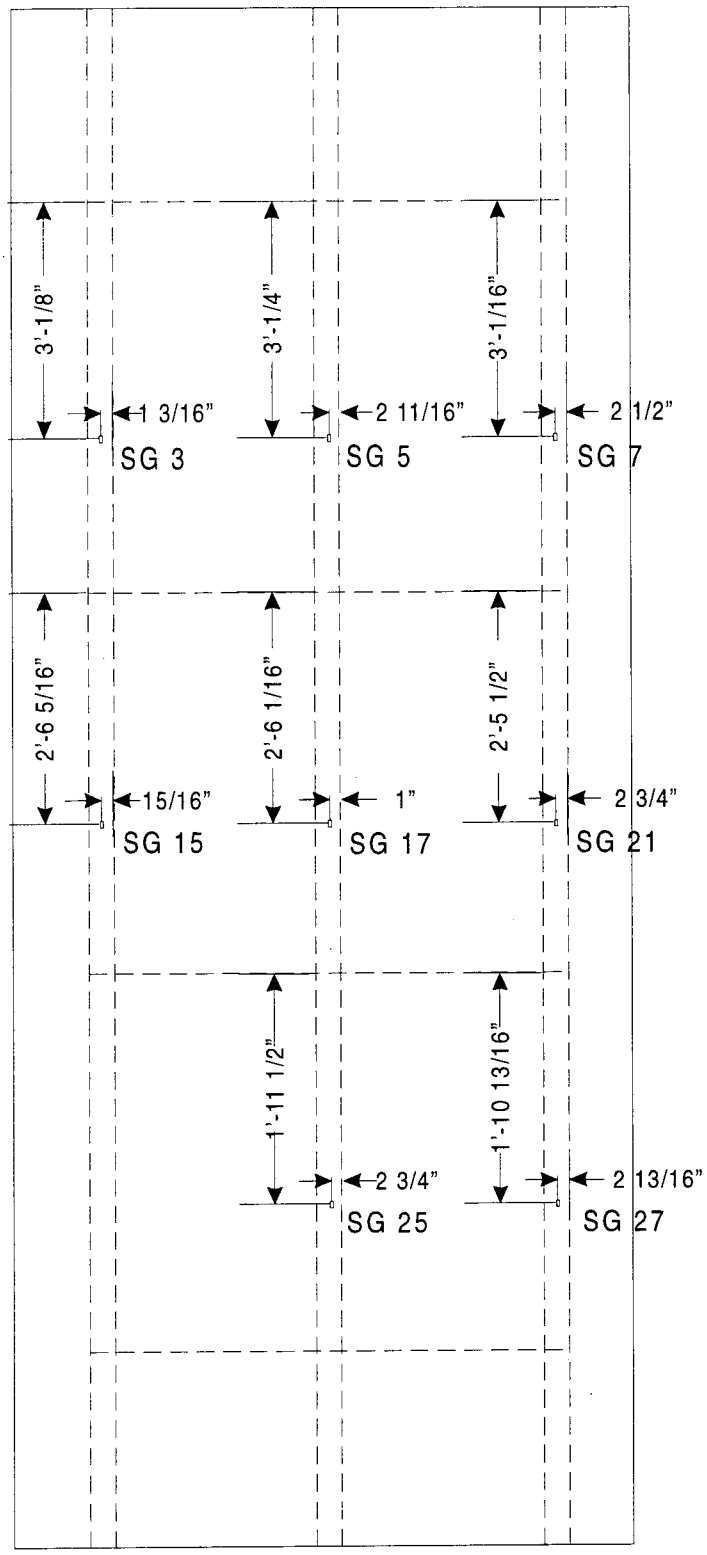

Note: 1 in. = 25.4 mm.

Figure 5.14 Locations of Strain Gages and Clip Gages (Cont.)

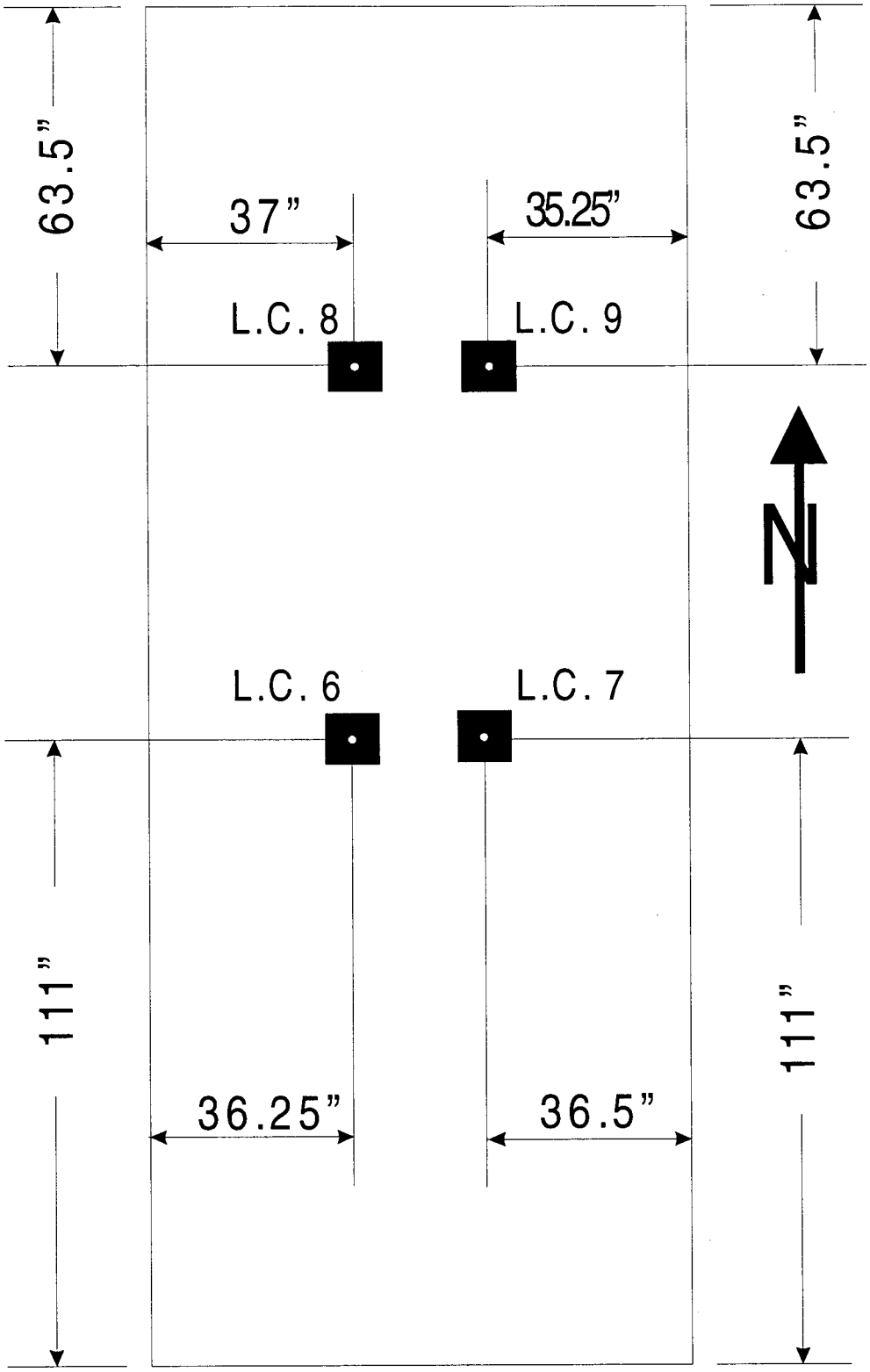

Note: 1 in. = 25.4 mm.

Figure 5.15 Location of Load Cells for Static Test

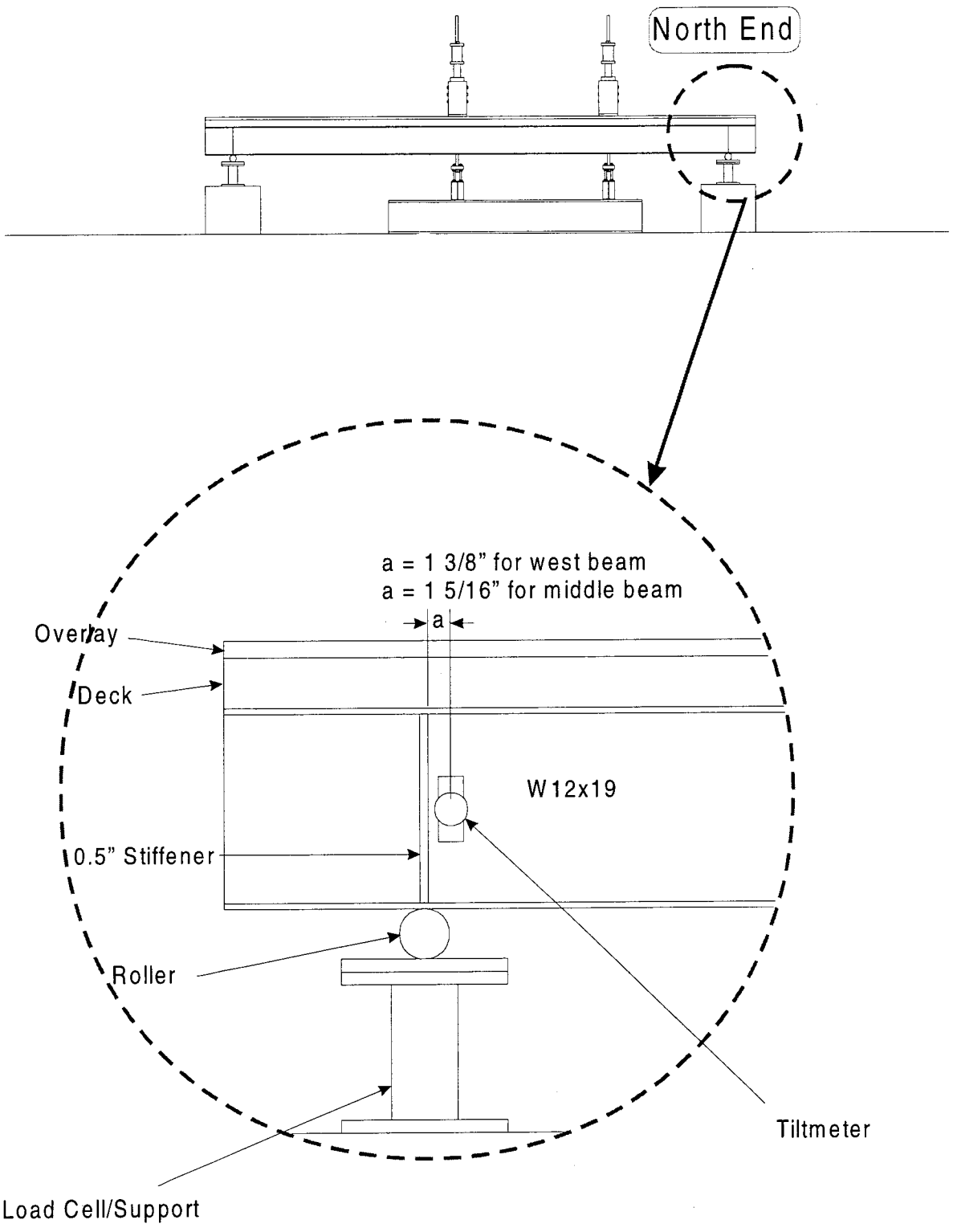

Note: 1 in. = 25.4 mm.

Figure 5.16 Location of Tilt Meters

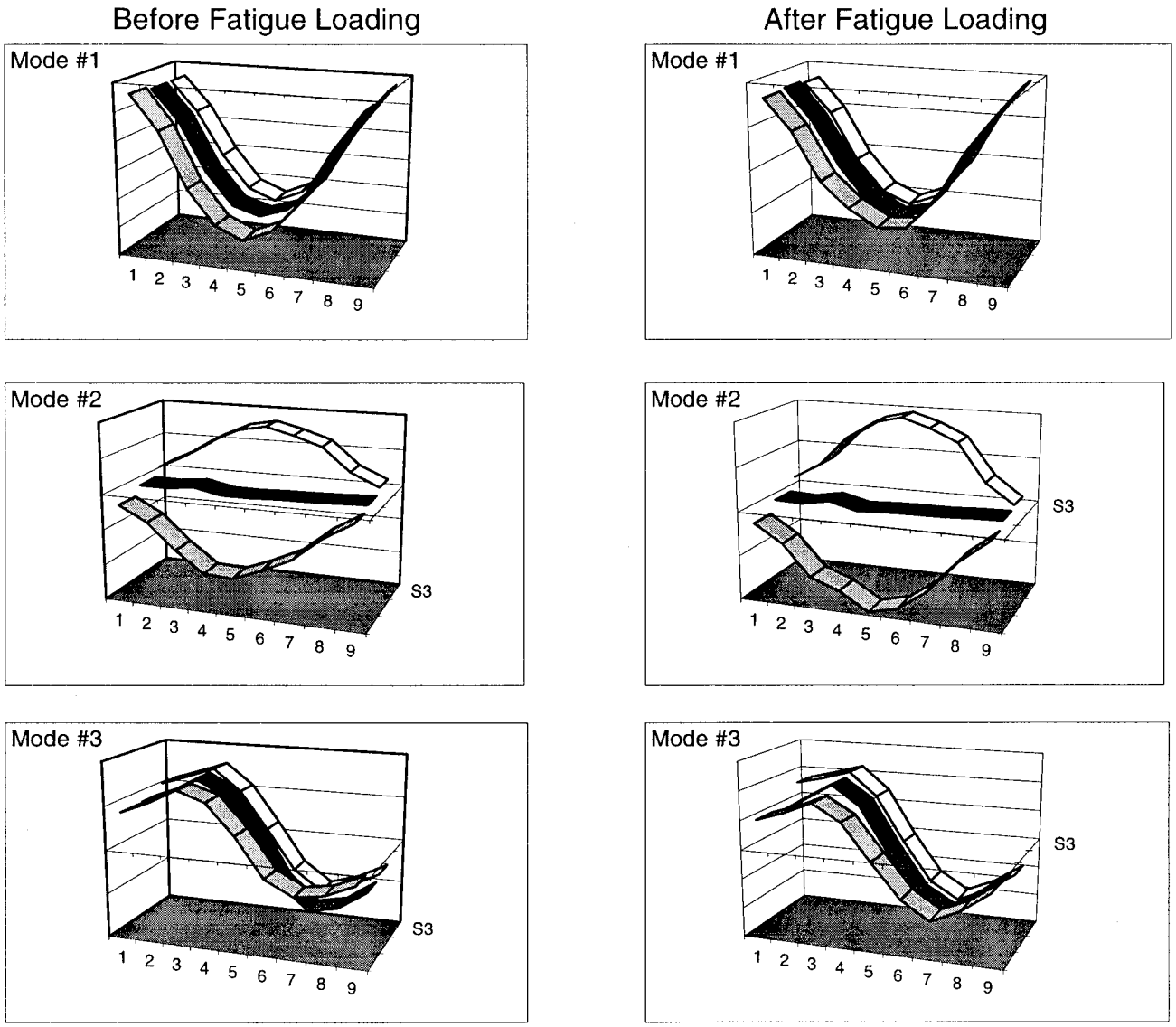

Figure 5.17 Comparison of Mode Shapes Before and After Fatigue Loading

Before Fatigue Loading

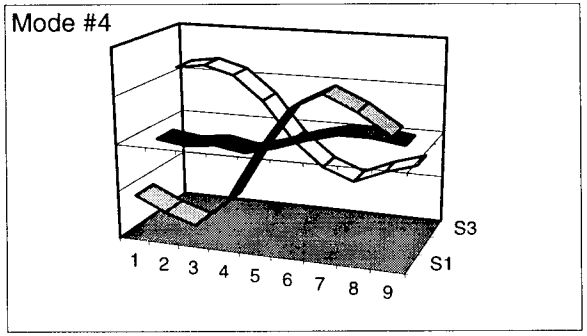

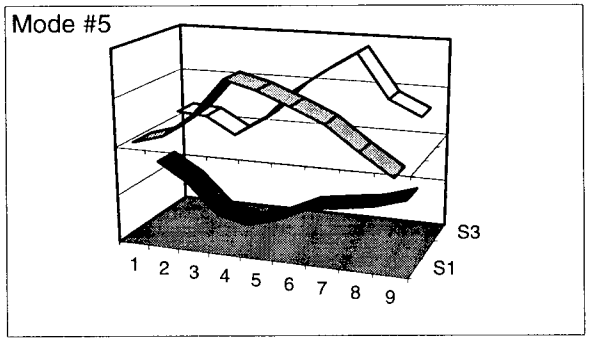

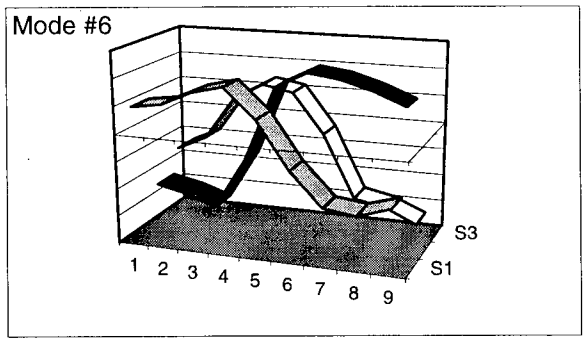

After Fatigue Loading

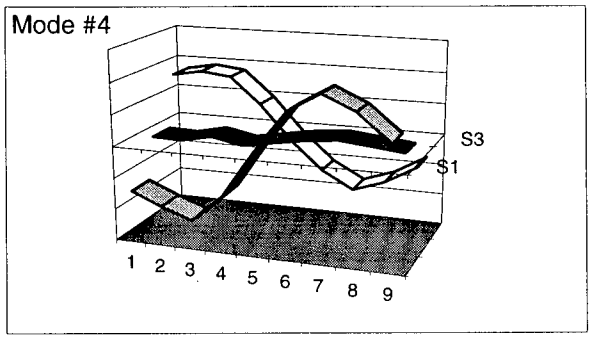

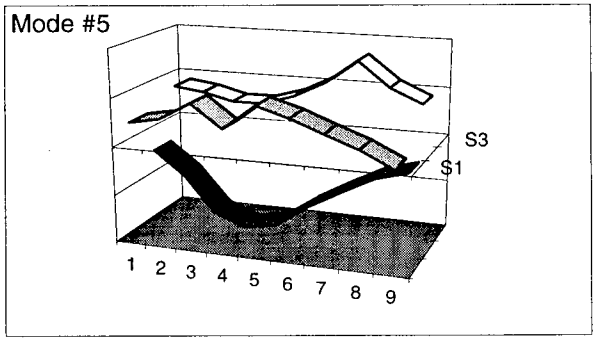

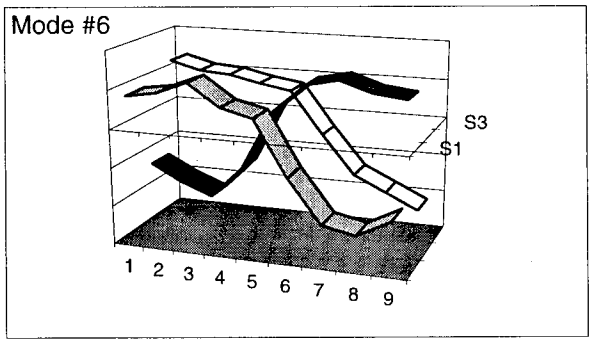

Figure 5.17 Comparison of Mode Shapes Before and After Fatigue Loading (Cont.)

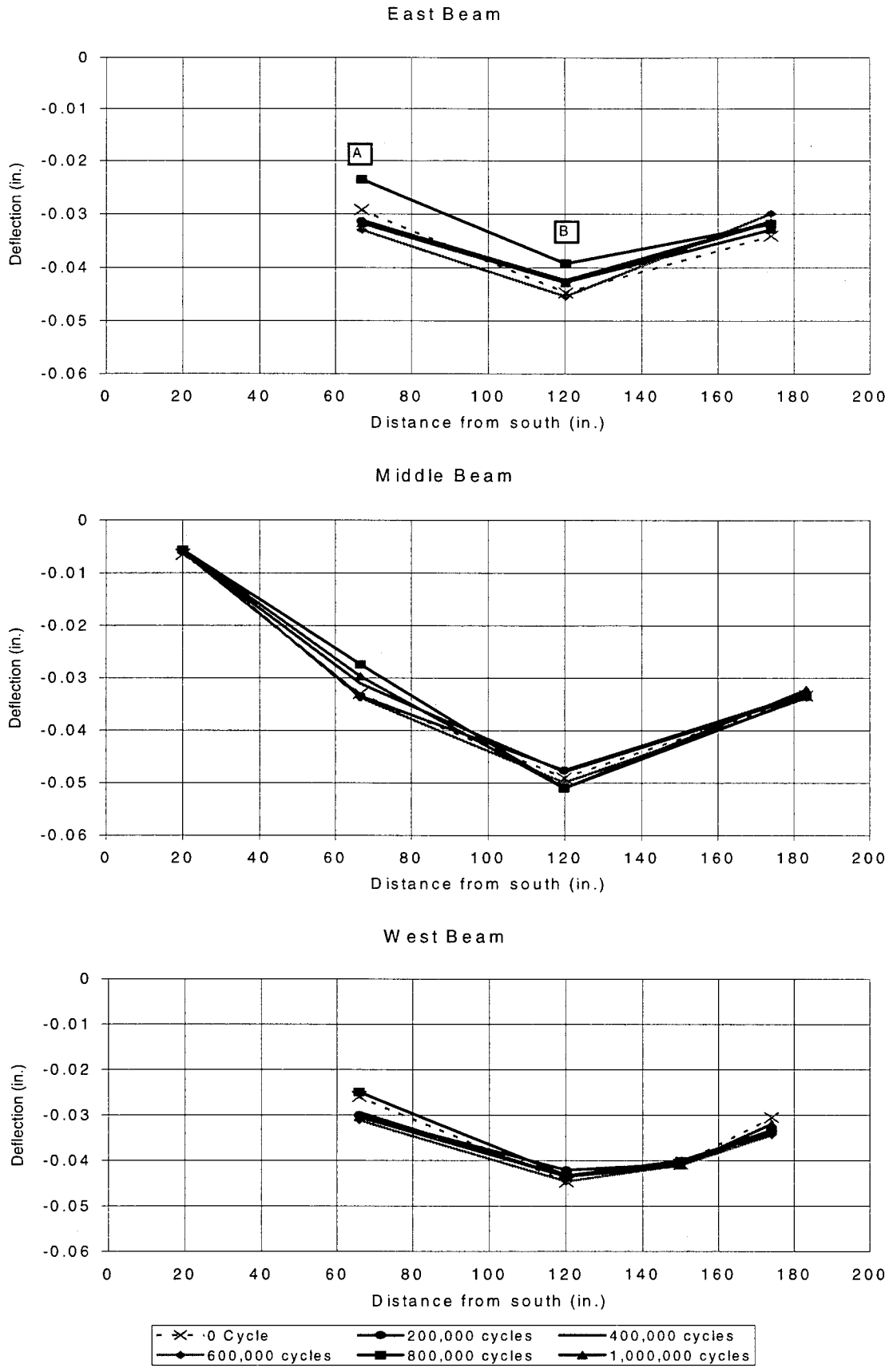

Figure 5.18 Deflected Shapes Under 49 kN (11 kips) of Static Load After Fatigue Cycles

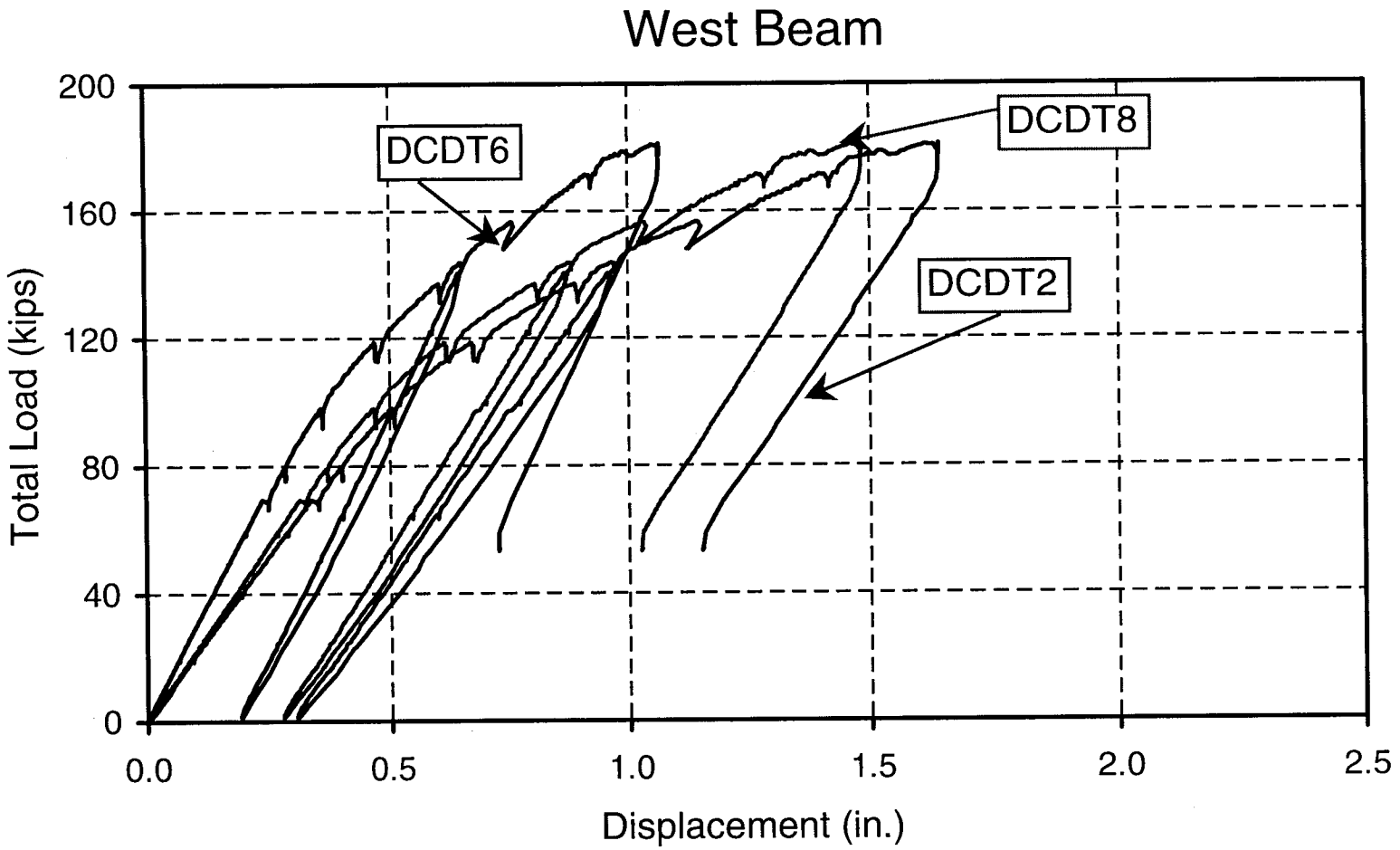

Figure 5.19 Measured Load-Deflection Curves

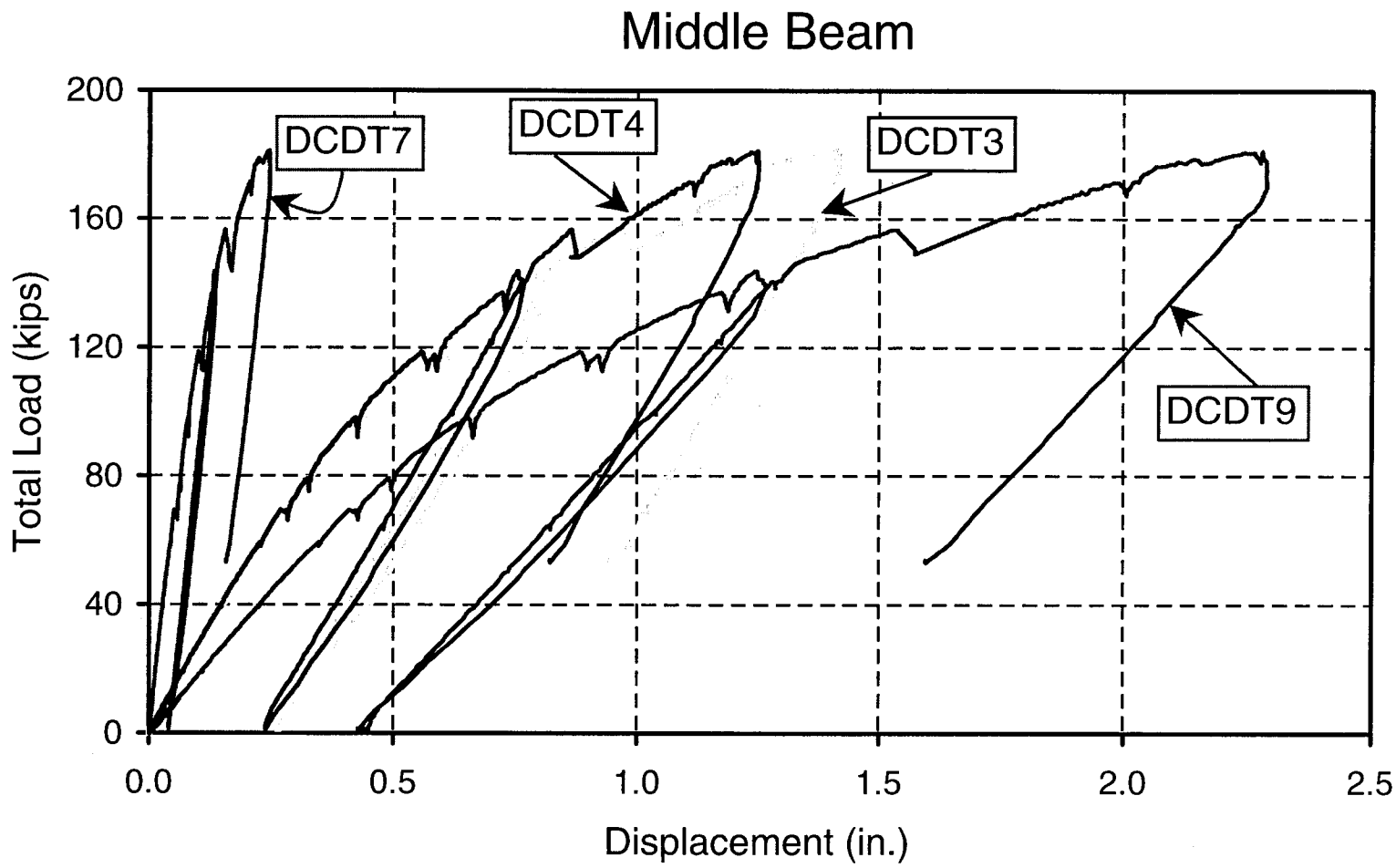

Figure 5.19 Measured Load-Deflection Curves (Cont.)

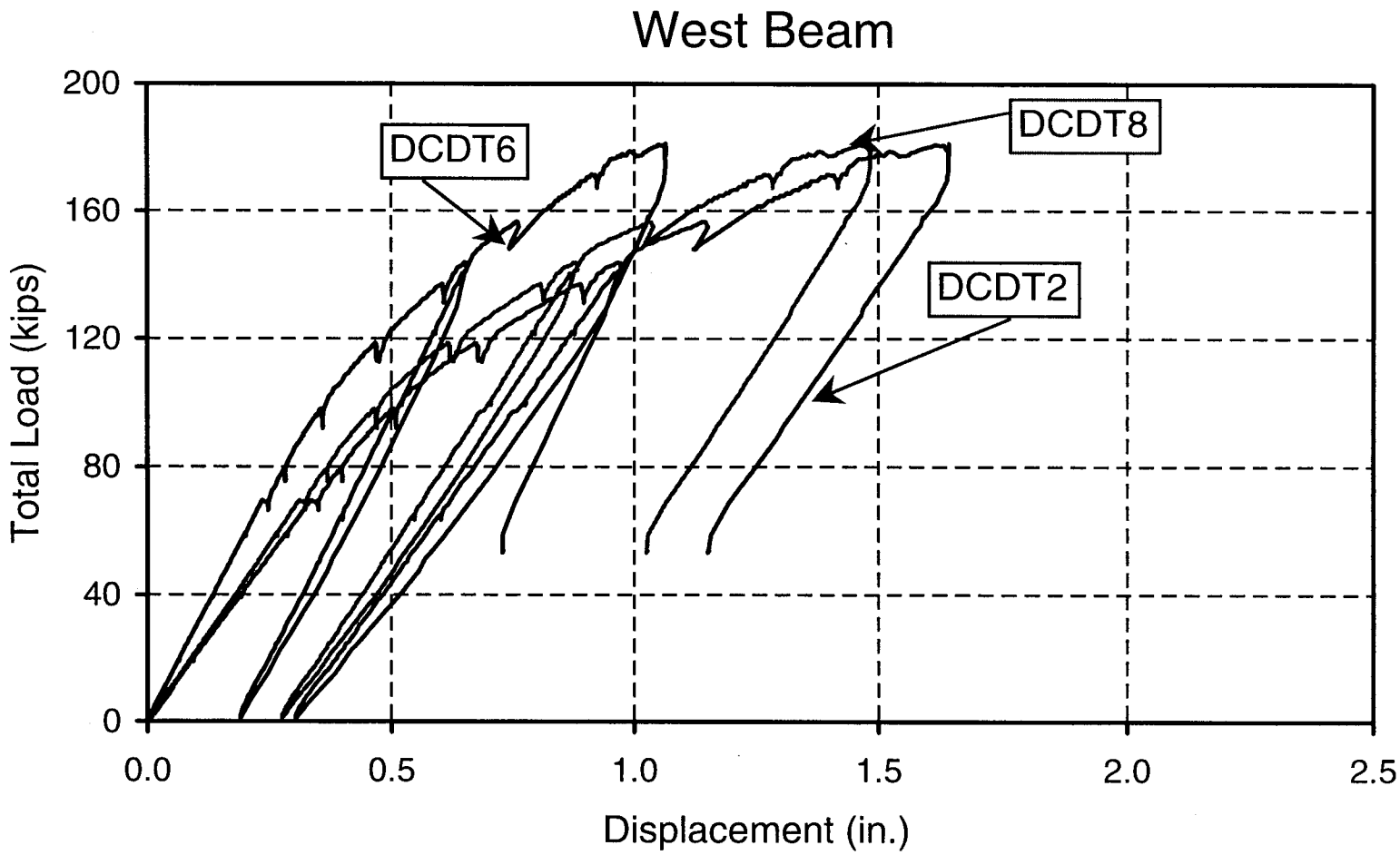

Figure 5.19 Measured Load-Deflection Curves (Cont.)

CHAPTER 6

SUMMARY, CONCLUSIONS, AND RECOMMENDATIONS

6.1 Summary of Research

The research presented in this report involved testing for the bond strength between existing bridge deck concrete and overlay concrete. The main objectives of the research were to (1) establish expected bond strength of overlays to sealed bridge decks using epoxy resin and high molecular weight methacrylate sealers (HMWM), and (2) to evaluate the influence of different testing methods for establishing bond strength. To achieve these objectives, a coordinated program involving field and laboratory testing was combined with detailed analytical studies.

Field testing was conducted on 12 bridges. Three different types of overlays were represented in the field tests: micro-silica modified concrete (MSC), super dense plasticized concrete (SDC), and latex modified concrete (LMC). The direct shear and direct tension tests were conducted on each bridge for bond strength.

Laboratory tests were performed using three different test methods to determine the bond strength of an overlay to a sealed and unsealed bridge deck surface. The test methods were (1) direct shear, (2) SHRP interfacial bond test, and (3) flexural beams. The test variables for direct shear and SHRP interfacial bond specimens were type of sealer on the interface (no sealer, HMWM, or epoxy resin), and type of overlay (MSC, LMC, SDC). Test variables used in the flexural beam tests included type of sealer (no sealer, or HMWM) and whether the overlay concrete was subjected to compressive or tensile stress during testing (negative or positive moment). In addition, a 1/3-scale specimen representing typical steel stringer bridges in Ohio was tested to examine the behavior of overlays placed on sealed decks. The relatively large-scale specimen was subjected to 1,000,000 cycles of equivalent HS-20 truck loading with an amplification factor of 1.3. Upon completion of fatigue loading, the specimen was statically pushed to its ultimate limit state. At

various stages, comprehensive measurements were made to monitor the behavior of overlays applied to sealed bridge decks.

6.2 Conclusions

1. The direct shear and direct tension tests conducted on actual bridge decks in ODOT District 12 show identical trends for bond strength. Either test may be used to obtain relative magnitudes for bond strength on bridge decks with concrete overlays. Hence, either test method is a viable option for quality control testing.

2. The use of a sealer at the interface surface will affect bond strength. Specimens from the direct shear, SHRP interfacial bond, and flexural beam tests indicate epoxy resin or HMWM sealer will lower bond strength compared to identical unsealed specimens.

3. The magnitude of strength reduction was found to depend on the type (manufacturer) of HMWM sealer. When SikaPronto 19 HMWM was applied, the bond strength was approximately 50% of the corresponding unsealed specimens. Transpo Sealate T-70 acted as a bond breaker, and hence no bond strength was measured. This type of HMWM sealer is not appropriate for the goals studied in this research. The strength reductions for the epoxy resin sealer used in this study (Sikadur 55SLV) was very similar to that measured for SikaPronto HMWM sealer. The level of moisture that the test specimens were subjected was found to dramatically alter the behavior of the specimens sealed with epoxy (refer to Appendix C). When wet cured continuously for 56 days, the bond strength reduction for those specimens was 84% of the corresponding unsealed specimens, while the bond strength for specimens which were wet cured for only 3 days was 35%. HMWM specimens were not sensitive to the type of specimen curing.

4. Extra surface preparation techniques applied to the HMWM sealed specimens significantly increased the bond strength. Sandblasting the interface after applying HMWM sealer, or broadcasting sand over the sealed interface was found to be effective means for enhancing the bond strength. The resulting strengths were close to those for identical specimens without sealer. Sandblasting the HMWM sealed surface, or broadcasting sand over the HMWM resulted in strengths that were 80% and 85% of the unsealed specimens bond strength, respectively. HMWM specimens were not sensitive to the type of specimen curing.

5. The direction of bending has a significant effect on creating failure at the interface surface. When the overlay is in tension, flexural cracks limit the transfer of longitudinal forces and; hence, shear stress in the overlay concrete. Therefore, bond strength at the concrete-overlay interface due to negative moments is not critical. Bond strength becomes critical when the concrete overlay is subjected to compressive stresses.

6. The relative importance of factors such as type of overlay and conditions of the existing concrete surface prior to overlay application can be examined by different test methods. However, the values of bond strength are different depending on the testing procedure, and should not be directly compared. This difference is due to the different state of stresses induced by each test method.

7. The application of sealers lower the available bond strength; however, finite element analyses of representative bridges indicate that the maximum in-plane shear stress would not exceed the bond strength of a surface sealed with a suitable HMWM or epoxy resin. The maximum computed shear stress is smaller than the lowest available bond strength of surfaces sealed with epoxy resin or HMWM.

8. Comprehensive laboratory tests conducted on the 1/3-scale bridge specimen verify that bridge decks may be sealed so long as an appropriate secondary surface preparation technique (e.g., broadcasting sand over the sealer while it is curing, or light sandblasting of the sealed deck) is used prior to the application of overlay.

6.3 Recommendations

1. **Use additional surface preparation techniques to increase bond strength.** Sandblasting the sealed surface at the interface removes residue and creates a better bond at the surface. Another surface preparation technique which increases bond strength is sand broadcasting. The application of a dry sand over the sealed surface (immediately after sealer application) at approximately 100 kg/m^2 (20 lb/ft^2) also will significantly increase the available bond strength

2. **Apply HMWM sealer over regions of negative moment.** Over bridge piers, loss of bond is not an issue, as the level of stress at the overlay concrete interface cannot reach critical levels. Because cracks occur in the bridge deck over the piers, sealing these cracks will help to stop the penetration of water and chlorides. Hence, the bridge superstructure will be protected from deterioration.

3. **Use field tests for quality control.** The direct shear or direct tension test are both appropriate for evaluating available bond strength in bridge decks.

References

ACI Manual of Concrete Practice, Committee 318 "Building Code Requirements for Structural Concrete (ACI 318R-95)," American Concrete Institute, Detroit, Michigan.

ACI Manual of Concrete Practice, Committee 345 "Concrete Highway Bridge Deck Construction (ACI 345R-91)," American Concrete Institute, Detroit, Michigan.

ACI Manual of Concrete Practice, Committee 503 "Use of Epoxy Compounds With Concrete (ACI 503R-93)," American Concrete Institute, Detroit, Michigan.

ACI Manual of Concrete Practice, Committee 548 "Standard Specification for Latex Modified Concrete Overlays (ACI 548.4-93)," American Concrete Institute, Detroit, Michigan.

Cole, J. "Testing and Evaluation of a Large-Scale Composite Steel Stringer Bridge Subassembly", M.S. Thesis, University of Cincinnati, 1999

Emmons, P.H., Vaysburd, A.M. and McDonald, J.E., "Concrete Repair In The Future Of The Century - Any Problems?," Concrete International, ACI, March 1994, pp. 43 - 49.

Grtimmelsman, K.A., "Instrumented Monitoring of a Reinforced Concrete Deck on Steel Stringer Highway Bridge Through Construction: Steel Elements", Master of Science Thesis, Department of Civil and Environmental Engineering, University of Cincinnati, 1997.

Keeran, K.D., "A Field Evaluation of Bond Strength of Bridge Deck Overlay Materials on Slabs with Varying Moisture Conditions and Bonding Grout Conditions", Ohio Department of Transportation, Columbus, Ohio, p. 38.

Luther, M.D., "Silica Fume (Microsilica) Concrete in Bridges," Concrete International, ACI, April 1993, pp. 29 - 33.

Metha, P.K. and Montiero, P.J., *Concrete, Structure Properties and Materials*, Prentice Hall, Englewood Cliffs, New Jersey, 1993.

McDonald, D.B., Krauss, P.D., and Rogalia, E.A., "Early - Age Transverse Deck Cracking,"Concrete International, ACI, May 1995.

O'Connor, D.N. and Saiidi, M., "Polyester Concrete for Bridge Deck Overlays," Concrete International, ACI, December 1993, pp. 36 - 39.

Pfiefer, D.W., Perenchio, W.F., and Marusin, S., "Coatings, Penetrants and Specialty Concrete Overlays For Concrete Surfaces," ACI Seminar for Structural Repair - Corrosion Damage and Control, 1985.

Pfiefer, D.W., Perenchio, W.F., and Marusin, S., "Cost Protective Protection Of Rebars Against Chlorides, Sealers or Overlays?," Concrete Construction, May 1984.

Saraf, V.K., "Effects of Repair on Behavior of Deteriorated Reinforced Concrete Slab Bridges", M.S. Thesis, University of Cincinnati, p. 140.

Silfwerbrand, J., "Improving Concrete Bond In Repaired Bridge Decks," Concrete International, ACI, September 1990, pp. 61 - 66.

Shahrooz, B.M., "CEE 482 - Reinforced Concrete", University of Cincinnati, Department of Civil and Environmental Engineering, 1997.

SHRP-C-361, "Mechanical Behavior of High Performance Concretes, Volume 1, Summary Report", Strategic Highway Research Program, National Research Council, Wahsington DC, 1993, pp. 93 - 98.

Turer, A., "Finite Element Modeling of Seymour Ave. Bridge No. HAM562-0683", Personal Communications, 1998.

APPENDIX A
COMPARISON OF TEST METHODS

In order to simulate the shear transfer between the interface of overlays to existing bridge decks, four different types of tests were selected for this investigation.

- Direct Shear
- Direct Tension
- SHRP Interfacial Bond Test
- Flexural Beam Test

The first two tests may be conducted in the field and laboratory, but the SHRP and flexural beam tests must be conducted in the laboratory. Chapter 2 describes each of the test methods in detail.

The direct tension and direct shear tests were compared based on results obtained from six bridge decks in ODOT district 12. As mentioned in Chapter 3, the tests indicate identical trends for bond strength (MSC overlay strongest, LMC weakest). However, the measured values were found to be different. The Direct tension test values were much lower than the direct shear test, about 35% lower on average. This difference was expected due to the different state of stress occurring at the interface.

The second comparison involved the direct shear test, SHRP bond test, and the flexural beam test. Specimens were cast from the same base concrete, and received the same micro-silica concrete overlay. Unfortunately, the flexural beam tests did not experience shear failure at the interface; therefore, bond strength could not be obtained for comparison. The direct shear specimens had an average bond strength of 3.2 MPa (415 psi), and the SHRP bond test specimens had an average bond strength of 2.9 Mpa (465 psi). These values are reasonably close (approximately a 10% difference). Note that the number of test specimens are deemed to be insufficient to obtain statistically viable averages. Additional specimens would have allowed a more in-depth comparison of the two test methods.

APPENDIX B

FINITE ELEMENT STUDY

For comparison purposes, finite element models of two types of bridges were analyzed for maximum shear stress achieved over the depth of a bridge deck slab. The first bridge was a continuous reinforced concrete slab bridge (CLN-729-1588). This bridge is a three span, two lane bridge. The end spans are 10m. (32ft.-8in.) each with a 12.2m. (40ft.) center span. The deck was 412 mm. (16.25 in.) thick over the entire length and width. The bridge deck was modeled by solid elements with the nodes at the mid-depth of the slab. The piers and pier caps were modeled as frame elements. The bridge deck was assumed to be simply supported at the abutments, with rigid frame elements connecting the solid deck element nodes to the rollers along each abutment. Rigid end zones were also incorporated between the pier caps and nodes at the mid-depths of the slab over the piers. The analytical model is illustrated in Figure B.1. Four single axle dump trucks (142 kN or 32 kips each) were used to load the bridge. The trucks were positioned to create (a) maximum moment in the center span, (b) maximum moment in the end span, and (c) maximum moment over the piers. The maximum in-plane shear stress of 971 kPa (141 psi) was achieved by creating moment in the end span.

The second bridge was a steel stringer bridge in Cincinnati, over Seymour Avenue (HAM-561-0683). The bridge consists of three continuous spans of 12.2 m. (40 ft.), 15.2m (50 ft.), and 12.2 m (40 ft.). The bridge deck is a 165 mm. (6.5 in.) thick reinforced concrete deck supported by six steel girders at 2.3 m (7ft. - 7in) on center. The four interior beams are W27x94, with two exterior W21x73. The bridge is a four lane bridge with a 12.2 m (40 ft.) wide deck. Similar to the continuous reinforced concrete slab bridge, the piers and pier caps were modeled using frame elements, solid elements were used for the concrete deck. The stringers were connected to the abutments by pin connections. Rigid links were used to connect the pins to the nodes at the slab

mid-depth as seen from Figure B.2. Two different load cases were modeled incorporating four single axle dump trucks (142 kN, or 32 kips each) were considered. The trucks were arranged to produce maximum moment in the end spans, and maximum moment in the midspan. The maximum in-plane shear stress obtained from the analysis was 400 kPa (60 psi) resulting from creating maximum moment in the end spans.

Therefore, the shear stress due to structural loading in typical bridges dos not reach large values. The computed values of in-plane shear stress are lower than the available shear strength as obtained from the laboratory tests. Bond strengths obtained from specimens sealed with high molecular weight methacrylate ranged from 1.4 MPa to 4 MPa depending on the testing method. Therefore the available bond strength for cases in which the deck is sealed is larger than the maximum expected demand in typical bridges subjected to normal loads.

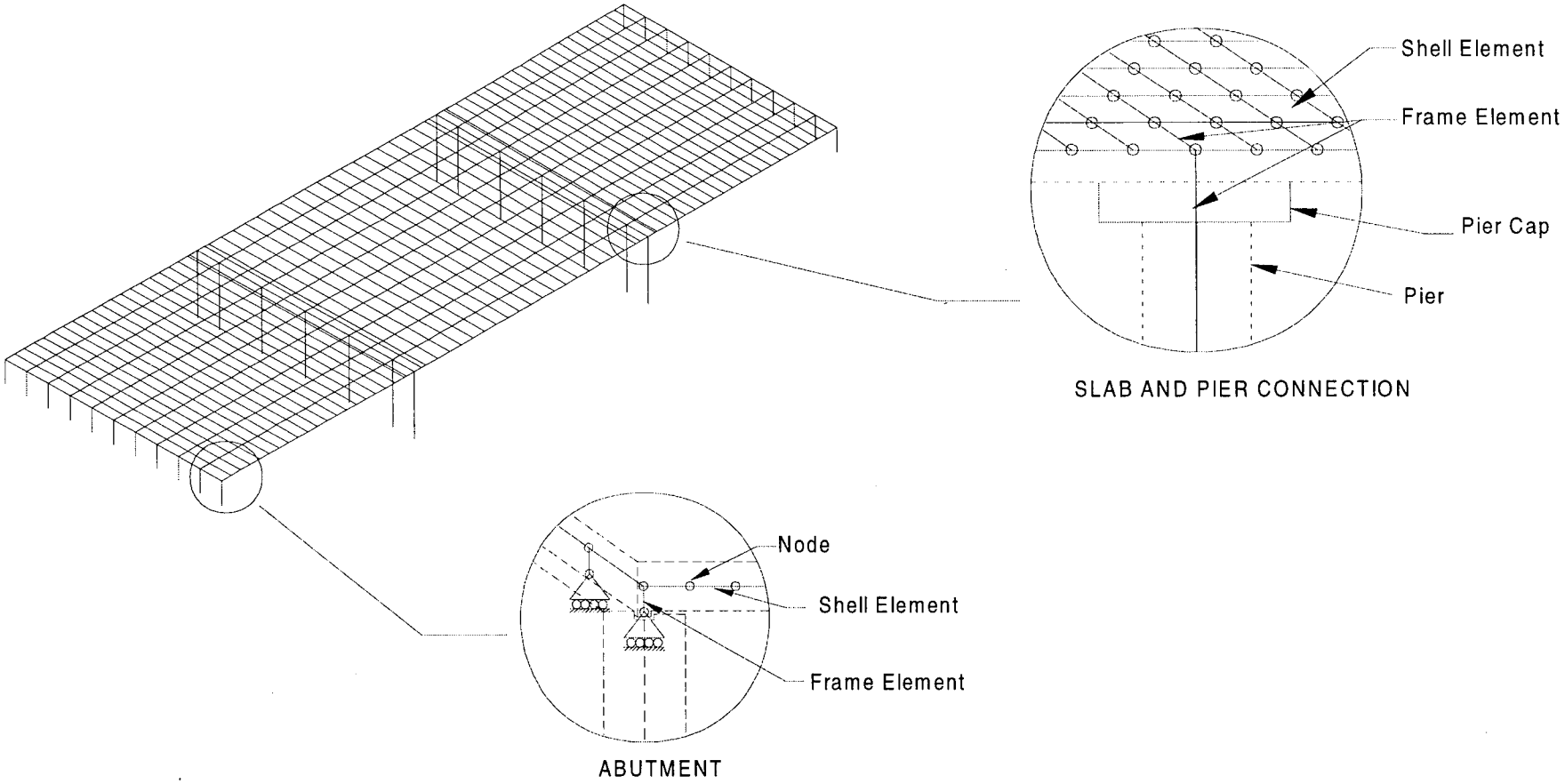

Figure B.1 Finite Element Modeling of CLN-729-1588 Bridge

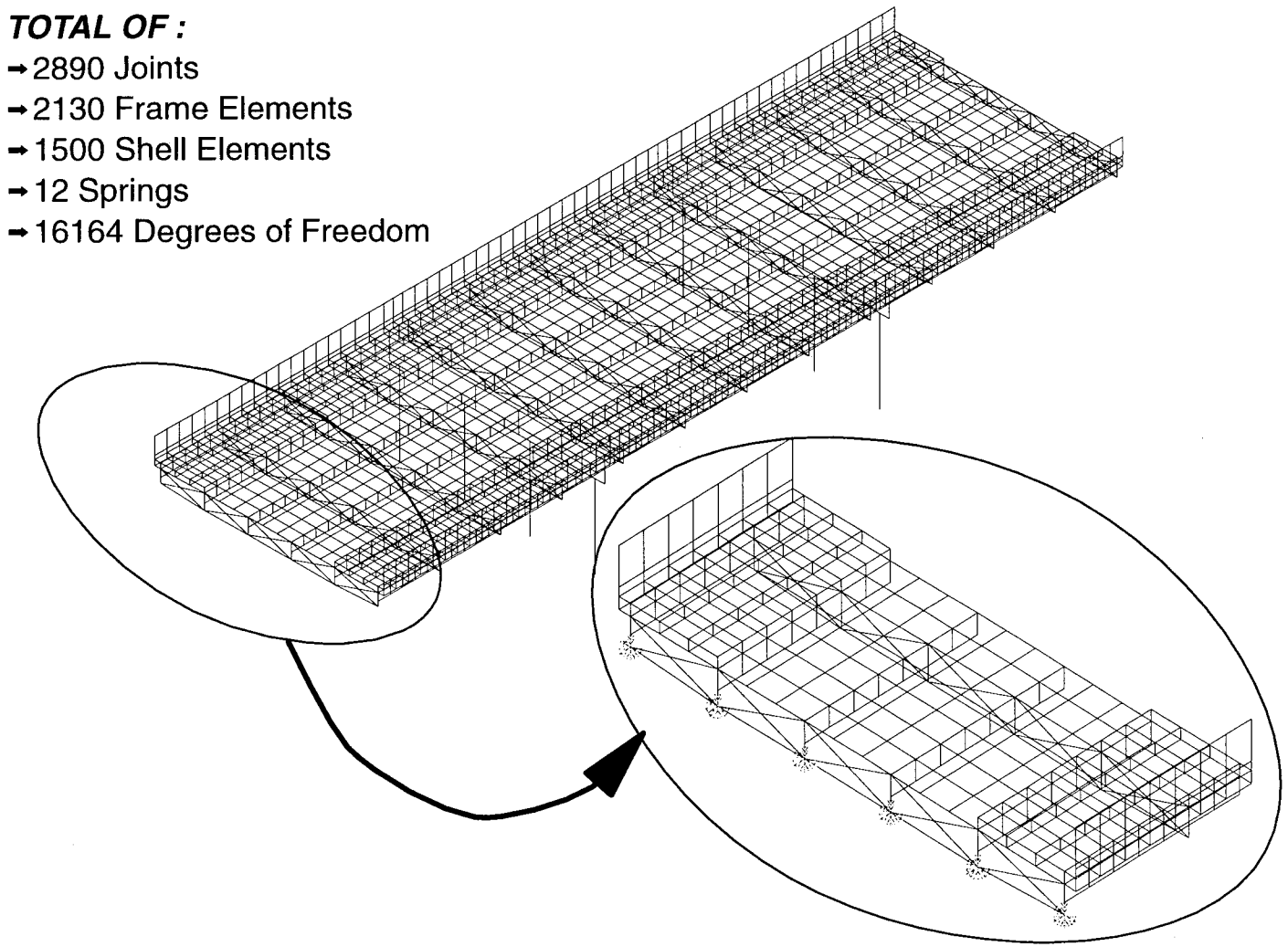

Figure B. 2 Finite Element Modeling of HAM-561-0683 Bridge (Turer, 1998)

APPENDIX C

EFFECT OF CURING METHOD ON BOND STRENGTH

During the process of deciding what variables to include in the test matrix of the laboratory tests, the method of curing became a concern for the testing. Because concrete shrinks over time if it is not exposed to a wet environment, the shrinkage of the overlay and the base concrete could have an effect on the bond strength at the interface. Due to this concern, the direct shear and SHRP specimens used in the series 1 (see Chapter 3) were divided into two groups to examine the effect of shrinkage. Half of the specimens were cured in a mist room until testing, and the remaining half were cured similar to current ODOT specifications. ODOT requires that the base concrete (Class "S" concrete) be wet cured under burlap for a minimum of seven days, and the overlay concrete (MSC, LMC, or SDC) be wet cured for a minimum of three days.

The fabrication procedure for the wet cured specimens was as follows: (1) cast the base concrete and place them into a wet room after 24 hours. (2) Cure the base concrete for a minimum of 56 days. (3) Prior to receiving an overlay, remove the base specimens from the mist room and allow them to dry to a saturated surface dry (SSD) condition. (4) After drying, sandblast and seal with epoxy resin or high molecular weight methacrylate (the benchmark specimens do not get sealed). (5) After 24 hours, place the specimens back in the mist room for 56 days (see Figure C.1).

The curing procedure for field cured specimens is similar to the descrption above, except the base concrete only wet cured for seven days, and the overlay for 3 days (refer to Figure C.2). After curing, the field specimens are placed in a dry storage room until testing.

The results from the direct shear tests indicate that shrinkage does not have a notable effect on the bond strength. However, the presence of moisture did create a noticeable decrease in bond strength depending on the type of sealer used at the interface (see Figures C.3 and C.4). When epoxy resin was used, a dramatic decrease in bond strength was found for each type of overlay. The bond strengths obtained for MSC, LMC, and SDC overlays when field cured were 3.4 MPa

(490 psi), 4.4 MPa (640 psi), and 5.4 MPa (780 psi), respectively. Wet cured specimens sealed with epoxy resin decreased to 1 MPa (145 psi), 0.8 MPa (115 psi), and 1.0 MPa (145 psi) for MSC, LMC, and SDC overlays, respectively. This decrease corresponds approximately to 78% decrease in bond strength. The curing method did not have an appreciable effect on the bond strength of surfaces sealed with HMWM.

The observed loss in strength was verified in discussions with SIKA representatives. The SIKADUR 55 SLV epoxy resin used as a sealer may be applied to a damp concrete surface, but it can not be subjected to moisture for a long period of time. A chemical reaction occurs at the surface of the epoxy, leading to debonding of the epoxy from both the overlay and the base concrete. Because of this bond strength loss, epoxy resins may not be suitable for use as a sealer between an existing deck concrete and a concrete overlay. If sealers are applied, testing should be conducted to determine which materials may be affected by moisture or other environmental variables.

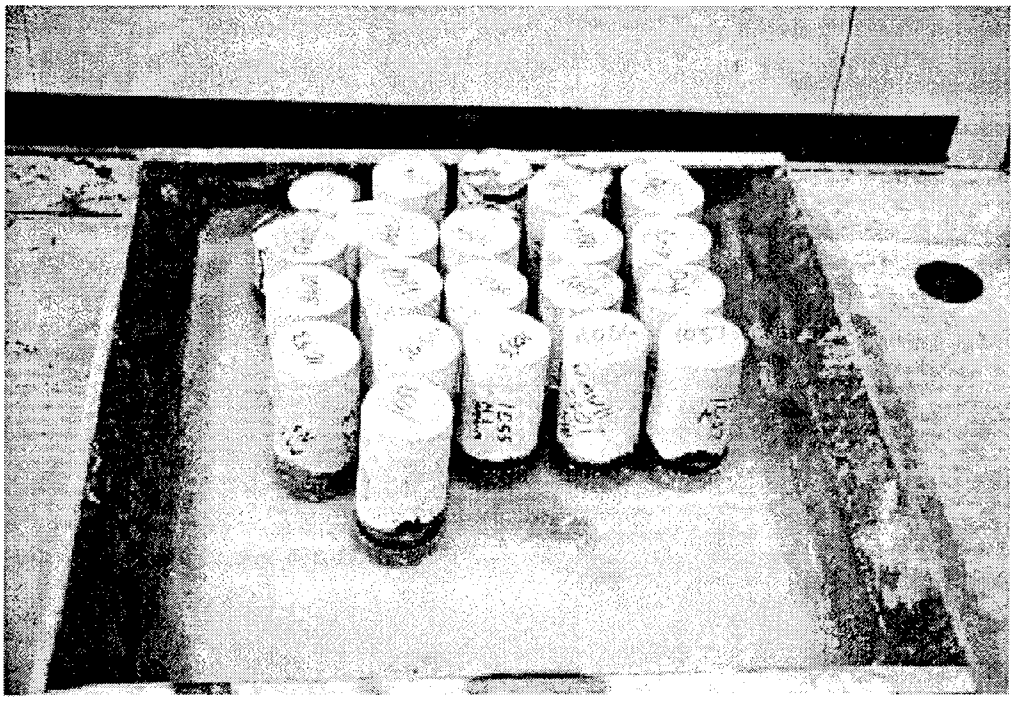

Figure C.1 Field Curing of Overlay for Direct Shear Specimens in a Trough of Water

Figure C.2 Continuous Wet Curing for Direct Shear Specimens in the Mist Room

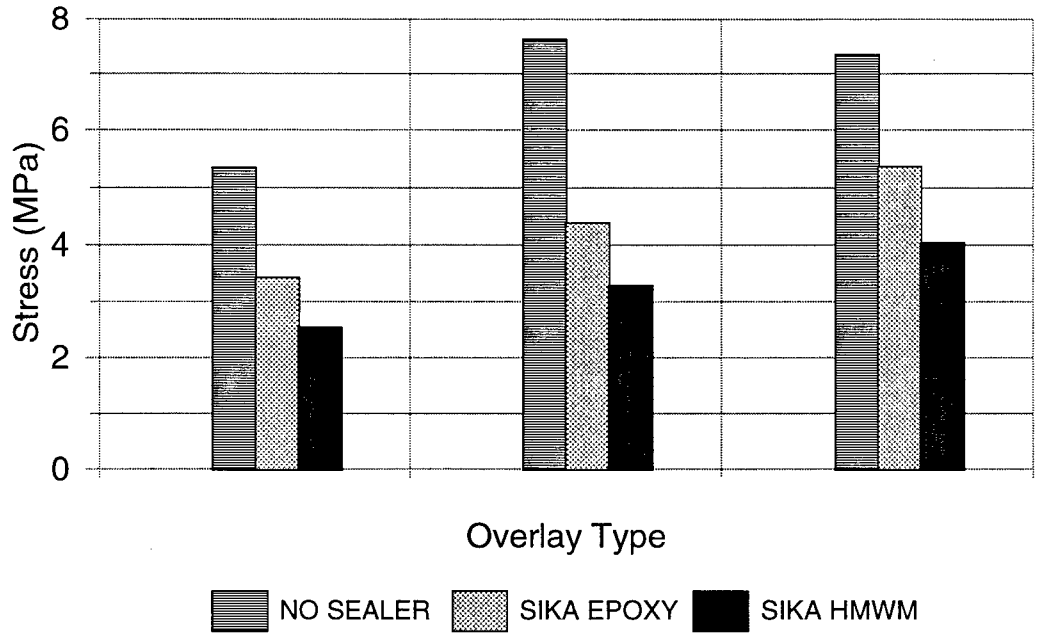

Figure C.3 Direct Shear Test Results for Field Cured Specimens

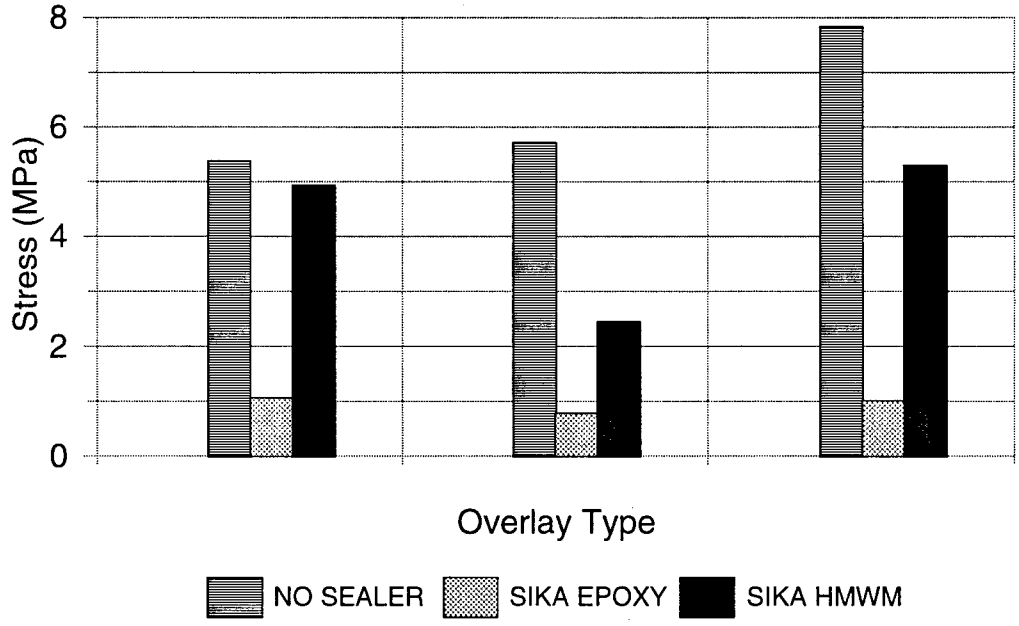

Figure C.4 Direct Shear Test Results for Wet Cured Specimens

APPENDIX D

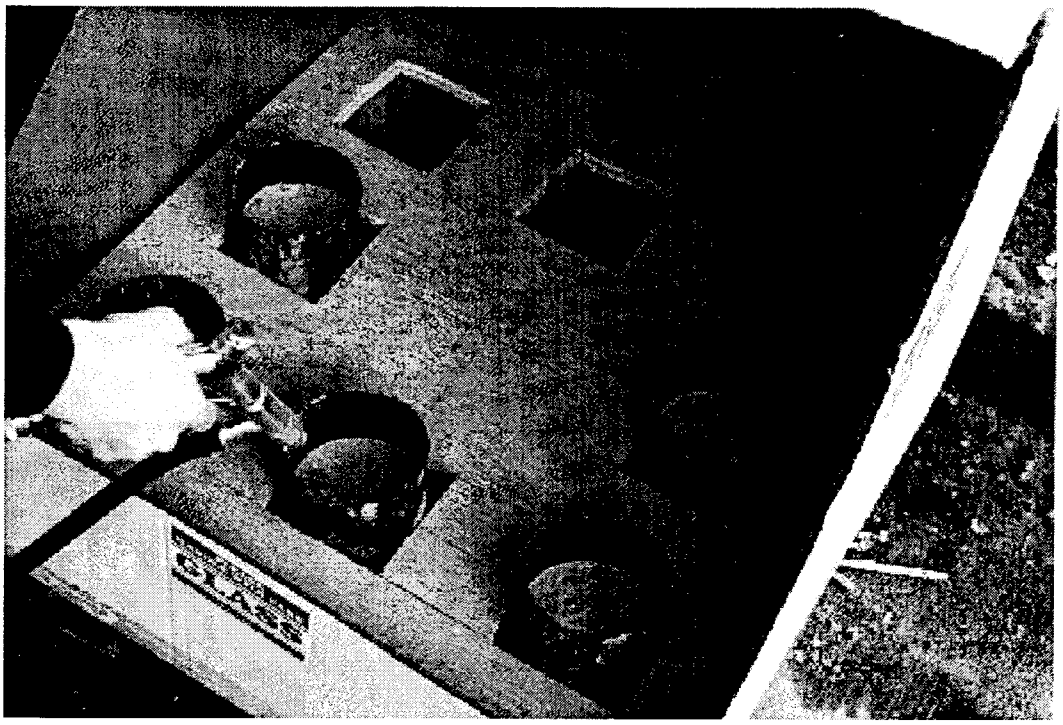

Figure D.1 Sandblasting bond interface surface

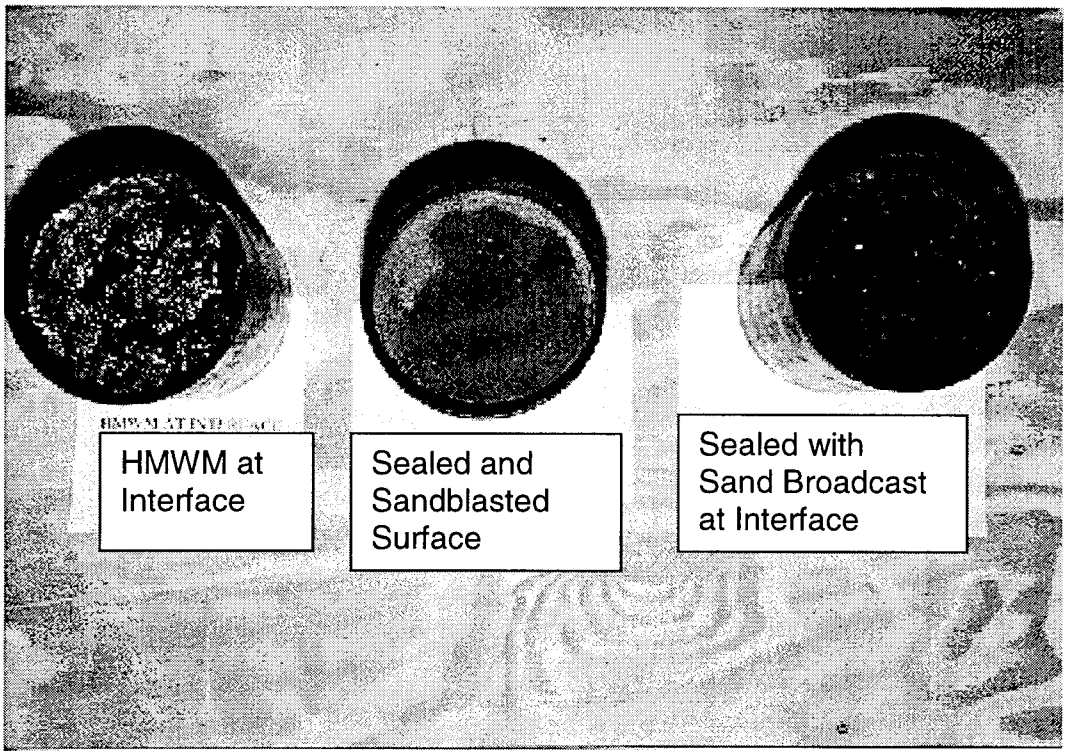

Figure D.2 Alternative surface preparation techniques (Series 2 Tests)

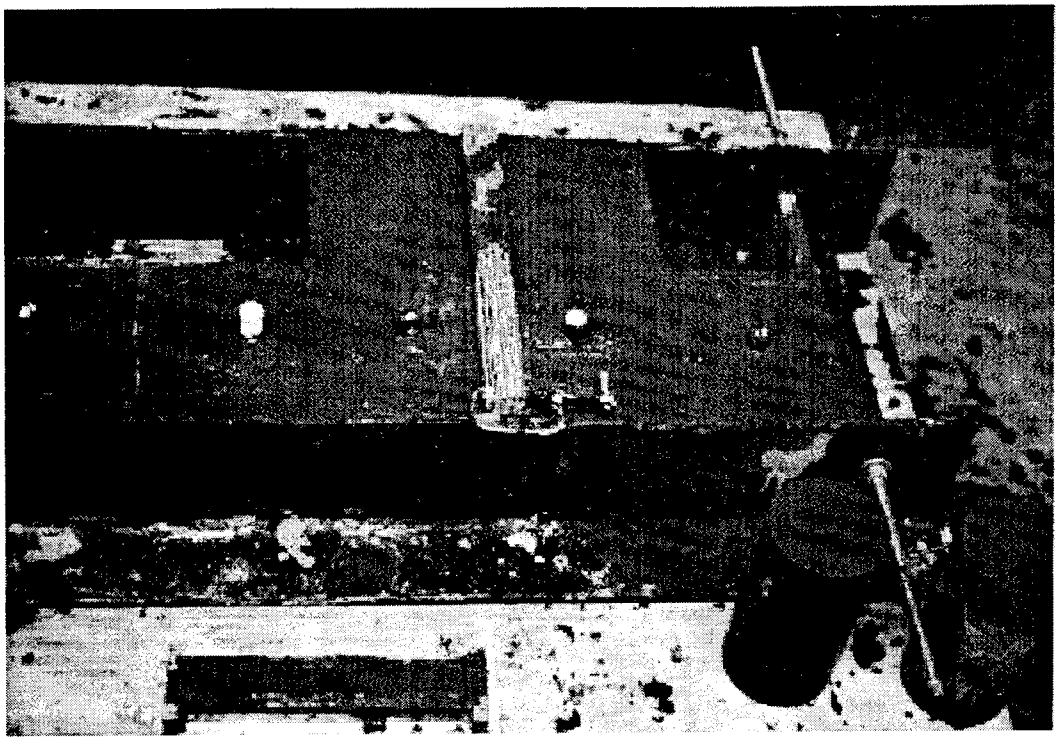

Figure D. 3 Form for concrete base of SHRP specimens

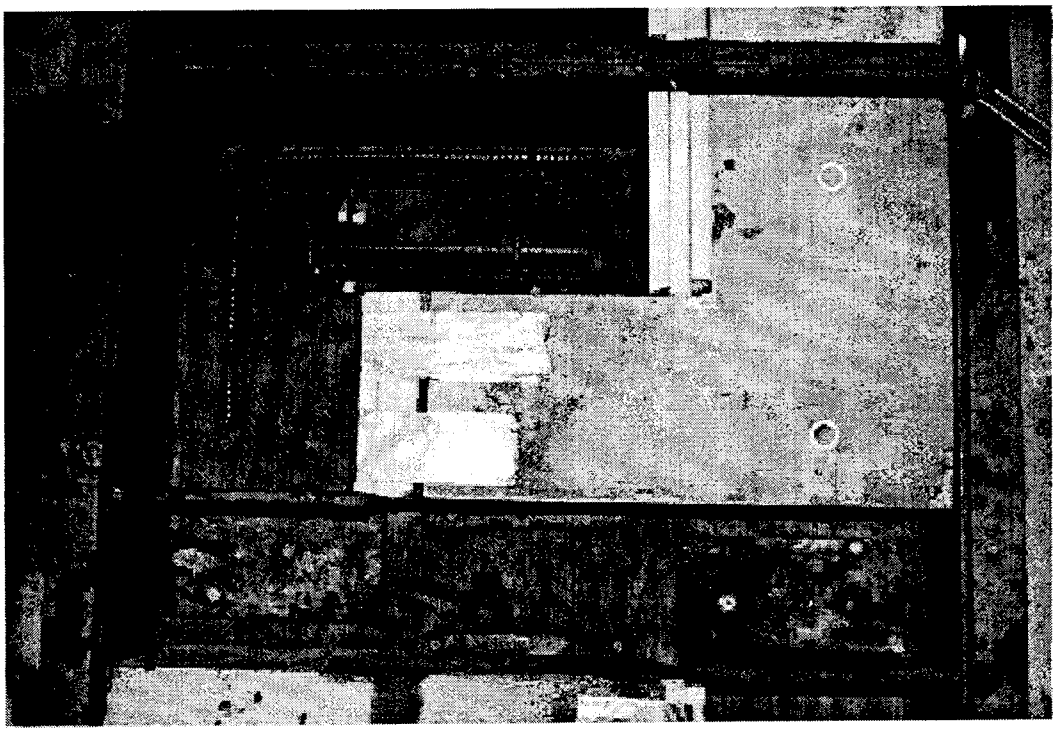

Figure D.4 SHRP base in forms ready to be overlaid

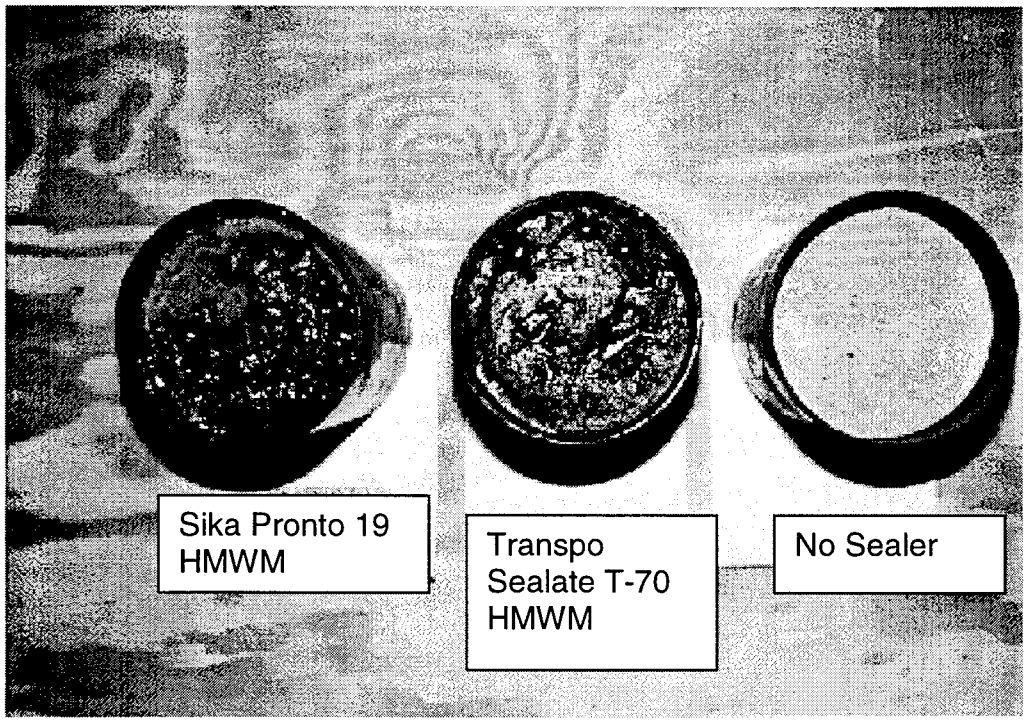

Figure D.5 Direct shear surface condition after sealer application

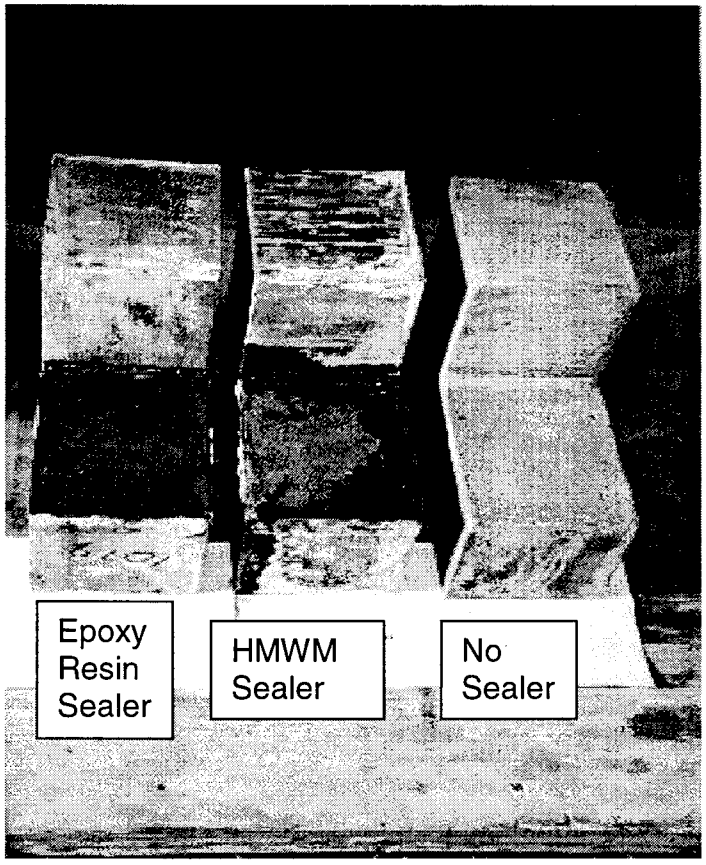

Figure D.6 SHRP surface condition after sealer application

Figure D.7(a) Direct shear test for a specimen without sealer at the Interface. Failure occurred in the base concrete. Note the broken aggregate in the overlay and base concrete.

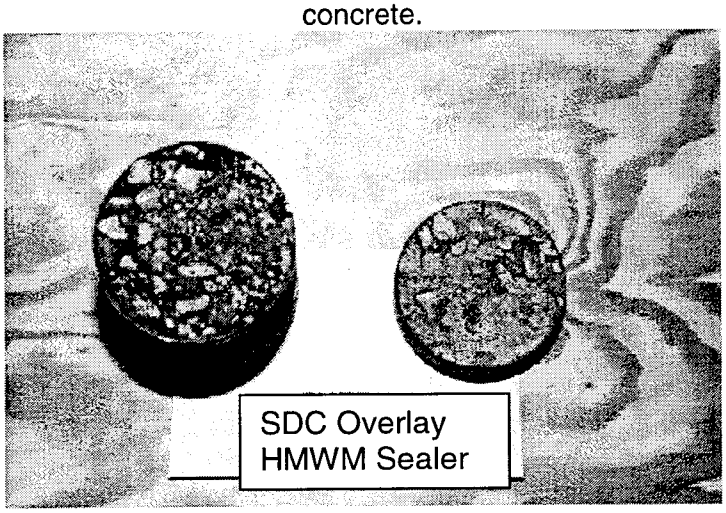

Figure D.7(b) Direct shear test for a specimen with HMWM sealer at the interface. Failure occurred at the interface.

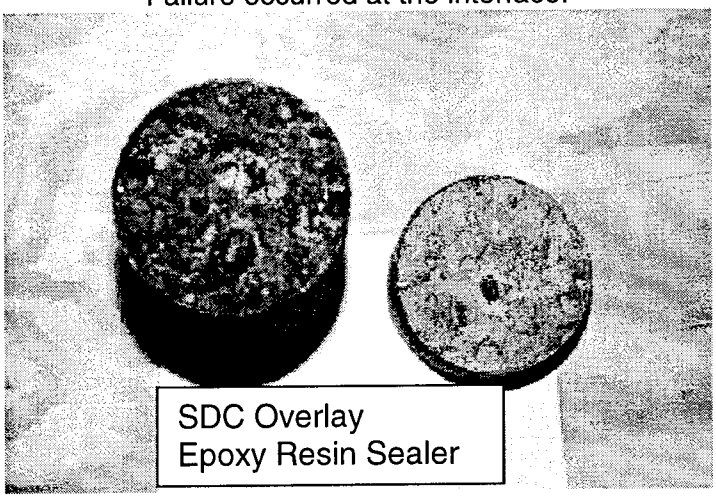

Figure D.7(c) Direct shear test for a specimen with epoxy resin sealer at the interface. Failure occurred at the interface.

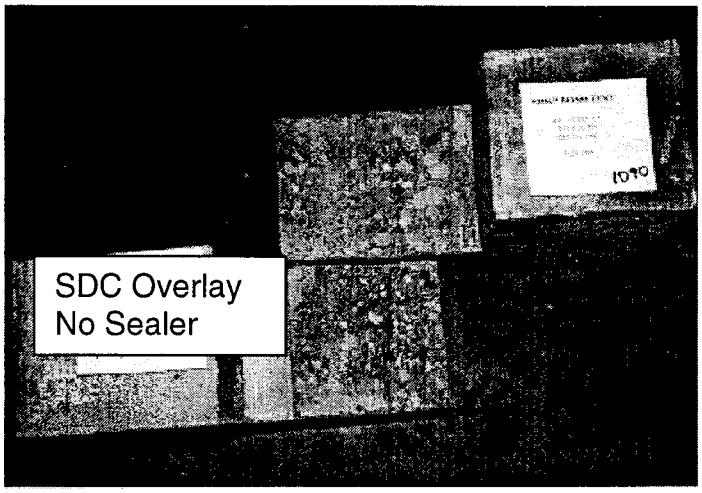

Figure D.8(a) SHRP test specimen with no sealer at the interface.
Failure occurred in the overlay concrete. Note the broken aggregate in the overlay and base concrete.

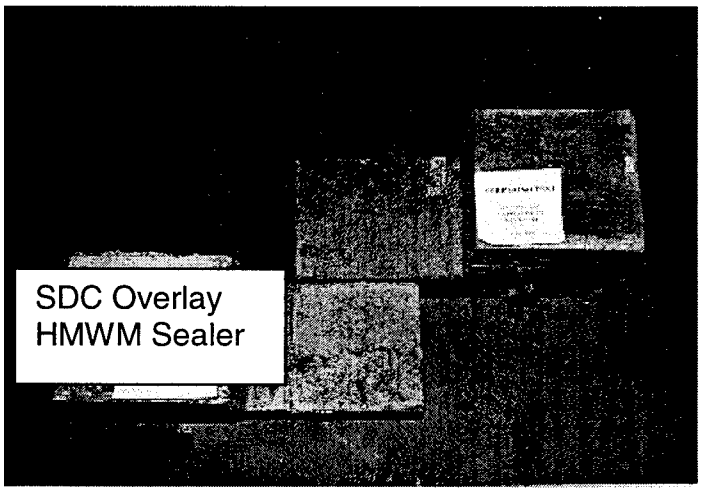

Figure D.8(b) SHRP test specimen with HMWM sealer at the interface.
Failure occurred at the interface.

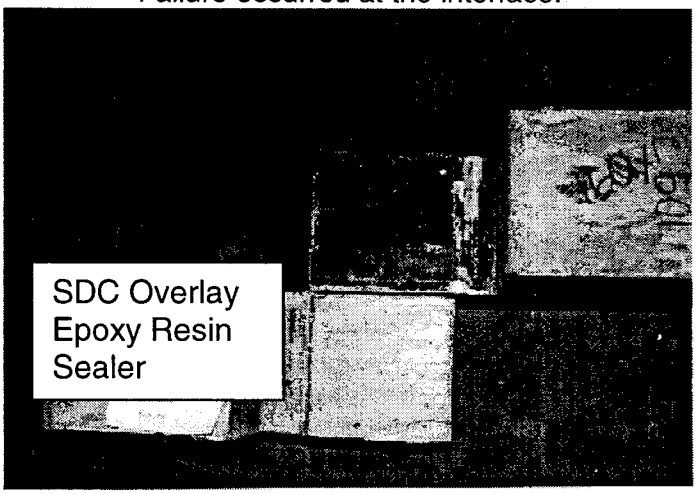

Figure D.8(c) SHRP Test specimen with epoxy resin sealer at the interface.
Failure occurred at the interface.

APPENDIX E

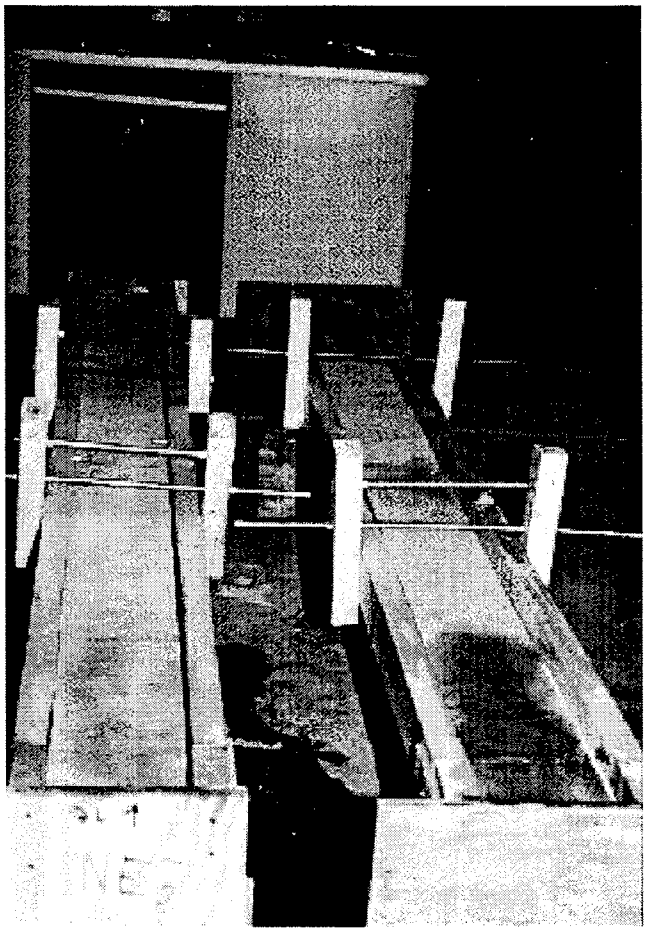

Figure E.1 Overlay Forms for Flexural Beam Test

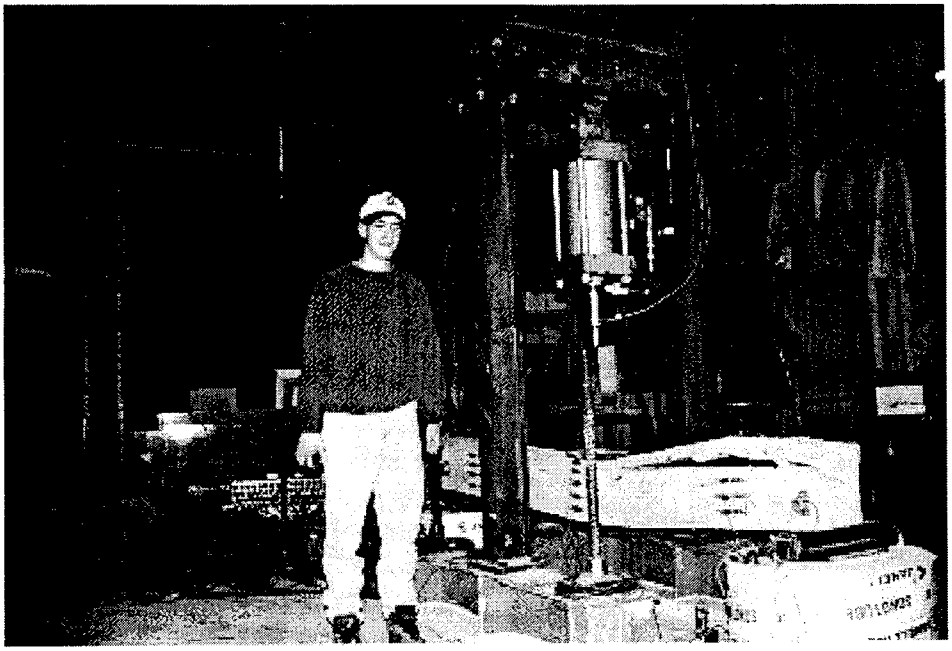

Figure E.2 Completion of Last Flexural Beam Specimen

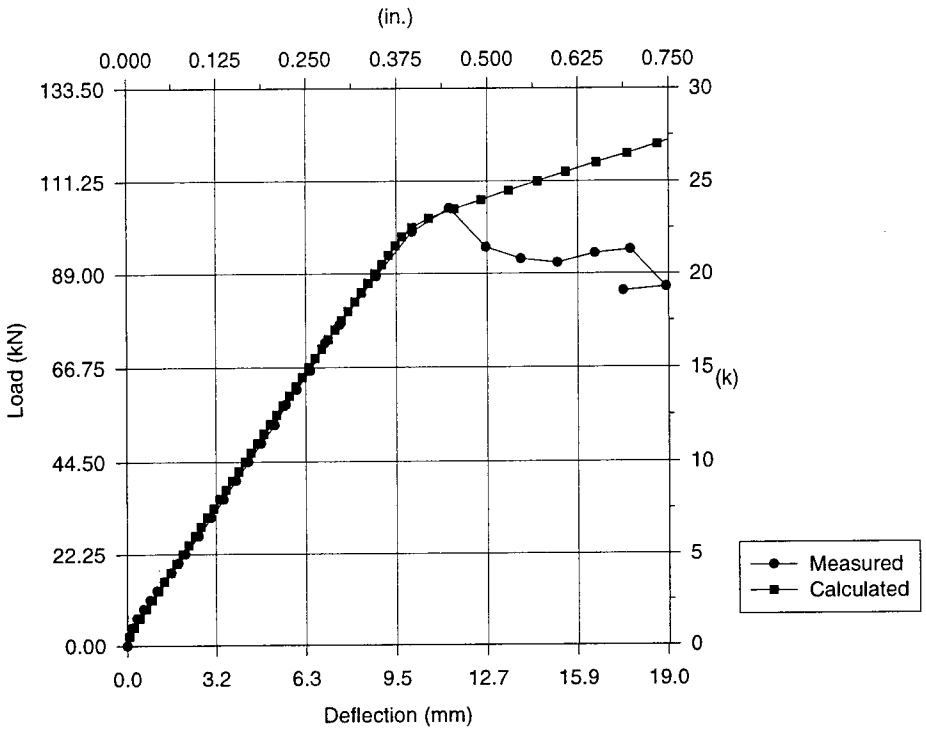

Figure E.3 Load-Deflection Comparison for Specimen No. 2

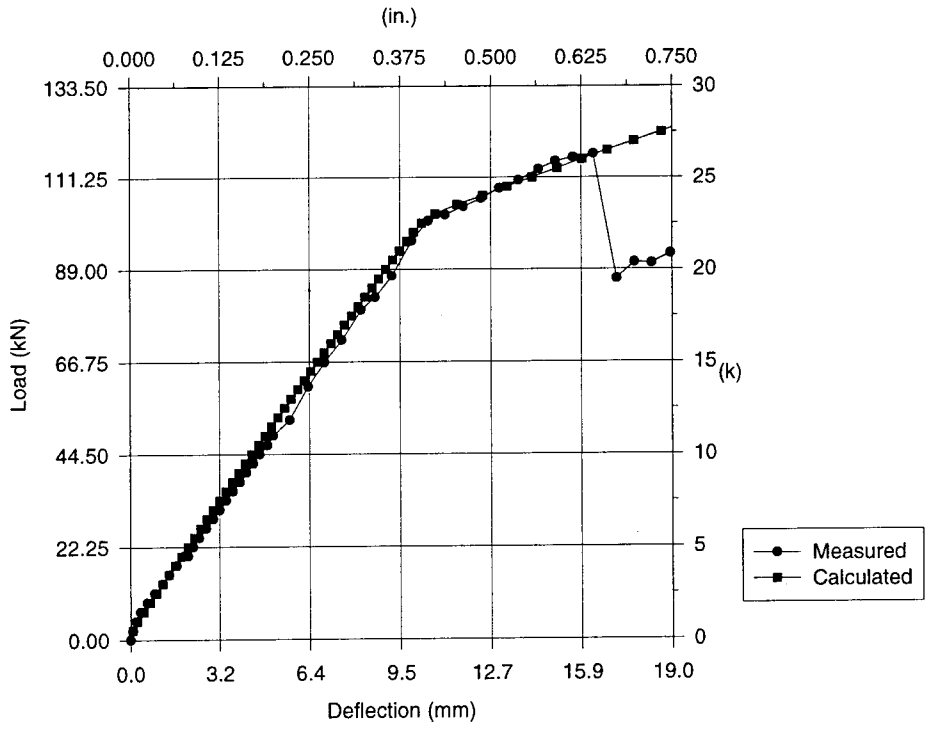

Figure E.4 Load-Deflection Comparison for Specimen No. 4

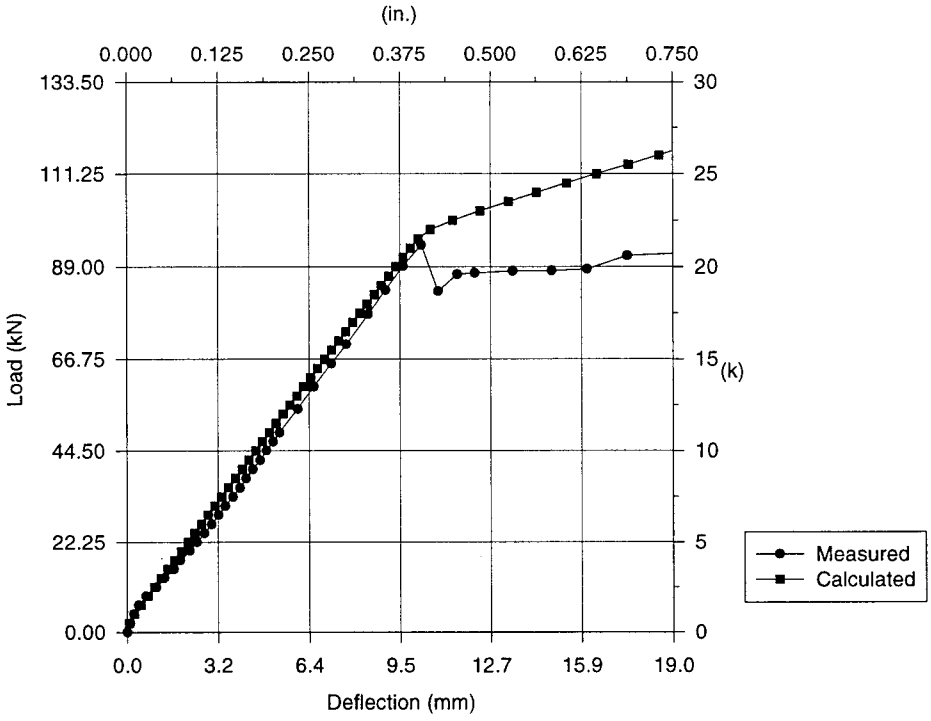

Figure E.5 Load-Deflection Comparison for Specimen No. 6

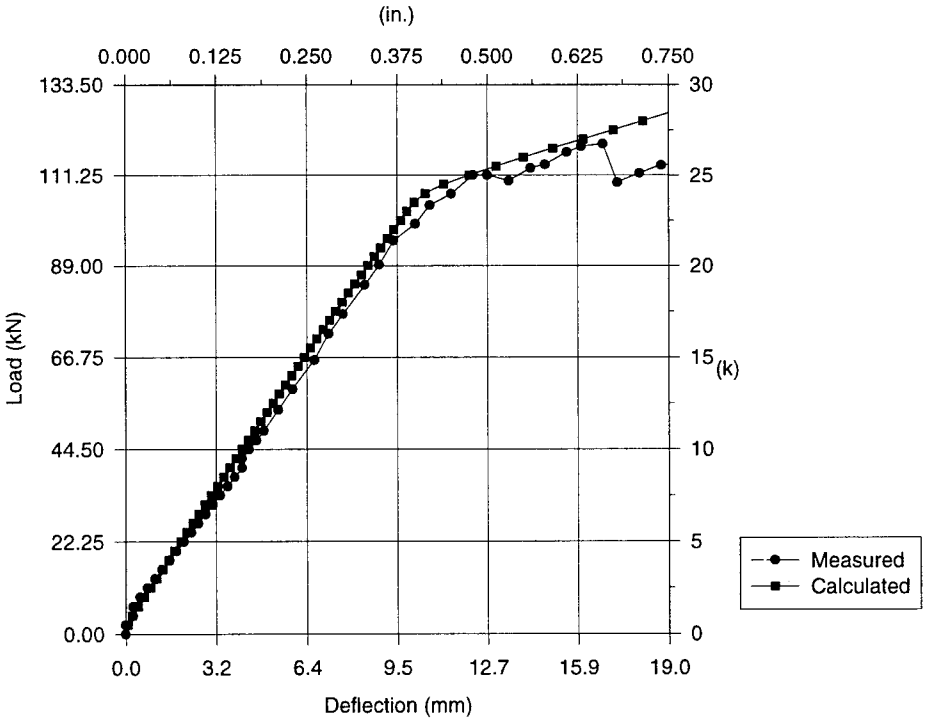

Figure E.6 Load-Deflection Comparison for Specimen No. 10

APPENDIX F

LOAD CELLS

In an effort to measure the load distribution between the three girders in the test specimen, special load cells were fabricated and placed under five supports. Each load cell consists of a 102 mm. x 102 mm. x 4.77 mm. (4 in. x 4 in. x 3/16 in.) structural tube connected to top and bottom steel plates through full-penetration weld all around the tube. Each plate is 254 mm. x 254 mm. x 19.1 mm. (10 in. x 10 in. x 3/4 in.). To eliminate warping in the plates due to welding and ensure that the plates are parallel to each other, the load cell assembly was machined with a 0.051 mm. (0.002 in.) accuracy. The general layout of the load cell is shown in Figure F.1. Two longitudinal 300-ohm strain gages were bonded to the opposite faces of the tube, and the two other faces were gauged with two 350- ohm gages in the transverse direction (so called Poisson gages). All the strain gages were placed on the center of each face. The bonding agent was oven cured for about two hours according to the product literature. The strain gages were subsequently wired to complete a Wheatstone full bridge.

Each load cell was calibrated so that the cell readings can be related to the applied load. For this purpose, each load cell was loaded up to about 311 kN (70 kips) by a concentric compressive load. By relating the applied load to the cell reading, a calibration factor was established. Note that because of the residual stresses in the tube as well as those introduced during welding, it was necessary to load and unload each load cell several times. With each loading and unloading cycle, the relationship between the applied load and cell reading became more linear as the influence of residual stresses diminished. On the average, each load was loaded and unloaded four times. A typical graph used to establish the calibration factors is shown in Figure F.2. The calibration factors for all the load cells are summarized in Table F.1. The load cells were calibrated based on a linear range of 289 kN (65 kips).

Table F.1 Summary of Calibration Factors

Load Cell	Calibration Factor (kips/volt) (Note: 10 volts of excitation was used)
1	5516.35
2	5480.53
3	5535.93
4	5754.59
5	5520.07

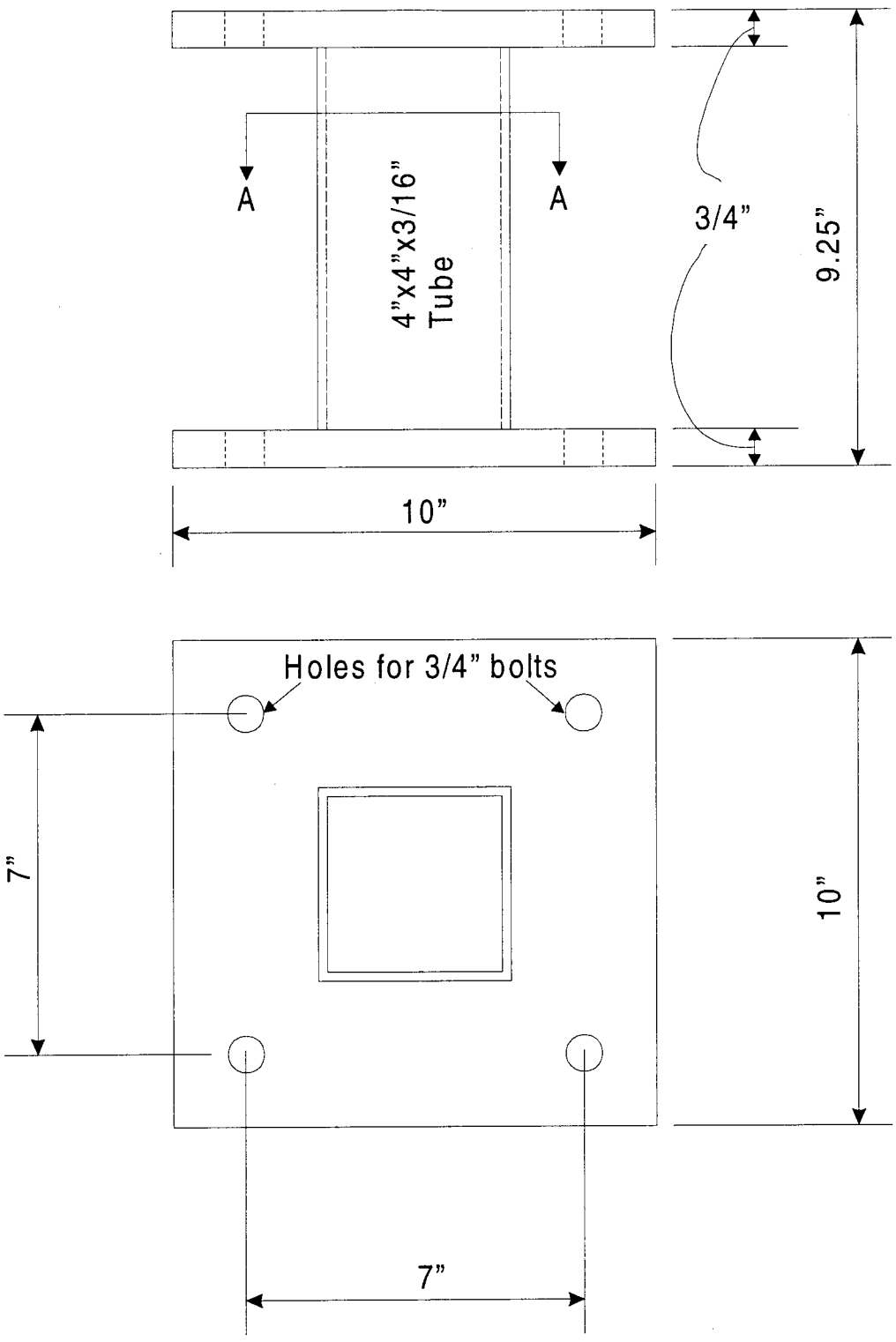

Figure F.1 Details of Load Cells

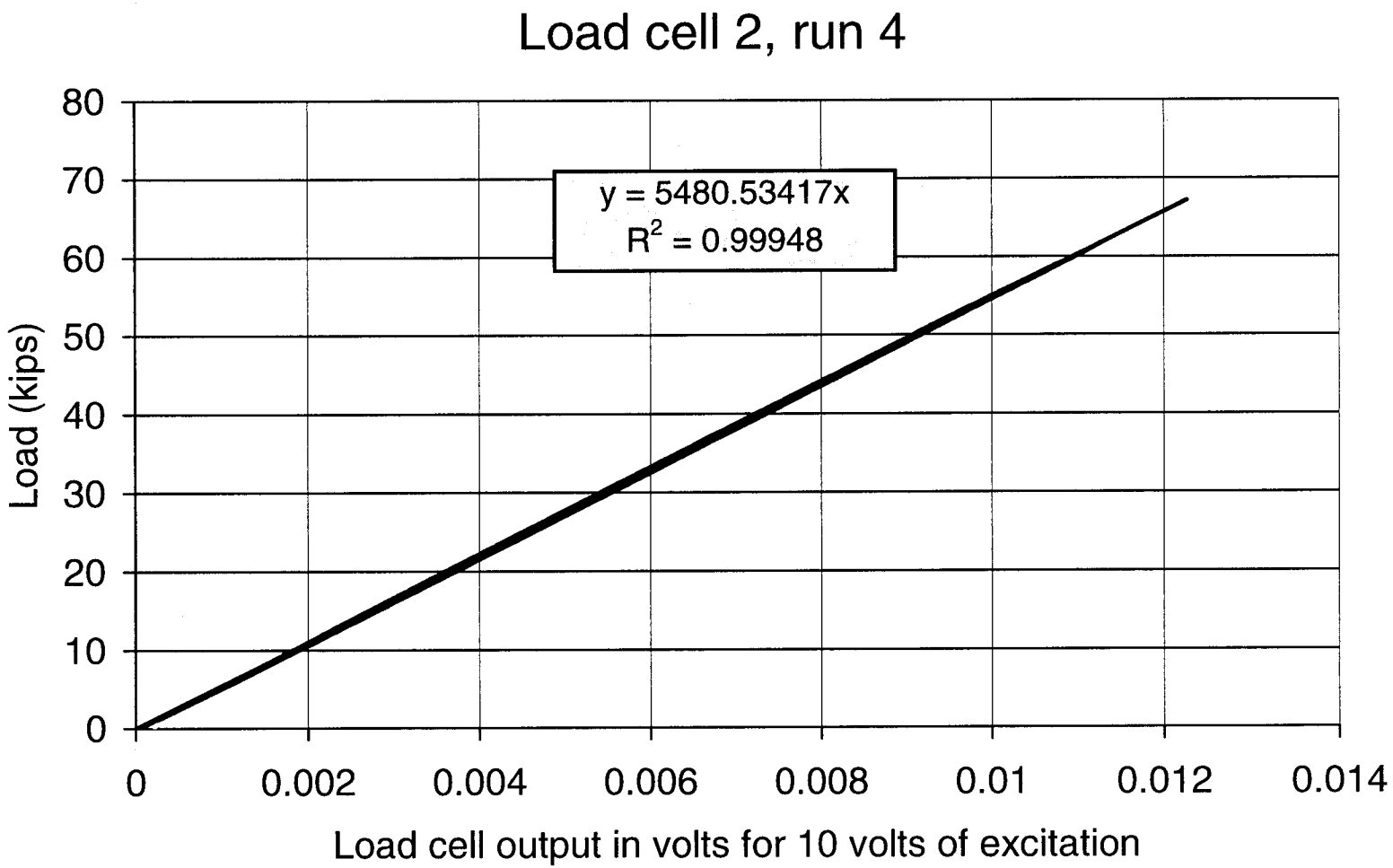

Figure F.2 Example of Calibration Data

APPENDIX G

MODAL TESTING

The critical responses of the test specimen were established by performing modal test using 27 point multi-reference impact testing techniques. A general description of the methodology is presented in this appendix.

The multiple reference impact testing (MRIT) technique was used to obtain frequency response data for post-processing. The MRIT, or roving hammer, technique uses multiple input responses in conjunction with fixed outputs. The roving hammer technique is commonly used for many reasons including minimal equipment and relatively short test time. The following equipment was:

- Four channel digital signal analyzer
- MRIT software
- 15 lb Impact sledge hammer
- Three accelerometers
- External power supply for the accelerometers
- Various lengths of BNC cables

Prior to testing, an adequate grid layout and frequency range of interest had to be decided. For this purpose, an elastic finite element model of the test specimen was constructed by using ANSYS professional analysis software, see Figure G.1. Using the calculated mode shapes, the accelerometer locations were decided at an optimal layout to capture the most of the possible mode shapes. During placement, special care was taken not to place the accelerometers at the "dead points" of the mode shapes. Six of the 27 points were chosen over the supports to capture their behavior. The spacing between the selected nodes was 2'6" except the support nodes which were 1'6" away from the closest node and 1" away from the edge of

the lab-bridge. The points were located along the length of the girders to minimize the effect of local modes of vibration in the slab between the steel girders. The configuration is shown in Figure G.2. The frequency range of interest was decided to be 200 Hertz as the first ten modes of the specimen were predicted to be less than 200 Hertz.

The accelerometers were calibrated using a hand held calibration unit. The hammer was calibrated by using a calibrated accelerometer attached to a known mass in a pendulum system. With the known mass (m) and measured acceleration (a), the calibration value (c) is computed by equating the measured signal (V) from the hammer to the inertia force (Vc = ma), refer to Figure G.3.

Finally, a four-channel dynamic analyzer was to set up to measure the data which were processed by X-Modal developed by the University of Cincinnati's Structural Dynamics Research Lab. Using the 200 Hertz frequency span, 800 spectral lines were chosen to maximize the resolution of the results and minimize leakage. This setup corresponds to a time record of 4 seconds which allowed enough time for the transient response of the impact to dissipate. The windowing applied to the data was a force/exponential window with 1% at the end.

The actual testing of the bridge consisted of impacting each point on the bridge multiple times and averaging the results, as seen in Figure G.4. The averaging serves to minimize random noise on the data. The established value of 5 averages was used at each point in obtaining the frequency response data.

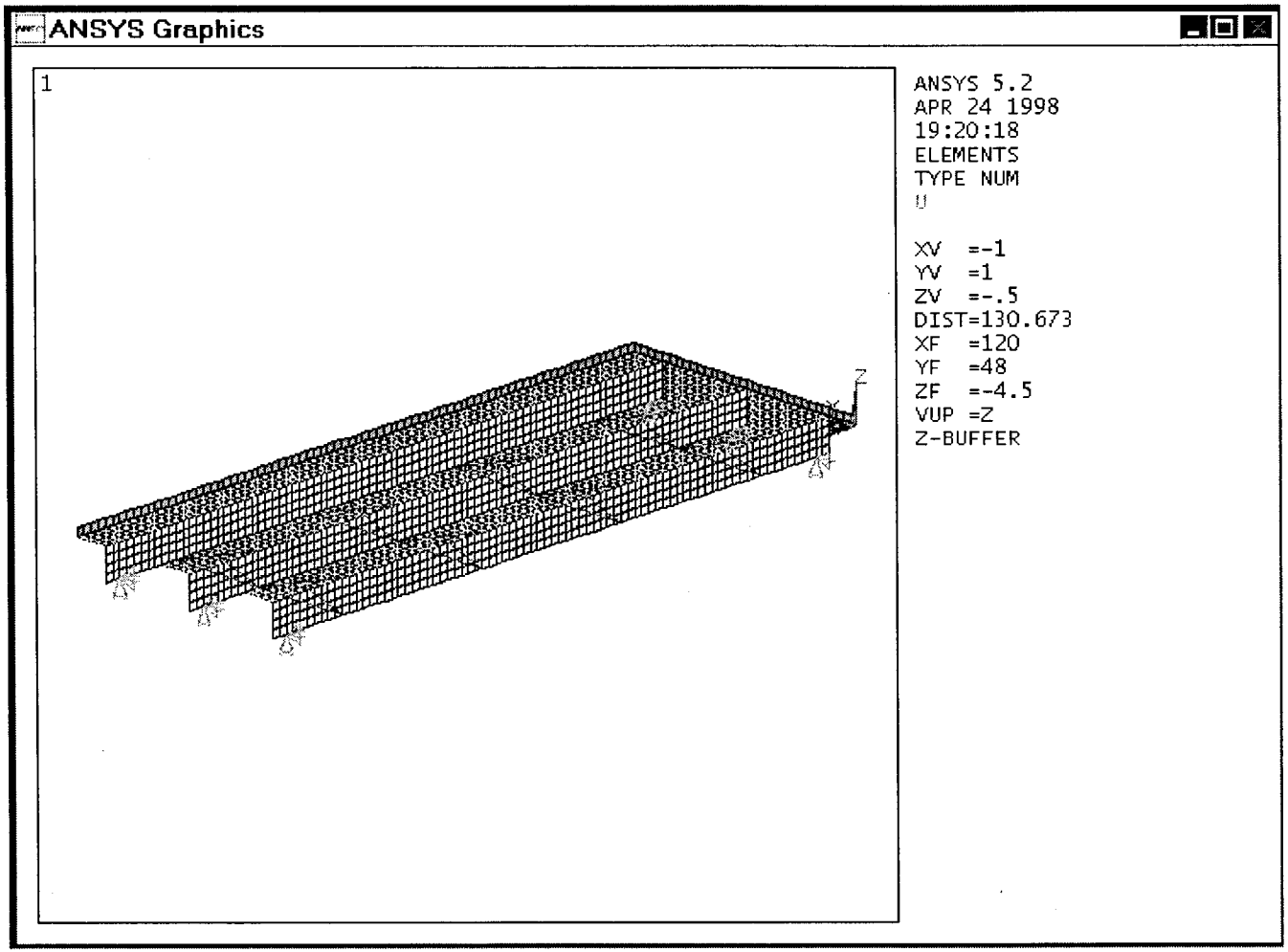

Figure G.1 Finite Element Modeling of Test Specimen

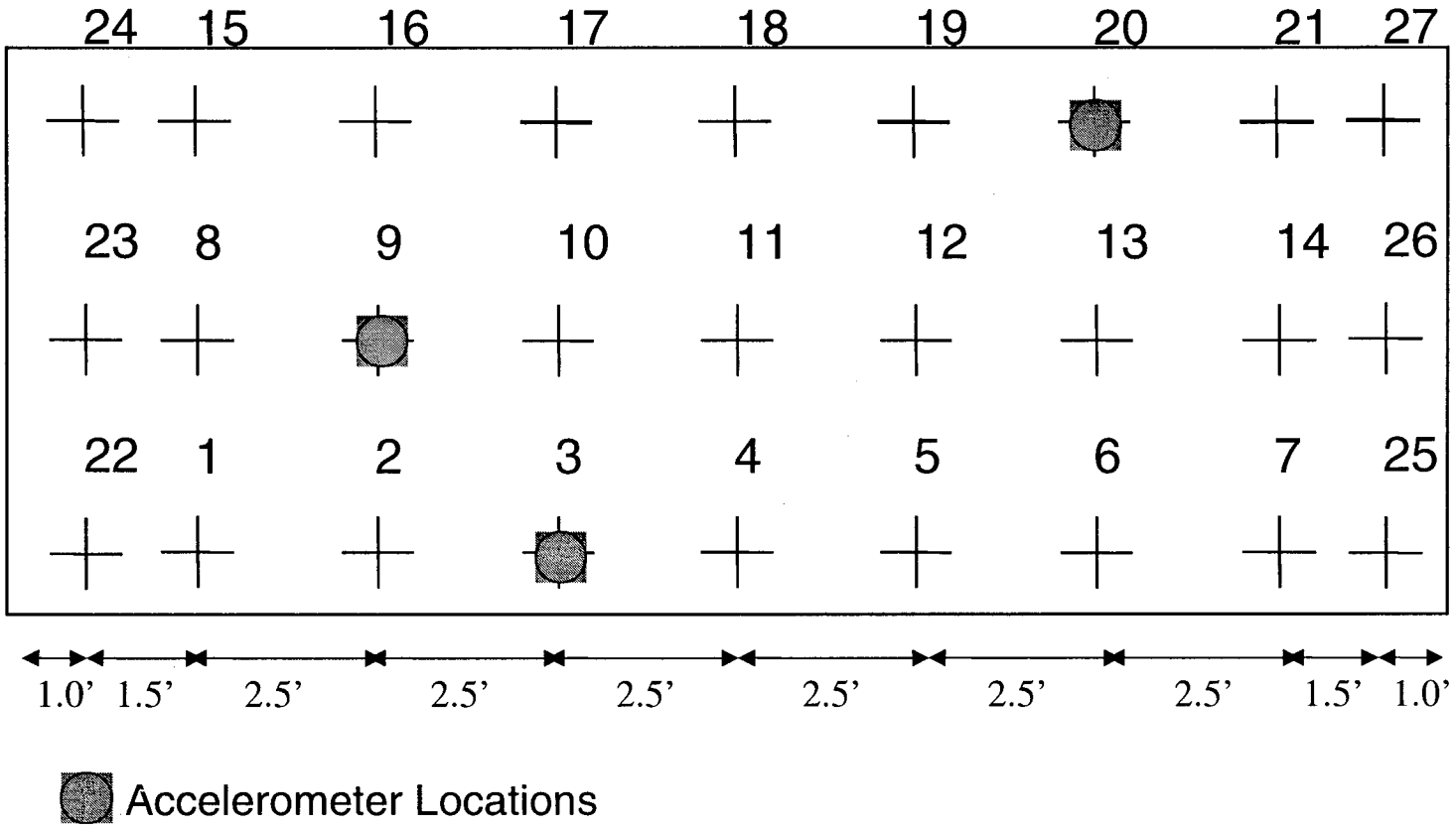

Figure G.2 Grid layout and numbering of accelerometers

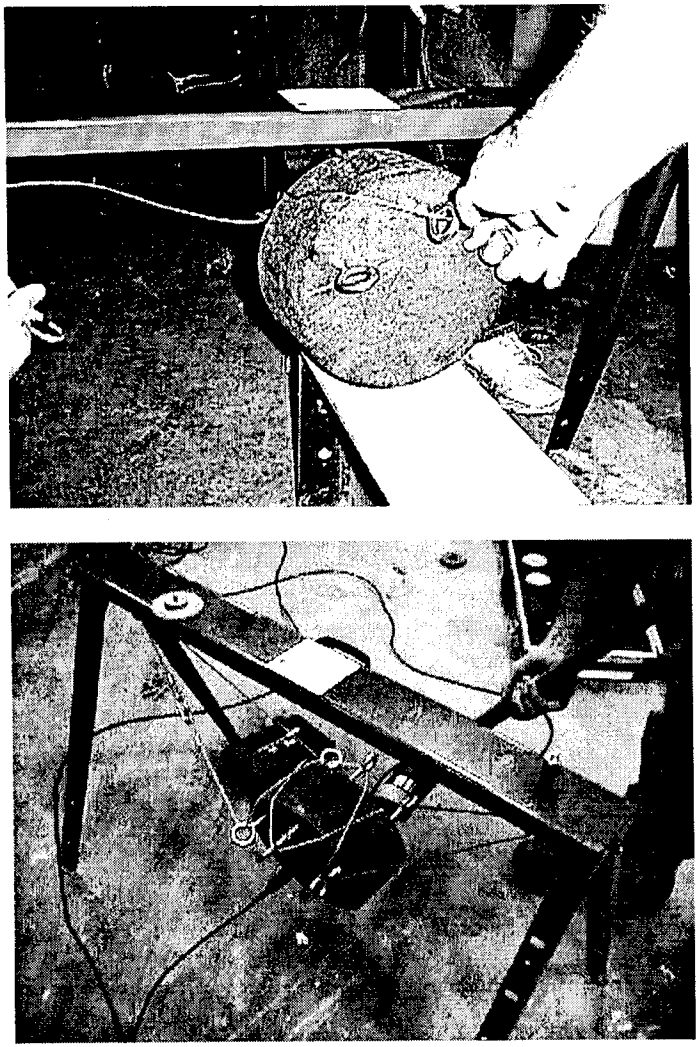

F=m.a, F=c.(Voltage)
a is measured from calibrated acceleration
m is measure from the scale. (97lb)
c=m*a/(Voltage)
0.95 mV/lbf is computed as calibration factor for the hammer

Figure G.3 Calibration of Hammer

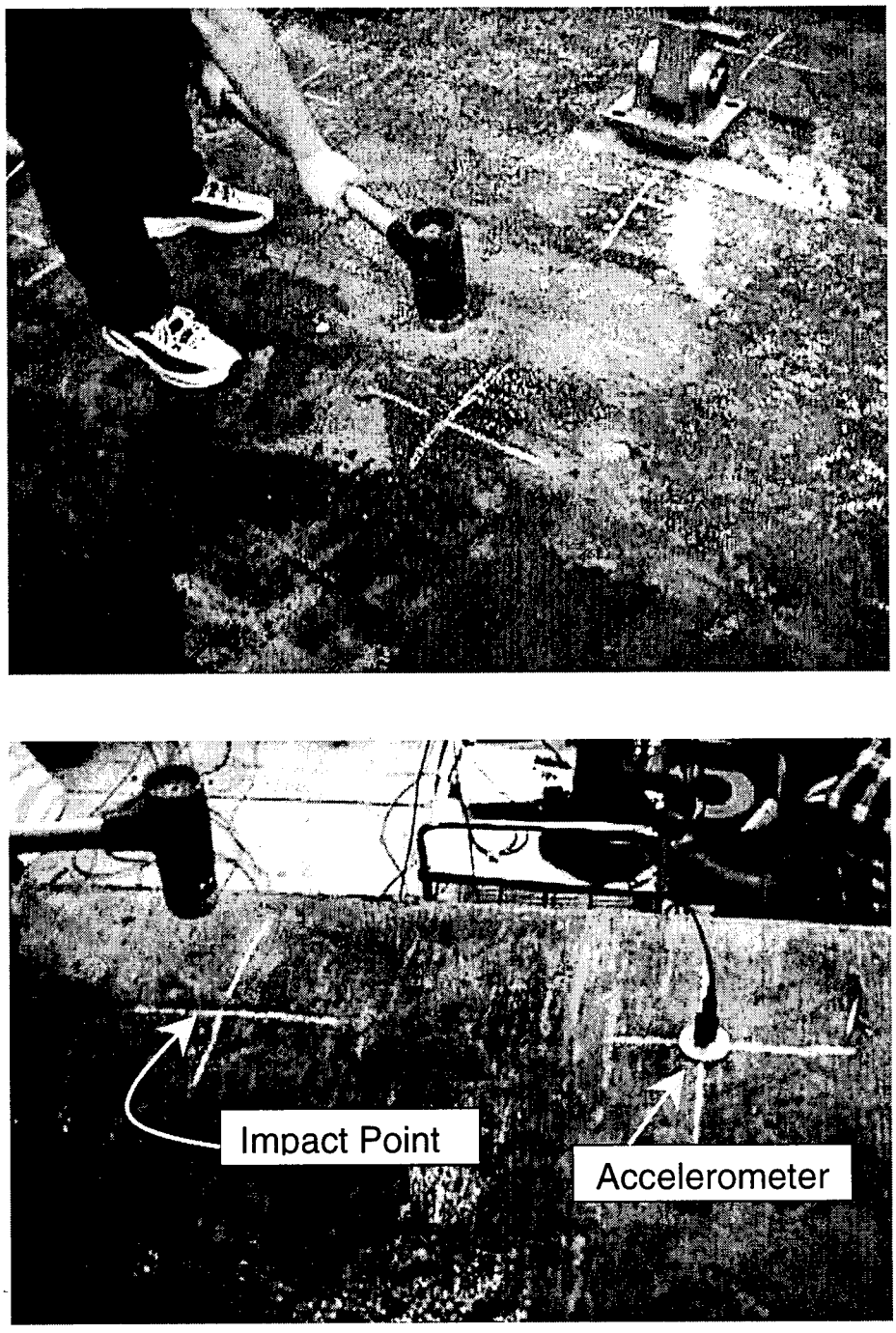

Figure G.4 Impacting of the Test Specimen